Quantum critical metals at vanishing fermion flavor number

Säterskog, K.P.W.

Citation

Säterskog, K. P. W. (2017, November 23). *Quantum critical metals at vanishing fermion flavor number*. Retrieved from https://hdl.handle.net/1887/59464

Cover Page

Universiteit Leiden

Leiden University Repository

The following handle holds various files of this Leiden University dissertation:
http://hdl.handle.net/1887/59464

Author: Säterskog, K.W.P.
Title: Quantum critical metals at vanishing fermion flavor number
Issue Date: 2017-11-23

Quantum critical metals at vanishing fermion flavor number

Petter Säterskog

geboren te Göteborg, Zweden in 1989

Promotor:	Prof. dr K. E. Schalm
Promotiecommissie:	Prof. dr A. V. Chubukov (University of Minnesota, Minneapolis, USA)
	Dr. S. Raghu (Stanford University, Stanford, USA)
	Dr. V. Cheianov
	Prof. dr E. R. Eliel
	Prof. dr J. Zaanen

The front cover shows the momentum distribution function of both a non-interacting Fermi surface (left) and an interacting Fermi surface in the vanishing fermion flavor number limit (right). The action for the interacting theory is shown on the rear side with values of dimensionful parameters indicated with arrows.

The diagrams on the front center represent the infinite set of perturbative corrections in the vanishing fermion flavor number limit. The sum of these corrections gives the fermion two-point function. The solution to this infinite sum is shown on the rear side in terms of an implicit equation.

*To my parents Christina and Michael
and my siblings Erik and Hanna*

Contents

Chapter 1

Introduction

The fundamental laws necessary to describe with high accuracy matter at room temperature and below have been known since the development of quantum mechanics in the 1920s[1]. These laws describe the interactions between atomic nuclei, electrons and the electromagnetic field. They provide a microscopic description of a physical system. This microscopic description is in principle sufficient to derive the physics of most condensed matter systems. However, to do so is not an easy task.

The microscopic description can be used to derive the energy levels of a hydrogen atom with paper and pencil. With a computer we can find the energy levels of a hydrogen molecule. For larger collections of particles it becomes increasingly difficult to apply this microscopic description. Additionally, as system size is increased, new phenomena emerge that—while in principle governed by the same microscopic laws—are not easily described by them. In Marx's words: "Merely quantitative differences beyond a certain point pass into qualitative changes." [1]

Almost anything we experience in daily life is in principle governed by the very same microscopic description, but understanding the laws of physics gives no further understanding of e.g. politics. To some extent this applies to condensed matter too, having a microscopic description is far from enough to understand a system. Condensed matter systems are however, in relation to politics, quite close to the microscopic description. We can therefore hope to understand emergent condensed matter phe-

---

[1]Using the more accurate standard model of today only gives small corrections to low-energy physics. Taking these effects into account in the case of the hydrogen atom gives rise to Lamb shift, a relative change of the energy levels on the order of 10^{-6}.

nomena in terms of microscopic laws at some point, but we are not there yet.

There has been much progress in condensed matter physics since the 1920s, both in terms of understanding implications of the microscopic description and in experimentally studying different systems. A hallmark of the theoretical developments is Landau's Fermi liquid theory (FLT) formulated in the 1950s [2]. It is a theory describing large collections of interacting fermions, a class of particles that includes the electrons. This theory can beautifully describe many physical systems composed of fermions such as liquid helium-3, elemental metals like copper or complex compounds with large interaction effects. The work to understand this— initially phenomenological—theory in terms of the microscopic description of interacting fermions has continued into the current century [3].

Another 1950s hallmark of condensed matter theory is the Bardeen-Cooper-Schrieffer (BCS) theory of superconductivity [4]. This explains why some of the electron systems have zero electrical resistance below a critical temperature, they become superconducting.

Despite the success of FLT and BCS theory, there are phases of electronic matter that fall outside of their description and for which we do not have an alternative theory. The most prominent examples are the high-temperature superconductors. These are materials that become superconducting at a temperature significantly higher than what can be obtained in BCS theory. In fact in their non-superconducting phase, they can not be understood within FLT and are referred to as non-Fermi liquids (NFL). The potential applications of room-temperature superconductors makes the understanding of these materials of utmost interest[2].

Since we have a microscopic description of these materials we could in principle put the governing equations in a computer and numerically calculate any property of interest. However, it has been proven that a numerical solution of this type of fermionic systems generally fall into a class of mathematical problems called NP-hard [6]. It is conjectured, and generally believed, that no classical algorithm with polynomial complexity can solve an NP-hard problem. This means that while in principle possible, such an approach would take too long time.

We know however that it is possible to obtain physical observables

---

[2]Nearly 200,000 high-T_c papers had been published on the 25th anniversary of the discovery [5].

in polynomial time. Nature provides them when we do experiments[3]. It should therefore be possible to construct a device to simulate these systems in polynomial time. The crux is that this device needs to operate quantum mechanically. An ordinary computer does not. Large efforts are currently under way to create a device that can perform controlled quantum computations, a quantum computer. These will—just like nature—be able to simulate quantum systems in polynomial time.

Although a quantum computer will eventually be able to simulate NFLs, there will be a need for a theoretical understanding. In the end, just being able to simulate these materials without understanding them is not much different from being able to do experiments. Trying to design a useful NFL without a theory would be like designing an airplane knowing about the molecules that make up air but only relying on experiments and simulations. The whole design process would be trial and error. However, if we have an effective description of air like the Navier-Stokes equations, then we know about phenomena like vortices, boundary layers, shockwaves, and turbulence. Knowing about these lets us make informed design decisions.

With this motivation, we focus in this thesis on developing general tools for studying non-Fermi liquids. We do so by considering a particular scenario in which a NFL arises, the quantum critical metals. Since there is currently no way of solving these theories we do not attempt to study a realistic model but instead study the most simplified possible model that still contains the essence of quantum critical metals, a toy-model. We furthermore limit ourselves to not study superconducting and other instabilities, but focus on NFL physics.

This thesis is structured as follows. In this first chapter we give some background, first on Fermi liquid theory in Section 1.1 and on some cases where this theory breaks down in Section 1.2. We there settle on a particular case where FLT breaks down, a quantum critical metal, that will be the main focus of the rest of this thesis. In Section 1.3 we study some general features of the perturbation theory of the chosen theory and in Section 1.4 we review some non-perturbative approaches to this and other NFL theories. In the following Chapters 2-5 we present new results using one of these non-perturbative approaches, the small N_f limit.

---

[3]The time it takes to perform a condensed matter experiment is polynomial in the system size for typical observables. It is of course possible to construct exponentially complex observables for which this is not true.

1.1 Fermi liquid theory

In this section we review the physics of fermions at finite density. We start by describing free fermions, the Fermi gas. We go on to study interacting fermions, first by presenting Landau's phenomenological theory, Fermi liquid theory, and then by giving a modern motivation for this theory in terms of renormalization group flows. We conclude with some implications of FLT in a field theory language.

Throughout this chapter and this thesis we consider an isotropic and translationally invariant system of spinless fermions. Neither of these assumptions is true for electrons living in a periodic lattice. However, for the questions that we explore, spin and the presence of a lattice are not relevant. Once the physics in the simplified case is satisfactorily understood, then a more general model should be explored, but until then these generalizations only make things more complex.

1.1.1 Fermi gas

The total energy of a free particle of mass m, momentum $\mathbf{p}$ and at a potential $-\mu$ is given by $\epsilon(\mathbf{p}) = \mathbf{p}^2/2m - \mu$. In a square box of side-lengths L, the momentum is discretized as $\mathbf{p} = (n_1, n_2, ..., n_d)\hbar 2\pi/L$, $n_i \in \mathbb{Z}$, where d is the number of spatial dimensions. Here and henceforward we use units such that $\hbar = 1$. The Hamiltonian for a system of such free fermions is

$$H_0 = \sum_{\mathbf{p}} \psi_{\mathbf{p}}^\dagger \psi_{\mathbf{p}} \epsilon(p) \tag{1.1}$$

where $\psi_{\mathbf{p}}^\dagger, \psi_{\mathbf{p}}$ are the creation and annihilation operators for a fermion in momentum state $\mathbf{p}$. All momentum states are decoupled from each other and form individual two level systems, the unoccupied state with energy 0 and the occupied state with energy $\epsilon(\mathbf{p})$. Each state can be occupied by maximally one fermion by the Pauli exclusion principle. The ground state is when all states with negative $\epsilon(\mathbf{p})$ are occupied, i.e. al states with $\mathbf{p}^2/2m < \mu$, and all states with positive $\epsilon(\mathbf{p})$ are unoccupied. The set of occupied momenta thus forms a ball in d-dimensional momentum space of radius $k_F = \sqrt{2m\mu}$. The surface of this ball is referred to as the Fermi surface (FS) and the momentum k_F the Fermi momentum. Note that this is only a surface for $d = 3$, for e.g. $d = 2$ the Fermi surface will be a line. See Fig. 1.1.
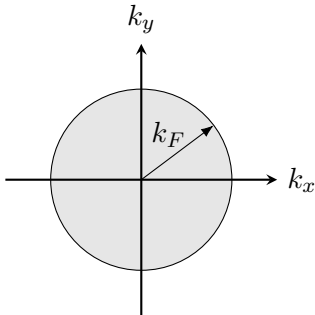
Figure 1.1. Momentum space of a two-dimensional Fermi gas. The shaded area shows occupied momentum states. The solid circle is the FS.

An excited state has a number of *particles* - occupied momenta with positive $\epsilon(\mathbf{p})$, and *holes* - unoccupied momenta with negative $\epsilon(\mathbf{p})$. The energy (above the groundstate) of an excitation is given by $|\epsilon(\mathbf{p})|$ and all the low energy states will thus be close to the Fermi surface. These low energy excitations closest to the FS dictate the low energy physics. Their dispersion is given by $\epsilon(\mathbf{p})$. For low energies we can expand this around the FS:

$$\epsilon(\mathbf{p}) = v_F(p - k_F) + \mathcal{O}\left((p - k_F)^2\right) \tag{1.2}$$

where $v_F = \sqrt{2\mu/m}$, the Fermi velocity, determines the dispersion of the low energy excitations. Here p is the magnitude of the momentum $\mathbf{p}$. The higher order terms are typically not important; however, a more general $\epsilon(\mathbf{p})$ resulting from the lattice potential can have a direction dependent k_F and v_F. This near FS expansion is very telling of the nature of fermions at finite density. Only a small fraction of the fermions can be excited at low energies and they are effectively one-dimensional and chiral, meaning particles move in one direction and holes the other. This is independent of the dimensionality. Dimensionality is only important for calculating the FS size at this level of accuracy.

To calculate thermodynamic properties of the Fermi gas we can calculate the partition function for these modes. If we are only interested in the strict limit where $k_B T \ll \mu$ then only the modes closest to the FS contribute and we can use the above expansion. Here T is temperature and k_B Boltzmann's constant, which by a choice of temperature units is set to 1 henceforth. The partition function for a mode of momentum p is

then simply given by

$$Z(p) = \exp(0) + \exp\left(v_F|p - k_F|/T\right) \tag{1.3}$$

For the total partition function we need to take a product of the partition functions of all modes by considering all the integers n_i. We can write this as

$$\log Z = \sum_{\mathbf{n} \in \mathbb{Z}^d} \log Z\left(\frac{2\pi|\mathbf{n}|}{L}\right) \tag{1.4}$$

In the thermodynamic limit $L \to \infty$ we can approximate this sum as an integral. We are not interested in finite-size effects that depend on the shape and boundary conditions of the Fermi gas so we work in this limit. We then have

$$\log Z = \frac{2\pi^{d/2}}{\Gamma(d/2)} \int_0^\infty \mathrm{d}n\, n^{d-1} \log\left(1 + \exp\left(\frac{v_F}{T}\left|\frac{n2\pi}{L} - k_F\right|\right)\right) \tag{1.5}$$

The logarithmic term dies off exponentially away from the FS. The FS is at $n = Lk_F/2\pi$ and since the width is small compared to this within our current limits we can fix n to this value outside of the logarithm and also extend the integration range to $\mathbb{R}$. We then have

$$\begin{aligned}
\log Z &= \frac{2\pi^{d/2}}{\Gamma(d/2)}\left(\frac{Lk_F}{2\pi}\right)^{d-1} \int_{-\infty}^\infty \mathrm{d}n \log\left(1 + \exp\left(\frac{v_F}{T}\left|\frac{n2\pi}{L} - k_F\right|\right)\right) \\
&= \frac{\pi^{2-d/2}k_F^{d-1}L^d T}{2^d 3\Gamma(d/2)v_F} = \frac{\pi^2}{6}N_0 L^d T \tag{1.6}
\end{aligned}$$

where the density[4] of states at the FS, N_0, is given by

$$N_0 = k_F^{d-1}\frac{2^{1-d}\pi^{-d/2}}{\Gamma(d/2)v_F} \tag{1.7}$$

From this we find the entropy and heat capacity:

$$S = \partial_T(T \log Z) = \frac{\pi^2}{3}N_0 L^d T \tag{1.8}$$

$$C_v = \partial_T(T^2 \partial_T \log Z) = \frac{\pi^2}{3}N_0 L^d T \tag{1.9}$$

Only the prefactor $N_0 L^d$ depends on the dimension d; as far as these low-temperature thermodynamic quantities are concerned we only have a collection of chiral fermions with linear dispersion.

---

[4]This is the number of states per unit volume of the system of size L^d, and per infinitesimal energy interval $\mathrm{d}\omega$ at the FS.

1.1.2 Landau's Fermi liquid theory

The non-interacting quantum mechanical system described above is of course rather special compared to a generic quantum system. The different momentum modes are completely decoupled and can be treated individually, they are free particles and holes. If we excite a momentum p_1 or p_2 in a Fermi gas, we find excited states with energies $E_0 + \delta E_1$ or $E_0 + \delta E_2$, however we can also excite them both at once and find an excitation of energy $E_0 + \delta E_1 + \delta E_2$. A generic interacting quantum system with the same degrees of freedom will also have many excited states, however one can generally not expect it to be possible to combine excitations this way. The eigenstates of the theory will be more complicated linear combinations of the eigenstates of the free theory.

In 1957 Landau proposed a phenomenological model of an interacting Fermi gas, the Fermi liquid. Landau's Fermi liquid theory postulates that the above picture is qualitatively correct and only receives minor corrections [2]. This was in the following years shown to be consistent within perturbation theory.

We here review the main features of Fermi liquid theory and in the next section we show how to motivate FLT using the modern approach of renormalization group flow. For a more complete description of FLT see e.g. [7].

The main idea of FLT is that as we turn on interactions, the spectrum of states found in the previous section moves continuously in energy but still provides approximate eigenstates of the Hamiltonian. Since translational symmetry is unbroken we can still label them by momentum and there is a one-to-one correspondence between the Fermi gas eigenstates and these approximate Fermi liquid eigenstates. Since they are not true eigenstates they all have a finite lifetime τ, but crucially this lifetime diverges near the FS as $\tau \sim (k - k_F)^{-2}$. This means that for low enough energies, these states are arbitrarily close to being true eigenstates of the Hamiltonian. Their energies shift as interactions are turned on and the property that excitations can be combined with summed total energy will be broken continuously, these particles are interacting. We thus still have a theory of particles, as opposed to a generic set of eigenstates. These excitations are not the original particles and holes however so we refer to them as *quasiparticles*.

When adding a quasiparticle at momentum $\mathbf{k}$ we increase the energy by an amount $\epsilon[n](\mathbf{k})$. Here $n(\mathbf{k}')$ describes the current state, it is a function

of momentum corresponding to the occupation of every quasiparticle state. This is necessary since now combining two excitations does not simply add their energies. In the free Fermi gas $\epsilon_\mathbf{k}$ is independent of $n(\mathbf{k}')$. We write $n_0(\mathbf{k}') = \theta(k_F - k)$ for the ground state occupation. Note that k_F is independent of interactions. Luttinger showed [8] that the total volume of the FS remains constant when adding interactions. For a spherically symmetric system this means k_F is fixed by the charge density. Once again expanding around the FS we have

$$\epsilon[n_0(\mathbf{k}')](\mathbf{k}) = v_F^*(k - k_F) + \mathcal{O}\left((k - k_F)^2\right) \qquad (1.10)$$

where v_F^* is now an effective Fermi velocity. From this it is common to also introduce the effective mass $m^* = k_F/v_F^*$. Away from the ground state we parametrize the effect of additional excitations by what is called the Fermi liquid interaction $f_{\mathbf{k},\mathbf{k}'}$

$$\epsilon[n](\mathbf{k}) = \epsilon[n_0](\mathbf{k}) + \sum_{\mathbf{k}'} f_{\mathbf{k},\mathbf{k}'} \left(n(\mathbf{k}') - n_0(\mathbf{k}')\right) \qquad (1.11)$$

$f_{\mathbf{k},\mathbf{k}'}$ can only depend on the angle θ between $\mathbf{k}$ and $\mathbf{k}'$ since we have an isotropic system, $f_{\mathbf{k},\mathbf{k}'} = f(\theta)$. In $d = 2$ we can write

$$f(\theta) = \frac{1}{N_0}\left(F_0 + 2\sum_{i=1}^\infty F_i \cos(\theta)\right) \qquad (1.12)$$

This parametrization is useful since the sum of (1.11) (or integral in the macroscopic limit) defines an inner product under which this basis is orthogonal. In higher dimensions this angular integral receives a measure and we use a different basis, the Legendre polynomials in $d = 3$. The normalization by the density of states makes these parameters dimensionless. The numbers F_i are called the Landau parameters and they completely characterize the interactions of the Fermi liquid state.

We will not do so here, but by calculating the change in total energy δE under an infinitesimal change in $n(\mathbf{k})$ at the FS and demanding that $0 < \delta E$ for all k one finds the stability condition $-2i - 1 < F_i$ (in the case of $d = 3$) [9]. An instability at $0 < i$ is called a Pomeranchuk instability. In this case the spherical FS is not the lowest energy state and it will spontaneously break rotational symmetry by deforming the FS. See Fig. 1.2.

This theory of interacting fermions was at the time just a phenomenological model able to describe experimental results, based on the intuition
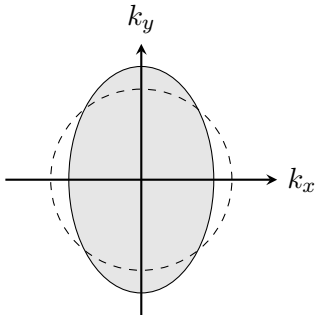
Figure 1.2. For strong enough interactions the rotationally symmetric FS (dashed) might not be the lowest energy configuration and the interacting fermions spontaneously deform the FS to a less symmetric configuration (solid).

of Landau. Despite its remarkable success in describing experiments on interacting fermions, a rigorous motivation was missing. Landau and others provided some microscopic motivation but understanding remained elusive for a long time. Progress was made in the early 90's by the use of renormalization group flow, initially by Feldman et al. [10]. This is the topic of the next section. In 2004 Feldman et al. published a series of ten papers proving the convergence of the perturbative expansion of a class of systems of interacting fermions in 2 dimensions [3]. They find that they are indeed described by FLT.

1.1.3 Renormalization group flow of interacting fermions

Low energy effective theory has been a powerful tool in characterizing the low energy physics of quantum field theories. By performing a scaling analysis one can separate out interactions and degrees of freedom that are relevant for low energy physics and those that are not and obtain a physical model with few parameters that only contains the essence of the physics of interest.

Exactly how this is done depends on the details of the theory. We will do this explicitly for the theories we are interested in but first we describe the general framework. One approach to this scaling analysis is to consider a theory with a UV cutoff Λ and separate degrees of freedom into those below a certain energy scale $\Lambda^- = \Lambda e^{-t} < \Lambda$ and those above Λ^-. One then integrates out the degrees of freedom between the scales Λ^- and Λ. This introduces effective interactions between the low energy

degrees of freedom. We now want to rewrite this effective theory into a similar form as to what we started with so that we can compare apples to apples and see what happens to the various terms as we approach low energies. To do this we rescale coordinates by a factor e^t ($\omega \to e^{-t}\omega$) to return the cut-off to $|\omega| < \Lambda$ and we rescale the fields by a factor that has to be determined case-by-case to get the same normalization of a chosen term of the action. We are then left with a similar-looking theory with some of the high energy degrees of freedom missing, however the low energy degrees of freedom behave the same since the effects of interactions with the high energy modes are absorbed in coupling constants. This can be done repeatedly for an infinitesimal t and the result is a flow of the coupling constants of the theory. This flow, called the renormalization group (RG) flow, represents a zooming in on the low-energy physics and provides a precise way of getting an effective action describing only the low energy physics. It is important to start with a theory containing all couplings that may be generated under the RG flow. Here symmetries play a crucial role in determining and limiting the possible couplings that can be generated. In addition, terms of high order in fields and derivatives of the coordinates are generally scaled to smaller values during the coordinate and field rescaling steps. This means that one can, even before performing the integration of high-energy modes, see that terms higher than a certain order will decay under the flow.

The RG flow is a flow in the space of physical theories. Starting with a microscopic description of the theory describing it at both high energies (UV) and low energies (IR) this flow results in a theory only describing the IR. The flow is governed by a differential equation of the form

$$\frac{\partial g_i}{\partial t} = \beta_i(\{g_j\}) \tag{1.13}$$

where the g_i are the couplings of the theory and β a function found from the above procedure of integrating out modes and rescaling the theory. If the β-functions have a 0 for a set of couplings g_i^* then there is no flow. If the eigenvalues of the Jacobian of β_i with respect to the couplings only has eigenvalues in the left half plane, then the flow will be attracted to this IR fixed point for a region of UV couplings g_i. The form of the β-functions only depends on the fields present in the theory so the couplings at the fixed point are not sensitive to details of the UV theory. This means that many vastly different physical theories share the same behavior at the very lowest of energy scales.

Couplings can be classified according to their behavior under the RG flow at a fixed point. Couplings that grow as $t \to \infty$ are called relevant couplings. Adding those to a theory will result in a different IR fixed point. Couplings that decrease as $t \to \infty$ are called irrelevant couplings and do not modify the fixed point. Couplings that do not flow are called marginal and in a theory with marginal couplings the fixed point will not be a point in the space of theories but be a set parametrized by the marginal couplings.

We have now roughly outlined how the renormalization group can be used to find low energy effective theories. This framework of low energy effective field theory was first used in high energy physics but was later brought to Fermi liquid theory, initially by Feldman et al., Polchinski and Shankar [10–12]. We will now review their findings that gives a justification for the FLT of the previous section. For a more in-depth discussion see [12].

The low energy excitations of a Fermi liquid reside on the Fermi surface which makes the analysis slightly more complicated than for a theory with low energy modes at zero momentum. Instead of introducing a spherical cut-off in energy-momentum space we will introduce a cut-off on both sides of the FS such that only modes of momenta $|k - k_F| < \Lambda$ are considered and the flow will proceed by decimating modes progressively closer to the FS. See Fig. 1.3.

Consider first the free Fermi gas theory. We write down the action corresponding to the Hamiltonian in Eq. (1.1)

$$S_0 = \int_{-\infty}^{\infty} \frac{\mathrm{d}\omega}{2\pi} \int_{-\Lambda}^{\Lambda} \frac{\mathrm{d}k}{2\pi} k_F^{d-1} \int_{S^{d-1}} \frac{\mathrm{d}^{d-1}\mathbf{\Omega}}{(2\pi)^{d-1}} \psi^{\dagger} \left(i\omega - vk \right) \psi. \qquad (1.14)$$

As in the previous section we have linearized around the FS where the low-energy modes live. Also the measure has been linearized around $k = k_F$. Subsequently we have shifted k so that the FS is at $k = 0$. The higher order in momentum terms are in the language of RG irrelevant couplings. The action is written in polar coordinates where $\mathbf{\Omega}$ is a unit vector in d-dimensional space.

Now we consider the rescaling of fields and coordinates before we do the integrating out of modes. The order of these infinitesimal transformations does not matter. We perform a redefinition of the coordinates and fields of this theory such that the above free theory is preserved:

$$(\omega, \ k, \ \psi) \to (\mathrm{e}^{-t}\omega, \ \mathrm{e}^{-t}k, \ \mathrm{e}^{3t/2}\psi) \qquad (1.15)$$
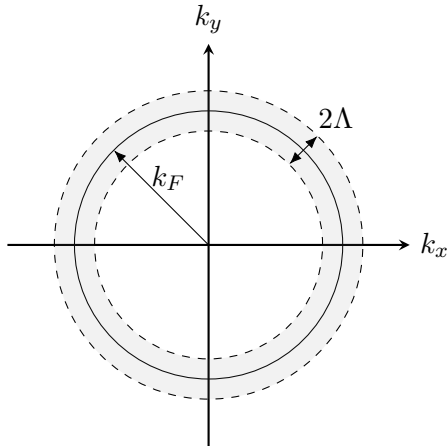
Figure 1.3. This figure shows a decimation scheme for the RG flow of a Fermi liquid. The solid circle is the FS. Only modes in the shaded are are kept in the low-energy effective theory. The shell is surrounded by two hard cut-offs at $k = k_F \pm \Lambda$, as indicated by the dashed circles.

Note that k here refers to the k in (1.14) and is thus scaled away from the FS. The physics of this theory is trivially identical to the one we started with. The cut-off is now effectively rescaled to $e^t \Lambda$. To get a theory of the same form as we started with the next step is to integrate out all momenta k between $\Lambda < |k| < e^t \Lambda$. The free theory is gaussian so performing this integral only results in a prefactor. The value of Λ is then decreased by a factor e^{-t}. Note that k_F is not scaled so the ratio Λ/k_F flows to 0. This means that k_F becomes a very large scale in the effective theory. We now move to the Fermi liquid by adding interactions.

We write down a general four-fermion interaction parametrized by the function $u(\mathbf{k}_4, \mathbf{k}_3, \mathbf{k}_2, \mathbf{k}_1)$ of momenta. This is the lowest order operator we can write so unless this is relevant we do not need to consider further operators. Every component of the function u should be regarded a coupling and has to be studied under the RG. RG without a FS typically has a finite number of couplings since a momentum dependence would be higher order in momentum and thus irrelevant. However in our case the scaling is towards the FS and the angular dependence cannot be deemed irrelevant.

$$S_0 = \frac{1}{4} \int_{123} \psi^\dagger(4)\psi^\dagger(3)\psi(2)\psi(1) u(\mathbf{k}_4, \mathbf{k}_3, \mathbf{k}_2, \mathbf{k}_1)\theta(\Lambda - |\mathbf{k}_4|) \qquad (1.16)$$

Here the integrals and measures are the same as in the integral of the free action above, $\mathbf{k}_i = k_i \mathbf{\Omega}_i$ and $\psi(1)$ is shorthand for $\psi(\omega_1, \mathbf{k}_1)$. From momentum conservation we have that $\mathbf{k}_1 + \mathbf{k}_2 = \mathbf{k}_3 + \mathbf{k}_4$ and we need only integrate over three momenta. The momenta are constrained within our cut-offs but the fourth momentum given in terms of the first three can still end up outside the cut-offs. This is the reason for the Heaviside θ-function above. The fourth momentum is given by

$$k_F + k_4 = |(k_F + k_1)\mathbf{\Omega}_1 + (k_F + k_2)\mathbf{\Omega}_2 - (k_F + k_3)\mathbf{\Omega}_3| \qquad (1.17)$$

Since Λ/k_F flows to zero and $|k_i| < \Lambda$, in the effective theory we have

$$k_4 = k_F \left(|\mathbf{\Omega}_1 + \mathbf{\Omega}_2 - \mathbf{\Omega}_3| - 1\right) + \mathcal{O}(\Lambda) \qquad (1.18)$$

For k_4 to be within the cut-offs we see that the unit vectors $\mathbf{\Omega}_i$ are greatly constrained. Performing the above tree-level scaling one finds (see [12]) that the coupling u is irrelevant for all momentum configurations apart from three exceptional cases corresponding to the solutions to $|\mathbf{\Omega}_1 + \mathbf{\Omega}_2 - \mathbf{\Omega}_3| = 1$. The tree-level marginal parts of u can for $d = 2$ be written as

$$u(\mathbf{\Omega}_3 = \mathbf{\Omega}_1, \mathbf{\Omega}_4 = \mathbf{\Omega}_2) = F(\theta_{12})$$
$$u(\mathbf{\Omega}_4 = \mathbf{\Omega}_1, \mathbf{\Omega}_3 = \mathbf{\Omega}_2) = -F(\theta_{12})$$
$$u(\mathbf{\Omega}_4 = -\mathbf{\Omega}_3, \mathbf{\Omega}_2 = -\mathbf{\Omega}_1) = V(\theta_{13}) \qquad (1.19)$$

where θ_{ij} is the angle between $\mathbf{\Omega}_i$ and $\mathbf{\Omega}_j$. These three momentum configurations that contribute to the low energy scattering processes can be understood geometrically. The first two processes have identical momentum before and after the scattering. They are therefore referred to as *forward-scattering* processes. The third process involves fermions at two opposite points of the FS scattering to two new opposite points of the FS.

In three dimensions there will be more solutions to Eq. 1.18. The first two processes do not require each individual momenta to be conserved anymore, however the angle between the two fermions momenta is conserved before and after the scattering process. The F and V will additionally depend on the angle between the planes of the two momenta before and after the scattering.

To find out the behavior of these tree-level marginal couplings one needs to performing the integration of the modes that are scaled out. Doing this perturbatively in the coupling u amounts to calculating several one-loop diagrams of this field theory. We just quote the result from [12]

13
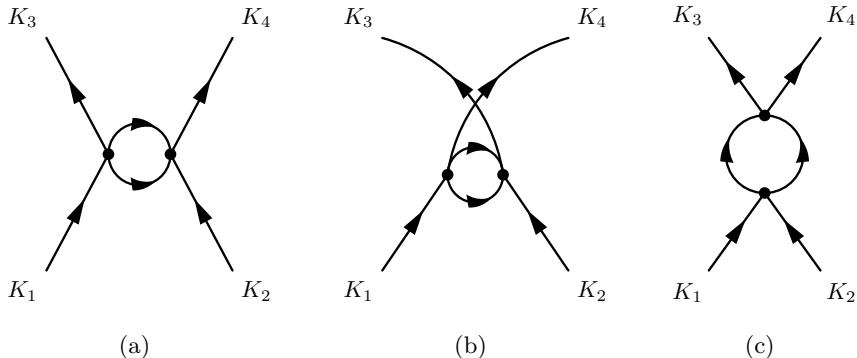
Figure 1.4. (a,b) These two diagrams do not contribute to the flow of the Fermi liquid coupling function due to kinematic constraints [12]. (c) The BCS-type diagram is the only one that contributes to the flow of the Fermi liquid coupling function at one loop.

here. All diagrams contributing to the flow of F turn out to vanish and F is still marginal at one loop. We should then go to higher loops to see in which direction F flows. Feldman et. al have found that [13] the limit $\Lambda/k_F \to 0$ suppresses the effect of higher loops such the flow of F, at the end of the flow when Λ/k_F is small is exact. They describe this in terms of a vector large N limit, similar to what we describe in Section 1.4.2. F is thus marginal and remains as a parameter at any fixed point.

We proceed by studying the flow of V. One diagram, see Fig. 1.4(c), contributes to the flow of V. It is given by

$$
\begin{aligned}
\mathrm{d}u(\mathbf{k}_4, \mathbf{k}_3, \mathbf{k}_2, \mathbf{k}_1) = -\frac{1}{2} \int_{-\infty}^{\infty} \frac{\mathrm{d}\omega}{2\pi} \int_{\mathrm{d}\Lambda} \frac{\mathrm{d}k}{2\pi} \int_{0}^{2\pi} \frac{k\mathrm{d}\theta}{2\pi} \times \\
\times u(\mathbf{k}_1 + \mathbf{k}_2 - \mathbf{k}, \mathbf{k}, \mathbf{k}_2, \mathbf{k}_1) G_0(K) \times \\
\times G_0(K_1 + K_2 - K) u(\mathbf{k}_4, \mathbf{k}_3, \mathbf{k}_1 + \mathbf{k}_2 - \mathbf{k}, \mathbf{k})
\end{aligned} \tag{1.20}
$$

The upper-case K denotes $(\omega, \mathbf{k})$. The spatial part of this will only be over the infinitesimal shells that we integrate out, see Fig. 1.3. Let us now set the momenta to a configuration that generates the coupling V, we set

$\mathbf{k}_2 = -\mathbf{k}_1$ and $\mathbf{k}_4 = -\mathbf{k}_3$ and external frequencies to 0.

$$dV(\theta_{13}) = -d\Lambda \sum_{k=k_F \pm \Lambda} \frac{1}{2} \int_{-\infty}^{\infty} \frac{d\omega}{(2\pi)^2} \int_0^{2\pi} \frac{k d\theta}{2\pi} u(-\mathbf{k}, \mathbf{k}, -\mathbf{k}_1, \mathbf{k}_1) \times$$
$$\times G_0(K) G_0(-K) u(-\mathbf{k}_3, \mathbf{k}_3, -\mathbf{k}, \mathbf{k}) \tag{1.21}$$

We find that both momentum configurations for the coupling function corresponds to the case parametrized by V. The frequency integral can be done using the residue theorem, we always have one pole in either half plane. We can rewrite this in terms of the flow parameter $d\Lambda = \Lambda dt$ to find

$$\frac{dV(\theta_{13})}{dt} = -\Lambda \frac{1}{8\pi} \int_0^{2\pi} \frac{d\theta}{2\pi} V(\theta) V(\theta - \theta_{13}) \times$$
$$\times \left(\frac{k_F - \Lambda}{|\epsilon(k_F - \Lambda)|} + \frac{k_F + \Lambda}{|\epsilon(k_F + \Lambda)|} \right) \tag{1.22}$$
$$= -\frac{k_F}{4\pi v_F} \int_0^{2\pi} \frac{d\theta}{2\pi} V(\theta) V(\theta_{13} - \theta) \tag{1.23}$$

To solve the resulting integro-differential equation we decompose $V(\theta)$ into Fourier modes

$$V(\theta) = \sum_{n=0}^{\infty} V_n e^{-in\theta} \tag{1.24}$$

to obtain

$$\frac{dV_n}{dt} = -\frac{k_F}{4\pi v_F} V_n^2. \tag{1.25}$$

the solution to this is given by

$$V_n(t) = \frac{V_n(0)}{1 + t \frac{k_F}{4\pi v_F} V_n(0)} \tag{1.26}$$

We thus find that all positive V_n flow to zero under the RG whereas any negative V_n diverges at a finite t, signaling an instability. This is the Bardeen-Cooper-Schrieffer superconducting instability. There are thus many possible instabilities and these are the formations of condensates with different symmetry properties. Performing this calculation in $d = 3$ we find that V depends on a unit vector in three dimensions and we instead have to decompose it in spherical harmonics to separate the flow equations. Instabilities for the first three harmonics correspond to s, p and d wave superconductivity.

1.1.4 Fermi liquid fixed point

To conclude this section on Fermi liquids we summarize by giving some properties of the Fermi liquid fixed point found in the previous section and make connection to the phenomenological theory put forward by Landau.

The two-dimensional isotropic Fermi-liquids we studied above generally have the instability where some component of V diverges under the RG flow, even for purely repulsive interactions [14–16]. This means that the true ground-state of interacting fermions is a superconductor and not a Fermi liquid. The superconducting instability sets in at late stages of the RG flow, corresponding to low temperatures. In many cases this instability sets in at exponentially low temperatures meaning it is typically not relevant for experimental observations. We would like to study how these interacting fermions behave above the critical temperature T_c. We consider interacting fermions with suppressed, but non-zero, T_c. From the above analysis we found that the low-energy interaction is governed by the functions F and V. Most components of V flow to 0 but a few will, at now a very late stage, grow exponentially. We can then ask how the theory behaves in this long flow before finally one component of V becomes large. In this region the system is described by Fermi liquid theory.

In FLT we thus have $V \approx 0$ and a non-zero F that does not flow. The fixed point is therefore parametrized by the infinite set of Fourier components making up the function $F(\theta)$, the Landau parameters F_n. The function F is thus the same as f in the phenomenological model of Landau in the beginning of this section.

The Landau parameters together with the, fixed under RG, Fermi momentum k_F and the fermion mass completely characterize the fixed point. This fixed point is interacting, however it only has forward scattering processes. To see how this interacting theory differs from the Fermi gas we consider the fermion two-point function in terms of the bare fermionic field in a field theory description of the above FL. We write this two-point function as

$$G(\omega, k) = \frac{1}{i\omega - v_F(k - k_F) - \Sigma(\omega, k)} \tag{1.27}$$

where $\Sigma = 0$ denotes the free theory. This equation can just be seen as a definition of the fermion self-energy Σ, a quantity capturing all effects of interactions on the two-point function. The decay rate Γ of quasiparticles

is given by the imaginary part of the self-energy

$$\Gamma(\omega, k) = \text{Im}\,\Sigma(\omega, k). \tag{1.28}$$

The quasiparticle lifetime is given by $\tau = 1/\Gamma$. For well-defined quasiparticles at the FS we need τ to diverge as $\omega, k \to 0, k_F$ and $\text{Im}\,\Sigma(\omega, k)$ approach 0. The size of the FS is not affected by interactions by Luttinger's theorem. This means that $\text{Re}\,\Sigma(\omega, k)$ additionally has to approach 0 at the FS. We can thus write the two-point function near the FS

$$G(\omega, k) = \frac{Z}{i\omega - v_F^*(k - k_F) + \dots} \tag{1.29}$$

where the ω, k-linear terms of $\text{Re}\,\Sigma(\omega, k)$ have been absorbed in the quasiparticle residue Z and the effective Fermi velocity v_F^* respectively

$$Z^{-1} = (1 + i\partial_\omega \Sigma(\omega, k))_{\omega=0, k=k_F} \tag{1.30}$$

$$v_F^* = Z\left(v_F + \partial_k \Sigma(\omega, k)\right)_{\omega=0, k=k_F}. \tag{1.31}$$

The ellipsis in (1.29) denote terms higher order in ω and $k - k_F$.

To see some physical implications of this form of the two-point function we study the spectral function. The spectral function shows the density of excitations in energy-momentum space, see e.g. [17] for a more in-depth description. This is a real-time quantity and can be expressed in terms of the retarded two-point function:

$$A(\omega_R, k) = -2\,\text{Im}(G_R(\omega_R, k)). \tag{1.32}$$

The retarded two-point function G_R is related to the Euclidean two-point function G we have considered so far, by analytical continuation in frequency. $G_R(\omega_R, k)$ is analytic in the upper half plane of complex ω_R. When evaluated on the upper imaginary axis it equals the Euclidean two-point function, $G_R(i\omega, k) = G(\omega, k), 0 < \omega$. We can thus also find G_R by analytically continuing G. This is simply done by replacing $\omega \to -i\omega_R + \epsilon$ where ϵ is an infinitesimal number indicating that we are in the right half plane of ω in the case where there is a discontinuity on the imaginary ω-axis. In the free theory where $\Sigma = 0$, G_R has a simple pole at $\omega_R = v_F(k - k_F) + \dots$ of residue 1. When taking $\epsilon \to 0$ this pole becomes a δ-function of the spectral function

$$A(\omega_R, k) = 2\pi\delta(\omega_R - v(k - k_F) + \dots) \tag{1.33}$$
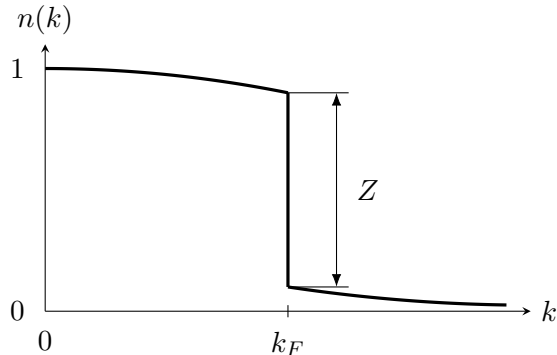
Figure 1.5. Sketch of a Fermi liquid zero temperature momentum distribution function. There is always a discontinuity at the FS for well-defined quasiparticles. The size of the discontinuity is given by the quasiparticle residue Z.

With interactions this δ-function is smeared out but close to the FS it becomes sharp but moves in accordance with the effective Fermi velocity and receives a weight Z. The lost spectral weight $1 - Z$ is distributed into the continuous part of $A(\omega_R, k)$. From the spectral function we find the momentum distribution function

$$n(k) = \int_{-\infty}^{\infty} \frac{\mathrm{d}\omega_R}{2\pi} n_F(\omega_R) A(\omega_R, k) \tag{1.34}$$

where $n_F(\omega_R)$ is the Fermi-Dirac distribution. At zero temperature the Fermi-Dirac distribution is given by a step function $n_F(\omega_R) = \theta(\omega_R)$ and the ω_R integrals are only over the negative real line. The δ-function is only included in this integral when $k < k_F$ and there is therefore a discontinuity of size Z in the zero temperature momentum distribution function at $k = k_F$, see Fig. 1.5.

1.2 Non-Fermi liquids

In this section we look at the cuprate superconductor phenomenology as an example and note the need for models of fermions at finite density in two dimensions which are not Fermi liquids. We then review some scenarios where such models may show up in physical systems. We conclude by settling on a specific action for such a model and this is the subject of study for the subsequent chapters.

1.2.1   Breakdown of Fermi liquid theory

From the scaling analysis of Section 1.1.3 we saw that Fermi liquid results are robust against any fermion self-interactions. There are instabilities that can result in BCS superconductivity or deformations of the FS but apart from these we have robust expectations of the behavior of a FS, even with interactions.

As we mentioned in the first part of the introduction there are several experimental systems of finite density fermions that do not adhere to the expectations from FLT. One of these are the high temperature cuprate superconductors. The first of these superconductors was found in 1986 [18] and the (at the time) very high critical temperature (T_c) of 35 K was a surprise since it does not fit within the conventional theory of BCS superconductivity. These high-T_c cuprates are layered materials with weakly coupled copper-oxide layers. Between these layers there are many different elements to provide structure and dope electrons or holes onto the copper-oxide layers. The specific structure of these supporting layers are different for the different cuprates, in the case of [18] the chemical formula is given by $Ba_xLa_{5-x}Cu_5O_{5(3-y)}$ where different values of x, y were used. Despite thirty years of intense research there is presently still no understanding of the mechanism generating superconductivity in these materials and with the prospect of creating superconducting materials with higher critical temperatures there is obviously a large interest in understanding these. A less direct but even more striking characteristic is that above T_c, these materials behave like metals in some ways but conventional FLT does not apply at all. They are therefore referred to as non-Fermi liquids or strange metals. E.g. the low temperature resistivity of a clean Fermi liquid generically has a quadratic resistivity $\rho \sim T^2$ however for the cuprates (and many other non-Fermi liquid) a linear resistivity, $\rho \sim T$, is found [19]. The spectral function of strange metals can be measured using angle-resolved photoemission spectroscopy (ARPES). A sharp FS is found, however the excitations are not long lived near it meaning that the quasiparticle picture breaks down.

BCS theory cannot account for the high T_c-superconductivity and FLT can not accommodate the linear in T resistivity nor the short-lived excitations near the FS. The robustness of FLT means that we need to quite radically change the premise of this theory for it to not apply. In the language of RG-flows: we need to add a relevant interaction driving the flow to a new fixed point. We saw in the previous section that there is

not such an interaction when just considering the fermionic fields $\psi, \psi^\dagger$. We have to add another field interacting with these fields. We call this for now unspecified field ϕ. For the interactions between ϕ and the gapless excitations at the Fermi surface to have any effect, the field ϕ also has to be gapless. If it is not then it can simply be integrated out yielding an effective theory for the physics below the gap. The effect of the interactions between the fermions and ϕ will then only show up as a correction to fermion interactions, which we have concluded can not result in non-Fermi liquid behavior.

Whether coupling to a massless field is responsible for the non-Fermi liquid behavior seen in the cuprates is not definite. It is, however, clear that such a coupling appears in physical systems and understanding such models is desirable regardless of whether they are responsible for cuprate non-Fermi liquidity or not. This is the premise we shall pursue in this thesis.

It does raise the obvious question how such a massless field might show up in a fermionic system? There are a few different scenarios where this might happen [20] and we list some of them here.

Goldstone boson

By Goldstone's theorem there will always be a gapless mode when a continuous symmetry is spontaneously broken. A condensed matter example of this is an atomic lattice spontaneously breaking the continuous translational symmetry. The Goldstone bosons are in this case the phonons. Since the gaplessness of these modes is protected by the theorem they may seem like good candidates for ϕ. However since the action of the theory remembers the symmetry that is broken, these bosons still observe a shift symmetry in their coupling to other fields. This means that if the field ϕ were a Goldstone boson then its coupling to the fermions would need to contain a derivative, otherwise it wouldn't be invariant under a constant shift $\phi \to \phi + \Delta_\phi$. This derivative coupling is then not relevant under the RG flow and a Goldstone coupling falls back to FLT.

Emergent gauge field

Gauge fields are massless by symmetry so they provide a natural candidate for ϕ. The electromagnetic gauge field however can not lead to NFL behavior. The electric field is screened in FLT and the coupling

to the magnetic field suppressed by $1/c^2$. On the other hand, there are mechanisms by which emergent gauge fields can arise from the underlying electrons.

One proposed scenario is at a Mott transition, the critical point between a Fermi liquid and an insulating state with interactions strong enough to prevent formation of a Fermi surface. The proposed mechanism [21] considers spin-1/2 electrons on a lattice with strong repulsive interactions such that each lattice site only hosts one particle. The theory can be cast in terms of spin up and down particles, spinons $s_{i,\alpha}$, and holes, holons h_i. Each site hosts exactly one of these which leads to a constraint on each site. This new redundant description of electrons on a lattice in terms of spinons and holons leads to a local symmetry. The original electrons ψ_i create a spinon and annihilate a holon and are therefore given by $\psi_{i,\alpha} = s_{i,\alpha} h_i$. Rotation of the spinons and holons by opposite phases leave $\psi_{i,\alpha}$ invariant. This symmetry can be promoted to a dynamical gauge symmetry interacting with the spinons, see e.g. [22] for details.

Another case where non-Fermi liquid physics might show up due to interaction with an emergent gauge field is when electrons in two dimensions are subject to an external magnetic field. Electrons in a magnetic fields travel in circular orbits. When treated quantum mechanically these quantize into Landau levels. This gives rise to interesting phenomena for solids in magnetic fields such as the quantum Hall effect. Depending on the field strength and the number of available electrons the Landau levels will have different filling fractions ν. Halperin, Lee and Read showed [23] that for $\nu = 1/2$ this system can be understood in terms of a dual description by a theory of electrons interacting with a Chern-Simons gauge field. This dynamical gauge-field can also act as the field ϕ.

These scenarios will not be further discussed in this thesis. However, we note that once one fixes the gauge, the analysis of fermions coupled to a gauge field very much parallels that of fermions coupled to a scalar. This is the scenario we describe below. Therefore many of the results we find can with only minor modifications be applied to these theories as well. In [24] the authors study both the case of coupling fermions to an emergent gauge field and to the order parameter fluctuations at a quantum critical point, described in the next section, simultaneously. They indicate the few points where these two different set-ups differ.
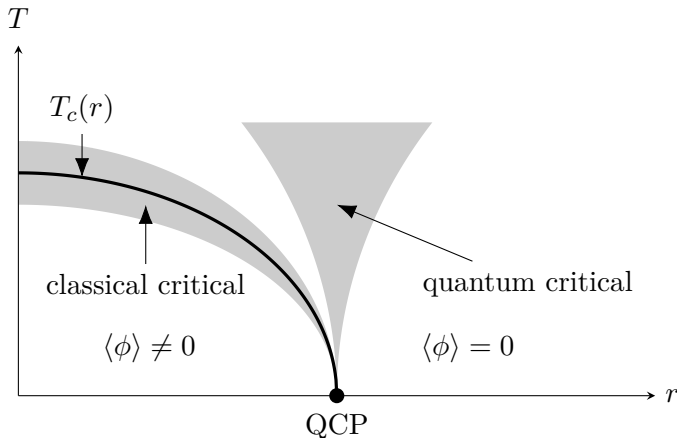
Figure 1.6. Phase diagram of a theory with a continuous phase transition terminating at a quantum critical point. The region marked with $\langle \phi \rangle \neq 0$ is an ordered phase where the order-parameter ϕ has an expectation value. It is surrounded by a second order phase transition at a critical temperature $T_c(r)$ that goes to 0 as some parameter r approaches a critical value r_c. The point $r = r_c, T = 0$ is the quantum critical point. Here the ground state changes from a symmetry broken state to a symmetric state $\langle \phi \rangle = 0$. The region around the temperature driven transition, where $(T - T_c(r))/T$ is small, has long-range classical fluctuations in the field ϕ. The region right above the QCP has critical fluctuations in ϕ that has to be treated quantum mechanically.

Quantum critical point

Now we come to the third scenario which is what we focus on in this thesis. As physical systems can have phase transitions when temperature is varied, it is also possible to have a transition at zero temperature as some other parameter r is varied (e.g. pressure, doping or a magnetic field). This is called a quantum phase transition and the point where it occurs the quantum critical point (QCP). We review these briefly and refer to [25] for a more in-depth discussion. Similarly to how temperature driven transitions are classified as discontinuous or continuous, so are the quantum phase transitions. Fluctuations in the order parameter field become strong as we approach a continuous quantum phase transition from the disordered phase and at the QCP these fluctuations become massless. Continuing into the ordered phase these fluctuations get a negative "mass"-term and they acquire an expectation value. See Fig. 1.6.

The order-parameter fluctuations of thermal phase transitions can be treated classically as the critical temperature is approached. The relevant energy scale goes to 0 as the critical point is approached while the temperature remains constant in magnitude. The relevant energy scale also goes to 0 as the QCP is approached but here temperature is 0 and the order parameter fluctuations have to be treated quantum mechanically. A system of fermions undergoing a quantum phase transition will thus have massless quantum fluctuations at the critical point. This provides the massless field ϕ. ϕ is generally a bosonic collective excitation of the underlying degrees of freedom undergoing the phase transition. We will go into details of what the exact phase transition might be in the next section.

This mechanism for massless field is not as natural as a gauge field or the Goldstone bosons in the sense that it requires fine tuning. Masslessness is not protected by a symmetry. The field ϕ has a mass-term that becomes zero right at the QCP: $m^2 \propto r - r_c$. If we however consider a temperature $T \gg |r - r_c|$, then this mass is not very important and we can treat the field as effectively massless. This means that there is a region of finite r-width in the phase diagram above the QCP where physics is still in influenced by the vicinity of the QCP. The higher the temperature, the less important a small departure from $r = r_c$ is, so this region is roughly cone-shaped. The critical theory will not be a good description for high enough temperatures where other energy-scales that are not tuned to be small at the QCP become important. Therefore the cone where the theory is governed by quantum critical behavior terminates smoothly at some upper temperature.

1.2.2 Quantum critical metals

In this section we describe several orderings that can give rise to quantum phase transitions in two-dimensional fermionic systems and thus a route to non-Fermi liquid behavior, the quantum critical metals (QCM). We go into some detail for each example by describing the phase transition and the properties of its order parameter fluctuations and its coupling to fermions.

Second order phase transitions can be split into two classes, those with order parameter fluctuations peaked at 0 momentum and those at a finite momentum $\mathbf{Q}$. The latter case corresponds to systems where the expectation value of ϕ has spatial modulations breaking the translational

symmetry of the disordered phase. Before receiving corrections from other gapless excitations, the ϕ fluctuations are generally described by the following two-point function at low energies

$$D_{\mathbf{Q}}(\omega, \mathbf{q}) = \frac{1}{r - r_c + \omega^2 + c^2(\mathbf{q} - \mathbf{Q})^2} \tag{1.35}$$

where c is the speed of the order parameter fluctuations (not the speed of light), from here on we use coordinates such that $c = 1$. In the above expression we have let r be defined such that the mass term is given directly by it. At the critical point $r = r_c$ and ϕ is massless. The form of this is deduced by considering rotational symmetry and in the spirit of low-energy effective action only writing the lowest order terms. We perform an RG treatment of such critical theories in Sec. 1.3. The field ϕ couples to the fermions with a coupling of the form

$$S_{\text{int}} = \int \frac{\mathrm{d}^{d+1}k\mathrm{d}^{d+1}q}{(2\pi)^{2(d+1)}} \lambda(\mathbf{k}, \text{II}) \psi^\dagger(\mathbf{k} + \mathbf{q}) \psi(\mathbf{k}) \phi(\mathbf{q}) \tag{1.36}$$

We describe both the finite and zero $\mathbf{Q}$ cases in this section but the $\mathbf{Q} = 0$ case is the focus of the rest of the thesis. Let us start with the finite $\mathbf{Q}$ case.

By rotational symmetry we typically have several different $\mathbf{Q}$ vectors at the QCP; with full rotational symmetry there is a continuum of them. All low-energy fermions live close to the FS and low energy fluctuations of ϕ live close to $\mathbf{Q}$. The translational symmetry of the lattice means that momentum at each vertex is conserved, up to multiples of the reciprocal lattice basis vectors in the case of a lattice. The vertex in Eq. 1.36 consists of two fermions and one boson. We thus have a constraint that both $\mathbf{k}, \mathbf{k} + \mathbf{q}$ are on the FS and that $\mathbf{q} \approx \mathbf{Q}$. There are only a few spots on the FS that satisfy this constraint. This gives rise to a finite number of so called "hot-spots" which are the only points where the interactions to the field ϕ are important for fermions' low-energy physics. See Fig. 1.7. If we have a rotationally invariant system then all fluctuations with $\mathbf{Q}$ of a certain magnitude where the instability sets in will be important. In the case without a lattice, momentum is completely conserved so if $2k_F < |\mathbf{Q}|$ then the ϕ interaction is irrelevant. For $|\mathbf{Q}| < 2k_F$ all points of the FS will be influenced by ϕ and the whole FS will be "hot". This is however not very relevant to experimental systems and generally only a finite set of $\mathbf{Q}$ are important.
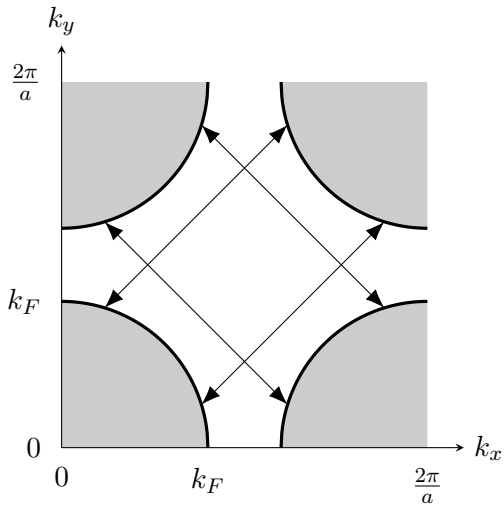
Figure 1.7. Sketch of spherical FS coupled to order parameter fluctuations at momenta $\mathbf{Q} = (\pm\pi, \pm\pi)/a$ where a is the lattice constant of a square lattice. The gray quarter circles are the occupied states of a FS (this figure is not to be confused with the similar cuprate FS where the occupied states are in the white area and origin of momentum space in the center). There are four copies of it visible due to identification by the reciprocal lattice vectors. The arrows indicate the $\mathbf{Q}$-vectors. We see that only four possible pairings of low energy fermionic excitations are related by these vectors. This gives rise to "hot-spots" at the ends of the arrows where the interaction is important at low energies.
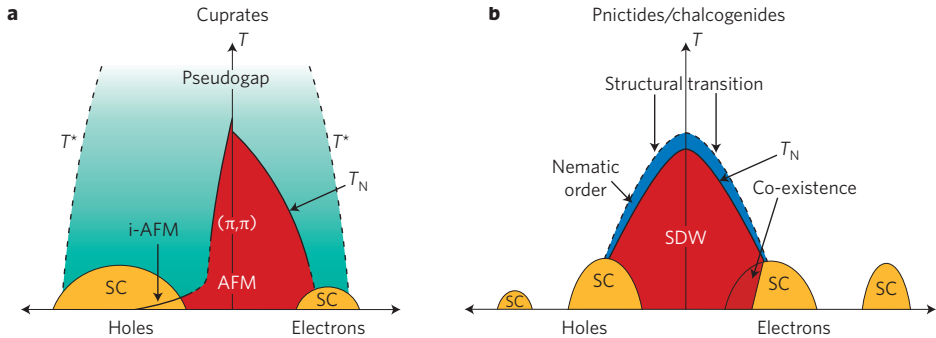
Figure 1.8. Schematic phase diagrams of cuprate superconductors (a) and iron-pnictide superconductors (b). These schematic is based on many different experiments on compounds with different compositions and shouldn't be taken as literal phase diagrams, more like maps of where some of the different phases of cuprates and iron-pnictides have been found. Image taken from [27].

There are three main ordered phases at finite **Q** that can give rise to non-Fermi liquid behavior: antiferromagnetic order (AFM), spin density wave order (SDW) and charge density wave order (CDW). AFM order is the alternating ordering of interacting spins that are fixed on a lattice. Such interacting spin degrees of freedom are described by the Heisenberg model. Since the spins are attached to lattice sites, the order parameter will always have a spatial periodicity that is a multiple of the lattice constants. SDW order is similar however here the spins are not fixed to a lattice but are mobile and the order parameter can have a periodicity that is a rational fraction of the lattice constant: commensurate order, or an irrational fraction: incommensurate order. Interactions with spin fluctuations is a candidate for the mechanism of high T_c superconductivity and non-Fermi liquid behavior in the cuprates [26] and also the iron-pnictides, another class of high-T_c materials [27]. Figure 1.8 shows schematic phase diagrams of both the copper and iron based high-T_c superconductors. The main superconducting domes cover the QCPs associated with AFM/SDW transitions in both of these materials.

CDW order is the onset of symmetry-breaking periodic fluctuations in the charge density, that once again can be commensurate or incommensurate with the periodicity of the underlying lattice. The charge density affects the lattice as well so it can be hard to separate whether this instability is a structural instability or driven by the itinerant electrons.

Evidence of CDW order has been found in x-ray scattering experiments

in the cuprate superconductor $(\mathrm{Y}, \mathrm{Nd})\mathrm{Ba}_2\mathrm{Cu}_3\mathrm{O}_{6+\mathrm{x}}$ [28]. They report a period of $\approx 3.2a$ where a is the lattice constant.

Let us now turn to the case of $\mathbf{Q} = 0$. In this case the field ϕ couples low energy excitations at each part of the FS to excitations with similar momenta. The whole FS is thus interacting and is sometimes referred to as a "hot FS". Depending in the mechanism the coupling might be zero for some specific momenta and we instead have a few "cold spots".

Orderings with $\mathbf{Q} = 0$ relevant for non-Fermi liquid behavior include, ferromagnetic ordering (FM), electron-nematic ordering and loop-current order.

FM ordering is the alignment of spins, resulting in a net magnetic field. As opposed to the AFM case this happens at $Q = 0$ and it does not break the translational symmetry of the disordered phase. The FM-paramagnetic ordering transition is typically first-order in disorder-free systems [29].

We will focus on the electron-nematic phase transitions. A nematic phase spontaneously breaks the rotational symmetry of a system. Nematic phases traditionally show up in liquids, the so-called liquid crystals. Electron nematics are electron liquids where interactions drive a transition to a state breaking rotational symmetry, but not translational symmetry. The atomic lattice necessarily also breaks the symmetry so it is not always entirely clear whether the symmetry breaking is driven by the interacting electron liquid or if it is a structural instability. A crystal with C_4 rotational symmetry can for example spontaneously break the symmetry to C_2. The ground state in this case is two-fold and it is referred to as an Ising-nematic transition. Similarly the academic case of C_∞ rotational symmetry broken down C_2 is called an XY-nematic transition. There are many possible nematic orders and transitions in 2 dimensions, a thorough classification of these is provided in [30].

We saw one mechanism for a electron-nematic transition in Sec. 1.1.2, the Pomeranchuk transition. For negative Landau parameters with large enough magnitude the spherical FS is not the lowest energy configuration and the ground state will be a deformed FS. Depending on the values of Landau parameters the deformed FS can have different subgroups of C_∞ (Or C_4 in the case of a square lattice) as its symmetry. Jakubczyk et al. showed [31] that although first order when treated in mean-field theory these transitions are continuous when accounting for fluctuations and they can thus provide the field ϕ.
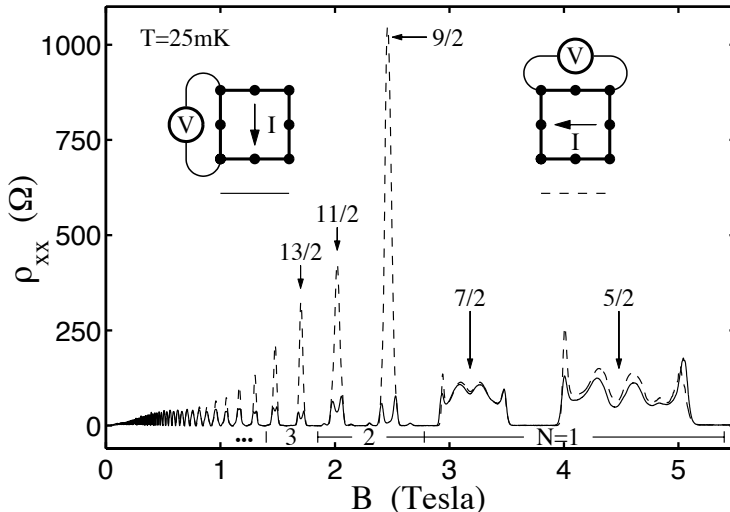
Figure 1.9. In-plane resistivity measurement of GaAs/AlGaAs heterostructures under a varying perpendicular magnetic field. The different peaks are due to the fractional quantum hall effect. The interesting point is that as the supposedly C_4 rotationally invariant system is rotated by 90° and the measurement is repeated a different result is found if at low temperatures, cf. solid and dashed lines. The plot is taken from [32].

Another mechanism for electron-nematic phases is the partial melting of a striped phase such as the $\mathbf{Q} \neq 0$ phases we covered earlier. The partial melting restores translational symmetry of the underlying lattice by proliferation of defects however rotational symmetry can remain broken.

GaAs/AlGaAs heterostructures are a system where an electron-nematic has been found. These layered systems hold two-dimensional electron liquids. Applying a transverse magnetic field shows a great anisotropy in the fractional quantum hall effect, see experiment by [32] in Fig. 1.9. The low-energy electrons spontaneously break the lattice symmetry at low temperatures. The mechanism for this is not known. Existence of nematic phases have been suggested both in the cuprate and iron-pnictide superconductors [33].

Loop current order is the onset of current loops within the lattice unit cells. This ordering, first suggested by Varma [34], breaks time-reversal symmetry and rotational symmetry however does not break translational symmetry and does not result in a net magnetic field due to counter-
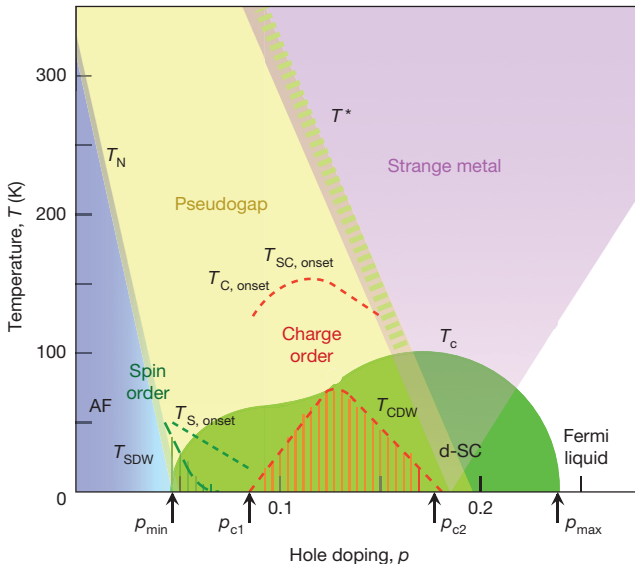
Figure 1.10. Schematic phase diagram of cuprate superconductors. The green area shows the superconducting phase. Both the CDW QCP and a tentative pseudogap QCP are located below optimal doping and the strange metal regime. Image taken from [39].

rotating current loops. Experimental evidence for such a phase has been observed [35–38], though a mechanism for its onset is not known.

Assuming that the NFL behavior observed in high-T_c cuprates is driven by electrons interacting with a QCP, there are thus several different proposals for the QCP. [39] provides an overview of these. The cuprate phase diagram they present is shown in Fig. 1.10.

1.2.3 A quantum critical metal toy model

We would now like to have a concrete model to study that contains the essential physics of the above quantum critical systems.

As we will see in Section 1.3, studying fermions interacting with massless fluctuations is notoriously difficult and demands new tools. Therefore our immediate goal is not to find an accurate description of the physical phenomena of the experimental systems of the preceding section, but to develop tools useful for doing so. Developing these tools is the topic of the following chapters of this thesis. We can then get away with a sim-

plified model, that we will see still requires a non-perturbative treatment. In this spirit we look for the simplest possible model containing fermions at a finite density interacting with a massless boson—the putative order parameter at the critical point.

We consider two-dimensional systems since that is what is relevant for most systems mentioned above and as we will note later the three-dimensional case is rather well understood. We get rid of the periodic lattice of positive charge from atomic nuclei and instead consider a homogenous chemical potential μ. We consider spinless fermions. We limit ourselves to studies of the case with $\mathbf{Q} = 0$, and add a boson kinetic term corresponding to Eq. 1.35 at the critical point $r = r_c$. We could consider a ϕ^4 interaction term, however we drop this for simplicity, keeping in mind that it might be important depending on what IR scaling we find. The coupling between the fermion and the boson is taken to be momentum independent, giving a completely rotationally symmetric model:

$$ S = \int \mathrm{d}x \mathrm{d}y \mathrm{d}\tau \left[\psi^\dagger \left(\partial_\tau - \frac{\nabla^2}{2m} - \mu \right) \psi + \frac{1}{2} \left(\partial_\tau \phi \right)^2 + \frac{1}{2} \left(\nabla \phi \right)^2 + \lambda \phi \psi^\dagger \psi \right] $$
$$ (1.37) $$

This toy model, dubbed a quantum critical metal, will be the focus of this thesis.

1.3 Perturbation theory and RG flow of a quantum critical metal

In this section we study the quantum critical metal (1.37) by an expansion in the coupling constant λ. We first calculate the fermion and boson one-loop self energies and discuss their physics. We then apply the framework of RG flows to the toy model and using the one-loop calculations and results from the literature [40–44] we see what can be said about the IR of this toy model both in two and three dimensions. We then conclude by considering some general features of the perturbation theory of (1.37), some of which are used in the rest of this thesis.

1.3.1 Free propagators and conventions

We denote collections of energy and momentum by k, and when referring to the spatial part we use a boldface $\mathbf{k}$. We denote Euclidean frequency
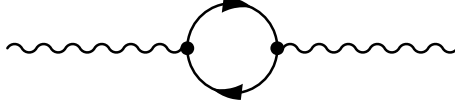
Figure 1.11. One-loop correction to boson two-point function.

by ω. The free propagators for the fermion and boson are respectively

$$G_0(\omega, \mathbf{k}) = \frac{1}{i\omega - \mathbf{k}^2/2m + \mu}, \tag{1.38}$$

$$D_0(\omega, \mathbf{k}) = \frac{1}{\omega^2 + \mathbf{k}^2}. \tag{1.39}$$

The vertex is simply given by the coupling constant λ. We define the fermion and boson self-energies through

$$G(\omega, \mathbf{k}) = \frac{1}{i\omega - \mathbf{k}^2/2m + \mu - \Sigma(\omega, \mathbf{k})} \tag{1.40}$$

$$D(\omega, \mathbf{k}) = \frac{1}{\omega^2 + \mathbf{k}^2 - \Pi(\omega, \mathbf{k})} \tag{1.41}$$

In perturbation theory we will denote contributions at order λ^n with λ^n as a subscript.

1.3.2 Boson one-loop self-energy

We start by calculating the boson self-energy to at order λ^2. The integral, represented by the diagram in Fig. 1.11, is given by

$$\begin{aligned}
\Pi_{\lambda^2}(\omega, \mathbf{k}) &= \lambda^2 \int \frac{\mathrm{d}^3 k_1}{(2\pi)^3} G_0(\omega + \omega_1, \mathbf{k} + \mathbf{k}_1) G_0(\omega, \mathbf{k}) \\
&= \lambda^2 \int \frac{\mathrm{d}^3 k_1}{(2\pi)^3} \frac{1}{i\omega_1 - k_1^2/2m + \mu} \frac{1}{i(\omega_1 + \omega) - (\mathbf{k}_1 + \mathbf{k})^2/2m + \mu}
\end{aligned} \tag{1.42}$$

This integral is UV divergent[5]. We can isolate the divergent piece by subtracting the asymptotic behavior of the integrand

$$
\Pi_{\lambda^2}(\omega, \mathbf{k}) = \lambda^2 \int \frac{\mathrm{d}^3 k}{(2\pi)^3} \frac{1}{(i\omega - \mathbf{k}^2/2m)^2} +
$$
$$
+ \int \frac{\mathrm{d}^3 k_1}{(2\pi)^3} \left(G_0(\omega + \omega_1, \mathbf{k} + \mathbf{k}_1) G_0(\omega, \mathbf{k}) - \frac{1}{(i\omega - \mathbf{k}^2/2m)^2} \right)
$$
$$
(1.43)
$$

Here the first integral is UV divergent and needs to be regularized. The second integral however converges. The first term is independent of ω, k and can be cancelled by a mass counterterm for the boson. If we regularize with cut-offs symmetric under $\omega \to -\omega$, then the counterterm is actually finite as we take the cut-offs to ∞. We then have (See e.g. [45])

$$
\Pi_{\lambda^2}(\omega, \mathbf{k}) = \lambda^2 \frac{m \left(\mathrm{Re} \left(\sqrt{\left(|\mathbf{k}| - \frac{2im\omega}{|\mathbf{k}|} \right)^2 - 4k_F^2} \right) - |\mathbf{k}| \right)}{2\pi |\mathbf{k}|} + C \quad (1.44)
$$

We need a renormalization condition to fix the counterterm. We demand that the theory is critical, for any larger C an instability should develop. In the static limit $\omega \to 0$ we have $\Pi_{\lambda^2}(\omega = 0, \mathbf{k}) = -\lambda^2 m/2\pi + C$ for $|\mathbf{k}| < 2k_F$. No larger Π_{λ^2} is obtained for $|\mathbf{k}| > 2k_F$. For $C < \lambda^2 m/2\pi$ we thus have a negative mass-term for the boson which leads to an instability. Larger C are stable but since we are interested in the critical theory we by hand set $C = m/2\pi$. For a similar argument in $d = 3 - \epsilon$ dimensions see [46]. For low energies we expect $\mathbf{k}^2 \ll k_F^2, m\omega$ and we can approximate this as

$$
\Pi_{\lambda^2}(\omega, \mathbf{k}) = -\frac{\lambda^2 m^2 |\omega|}{2\pi \sqrt{\mathbf{k}^2 k_F^2 + m^2 \omega^2}} \left(1 + \mathcal{O} \left(\frac{|\mathbf{k}|^6 k_F^2}{(\mathbf{k}^2 k_F^2 + m^2 \omega^2)^2} \right) \right) \quad (1.45)
$$

This low energy limit can also be found by right from the start linearizing the fermion dispersion as in Eq. 1.2.

We see that for low energies, this term will always dominate the ω^2 term in the free boson propagator. If this first-order contribution were the

[5]One encounters no divergencies by performing the ω or $\mathbf{k}$ integrals, in either order. There are however subsets of the integration domain where the integral diverges.

whole story, then the boson low-energy dispersion would be $\mathbf{k}^2 \sim |\omega/k|$ and for low energies we can approximate the boson self energy as

$$D_{\mathrm{LD}}(\omega, \mathbf{k}) = \frac{1}{\mathbf{k}^2 + \frac{\lambda^2 k_F |\omega|}{2\pi v_F^2 |k|}}. \tag{1.46}$$

This indicates a new scaling relation between space and time that emerges in the IR. In a Lorentz invariant theory with a scaling symmetry, space and time necessarily scale with the same power. In a scale invariant theory without Lorentz invariance this need not be the case and we can have a scaling where $\omega, k \to s^z \omega, sk$. z is called the dynamical critical exponent. With the above polarization we see if the one-loop result were the whole story then we would have $z = 3$ for the boson.

Analytically continuing this to real time with a retarded contour we get the retarded two-point function

$$D_{R,\mathrm{LD}}(\omega, \mathbf{k}) = \frac{1}{\mathbf{k}^2 - i\frac{\lambda^2 k_F \omega_R}{2\pi v_F^2 |\mathbf{k}|}}. \tag{1.47}$$

This is a damped boson, the sharp excitation has completely disappeared for low energies. This effect, called Landau-damping, greatly influences the IR of this theory.

Our calculation so far has only been to order λ^2. We saw that the first correction at order λ^2 actually dominates over the bare term in the IR. The higher order corrections similarly turn out to dominate over this in the IR so perturbation theory can not be used to understand the IR and the above result is of limited use. We discuss this further in Section 1.3.7.

1.3.3 Fermion one-loop self-energy

The single one loop correction to the fermion two-point function is given by the diagram in Fig. 1.12(a). The integral corresponding to this diagram is

$$\Sigma_{\lambda^2}(k) = \lambda^2 \int \frac{\mathrm{d}^3 p}{(2\pi)^3} G_0(k+p) D_0(p) \tag{1.48}$$

As opposed to the boson self-energy, this diagram converges absolutely. For $\omega, |\mathbf{k} - k_F| \ll k_F$ we can expand the fermion propagator around the

external momentum $\mathbf{k} = (k_x + k_F)\hat{\mathbf{x}} + k_y\hat{\mathbf{y}}$

$$\Sigma_{\lambda^2}(k) = \lambda^2 \int \frac{\mathrm{d}p_0 \mathrm{d}p_x \mathrm{d}p_y}{(2\pi)^3} \frac{D_0(p)}{i(\omega + p_0) - v_F(k_x + p_x) - (k_y + p_y)^2/2m} \tag{1.49}$$

The quadratic in momentum term is necessary for convergence, but in the end we can take $m \to \infty$ (v_F constant) to obtain

$$\Sigma_{\lambda^2}(\omega, k_x) = \lambda^2 \frac{\log\left(\frac{iv\omega - k_x + \sqrt{(1-v^2)(k_x^2 + \omega^2)}}{iv\omega - k_x - \sqrt{(1-v^2)(k_x^2 + \omega^2)}}\right)}{8\pi\sqrt{1-v^2}} \tag{1.50}$$

This expression is valid for $0 < v_F < 1$ and $1 < v_F$. The square roots are defined by analytical continuation in the upper half plane for negative values. For $v_F = 1$ we have

$$\Sigma_{\lambda^2, v=1}(\omega, k_x) = \lambda^2 \frac{\sqrt{\omega^2 + k_x^2}}{4\pi(i\omega - k_x)}. \tag{1.51}$$

This simpler result can be shown to be due to an additional symmetry of the low-energy limit of diagrams contributing to the fermion two-point function. Chapter 5 of this thesis in fact explains that this is a universal feature of self-energy corrections to "boson dominated" quantum critical metals.

1.3.4 Tree-level RG flow

We will now repeat the scaling analysis of Section 1.1.3 with the action in Eq. 1.37. We use the same scaling as in Eq. 1.15 for the fermion energy and momentum but since the boson low energy excitations are centered around 0 momentum we can not scale it towards the FS as for the fermion. We let the boson energy ω_B and momentum $\mathbf{q}$ (measured from the origin and not the FS) scale as

$$(\omega_B, \ \mathbf{q}) \to (\mathrm{e}^{-t}\omega_B, \ \mathrm{e}^{-t}\mathbf{q}). \tag{1.52}$$

To preserve the boson kinetic term we have to scale the boson field as

$$\phi(\omega_B, \mathbf{q}) \to \mathrm{e}^{t(d+3)/2}\phi(\omega_B, \mathbf{q}). \tag{1.53}$$

Note that with this different fermion and boson scaling we do not keep the theory local in real space. This is not a problem. Even in the Fermi liquid

case the real space scaling does not preserve locality. The only important point with the choice of scaling is that the kinetic terms are unchanged, so whatever happens to the couplings can be interpreted as a change of the same theory we started with before integrating out high energy modes.

Let us now see what happens to the interaction term of Eq. 1.37. First we write this in momentum space

$$S_{\text{int}} = \lambda \int \frac{\mathrm{d}\omega_B \mathrm{d}^d q \mathrm{d}\omega \mathrm{d}k \mathrm{d}^{d-1}\boldsymbol{\Omega}}{(2\pi)^{2d+2}} \phi(\omega_B, \mathbf{q}) \times$$
$$\times \psi^\dagger(\omega_B + \omega, \mathbf{q} + (k_F + k)\boldsymbol{\Omega})\psi(\omega, (k_F + k)\boldsymbol{\Omega}) \tag{1.54}$$

We see that upon rescaling the energies, momenta and fields we effectively have $\lambda \to \mathrm{e}^{t(3-d)/2}\lambda$ and thus we have the tree-level β-function

$$\beta_\lambda(t) = \lambda \left(\frac{3-d}{2} + \mathcal{O}(\lambda^2) \right). \tag{1.55}$$

The last term comes from interactions between degrees of freedom above and below the cut-off. It is obtained when integrating out the high-energy terms. At tree level in $d = 3$ we have no flow and the coupling is tree-level marginal at the UV fixed point. We need to integrate out the high energy modes to see in which direction λ flows.

At $d = 2$ we see that this coupling is relevant already at tree level and it makes the IR of this theory different from the UV fixed point. Formally this is what explains the emergence of a new NFL fixed point as the low-energy theory.

For completeness we briefly mention the RG behavior of a boson four-point interaction λ_ϕ. Performing the same analysis we find $\lambda_\phi \to \mathrm{e}^{t(3-d)}\lambda_\phi$ and

$$\beta_{\lambda_\phi}(t) = \lambda_\phi (3 - d + \mathcal{O}(\lambda_\phi)) + \mathcal{O}(\lambda^4). \tag{1.56}$$

This means that the ϕ^4 interactions is also tree-level marginal in $d = 3$ and relevant in lower dimensions.

1.3.5 Hertz-Millis theory

Before moving on to calculate the perturbative RG flow we mention an earlier approach that was successfully used to understand the same model we are studying but in $d = 3$. Hertz studied this model by simply integrating out the fermions to obtain an effective action for ϕ [47] (this

was later refined by Millis [48]). This generates couplings for ϕ at all orders, and since the fermions are gapless these couplings can be singular. We saw above that all boson self-interactions are marginal (marginally-irrelevant when taking quantum corrections into account) in $d = 3$ so only the correction to the kinetic term is important. This is given by a one-loop correction to the boson self-energy and results in a boson two-point function of the form (1.46) also in $d = 3$ but with a different prefactor of the self-energy. This is indeed a singular contribution giving rise to a dynamical critical exponent $z = 3$. Taking this exponent into account in the RG flow it looks as if the ϕ^4 interaction is irrelevant all the way down to $d = 1$ and by this argument Hertz theory was claimed to be valid also in $d = 2$. By performing a more careful RG-flow including both the fermions and bosons it is found to be incorrect and Hertz approach fails in $d = 2$ [49]. We perform this more careful RG analysis in the next section.

1.3.6 One-loop RG flow

Integrating out the high energy modes can only be done perturbatively. In $d = 3$ this is straightforward. We can assume a small λ in the UV and expand in λ. This is done in [41, 42]. These two works use slightly different renormalization schemes however they both find

$$\beta_\lambda(t) = \lambda \left(\frac{3 - d}{2} - B\lambda^2 + \mathcal{O}(\lambda^4) \right) \qquad (1.57)$$

where B is positive. There are two contributions to B. The first from the fermion field renormalization at one loop given by the fermion self energy cut-off dependence. The corresponding diagram is in Fig. 1.12(a). The second contribution is from the vertex correction seen in Fig. 1.12(b).

In [42] B depends on v_F which also flows in their renormalization scheme, however, B remains positive. This means that $\lambda = 0$ is a stable fixed point. If λ is small but non-zero in the UV, it will still flow to 0 in the IR.

The boson self-energy does not contribute to the ϕ field renormalization at 1 loop. The reason for this is that a boson with energy ω only receives corrections from fermions with energies lower than this. Changing the fermion (and boson) cut-off Λ does then not affect the boson self energy as long as $|\omega| < \Lambda$. Because of this Landau-damping is not seen in the one-loop RG flow. However, from the preceding section we know that

(a)   (b)
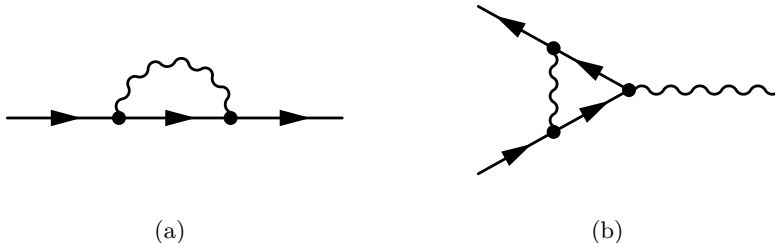
Figure 1.12. (a) One-loop contribution to fermion two-point function giving
rise to wave-function renormalization in the one-loop RG flow of the coupling λ.
(b) One-loop vertex correction contributing to the RG flow of the coupling λ.

it is an important effect for the low-energy physics. This does not mean
that the RG flow is incorrect, it is just not seen at one loop.

We can attempt the same analysis in $d = 2$. Here λ^2 is not dimen-
sionless so it has to be compared to some scale. The relevant scale is the
cut-off Λ. Assuming λ^2/Λ is small we can calculate β_λ perturbatively. The
tree-level flow makes λ grow exponentially until the one-loop correction
starts to become important. This happens at a scale $1/2 \sim \lambda^2/\Lambda$ how-
ever, which means that λ^2/Λ is not small anymore and we can not use a
perturbative calculation. In $d = 2$ we can use perturbative RG-flow to see
that for any finite UV coupling to a massless field ϕ we will depart from
Fermi liquid fixed point, but we can not tell what happens after that.

One approach is to not directly consider $d = 2$ but to work in $d = 3 - \epsilon$
dimensions with ϵ small. This approach has been successfully used to
understand interacting bosons in 2+1 dimensions by studying them in
"3.99" dimensions [50]. Our coupling is tree-level marginal in $d = 3$ but
it flows to stronger coupling for any $d < 3$ until loop corrections kick
in, $d = 3$ is the upper critical dimension. The first loop corrections are
comparable to the tree-level flow for $\epsilon/2 \sim \lambda^2/\Lambda^\epsilon$. If ϵ is small this now
happens for a small $\lambda^2/\Lambda^\epsilon$ and we can thus treat it perturbatively. We
find a fixed point at

$$\lambda^* = \sqrt{\frac{\epsilon}{2B}} + \mathcal{O}(\epsilon). \tag{1.58}$$

Whether this fixed point remains as ϵ is increased to 1 and we go to $d = 2$
is not clear. Higher order in ϵ corrections become important and Landau-
damping efffects set once higher loops are included. To analyze this, one

37

could calculate the first corrections in ϵ by going to higher loop order. It will not give a conclusive answer, since for $\epsilon = 1$, likely all orders in ϵ are necessary, but it could give an indication to what happens to this fixed point. Another approach was used in [43, 44] where the authors instead put the Landau-damping corrections in the action from the onset and studied the RG flow at one loop of the resulting theory. They found a flow that interpolates between the earlier one-loop flow in the UV and a $z_b = 3$ boson interacting with a $z_f = 1$ fermion in the IR.

1.3.7 Usefulness of perturbation theory

We have seen in the preceding subsections that perturbation theory in the coupling constant is not useful for studying energies of order λ^2 or lower of the two-dimensional quantum critical metal.

We do expect perturbation theory to be useful in the UV. Precisely what this means is not obvious. All orders in perturbation theory have the same dimension so the relevant powers of the dimensionful coupling constant will show up together with other dimensionful quantities. If we consider the fermion two-point function then the energy ω, momentum $\mathbf{k}$ and Fermi momentum all provide dimensionful parameters. Without more information about the perturbative expansion we do not know what combination of these show up in powers of λ. This means that we do not know in what part—if any—of energy-momentum space perturbation theory is useful. In a relativistic theory with no other scales there is only one Lorentz invariant dimensionful quantity, $\omega^2 + \mathbf{k}^2$ and we know that perturbation theory will be organized in terms of $\lambda^2/\sqrt{\omega^2 + \mathbf{k}^2}$. It is then clear what the UV is and for large enough $\omega^2 + \mathbf{k}^2$ we expect perturbation theory to be useful. In our case we do not have this, however in Chapter 5 we impose an additional symmetry, similar to Lorentz invariance but relevant to chiral fermions at a FS, and in this case we find the equivalent to $\omega^2 + \mathbf{k}^2$ and can say where perturbation theory is useful.

Since we can not expand to low orders in the coupling constant to understand the IR, could we perhaps find a way to sum up contributions to all orders in the coupling constant? Even if we could calculate all perturbative corrections, it is not clear that this would work. For starters, perturbation theory would only converge in the "UV-region" described above. If we can sum up all perturbative corrections there we might be able to use analyticity arguments to extend this to the IR. It is however not clear that perturbation theory converges anywhere, even in the "UV-

region" where the effective coupling constant is small. It is a common feature of quantum field theories that the perturbative series does not converge, but only gives an asymptotic series. This was first shown by Lipatov for a scalar field theory [51] but happens in more general field theories such as QED as well. This may well be the case for our theory (1.37) too. QED has a small dimensionless coupling constant $\alpha \approx 0.007$ whereas the coupling constant λ^2 of our theory has units of energy. Perturbative corrections to QED come with powers of α and are initially suppressed since $\alpha < 1$. The coefficient in front of α^n however grows as $n!$ so for $1 \lesssim n\alpha$, each perturbative correction is larger. This is called an asymptotic expansion. By truncating the series before the divergence, the error is of order $\exp(-1/\alpha)$ and can be made arbitrarily small for small α but cannot be captured perturbatively. The divergence is immaterial in the sense that the truncated series agrees with physical observables[6]. In our case with a dimensionful coupling constant we get powers of λ^2/w in perturbation theory, where w is some unknown combination of external energies, momenta and the Fermi momentum[7]. If also our theory has an asymptotic expansion, then in the UV we can sum of the order of w/λ^2 orders in perturbation theory before we hit the divergence. It is however not clear that the perturbative series of our QFT has 0 radius of convergence. Feldman et al. have shown that the radius of convergence is non-zero in a class of two-dimensional Fermi liquids [3]. Their model is not too dissimilar to ours so this might happen in our case too.

With these limitations mentioned, it is still useful to study the perturbative expansion. Any non-perturbative approach should match perturbation theory when expanded in the coupling constant so calculating the first few diagrams provides a strong check on any non-perturbative calculation.

A future study of the perturbative series of (1.37) to high orders would be interesting to "experimentally" see where in energy-momentum space this series converges. If a converging expansion is found in a limited ω-region, then analytic properties of n-point functions could perhaps be used to analytically continue into the regions without convergence. If only asymptotic convergence is found this would also be interesting. The asymptotic series can be studied using the framework of resurgence theory

---

[6]The error of order $\exp(-1/\alpha)$ is entirely out of experimental reach.

[7]This is a simplification. We do not know how the perturbative expansion is organized at high orders. There could be different classes of diagrams that have expansions in different combinations $\lambda^2/w_1, \lambda^2/w_2, ...$

and the nature of the divergence indicates presence of non-perturbative processes [52].

Additionally, even though the whole perturbation series can not be summed up, understanding the structure of the sum can tell us some properties of the non-perturbative answer as we will see in Chapter 5.

With this motivation we study some further features of the perturbative expansion in the following subsections.

1.3.8 Low-energy limit of general diagrams

We have seen that for low energies we can make several useful simplifications when evaluating diagrams. Without proof we here state general assumptions about the low-energy properties of the momentum integrals involved in the diagrammatic expansion. For this we consider a specific diagram with V vertices contributing to the correlation function $\langle \psi_1^\dagger ... \psi_{n_\psi}^\dagger \psi_1 ... \psi_{n_\psi} \phi_1 ... \phi_{n_\phi} \rangle$. All external fermions lines connect to another external fermion, possibly exchanging bosons before. Without loss of generality we assume $\psi_i^\dagger$ connects to ψ_i. There can also be internal fermion loops, we denote the number of them by L_ψ. The diagram comes with a factor λ^V. For a slightly more general theory with flavorful/spinful fermions we additionally get a factor $N_f^{L_\psi}$ where N_f are the number of fermion flavors/spins that are summed over for each fermion loop.

Now consider external energies much smaller than k_F ($v_F \sim 1$) and external momenta close to being on-shell (near the FS). For the dominant processes we have that

- All fermion momenta, k, are close to the FS, $|k| - k_F \ll k_F$

- All boson momenta, q, are much smaller than k_F, $|q| \ll k_F$

These assumptions can convincingly be seen to be true by performing several of the low order diagrams.

Using this we see that an external fermion line from $\psi^\dagger(k_1)$ to $\psi(k_2)$ will stay within a single patch of the FS. Each boson connecting to this fermion line adds a momentum q_i such that $k_1 + \sum q_i = k_2$. Since each $q_i \ll k_F$ we have $|k_1 - k_2| \ll k_F$ for a finite number of bosons. In evaluating diagrams we can then linearize any fermion propagator connected (indirectly) to an external momentum $\mathbf{k}_i$ as

$$G_0(\omega, \mathbf{k}) \approx G_{0, \hat{\mathbf{k}}_i}(\omega, \mathbf{k}) = \frac{1}{i\omega - v_F(\hat{\mathbf{k}}_i \cdot \mathbf{k} - k_F)}. \qquad (1.59)$$

Fermions that make up the internal fermion loops for $0 < L_\psi$ are not constrained to a single patch in the low-energy limit. However they still have momenta close to the FS and can be approximated by the linearized propagator

$$G_0(\omega, \mathbf{k}) \approx \frac{1}{i\omega - v_F(|\hat{\mathbf{k}}_i| - k_F)}. \qquad (1.60)$$

We have to be careful when employing the low energy limit. There are other limits involved in the description of our model and later we will consider even further limits by taking different parameters of our theory to extreme values in search of a further simplified model. These limits need not all commute, so it is important they are taken in the right order. If we wish to gain insights about the true IR of our model then the correct order to take these limits is

1. Limits associated with the path-integral formulation or—if we attempt to sum the full perturbative series—the limit in the infinite sum of perturbative corrections.

2. The limit of external energies smaller than k_F and momenta close to the FS.

3. Any auxiliary limits used to find regimes where we can do calculations and hope to still gain some insights about the IR.

The first limit is difficult to calculate and the subsequent limits are imposed to make the earlier ones simpler so in many works these limits are typically evaluated in the completely opposite order. In principle limit 2 and 3 can be useful even if evaluated in the right order, though when doing this great care has to be taken. In Section 1.4 we will see that neither the "small N_f" limit nor the "matrix large N" limit commute with the low energy limit and the results obtained from these are of limited use.

In our low energy consideration above we have considered limit 1 and 2 in the wrong order. For any diagram with a finite number of boson lines it is true that for low energies each fermion will stay within the same patch as the external momentum. However, the total boson momentum can be of order k_F even if each boson momentum is much smaller than k_F if the limits 1 and 2 are taken in the correct order. Whether this happens or not is not known and would be interesting to investigate. One could start by calculating a simple ladder diagram, see Figure 1.13, without relying on
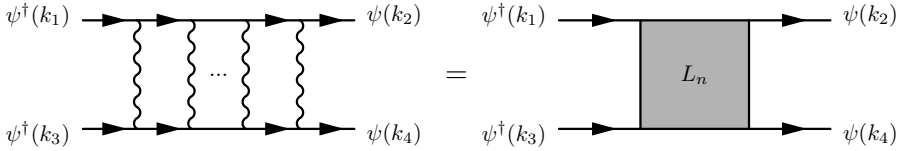
Figure 1.13. Ladder diagrams with many steps allow a stepwise transfer a momentum between the fermion lines. Here $L_n(k_1, k_2, k_3, k_4)$ represents the amputated ladder diagram with n rungs. $|\mathbf{k}_1 - \mathbf{k}_2| \ll k_F$ in the low-energy limit, however it is not obvious that this is true if first the large n limit is taken.
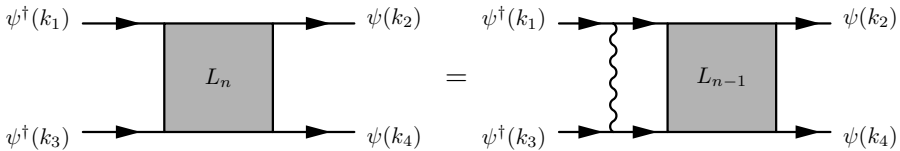
Figure 1.14. The amputated ladder diagram with n rungs satisfies this recursion relation.

any of the above assumptions and take the large n limit. Then it should be clear whether $|\mathbf{k}_1 - \mathbf{k}_2| \sim k_F$ processes are suppressed on not. Such a diagrams can be found through a simple recursion relation

$$L_n(k_1, k_2, k_3, k_4) = \lambda^2 \int \frac{\mathrm{d}^3 k}{(2\pi)^3} D_0(k) G_0(k_1 + k) G_0(k_3 - k) \times$$
$$\times L_{n-1}(k_1 + k, k_2, k_3 - k, k_4) \tag{1.61}$$

This is represented in Fig. 1.14. In the large n limit we only need to look for the largest eigenvalues of this linear operator.

1.3.9 Patch theory

In the previous section we have concluded that for low energies, a set of connected fermion propagators in a diagram will stay within the same patch of the FS, with the caveat that this low energy limiting behavior might not commute with the limit in the infinite sum of the perturbative expansion. Only considering a single patch for each fermion line simplifies calculations, however different fermion lines belonging to the same diagram generally have momenta in different patches. It has, however,

been shown that the use of FS patches can be taken even further. In [24] the authors study a model similar to (1.37). They argue that only bosons with collinear momenta are correlated. The reason for this can intuitively be understood as when a fermion in a certain patch of the FS scatters, the dominant boson momenta are influenced by the location of the patch. Further bosons scattered from the same fermion (and thus correlated) in the same way have a constrained momentum. Bosons are predominantly scattered in the directions transverse to to FS. Consider a fermion in the patch at $k_F \hat{x}$ and a boson line attached to this fermion with a momentum $q = (q_x, q_y)$. As a heuristic it is useful to consider the fermion to be on-shell. Then the energy penalty for scattering the fermion is $v_F(q_x + q_y^2/2k_F)$ and bosons are predominantly scattered in the directions transverse to the FS. If now a diagram contains many fermion lines, it is dominated by momentum configurations where all boson lines, on both ends, are connected to fermions in patches parallel to its momentum. This means that diagrams will be dominated by momentum configurations where all fermions are in parallel patches and all bosons transverse to these patches. For our circular FS there are pairs of antipodal patches where the coupling through the boson dominates. Note that this is also true for any convex FS. The other patches will be decoupled and one can consider an effective theory consisting only of two patches. This is precisely what was done in [24]. There they perform a more careful analysis by, as in the Hertz theory [53], integrating out the fermion to obtain a formal expression for a nonlocal action for ϕ. The action contains singular terms of all orders in ϕ, however the leading singularities only appear for collinear boson momenta. They then argue that the physics relevant for low energies is decoupled into different directions in boson momentum space and corresponding pairs of patches for the fermion. There are interactions between these decoupled theories, however they are only irrelevant corrections to the low energy effective theory.

1.4 Non-perturbative approaches to quantum critical metals

The open question at the basis of this thesis is that it is currently not possible to completely solve the theory of a Fermi surface interacting with a massless scalar in two dimensions. The coupling constant is as we have seen in Section 1.3.6 not a small parameter. We need to find another small

(or not so small) parameter to expand in. This relatively simple theory, however, does not have many parameters that provide useful expansions. This is what makes this theory so difficult and in a sense has led physicists to what might seem as desperate measures. One approach has been to first extend the theory to a slightly more complex theory with a new parameter, and then study a simplifying limit of this new parameter.

Although the expansions that have been explored so far do not give a precise understanding of our model, together one might hope that they can box in our theory in the landscape of different theories. Once we have explored the landscape thoroughly we might be able to find a natural point to expand from, different from that of a Fermi gas.

The two potential expansions parameters are:

- **Inverse coupling constant** ω/λ^2 is a small parameter in the IR. Unfortunately we do not have control over the strong coupling limit so we do not have a point to expand around. In the UV we have complete understanding of the free theory and we can add corrections to is as we depart slightly from the UV fixed point. The same is not true in the IR. Perhaps there is a dual description of our theory, or a closely related one, whose IR limit is a free theory that admits a perturbative treatment in ω/λ^2. Such weak-strong dualities exist for a number of theories (see e.g. [54]) though none is presently known which directly applies to (1.37).

- **Fermion-boson velocity ratio** The limit of small v_F/c corresponds at leading order to a static fermion interacting with a fluctuating scalar field. As we saw in the RG analysis, v_F has been found to flow to 0 so this might be a useful approximation of the IR. This limit was studied in [55]. The static limit was however not enough to solve the theory and they had to use additional approximations, the so-called "ϵ-expansion" and "matrix large N" limit. We cover these expansions in the next section.

  The opposite limit of small c/v_F corresponds to a FS coupled to slow bosonic modes. Since this limit is unstable under RG it is likely not a good description of the IR; the $v_F \to 0$ region is artificially suppressed. Vertex corrections are suppressed in this limit by Migdal's theorem [56]. This means that the Schwinger-Dyson equations of this theory close, and it can be solved so it would be an interesting case to study nevertheless.

None of the above parameters provide a directly useful approximation to determine the IR of our QCM. Our model (1.37) does not provide further dimensionless parameters so various extensions have been considered that contain further parameters. We will describe some of these now.

1.4.1 Dimensional continuation

In Section 1.3.6 we saw that by extending the theory to more dimensions we can perform a perturbative expansion in $\epsilon = 3 - d$. There are several different ways of performing such an expansion. The model we are ultimately interested in has 1 temporal and 2 spatial dimensions. When considering the patch theory as in Section 1.3.9, there is one spatial direction parallel to the FS and one direction perpendicular to the FS. The dimensions of all these three distinct directions can in principle be extended to general parameters $d_0, d_\parallel, d_\perp$.

In [57], I. Mandal and S.S. Lee study a Q = 0 QCM with $d_0 = 1$ and $d_\perp = d - d_\parallel$. $d_\parallel$ sets the dimension of the FS and thereby controls the extensiveness of gapless modes. For d greater than the upper critical dimension 3, (see Sec. 1.3.6) we have a Fermi-liquid. Below the upper critical dimension they find quite different behaviors in the cases of $d_\parallel = 1$ or $d_\parallel > 1$. For $1 < d_\parallel$ they find what they call UV/IR mixing; the UV scale k_F shows up in low energy observables. In the case of $d_\parallel = 1$ we can use the patch theory (see Sec. 1.3.9) with only two antipodal patches contributing to the fermion two-point function. For $1 < d_\parallel$ this does not work and global properties of the FS have to be taken into account. These results rely on an expansion in small $\epsilon = 3 - d$. How to extend dimensional expansions all the way down to $\epsilon = 1$ is not know.

1.4.2 Fermion flavor expansion: vector large N_f limit

We can extend the theory to have N_f flavors of fermions transforming in the fundamental representation of a global $U(N_f)$ flavor symmetry group. The fermion then has an index $i = 1, ..., N_f$: $\psi^i, \psi_i^\dagger$. The interaction term is written as $(\lambda/\sqrt{N_f})\phi\psi_i^\dagger\psi^i$. This extension has been extensively studied in the large N_f limit and it was first thought to provide a controlled expansion in $1/N_f$ valid at low energies [22, 58].

Consider the perturbative expansion of the boson two-point function. What is the power of N_f for each diagram? Each vertex comes with a factor $N_f^{-1/2}$. All fermionic loops contribute with a sum over N_f. The

45

power is thus $N_f^{F-V/2}$ where V is the number of vertices and F the number of fermion loops. The one-loop diagram calculated in Sec. 1.3.2 is thus the same order as the free two-point function, N_f^0. Adding more vertices to the fermion can only result in subleading diagrams since no more fermion loops are added. The only other diagrams at order N_f^0 are simply multiples of this loop and the boson two-point function can naively be thought to be given by the one-loop result in the large N_f limit. The first $1/N_f$ correction to the fermion self-energy is then given by the diagram in Fig. 1.12(a) but with this corrected boson. This leads to what are called the RPA two-point functions [59]

$$D_{\text{RPA}} = \frac{1}{\mathbf{k}^2 + N_f \frac{\lambda^2 k_F |\omega|}{2\pi v_F^2 |\mathbf{k}|}} \tag{1.62}$$

$$G_{\text{RPA}} = \frac{1}{i\omega - v_F(|\mathbf{k}| - k_F) + i\,\text{sgn}(\omega)\frac{v_F^{2/3}}{\sqrt{3}(2\pi\lambda\sqrt{N_f k_F})^{2/3}}|\omega|^{2/3}} \tag{1.63}$$

It thus seems like the large N_f limit provides a controlled low energy limit of (1.37) around which we can add corrections in $1/N_f$. There is however a caveat, as was first shown by S.S. Lee in [60]. Diagrams not included at lowest order in large N_f become increasingly important in the IR. In the case of a single FS patch, the set of diagrams to be considered at each order is given by a genus expansion of diagrams. The low energy theory still requires a nontrivial sum of an infinite set of diagrams.

1.4.3 Boson dynamical critical exponent

Mross et al. make a further extension of the theory to get the large N_f limit under control [61]. They modify the dynamical critical exponent z_b of the bare boson

$$D_0(k) = (\omega^2 + k_x^2 + k_y^2)^{-\frac{z_b-1}{2}}, \tag{1.64}$$

and expand in large N_f keeping $(z_b - 2)N_f$ finite. They show that this provides a controlled limit and that the RPA two-point functions in fact govern the low energy limit. z_b approaches 2 in this limit so it is not clear how relevant this result is to the case we are interested in with $z_b = 3$.

1.4.4 Boson flavor expansion

One might consider a similar extension but with the boson in the fundamental representation and the fermion in the trivial representation of a global $U(N_f)$ flavor symmetry group. However this just results in a sum over N_B for each boson propagator and since each boson propagator is connected to two vertices giving a factor of λ^2 this effectively just changes the coupling constant from λ to $\lambda\sqrt{N_B}$. An expansion in N_B is equivalent to the problematic expansions in the coupling constant.

1.4.5 Matrix large N

Similar to the vector large N_f limit we can extend (1.37) to have a global $SU(N)$ flavor symmetry with fermions transforming in the fundamental and bosons in the adjoint representation. The boson then has two flavor indices and the fermion one. The coupling constant of the theory is also normalized by the rank of the symmetry group and the interaction term is written

$$S_{\text{int}} = \int \mathrm{d}\tau \mathrm{d}^d x \frac{\lambda}{\sqrt{N}} \phi_j^i \psi_i^\dagger \psi^j. \tag{1.65}$$

For $N = 1$ we recover Eq. (1.37) but in general we have N flavors of fermions and N^2 flavors of bosons. Only certain classes of diagrams survive in the large N limit. One illustrative way of seeing what diagrams survive the large N limit is to draw the diagrams with one line for the fermion and two lines for the boson. The interaction contains sums over indices and these can potentially give diagrams factors of N. Each propagator, however, preserves the indices ($G_i^j \propto \delta_i^j$ and $D_{ij}^{kl} \propto \delta_i^l \delta_j^k$), so there are many constraints on the sum over them. A convenient way to count the N dependence is in so-called double-line notation. In the double-line notation each line corresponds to an index. A fermion propagator thus consists of a single line; but a boson propagator of a double line. At each vertex we connect the indices. In the end there are several disconnected continuous curves tracing the flow of each index. Some are connected to external fields and some form loops. The indices of the lines connected to external fields fix the external indices to be identical in both ends. All single line loops, however, will be summed over for all possible indices. They therefore give a factor of N each. Each vertex gives a factor of $1/\sqrt{N}$ in addition, so only diagrams where these two contributions cancel

contribute in the large N limit. An illustration of the double line notation for the case of the two-loop contribution to the fermion two-point function is shown in Figure 1.15. It turns out that in this limit all diagrams with fermionic loops vanish and additionally only planar diagrams survive the large N limit. A planar diagram is a diagram that can be drawn on a plane without any crossing lines. In the case of the fermion two-point function, all propagators leaving the fermion line have to be on the same side. The diagram of 1.15(a) has a fermion loop and thus vanishes. Diagram 1.15(c) is not planar and vanishes as well. 1.15(e) has no fermion loops and is planar and thus order 1 in the large N limit.

All important effects from Landau-damping disappear completely in the matrix large N-limit due to the lack of all fermion loops. This means that similarly to the large N_f limit this is not able to capture the IR of (1.37). In [62] the authors use the above large N limit to study quantum critical fermions in slightly below 3 dimensions. They have a similar model to ours, however, they additionally have a fermion four point interaction and a $\mathrm{tr}(\phi^2)^2$ coupling. The authors integrate out high energy and momentum modes and study the flow of the parameters of the theory. The fermion four point interaction flows to 0 and can be omitted from the onset. The fermions do not give any corrections to the bosons at leading order in the large N limit. Therefore the boson is described by a large N Wilson-Fisher fixed point [63]. The fermions do receive corrections from the boson and these are studied in three different ways. First they calculate the flow of the couplings (and velocity) using one-loop perturbation theory. They find a fixed point for the coupling $g \sim \sqrt{\epsilon}$ and a fermion anomalous dimension $\gamma = \epsilon/4$. g is thus small close to $d = 3$ and this perturbatively found fixed point can be trusted in a small vicinity of $d = 3$.

They also find that the Fermi velocity v_F flows to 0 in the IR, however they point out that as v_F goes to zero, higher order terms that could be neglected for a finite v_F now become important and the final fate of v_F is not certain. These higher order terms can be made arbitrarily small and then there will be a large region of $v_F \to 0$ where they can study the $v_F \to 0$ fixed point. They find the fixed point fermion two-point function:

$$G(\omega, \mathbf{k}) = \omega^{2\gamma - 1} f\left(\frac{\omega}{|\mathbf{k}| - k_F}\right) \tag{1.66}$$

They proceed by studying this fixed point, using what they call the fermion gap-equation. This is an equation for the fermion self-energy in the large
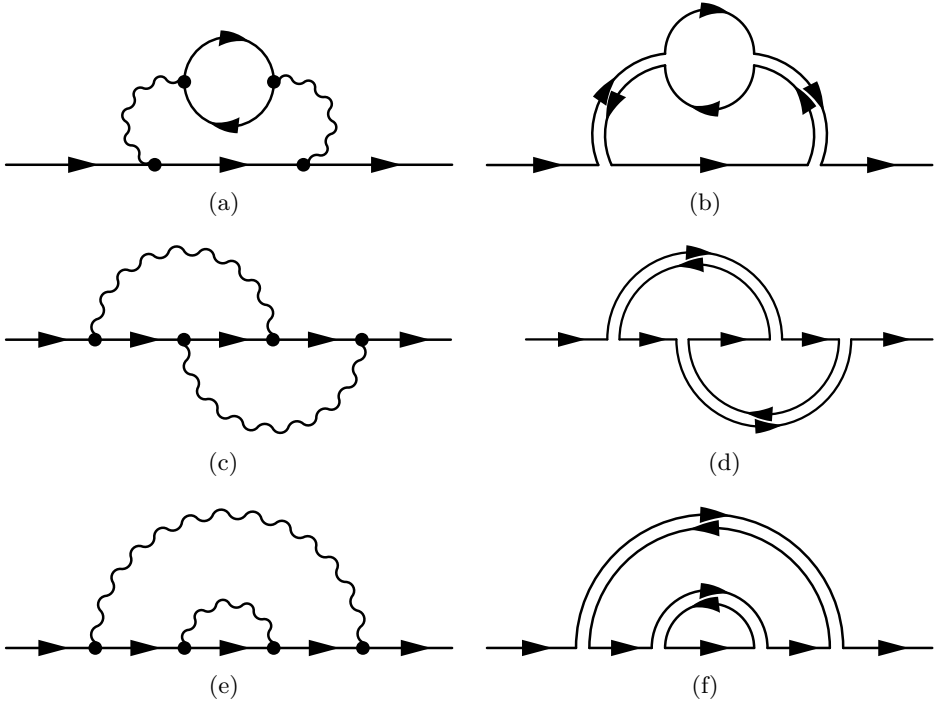
Figure 1.15. The left column show the three diagrams contributing to the fermion two-point function at order λ^4. Straight lines are fermion propagators and wavy lines are boson propagators. The right column shows the corresponding diagrams drawn using the double-line notation. Note that also the two lines making up the boson propagators have directionality and they have to be opposite. There is then just one unique way of connecting the double lines at vertices. Diagram (b) is seen to have one free single-line loop and thus scales as $1/N$. Diagram (d) has no disconnected single-lines and thus scales as $1/N^2$. Diagram (f) has two single-line loops and thus scales as N^0 and survives the large N limit.
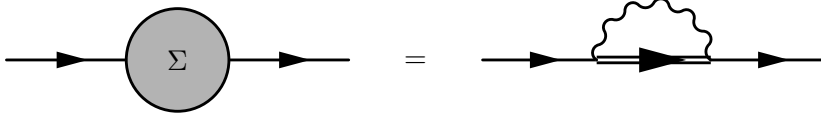
Figure 1.16. No boson lines cross in a planar diagram. Therefore the first boson to leave the fermion line also has to be the last to attach. We then have the above identity. The double line signifies all possible planar boson exchanges. This is just the full fermion propagator which is given by the self energy on the left side. This equation therefore closes.

N-limit, see Fig. 1.16. The equation is given by

$$\Sigma(k) = \lambda^2 \int \frac{\mathrm{d}^3 p}{(2\pi)^3} \frac{D(k-p)}{G_0^{-1}(p) - \Sigma(p)}. \tag{1.67}$$

Motivated by the $v_F \to 0$ flow the authors of [62] propose a Σ independent of k_x and write that order by order this does not produce a k_x dependence. They find a consistent solution in the IR, close to $d = 3$ that is independent of k_x and in agreement with Eq. 1.66 with a constant f.

1.4.6 Fermion flavor expansion: vector small N_f limit

We now describe the approximation pursued in this thesis. Instead of expanding in large N_f and rescaling the coupling constant by $1/\sqrt{N_f}$ we can keep the coupling independent of N_f and study the small N_f limit. Expanding in small N_f might seem less natural than the large N_f expansion since physical theories are only defined for positive integers N_f. There is a sequence of physical theories approaching the limit $N_f \to \infty$. For $N_f \to 0$ there is no such sequence. One can however define expectation values for any $N_f \in \mathbb{C}$ at any finite order in perturbation theory in a natural way. At order F in perturbation theory, any physical observable $\mathcal{O}$ (n-point functions of $\psi_i^\dagger, \psi^i$ and ϕ), as calculated in a proper theory with N_f a positive integer, is a polynomial in N_f:

$$\langle \mathcal{O} \rangle_F = \sum_{i=0}^{F} \lambda^i \sum_{j=0}^{i} N_f^j c_{ij}. \tag{1.68}$$

The summand at order j corresponds to all diagrams with j flavor indices summed over. These are the diagrams with j fermionic loops. These polynomials provide a natural extension to $N_f \in \mathbb{C}$. We define the polynomial $E_{\mathcal{O}}^{(F)}(N_f)$:

$$E_{\mathcal{O}}^{(F)}(N_f) = \sum_{i=0}^{F} \lambda^i \sum_{j=0}^{i} N_f^j c_{ij} \tag{1.69}$$

where the coefficients c_{ij} are defined by the perturbative expansion of the expectation value of $\mathcal{O}$ as in Eq. 1.68. These polynomials are now defined for all $N_f \in \mathbb{C}$. We denote the large F limit of this by $E_{\mathcal{O}}(N_f) = \lim_{F \to \infty} E_{\mathcal{O}}^{(F)}(N_f)$ and we write

$$E_{\mathcal{O}}(N_f) = \sum_{i=0}^{\infty} N_f^i c_i(\lambda) \tag{1.70}$$

For a theory with $N_f \in \mathbb{N}^+$ fermion flavors, the expectation value of $\mathcal{O}$ is then formally given by $E_{\mathcal{O}}(N_f)$. As we noted in Section 1.3.7, the large F limit might however not exist and this should not be taken literally[8].

If, however, the expansion in (1.70) converges for some $N_f = n$ (e.g. a positive integer corresponding to a physical theory) then the large F limit is guaranteed to exist for all $\{N_f \in \mathbb{C} : |N_f| \leq n\}$ and additionally the function $E_{\mathcal{O}}(N_f)$ is analytic in this disc. We will later in this section give a heuristic argument for why this is not the case. For reasons described in Section 1.3.7 we believe it is still interesting to study an expansion around $N_f = 0$ even if only an asymptotic expansion can be found. We will thus continue studying the function $E_{\mathcal{O}}(N_f)$ but keep in mind that the large F limit might only work asymptotically in the UV.

Equipped with this definition we can now formally define the $N_f \to 0$ limit of an expectation value as a limit of the function $E_{\mathcal{O}}(N_f)$. Calculating an expectation value in the $N_f \to 0$ limit amounts to summing up all diagrams without fermionic loops. Corrections at order N_f^L are found by summing up all diagrammatic contributions with L fermionic loops.

---

[8]Additionally, each $c_i(\lambda)$ is given by an infinite series that is not guaranteed to converge, however since the full perturbative series is split into a sum over both orders of the coupling constant and orders of N_f, one could expect that any divergence of the full perturbative expansion is somewhat tamed by this split and only occurs once both sums are performed. It indeed turns out that $c_0(\lambda)$ has finite radius of convergence in λ for all fermion n-point functions as we find in Chapter 4

When calculating the $N_f \to 0$ limit in this way, we are taking this limit before the low-energy limit and the large F limit. We noted in Section 1.3.8 that we lose information about the IR in doing this, so to get the true IR physics we need to either keep adding N_f corrections or figure out what part of these limits do not commute. We study this in Chapter 3.

Note that using the function $E_{\mathcal{O}}(N_f)$, one can formally define expectation values of e.g. $\psi_5^\dagger \psi_5$ for all N_f even though there clearly is not a fifth fermion flavor when $N_f < 5$. $\psi_5^\dagger \psi_5$ however is physical for $N_f \geq 5$ and it is given by a unique polynomial of N_f at each order of perturbation theory and this polynomial can still be evaluated at $N_f < 5$.

Similarly to how Freeman Dyson argued that QED observables can not be analytic functions of the electromagnetic coupling constant e [64], we can make an argument that the quantum critical metal observables are not analytic in the fermion flavor number. Dyson argued that for a negative e^2, opposite charges repel and through pair creation one can create configurations with lower energy than the vacuum. The vacuum thus breaks down for any negative e^2 and observables can thus not be analytic around $e^2 = 0$. To make a similar argument about analyticity around $N_f = 0$ for our theory we need an interpretation for negative N_f.

Consider, for contradiction, a theory as (1.37) but where $\psi_i^\dagger$ and ψ_i are not fermionic fields, but two components of a complex boson. Now we consider the perturbative expansion of an observable $\mathcal{O}_n$ of this theory. We will restrict ourselves to an operator of the form

$$\mathcal{O}_n = \prod_{i=1}^{n} \sum_{j_i=1}^{N_f} \psi_{j_i}(z_i) \psi_{j_i}^\dagger(w_i) \tag{1.71}$$

Differentiating with respect to the coupling constant gives a product of the interaction term. To construct diagrams we contract fields in all possible combinations. For fermions we would get a factor -1 every time we exchanged the order of two fermionic fields, but now with bosons this factor is 1. This is the only difference between the perturbative expansion of bosons and fermions. Now which diagrams will differ between the fermions and bosons? To calculate this we consider general fields $\psi_i^\dagger, \psi_i$ that obey

$$\psi_{i_1}(z_1)\psi_{i_2}(z_2) = \alpha \psi_{i_2}(z_2)\psi_{i_1}(z_1) \tag{1.72}$$

where $\alpha \in \{-1, 1\}$ and similarly where one or both fields have daggers.

Consider a diagram contributing to $\langle \mathcal{O}_n \rangle$ at order λ^F:

$$\langle \mathcal{O}_n \rangle_L = \langle \mathcal{O}_n \prod_{i=1}^{L} \sum_{j_i} \int \mathrm{d}^3 z \lambda \phi(z_i) \psi_{j_i}^\dagger(z_i) \psi_{j_i}(z_i) \rangle_0 \qquad (1.73)$$

This free-theory expectation value is evaluated by a sum of all possible contractions of these fields. We will now only focus on the part of these contractions that depend on α so we will omit the integrals and the field ϕ. There are $n + F$ fields $\psi_i^\dagger$ and each will be contracted with one of the $n + F$ fields ψ_i. This defines a permutation $\sigma \in S_{n+F}$ and we will sum over all such permutations. We can reorder the fields of (1.73) so that all contractions are between neighboring fields and thus independent of α. This reordering can be decomposed into the transpositions making up the permutation σ. Each transposition of fields will give a factor α. In the end we then have

$$\langle \mathcal{O}_n \rangle_F = ... \sum_{\sigma \in S_{n+L}} \alpha^{n+\sigma} \sum_{j_1,...,j_{n+L}} \prod_{i=1}^{n+L} \langle \psi_{j_i}^\dagger \psi_{j_\sigma(i)} \rangle_0 \qquad (1.74)$$

where by α^σ we mean α raised to the power of the number of transpositions making up σ. The reason we get σ^n is because the field-pairs in the definition of $\mathcal{O}_n$ are ordered opposite to that of the interaction term[9]. The number of transpositions making up a permutation is not unique, however the parity is and since $\alpha^2 = 1$ only the parity matters. We refer to this parity as the parity of the permutation. Each $\langle \psi_i^\dagger \psi_j \rangle_0$ is proportional to δ_i^j which constrains the sums over j_i. Each permutation can be decomposed into a set of cycles. We will consider elements fixed by the permutation to be in a one-element cycle. Each cycle, regardless of its length, will only contribute a single sum over N_f since the contractions fix the indices to be the same throughout each cycle. Each permutation will then have an N_f dependence of the form $N_f^{n_{\mathrm{cyc}}(\sigma)}$ where $n_{\mathrm{cyc}}(\sigma)$ is the number of cycles in σ. A permutation is odd if and only if it is composed of an odd number of even-length cycles. We denote the number of odd-length cycles by n_{odd} and the number of even-length cycles by n_{even}. We have $n_{\mathrm{odd}} + n_{\mathrm{even}} = n_{\mathrm{cyc}}$. The summed length of all cycles is $n + L$ since that is the number of vertices being permuted. If $n + L$ is odd, then n_{odd} is

---

[9]We could have defined the operator the other way around to avoid this however the above definition makes a generalization we perform later more elegant.

also necessarily odd, and the converse is true as well. We see from (1.73) that for L odd, the path-integral over ϕ is odd and the right hand side is 0. Therefore we can assume L to be even. To summarize we have

$$\alpha^{n+\sigma} = \alpha^{n+n_{\text{even}}} = \alpha^{n+n_{\text{cyc}}-n_{\text{odd}}} = \alpha^{n+n_{\text{cyc}}-n-L} = \alpha^{n_{\text{cyc}}}. \qquad (1.75)$$

Since n is fixed by the chosen operator $\mathcal{O}_n$, we have that parity of σ is fixed by the parity of n_{cyc} for all diagrams contributing to $\langle \mathcal{O}_n \rangle$ at all orders. This means that we can write[10]

$$\langle \mathcal{O}_n \rangle = \sum_{i=1}^{\infty} (-\alpha N_f)^i c_i, \qquad (1.76)$$

where the coefficients c_i depend on the details of the operator but are independent of both N_f and α. We can now define a number $\mathfrak{N}_f = -\alpha N_f$ that characterizes our theory both in terms of statistics and flavor number. We see that (1.76) is precisely the function $E_{\mathcal{O}_n}$ we defined earlier but now evaluated for the variable $\mathfrak{N}_f$. We thus have that for a physical theory of either N_f flavors of fermions *or* bosons[11] we have that

$$\langle \mathcal{O}_n \rangle = E_{\mathcal{O}_n}(\mathfrak{N}_f) \qquad (1.77)$$

The theory of bosons we have now considered contains bosonic modes inside the "FS" with negative energy and outside the "FS" with positive energy. For fermions this just means that the fermionic modes are occupied and the excitations are the holes. For bosons there is no limit to the occupation number of modes within the "FS". This theory is thus unstable towards infinite occupation of these modes and we do not have the correct vacuum of the theory. As in Dyson's argument we therefore do not expect the perturbative series to converge for any negative integer $\mathfrak{N}_f$. This means that the radius of convergence for $\mathfrak{N}_f$ in the large F limit is less than or equal to 1, $R \leq 1$. The perturbative expansion for any integer $\mathfrak{N}_f > 1$ therefore also diverges. See Figure 1.17. The strict inequality means that it is still possible that a theory with a single species of fermions is convergent.

---

[10]Another way to arrive at this result is to add sources to the fields $\psi^\dagger$ and ψ and integrate them out. All expectation values can still be obtained from differentiating w.r.t. the sources. The integral gives a determinant with a power of $\pm N_f$, depending on if the fields are bosonic or fermionic. The other terms of the action do not depend on N_f or α if the considered operator is similarly normal-ordered.

[11]Since we are in 2+1 dimensions it would be interesting to investigate the case of $\mathfrak{N}_f \in \mathbb{C}$. One could imagine that $\mathfrak{N}_f = N_f e^{i\theta}$ would correspond to a theory of anyons with exchange statistics $-e^{\pm i\theta}$.
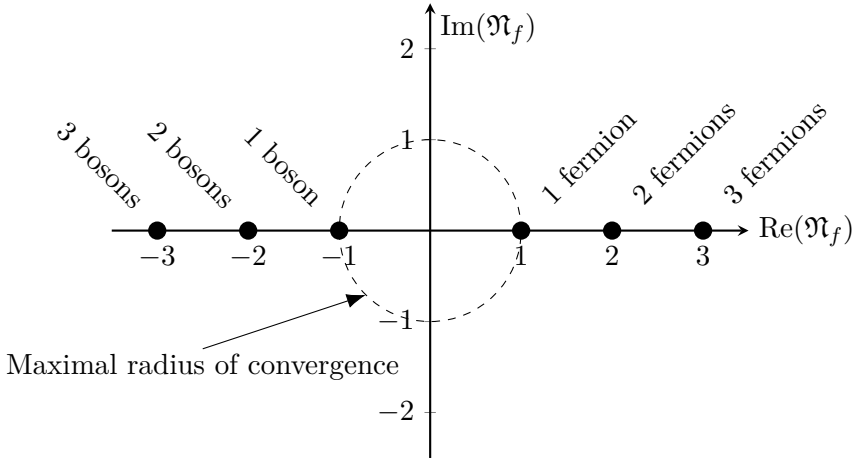
Figure 1.17. This figure shows the location of different theories in the complex $\mathfrak{N}_f$-plane. The bosonic theories are unstable and therefore the expansion around $\mathfrak{N}_f = 0$ is not expected to converge for $\mathfrak{N}_f = -1, -2, -3, \ldots$. This constrains the radius of convergence to at most include one of the fermionic theories.

1.5 This thesis

We now apply this small N_f limit to a study of the quantum critical metal. In Chapter 2 we calculate the fermion two-point function of the action in Eq. 1.37 in the ordered limit of first small N_f and then low energies. The fermion is essentially one-dimensional in this limit and we can find the fermion Green's function with a background field ϕ. Integrating out this field yields the non-perturbative fermion two-point function. This calculation is done in real space and we proceed by Fourier transforming to momentum space. An implicit expression for fermion-self energy is found. The dispersion is not monotonic and the momentum distribution function continuous so this is a non-Fermi liquid state. This chapter is based on [65].

We expand on this work in Chapter 3 by considering a more general limit where both $N_f \to 0$ and $k_F \to \infty$ with their product finite. It is found that fermionic loops with two vertices need to be included in this limit but a similar method to that of Chapter 2 can be used. It is found that taking the $N_f k_F \to 0$ limit (which corresponds to what was studied in the previous chapter) does not commute with the Fourier transform. The momentum distribution function still shows a non-Fermi liquid behavior

but the non-monotonicity is not found for any $N_f k_F$. The IR is given by a complicated function but governed by the scaling $\omega^2 \sim k_x^3$ as for the RPA results. This chapter is based on [66].

In Chapter 4 we again consider the ordered limit of Chapter 2 but now find a closed form expression for general fermion n-point functions. We use this to calculate the fermion density-density correlator and find an exponential decay of Friedel oscillations in the separation. This is contrary to the power-law decays found in Fermi liquids. This work is to be submitted [67].

In Chapter 5 we study a special case where the Fermi velocity is equal to the boson velocity, but we do so for a more general theory than the $N_f \to 0$ limit. We consider a general limit where fermionic loops are suppressed. We find that the additional symmetry provided by the equal velocities can be used to find many properties of the fermion two-point function, including the non-monotonic dispersion found in Chapter 2. This work is to be submitted [68].

Chapter 2

Non-perturbative emergence of non-Fermi liquid behaviour in $d = 2$ quantum critical metals

2.1   Introduction

A complete classification of infrared universality classes for phases of quantum matter at finite density is an open problem in condensed matter theory. Experimentally, a number of fermionic states of matter that exhibit breakdown of the quasiparticle Fermi-liquid paradigm [69] are known to exist, e.g. the strange metallic phase of unconventional superconductors [70] or the non-Fermi liquid phase of graphene [71, 72]. Theoretically, however, they are not understood. These phases are strongly interacting and this prevents the use of most conventional approaches that rely on perturbation theory.

One important scenario which is widely believed to cause the partial destruction of Fermi surfaces and substantial change of transport properties of the electronic state in high-T_c compounds [73], heavy fermion systems [74], and Mott insulators [75, 76] is the interaction of electronic quasiparticles with gapless bosons. The underlying physics is the proximity of a quantum critical point and these bosons are the protected emergent gapless collective degrees of freedom [77–79]. The nature of the fermion-

boson interaction is determined by the precise details of the quantum critical point — ferromagnetic [80] or antiferromagnetic [81] spin density waves, Kondo impurities [82], etc; see [83] for a review.

Qualitatively the simplest model that should already capture the nontrivial physics is the theory of spinless fermions at finite density interacting with a massless scalar through a straightforward Yukawa coupling. The action of this theory is:

$$S = \int \mathrm{d}x \mathrm{d}y \mathrm{d}\tau \left[\psi^\dagger \left(-\partial_\tau + \frac{\nabla^2}{2m} + \mu \right) \psi + \frac{1}{2} \left(\partial_\tau \phi \right)^2 + \frac{1}{2} \left(\nabla \phi \right)^2 + \lambda \phi \psi^\dagger \psi \right].$$
(2.1)

This model is believed to describe the Ising-nematic transition (see e.g. [79, 84]), observed for example in $YBa_2Cu_3O_y$, There, the meaning of the boson is the fluctuating order parameter related to the $C_4 \to C_2$ symmetry breaking of the electronic correlations. In the ordered phase the mass square of the boson is positive $M^2 > 0$, while in the disordered phase $M^2 < 0$. For non-zero mass we obtain a regular Fermi-liquid at low frequency. By choosing $M = 0$ we tune our theory to criticality where we expect non-Fermi liquid behavior. The model is also closely related to the theory of fermionic spinon excitations in a spin density wave minimally coupled to $U(1)$; at low energies only the transverse component of the gauge field survives and acts as the scalar above (see e.g. [85]).

Eq. (2.1) and related models of finite density fermions coupled to critical bosons were first studied in detail by Hertz [77] and Millis [78], but their results do not apply in 2+1 dimensions. For $d = 2$ the coupling λ is relevant [79], and can drive the system to a qualitatively new groundstate. This novel non-Fermi liquid groundstate is out of range of perturbation theory, and the fermion sign problem prevents us from using efficient numerical techniques.

Our work continues on a recent revival of interest in determining this groundstate. The crucial physics that is thought to control the non-Fermi liquid behavior is the Landau damping: the quantum fermion-loop corrections to the boson two-point correlation function/self-energy. By extending the model to an arbitrary number of fermions N_f and bosons N_b, one can enhance this physics in a limit where the number of fermion flavors N_f is much larger than the number of bosonic degrees of freedom ($N_f \gg N_b$); it is easily seen at the one loop level that this enhances the "Landau-damping" diagram in Fig. 2.1(b) compared to the self-energy Fig. 2.1(a).

(a) (b)
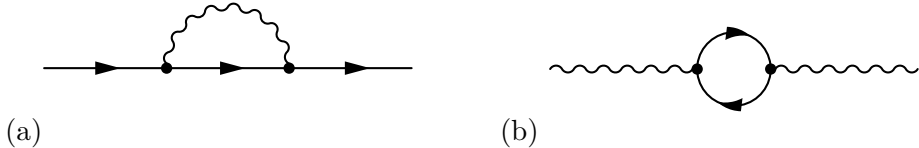
Figure 2.1. One loop corrections to fermion (a) and boson (b) self-energies due to Yukawa interaction. For a gapless boson (b) is the one loop contribution to Landau damping: this contribution to the self-energy can dominate in the IR. This term (b) is clearly proportional to the number of fermions N_f in contrast to the one-loop correction to the fermion self-energy (a). In the limit $N_f \gg N_b$ the boson self-energy/Landau damping therefore dominates, whereas it is suppressed in the opposite limit $N_f \ll N_b$.

In this $N_f \gg N_b$ regime the problem of a Fermi surface coupled to the Ising nematic and spin density wave order parameters has been considered in [84, 86] and an extensive perturbative renormalization group analysis has been performed up to three loops (higher order effects are investigated in [87, 88]). However, as pointed out in these papers and [85], in the (vector) large N_f expansion one still needs to sum infinitely many diagrams. (A well-defined expansion can be obtained by introducing an arbitrary dynamical critical exponent for the boson, z_b, as an extra control parameter [89].)

Here, however, we show that Landau damping is not essential to obtain exotic non-Fermi liquid physics in the IR. We will study correlation functions of the theory in the opposite limit $N_f \to 0$; $N_b = 1$. This so-called quenched limit discards all fermion loop contributions. As $N_f \ll N_b$ it shares common ground with recent matrix large N expansions of this model where the boson is taken to transform in the adjoint of an $SU(N)$ and the fermions in the fundamental, see e.g. the studies [90–93], but the strict quenched limit is more comprehensive. In the matrix large N limit where $N_f = N$ and $N_b = N^2$ with $N \gg 1$, not only the diagrams with fermion loops but also diagrams with crossed boson lines are suppressed (Fig. 2.2), whereas these are kept in the quenched approximation. By inspection of the associated momentum integral it is clear, however, that crossed boson corrections are important contributions to the IR physics. The IR of the quenched theory will therefore be different from the large N matrix limit and perhaps closer to that of the full theory.

Physically the quenched approximation we study here means the fol-

59
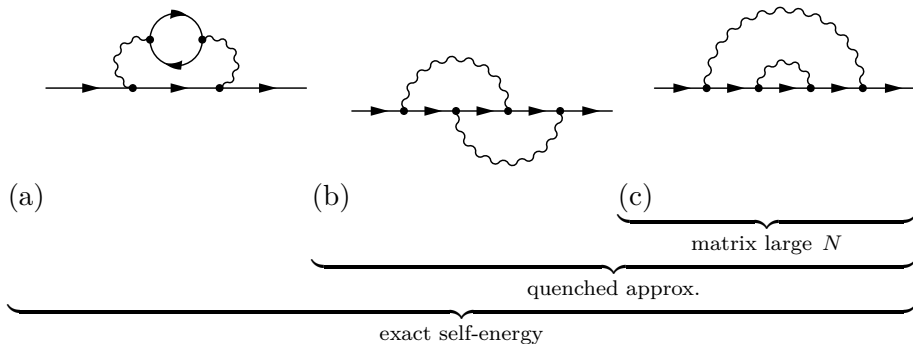
Same diagrams in double line notation:
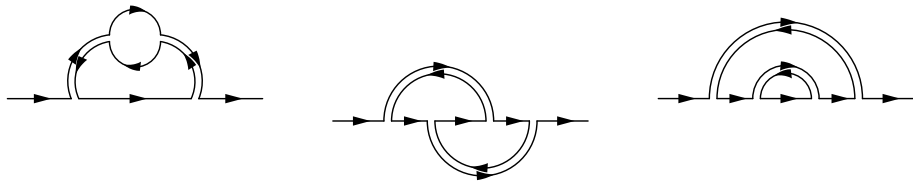
Figure 2.2. The two-loop contributions to the fermion self-energy in theory in Eq. (2.3). The quenched limit where $N_f \to 0$ only suppresses the fermion loop contribution Fig. (a), whereas matrix large N limits, where the boson is a $N \times N$ matrix $\phi_i{}^j$ and the fermion a N-component vector ψ_i also suppress crossed diagrams of type (b). This is evident in double line notation of the same Feynman diagrams where the fermion is written as a single line (it has one index) and the matrix-valued boson as two lines (it has two indices). Indices have to match at interactions; each closed loop therefore corresponds to a sum over this index and gives a weight N to the diagram. We then see that the crossed diagram has no loops and is thus sub-dominant in N to other diagrams at the same order in the coupling constant.

lowing: as pointed out in [93] there is a distinct energy scale where Landau damping becomes important. This is the scale where the fermion one-loop correction proportional to N_f becomes comparable to the leading boson dispersion — this happens at $E_{\text{LD}} \sim \sqrt{\lambda^2 N_f k_F}$ (see the end of section 2.2.1). By considering small N_f we are suppressing this scale and we are zooming in on the energy regime directly above the Landau damping scale E_{LD} (see Fig. 2.3).[1]

The quenched approximation has an additional benefit. Under the assumption that that the cut-off of the boson is much smaller than the Fermi momentum ($k_F \gg \Lambda_{\text{UV}}$), the small N_f limit also allows us to consistently focus on a small local patch (see Fig. 2.3) around the Fermi surface where the fermionic excitations disperse linearly. The reason the curvature effects are negligible and the global structure of the Fermi surface becomes irrelevant, is that their influence on the IR physics is also through Landau damping. If the Landau damping is not negligible, one does have to either work with the full Fermi surface (i.e. in [90–93] for the case of spherical Fermi surface) or at least consider the antipodal patch since the dominant contribution is coming from there [84, 86]. Specifically, as we discuss below, Landau damping depends both on the Fermi-surface curvature $\kappa \sim \frac{1}{k_F}$ and N_f as N_f/κ. After the quenched approximation $N_f \to 0$ for fixed κ, we may subsequently take κ small as well.

The remarkable fact is that with these approximations the fermion Green's function can be determined exactly (directly in $d = 2$ spatial dimensions). We achieve this by solving the differential equation for the Green's function in a background scalar field and then evaluating the bosonic path integral. Similar functional techniques have been used in high energy physics, for example in the study of high temperature QED plasma [94], lattice QCD [95] or for solving the so-called Bloch-Nordsieck model (which is QED in the quenched approximation) [96–100]. In condensed matter context, the fact that the fermion spectral function is exactly solvable in these limits was also observed for finite density fermions coupled to a transverse gauge field by Khveshchenko and Stamp [101] and independently by Ioffe, Lidsky, Altshuler and Millis [102, 103], though the latter solve the model by bosonization.

At the technical level, the reason the spectral function can be solved exactly in the quenched limit is that propagators of linearly dispersing

---

[1]There are other ways to suppress the Landau damping physics, e.g. by considering large (UV) Fermi velocity, but we will not be considering these cases here.
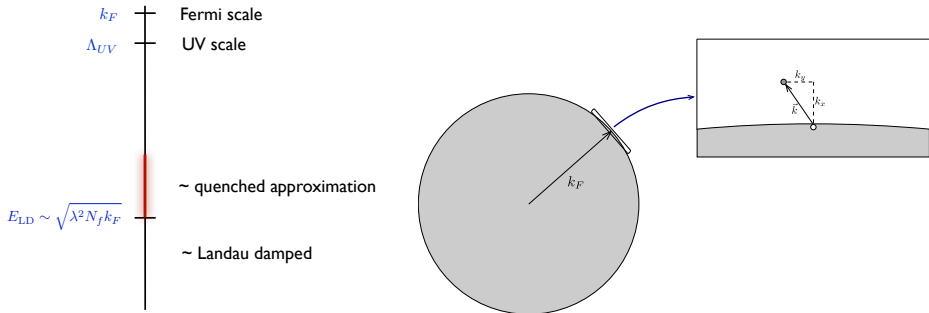
Figure 2.3. Left: The energy scales relevant to 2+1 dim. finite density fermions coupled to a massless boson. We assume the theory is already truncated at a UV cut-off Λ_{UV} lower than the Fermi scale k_F. The quenched $N_f \to 0$ limit focuses in on the intermediate energy regime right above the scale $E_{\mathrm{LD}} \sim \sqrt{\lambda^2 N_f k_F}$ where Landau damping becomes important.
Right: A small patch of the Fermi surface. In a small region near the Fermi level the surface curvature is negligible. Fermionic excitations can acquire both orthogonal k_x and tangent k_y momenta, but the latter does not contribute to the kinetic energy of the excitation. In the $N_f \to 0$ limit each patch decouples from other parts of the Fermi surface.

fermions (the local patch approximation) obey special identities. These allow a rewriting of the loop expansion in such a way that it can be resummed completely, or rather that it can be recast as the solution to a tractable differential equation. We show this in section 2.2. Note, that our method does not rely on renormalization group techniques. When we are to define an RG flow, we have to choose a proper decimation scheme. In relativistic field theories, it is natural to define the cut-off in a way that maintains the Lorentz invariance, while for the non-relativistic model of critical metals the choice of the cut-off is ambiguous, see e.g. [90].

These exact results in quenched approximation then allow us to establish that the IR fermion physics, even in the absence of Landau damping, is already that of a non-Fermi liquid. Specifically we show in section 2.3 that:

- The naive free Fermi surface breaks apart into three. A thin external shell of it splits apart from the rest, and we effectively have
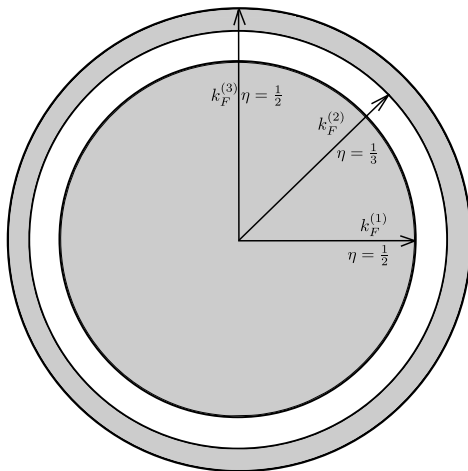
Figure 2.4. The emergent Fermi surface structure at low energy in the 2+1 dimensional quenched planar patch quantum critical metal. Due to the interactions the naive single Fermi surface is topologically unstable. The excitations around the Fermi surfaces are not well-defined quasiparticles, instead they have a continuous spectrum corresponding to a Green's function of the type $G(\omega, k) \sim (\omega - vk)^{-\eta}$ with scaling dimensions η. The different values of η at each of the emergent singular surfaces are mentioned.

three nested singular surfaces (see Fig. 2.4). This immediately follows from the fact that in a region around the original (free) Fermi level the dispersion of fermion changes sign, $\frac{d\omega}{dk_x} < 0$. This can be interpreted as a topological instability of the Fermi surface [87], as the dispersion curve must cross the Fermi energy two more times to connect to the free UV theory. Luttinger's theorem nevertheless continues to hold.

- The Fermi-liquid quasiparticle pole is destroyed by the interaction with the critical boson. Instead the spectrum is singular everywhere on the dispersion curve. Specifically near the three Fermi surfaces the singular Green's function takes a scaling form with different scaling dimensions. Around the original Fermi momentum the Green's function behaves as $G(\omega, k_x) \sim (\omega + ck_x)^{-1/3}$, where c is the dispersion velocity of the boson; around the two split-off Fermi surfaces behaves as $G(\omega, k) \sim (\omega - v^* k_x)^{-1/2}$ with v^* an emergent dispersion velocity $0 < v^* < v_F$.

We conclude this chapter with a brief outlook in section 3.6.

2.2 2+1 dimensional quantum critical metals in the patch approximation

As stated, the theory we study is that of N_f spinless fermionic flavours at finite density minimally coupled to a critical (relativistically dispersing) boson in $2 + 1$ dimensions. It has the Euclideanized action

$$S = \int \mathrm{d}x\mathrm{d}y\mathrm{d}\tau \left[\psi_j^\dagger \left(-\partial_\tau + \frac{\nabla^2}{2m} + \mu \right) \psi^j + \frac{1}{2} \left(\partial_\tau \phi \right)^2 + \frac{1}{2} \left(\nabla \phi \right)^2 + \lambda \phi \psi_j^\dagger \psi^j \right]$$

$$(2.2)$$

with $j = 1 \ldots N_f$; we will show below that the rotation back to real time has no ambiguities. Assuming that the theory is still weakly coupled at scales much below the Fermi momentum k_F, we may make a local approximation around a patch of the Fermi surface and truncate the fermion kinetic term to (Fig. 2.3) [79]

$$S_P = \int \mathrm{d}x\mathrm{d}y\mathrm{d}\tau \left[\psi_j^\dagger (-\partial_\tau + iv\partial_x)\psi^j + \tag{2.3}$$

$$+ \frac{1}{2} \left(\partial_\tau \phi \right)^2 + \frac{1}{2} \left(\partial_x \phi \right)^2 + \frac{1}{2} \left(\partial_y \phi \right)^2 + \lambda \phi \psi_j^\dagger \psi^j \right]. \tag{2.4}$$

Two comments are in order. (1) Though it is very well known that the leading "Fermi surface curvature" correction to the kinetic term $\mathcal{L}_{\mathrm{curv}} = -\kappa \psi_j^\dagger \partial_y^2 \psi^j / 2 + \ldots$ is a dangerously irrelevant operator important for fermion loops even at low energies, in the $N_f \to 0$ limit (where there are no fermion loops) this operator is safely irrelevant and can be consistently neglected for physics below the scale set by $1/\kappa$. We will show here through exact results that the minimal theory in Eq. (2.3) already has a very non-trivial IR. We shall comment on the relevance of $\mathcal{L}_{\mathrm{curv}}$ to our results below. (2) From a Wilsonian point of view, self-interactions of the boson should also be included. We leave the effect of this term for future investigations and take the action S_P as given from here on and study it on its own.[2]

---

[2]Note that, although the kinetic term is effectively (1+1)-dimensional, the properties of fermionic field are still strongly dependent on the dimensionality of the system, because the fermions interact with the $(d + 1)$-dimensional boson. An instructive way to think about the fermion dynamics in dimensions parallel to the Fermi surface, is to

Throughout this chapter we are mostly interested in the case where the characteristic speed $c = 1$ of the critical bosonic excitations is larger than the Fermi velocity, $c > v$. This need not be the case in the UV. However, as was recently argued [91, 93], the Fermi velocity decreases substantially under the RG flow and because in our analysis we consider energies below a cut-off $\Lambda_{\mathrm{UV}} \ll k_{\mathrm{f}}$, we take this condition for granted as a starting point.

In $d = 2$ spatial dimensions the Yukawa coupling is relevant — λ has scaling dimension $1/2$ — and the theory will flow to a new IR fixed point. Rather than focusing on a complete understanding of the IR of the action Eq. (2.3), we will focus only on understanding a single correlation function: the fermion spectral function. Coupling the fermionic fields to external sources

$$Z[J, J^\dagger] = \int \mathcal{D}\psi^j \mathcal{D}\psi_j^\dagger \mathcal{D}\phi \exp\left(-S_P - J_j^\dagger \psi^j - \psi_j^\dagger J^j\right), \qquad (2.5)$$

the fermionic integral is Gaussian and can be easily evaluated yielding

$$Z[J] = \int \mathcal{D}\phi \, \exp\left(-S_b[\phi] - S_{\mathrm{det}}[\phi] - \int d^3z d^3z' \, J_i^\dagger(z) G_j^i[\phi](z; z') J^j(z')\right) \qquad (2.6)$$

with

$$S_b = \int \mathrm{d}x \mathrm{d}y \mathrm{d}\tau \left[\frac{1}{2}\left(\partial_\tau \phi\right)^2 + \frac{1}{2}\left(\partial_x \phi\right)^2 + \frac{1}{2}\left(\partial_y \phi\right)^2\right]$$

$$S_{\mathrm{det}} = \int \mathrm{d}x \mathrm{d}y \mathrm{d}\tau \left[-N_f \mathrm{Tr} \ln G^{-1}[\phi]\right] \qquad (2.7)$$

and $G^i_{\ j}[\phi](z; z') = \delta^i_j G[\phi](\tau, x, y; \tau', x', y')$ is the fermionic propagator in presence of a background bosonic field configuration. By definition it satisfies

$$\left(-\partial_\tau + iv\partial_x + \lambda\phi(\tau, x, y)\right) G[\phi](\tau, x, y; \tau', x', y') = \qquad (2.8)$$

$$= \delta(\tau - \tau')\delta(x - x')\delta(y - y') \qquad (2.9)$$

Fourier transform in those directions. Because the kinetic term does not depend on these directions, the parallel momenta act as additional global quantum numbers. E.g. in $d = 2$, one therefore has an infinite set of one-dimensional fermionic subsystems, labeled by k_y. The Yukawa interaction with the bosons then describes the interactions between these many one-dimensional subsystems.

Taking functional derivatives with respect to the sources, the full fermion Green's function is then given by a path integral over only the bosonic field:

$$\langle \psi_j^\dagger(z)\psi^i(0)\rangle_{\text{exact}} = \delta_j^i G(z,z') = \delta_j^i \frac{\int \mathcal{D}\phi\, G[\phi](z,z') e^{-S_b[\phi]-S_{\text{det}}[\phi]}}{\int \mathcal{D}\phi\, e^{-S_b[\phi]-S_{\text{det}}[\phi]}}. \quad (2.10)$$

2.2.1   The $N_f = 0$ quenched approximation and Landau damping

We will evaluate this integral in the quenched or Bloch-Nordsieck approximation. This is a well known ad hoc approximation in lattice gauge theory [95] and finite temperature QED [96–98, 100] whereby all contributions from S_{det} are ignored: one sets the one-loop (fermion) determinant to one by hand. In our context we can make this approximation precise. Eq. (2.7) shows that S_{det} is directly proportional to N_f, whereas no other terms are. From Eq. (2.10) it is then clear that this approximation computes the leading contribution to the full fermion Green's function in the limit $N_f \to 0$. Note that we consider the N_f limit within correlation functions and not directly in the partition function.

Diagrammatically this means that one considers only contributions to the full Green's functions that do not contain fermion loops. Fermion loop corrections to the bosonic propagator, however, encode the physics of Landau damping. As discussed, this is important in the deep infrared and requires treatment of the dangerously irrelevant quadratic corrections to the kinetic term $\mathcal{L}_{\text{curv}}$ due to Fermi surface curvature. It is its Landau damping contribution that redirects the RG flow. This can be seen from the one-loop "polarization" correction Π to the boson-propagator at finite N_f.

$$G_B^{-1} = G_{B0}^{-1} + \Pi = q_0^2 - q_x^2 - q_y^2 + \Pi \quad (2.11)$$

The form of the polarization depends on the concrete form of the Fermi surface. In case of a spherical Fermi surface with Fermi momentum k_F its form at the one-loop level for large k_F equals

$$\Pi_{1S}(q_0, q_x, q_y) = \frac{(2\pi)^2 \lambda^2 k_F N_f}{v} \left(\frac{|q_0|}{\sqrt{q_0^2 + v^2(q_x^2 + q_y^2)}} \right). \quad (2.12)$$

The Fermi surface curvature κ is inversely proportional to the Fermi momentum $\kappa \sim 1/k_F$, therefore the polarization is controlled by the

combination N_f/κ. One immediately sees that there is an energy scale $E_{\text{LD}} \sim \sqrt{\lambda^2 N_f/\kappa}$ where the polarization becomes of order of the leading boson dispersion, where perturbation theory must break down and the theory changes qualitatively.[3] On the other hand, as we explained in the introduction, above this scale E_{LD} one ought to be able to neglect these contributions to the boson propagator [93, 105]. This is therefore the regime captured by the $N_f \to 0$ limit. Since this $N_f \to 0$ limit tames the dangerous nature of irrelevant Fermi surface curvature κ, this also justifies the patch approximation and linearization of the fermion dispersion relation. In this chapter we focus on this regime; we leave the effects of Landau damping captured by the (N_f) corrections for Chapter 4.

The remarkable fact is that in this regime $G_{\text{full}}(z; z')$ can be determined exactly, as we will now show. This is because the fermion two-point function in the presence of a background field $G[\phi](z; z')$ depends on the background bosonic field exponentially. The overall path integral over ϕ therefore remains Gaussian even in presence of the Yukawa interaction. This gives us qualitatively new insight in the physics right above E_{LD}.

2.2.2 The exact fermion Green's function

First, we determine the fermion Green's function in the presence of an external boson field $G[\phi]$. Rather then working in momentum space, it will be much more convenient to work in position space. Note that because the background scalar field $\phi(\tau, x, y)$ can be arbitrary, the fermionic Green's function $G[\phi]$ is not translationally symmetric. However, translational invariance will be restored after evaluating the path integral over ϕ.

Rewriting the background dependent Green's function as

$$G[\phi](\tau_1, x_1, y_1; \tau_2, x_2, y_2) = \\ \tilde{G}_0(\tau_1 - \tau_2, x_1 - x_2, y_1 - y_2) \exp\left(-\lambda V[\phi](\tau_1, x_1, y_1; \tau_2, x_2, y_2)\right),$$
(2.13)

---

[3] One may worry that at higher loop order a different scale arises. It turns out, however, that at higher order, contributions to Π are subleading in k_F compared to the one-loop result. This is because for linearized fermion dispersion ($\kappa \to 0$) the properly symmetrized closed fermion loops with more than two fermion lines vanishes [104]. In this chapter where we take the $N_f/\kappa \to 0$ limit we therefore use the unmodified boson propagator G_{B0}.

with $\tilde{G}_0$ the translationally invariant free Green's function in real space

$$\tilde{G}_0(\tau, x, y) = -\frac{i}{2\pi} \frac{\mathrm{sgn}(v)}{x + iv\tau} \delta(y) \equiv G_0(\tau, x)\delta(y), \qquad (2.14)$$

it is readily seen that the solution to the defining Eq. (2.8) is given by

$$V[\phi](\tau_1, x_1, y_1; \tau_2, x_2, y_2) = \int \mathrm{d}x\mathrm{d}y\mathrm{d}\tau \left[\tilde{G}_0(\tau_1 - \tau, x_1 - x, y_1 - y) \right.$$
$$\left. -\tilde{G}_0(\tau_2 - \tau, x_2 - x, y_2 - y) \right] \phi(\tau, x, y), \quad (2.15)$$

To be more precise, we need to ensure that the background dependent Green's function (2.13) satisfies proper boundary conditions as well. We did so by considering the problem at finite temperature and volume and taking explicitly the continuum limit. The compact analog of (2.13) has to satisfy antiperiodic boundary condition along the imaginary time direction and periodic boundary condition along the spatial direction. This can be achieved by taking the periodic free fermion Green's function $(\tilde{G}_0^P)$ in the exponent Eq. 2.15 and the antiperiodic one $(\tilde{G}_0^{AP})$ in Eq. 2.13. In the continuum limit, however, their functional forms are indistinguishable, and we denote them with the same symbol $(\tilde{G}_0)$.

The insight is that the only dependence on ϕ in the background dependent Green's function is in the exponential factor $V[\phi]$ and that this dependence is linear. In combination with the quenched $N_f \to 0$ limit, the path-integral over ϕ Eq. (2.10) needed to obtain the full Green's function is therefore Gaussian, and we can straightforwardly evaluate this to (2.10) to obtain

$$G(\tau_1, x_1, y_1; 0) = G_0(\tau_1, x_1)\delta(y_1)\exp\left[I(\tau_1, x_1; 0)\right] \qquad (2.16)$$

with

$$I(\tau_1, x_1; 0) = \frac{\lambda^2}{2} \int \mathrm{d}x\mathrm{d}\tau\mathrm{d}x'\mathrm{d}\tau' M(\tau_1 - \tau, x_1 - x; -\tau, -x) \cdot \qquad (2.17)$$
$$\cdot G_B(\tau - \tau', x - x', 0) M(\tau_1 - \tau', x_1 - x'; -\tau, -x), \qquad (2.18)$$

where

$$M(\tau_1, x_1; \tau_2, x_2) = G_0(\tau_1, x_1) - G_0(\tau_2, x_2) , \qquad (2.19)$$

and $G_B(\tau - \tau', x - x', y - y') = G_B(\tau, x, y; \tau', x', y')$ equal to the translationally invariant free boson propagator defined by

$$\left(\partial_\tau^2 + \nabla^2\right) G_B(\tau, x, y; \tau', x', y') = -\delta(\tau - \tau')\delta(x - x')\delta(y - y') . \quad (2.20)$$

Eq. (2.16) is a remarkable result. In the $N_f \to 0$ quenched approximation the full fermion Green's function still consists of a complicated set of Feynman diagrams that are normally not resummable. In particular at the two-loop level there are rainbow diagrams (Fig. 2.2(c)) and vertex-corrections of self-energies (Fig. 2.2(b)) that do not readily combine to a summable series. The reason why in this $N_f \to 0$ planar patch theory we can do so, is the existence of the following multiplicative identity of fermion propagators in the planar limit where the dynamics is effectively 1+1 dimensional.

$$G_0(\tau_1, x_1)G_0(\tau_2, x_2) = G_0(\tau_1 + \tau_2, x_1 + x_2)\left(G_0(\tau_1, x_1) + G_0(\tau_2, x_2)\right) \tag{2.21}$$

This identity follows directly from trivial equality

$$(G_0(\tau_1, x_1))^{-1} + (G_0(\tau_2, x_2))^{-1} = (G_0(\tau_1 + \tau_2, x_1 + x_2))^{-1}, \qquad (2.22)$$

and has many corollary multiplicative identities for products of $n > 2$ planar fermion propagators. The usual perturbative series and the exact result Eq. (2.16) may seem different but their equality can be proven to all orders. We do so in Appendix 2.A, thereby unambiguously establishing that this is the exact fermion two-point function in the planar theory in the quenched approximation.

2.3 The physics of the planar quenched quantum critical metal

We now show that this all order result for the fermion Green's function, albeit in the quenched $N_f \to 0$ approximation, describes very special physics. In this approximation the fermionic excitations constitute a continuous spectrum of excitations with power-law tails analogous to a critical theory; in particular, there are no distinct quasiparticle excitations. Importantly, in the low energy limit this continuous spectrum centers at three distinct momenta with different exponents for the power-law fall-off.

To exhibit this exotic physics from the exact $N_f \to 0$ Green's function (2.16), we substitute the explicit form of the boson and fermion Green's functions and Fourier transform the internal integrals. For the exponent $I(\tau, x; 0)$ we then have:

$$I(\tau, x; 0) = \frac{\lambda^2}{8\pi^3} \int d\omega dk_x dk_y \frac{\cos(\omega\tau - k_x x) - 1}{(i\omega - vk_x)^2 (\omega^2 + k_x^2 + k_y^2)} \tag{2.23}$$

This integral can be done analytically to obtain (for $v^2 \neq 1$)

$$I(\tau, x; 0) = \frac{\lambda^2}{8\pi(1 - v^2)} \left[\frac{(\tau - ivx)}{\sqrt{1 - v^2}} \log \left(\frac{\tau - ivx + \sqrt{(1 - v^2)(\tau^2 + x^2)}}{\tau - ivx - \sqrt{(1 - v^2)(\tau^2 + x^2)}} \right) \right.$$

$$\left. -2\sqrt{\tau^2 + x^2} \right]; \tag{2.24}$$

for $v^2 = 1$ one obtains

$$I_{v^2=1}(\tau, x; 0) = \lambda^2 \frac{(\tau + i\operatorname{sgn}(v)x)^2}{12\pi\sqrt{\tau^2 + x^2}}. \tag{2.25}$$

This gives us the all order $N_f \to 0$ Green's function in real space.

Analytically continuing in τ for $0 < v < 1$ yields the retarded Green's function. The physics follows from Fourier transforming this real time Green's function to momentum space; this is described in Appendix 2.C. The resulting retarded Green's function in momentum space is given by

$$G_R(\omega, k_x) = \frac{1}{\omega - k_x v + \frac{\lambda^2}{4\pi\sqrt{1-v^2}}\sigma(\omega, k_x)}, \tag{2.26}$$

where $\sigma(\omega, k_x)$ is the root, within $0 < \operatorname{Im}(\sigma) < i\pi$, of the equation

$$\frac{\lambda^2}{4\pi\sqrt{1 - v^2}}(\sinh(\sigma) - \sigma\cosh(\sigma)) + v\omega - k_x - \cosh(\sigma)(\omega - k_x v + i\epsilon) = 0 \tag{2.27}$$

A small positive parameter ϵ is introduced to identify the correct root when it otherwise would be on the real axis, which is the case for

$$(k_x + \omega)\left(\lambda^2 \sinh\left(\frac{4\pi\sqrt{1 - v^2}(vk_x - \omega)}{\lambda^2}\right) + 4\pi\sqrt{1 - v^2}(v\omega - k_x)\right) \geq 0. \tag{2.28}$$
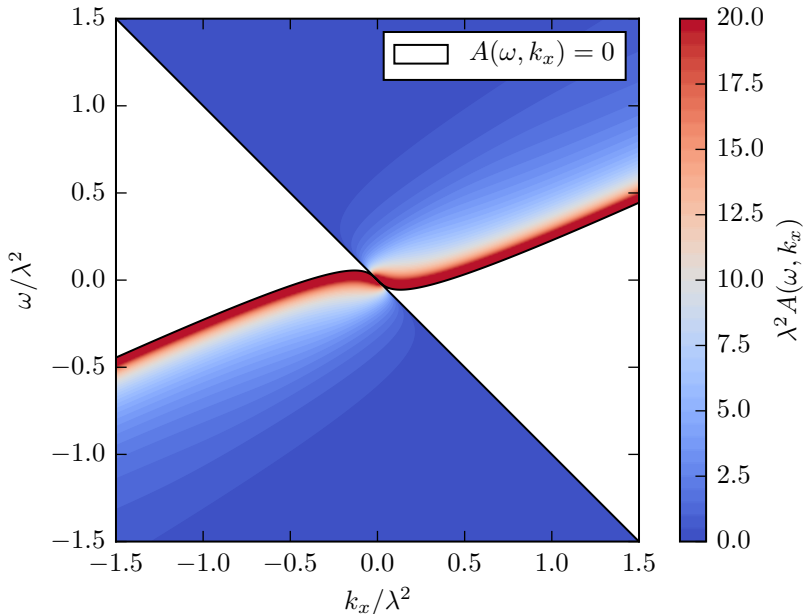
Figure 2.5. Fermionic spectral function for $v = 0.5$. It is identically zero in the white region.

Note that the center-combination $v\omega - k_x$ is correct; we are working in units in which the boson-dispersion velocity $c = 1$. The units can be made correct by restoring c.

Expression (5.24) together with (5.25) is the main technical result of the chapter. We can now extract the insights into the spectrum of fermionic excitations around the ground state of the planar quenched metal. Fig. 2.5 plots the spectral function $A(\omega, k_x) = -2\text{Im}G_R(\omega, k_x)$ as a function of the dimensionless combinations ω/λ^2, k_x/λ^2, as λ is the only scale in the problem. We immediately note that there is an obvious continuous peak, corresponding to a clear excitation in the spectrum. This excitation has the properties that:

- The dispersion relation is S-shaped in the infrared near $k_x = 0$, and now has three intersections with $\omega = 0$. A truncation of the theory to very low energies would therefore indicate three distinct Fermi surfaces. Similar topological Fermi surface instabilities due
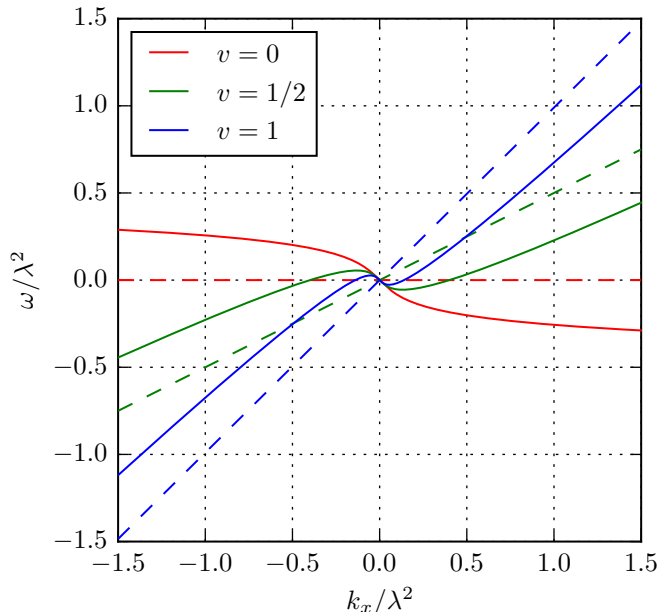
Figure 2.6. The dispersion relation (the zeros of G^{-1}) for different v in the interacting theory (solid line) and the free theory (dashed)

to electron interaction have been found e.g. in [106]. Curiously the dispersion is nearly identical to the one-loop result.

- As has been demonstrated before by means of a perturbative renormalization group analysis [91], we see the speed of fermions v decreases as we go from high to low frequency/momentum. The distinct S-shaped curve is outside of the regime of perturbation theory, however. With the exact result we see that the emergent Fermi-velocity at the innermost ($k_x = -k_x^* < 0$) and the outermost ($k_x = k_x^* > 0$) Fermi surfaces is non-universal, but positive and depends on the UV fermionic velocity v. These Fermi-surfaces are therefore particle-like.

  However, the reverse of direction due to the S-shape shows that the Fermi velocity at the emergent Fermi-surface at the original Fermi-momentum $k_x = 0$ is now in the opposite direction and the surface is therefore hole-like. Moreover, the value of the emergent Fermi-velocity at $k_x = 0$ is universal: it equals the boson-velocity $v_F = -1$

at $k = 0$ (near the middle Fermi surface), independent of the UV fermionic velocity v (Fig. 2.6). A way to perceive what happens is that the hole-like excitations at $k_x = 0$ become tied to the critical boson which completely dominates the dynamics.

- The three emergent Fermi surfaces are symmetric around $k_x = 0$; the hole-like one is at $k_x = 0$ and as follows from Eq. (5.24) and (5.25) the two particle-like ones are symmetrically arranged at $\pm k_x^*$. The precise value of k_x^* depends on the initial fermi velocity v. In the planar approximation where the Fermi surface is infinite in extent, this guarantees that Luttinger's theorem holds: the original Fermi surface (the region $-\infty < k_x < 0$) has the same volume as the emergent two regions enclosed by Fermi surfaces ($-\infty < k_x < -k_x^*$ and $0 < k_x < k_x^*$).

- The spectral function, $A(\omega, k_x) = -2\text{Im}G_R(\omega, k_x)$, is identically zero for the range of ω and k_x whenever $\sigma(\omega, k_x)$ is exactly real. This is whenever Inequality (2.28) is satisfied. Such a large range of zero-weight may seem to violate unitarity. As a consistency check, however, it can be demonstrated that the Green's function satisfies the sum rule for all v (Appendix 2.D)

$$\int\limits_{-\infty}^{\infty} \mathrm{d}\omega A(\omega, k_x) = 2\pi, \ \forall k_x \tag{2.29}$$

- Importantly, the weight of the spectral function is infinite at all points of the dispersion relation. Substituting the implicit dispersion relation $\sigma = \frac{4\pi\sqrt{1-v^2}}{\lambda^2}(\omega - vk_x)$ into the constraint Eq. (5.25), one can verify this explicitly. The spectrum is therefore a continuum, and not discrete. The excitation spectrum therefore resembles that of a scale-invariant critical theory, rather than that of interacting particles.

- Focusing on the low-energy regime, i.e. a narrow band in the spectral function around $\omega = 0$, we can determine the spectral weight analytically around the three different Fermi-surfaces — the three different crossings of the dispersion relation with $\omega = 0$. Expanding Eq. (5.25) around $(\omega, k_x) = (0,0)$ the retarded Greens's function behaves as

$$G_R(\omega, k_x) = C\lambda^{-4/3}|\omega + k_x|^{-1/3}, \tag{2.30}$$

with $C = (1 + v)^{1/3} \frac{4\pi}{(12\pi)^{1/3}} \left[i \frac{\sqrt{3}}{2} - \frac{1}{2} \operatorname{sgn}(\omega + k) \right]$, whereas near the outer Fermi surfaces $(\omega, k_x) = (0, \pm k_x^*)$ we have

$$G_R(\omega, k_x) \sim \lambda^{-1} (v^* k_x - \omega)^{-1/2}. \qquad (2.31)$$

In each case the IR $\omega \simeq 0$ spectral function thus has a clear power-law behavior with a branch-cut singularity, but it has a different exponent depending on the Fermi surface. Furthermore, at the $k_x = 0$ Fermi surface the spectral function is symmetric around ω, while in the other two it is zero for negative (positive) frequencies. This is clearly visible in Fig. 2.5.

Interestingly, in all three cases the power-law scaling conforms with a uniform scaling of energy and momentum corresponding to ground-state with a dynamical critical exponent $z_f = 1$ (consistent with [90, 93]). This is in contrast to the expectation that the 2+1 dimensional quantum critical metal has a $z_f \neq 1$ groundstate [79]. However, the role of Landau damping and Fermi surface curvature is crucial in this expectation, and both are ignored in the planar $N_f = 0$ approximation here.

All these insights are non-perturbative. This can be readily shown by comparing our exact result to the one-loop perturbative answer (Fig. 2.7 and Fig. 2.8). The one-loop result is only a good approximation in the UV, far away from the continuous set of excitations, i.e. the dimensionful Yukawa coupling $\lambda^2 \ll |\omega - v k_x|$. Perturbation theory therefore fails to capture any of the distinct non-Fermi liquid phenomenology of IR of the planar quenched model (with the exception of the shape of the dispersion-curve). Despite the fact that this is not the true IR of the full theory, where Landau damping must also be taken into account, for energies and temperatures slightly above E_{LD} the full physics will resemble this quenched critical non-Fermi-liquid result.

For completeness we can also compute the density of states and the occupation number as a function of momentum. The former gives (see Appendix 2.D)

$$N(\omega) = \int \mathrm{d}k_x \frac{A(\omega, k_x)}{2\pi} = \frac{1}{v} \left[1 + \theta(\lambda^2 \frac{\cosh^{-1}(v^{-1}) - \sqrt{1 - v^2}}{4\pi(1 - v^2)^{3/2}} - |\omega|) \right].$$
$$(2.32)$$
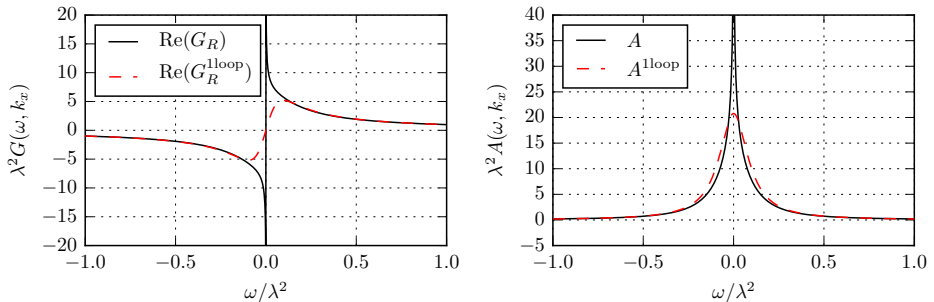
Figure 2.7. The real and the imaginary part of the Green's function at the middle Fermi surface ($k_x = 0$, $v = 0.5$) as a function of ω (solid line), compared with the corresponding one-loop result (dashed)
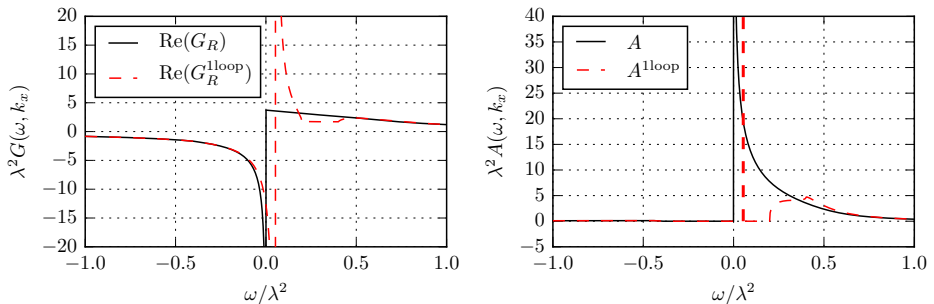
Figure 2.8. The real and the imaginary part Green's function at the outer Fermi surface ($k_x = k_x^* \approx 0.4\lambda^2$, $v = 0.5$) as a function of ω (solid line), and the one-loop truncated result (dashed). The spectral weight of the one-loop approximation is concentrated to a δ-function whereas the spectral weight of the full result is spread in the power-law singularity.
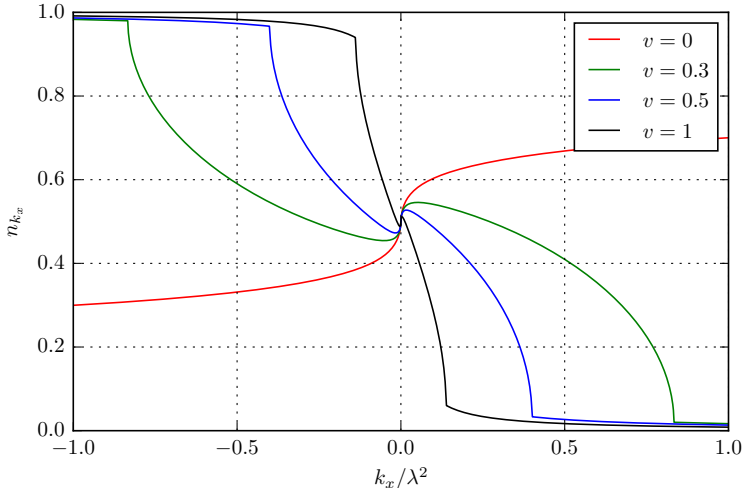
Figure 2.9. The occupation number for different v as a function of momentum. We can see the effect of the multiple sharp fermi surfaces, the non-fermi liquid behaviour is also apparent as a non-monotonic behaviour of the occupation number.

The occupation number can be obtained from the spectral function by using the formula

$$n_{k_x} = \int_{-\infty}^{0} d\omega \frac{A(\omega, k_x)}{2\pi} \qquad (2.33)$$

This evaluates to (Appendix 2.D)

$$n_{k_x} = \frac{1}{\pi} \arg \left[\frac{\cosh(\sigma(\omega = 0, k_x/\lambda^2, v)) - v}{v \cosh^{-1}(v) - \sqrt{1 - v^2}(i - 4\pi(1 - v^2)k_x/\lambda^2)} \right], \qquad (2.34)$$

where $\sigma(\omega, k_x)$ is defined by (5.25). It is plotted in Fig. 2.9. We can see the effect of the multiple Fermi surfaces as discontinuities in the derivative of the occupation number, even though the occupation number itself is continuous. This is another way to see that the fermionic excitation spectrum is that of a non-Fermi liquid. (Note that in the singular case of vanishing UV Fermi velocity $v = 0$, the occupation number has different asymptotics as $k_x \to \pm\infty$ than for any small but non-zero v. For $v \neq 0$ the occupation number approaches $n_{k_x} = 1$ at $k_x = -\infty$ and $n_{k_x} = 0$ at $k_x = \infty$, as it should.)

2.4 Conclusions

In this chapter we have shown that in the quenched $N_f \to 0$ limit the fermion Green's function in a 2+1 dimensional quantum critical metal can be determined exactly. The quenched limit neuters the dangerous nature of dimensionally irrelevant Fermi surface corrections and allows us to truncate to a linear dispersion relation for the fermions. This reduction to an effective one-dimensional system allows an explicit solution to the fermion Green's function in the presence of a background scalar field. The quenched $N_f \to 0$ limit further allows us to compute the full background scalar field path-integral when coupled minimally to the fermion.

Even though the quenched limit discards the physics of Landau damping, our result shows that the resulting physics is already very non-trivial. There are three distinct low-energy excitations as opposed to the excitations around a single Fermi surface of the free theory. Most importantly, the sharp excitations of the free theory broaden into a power-law singularity of the spectral function of the form $G \sim (\omega - \epsilon(k_x))^{-\eta}$, with either $\eta = 1/2$ or $\eta = 1/3$. The groundstate is a non-Fermi-liquid.

Beyond the quenched limit and including N_f corrections, i.e. fermion loops, Landau damping effects become important. These effects will show up below some energy scale $E_{\rm LD}$ set by both N_f and the Fermi surface curvature κ. Our model breaks down below this scale, but it is expected to describe the physics above $E_{\rm LD}$. What our results show is that, qualitatively, the physics is that of a non-Fermi-liquid both above $E_{\rm LD}$ and below $E_{\rm LD}$ [103], but in detail it will differ.

In order to access IR physics below $E_{\rm LD}$, the corrections in the Fermi surface curvature and the number of fermionic flavours must be treated systematically, but a (possible) shortcut deserves to be mentioned. Our analytic determination of the exact fermionic Green's analytically hinged on the free fermion dispersion being linear, but the approach taken in this chapter does not put any restrictions on the allowed form of the bosonic propagator. This opens up the possibility to implement the Landau-damping effects phenomenologically, just by modifying the background bosonic Green's function, and staying within the Gaussian approximation. This is the approach taken by Khveshchenko and Stamp [101] and Altshuler, Lidsky, Ioffe and Millis [102, 103]. Comparing to vector large N_f approaches [84, 86], it is not clear that this is sufficient to reliably capture the IR. The Landau damping is not the only important effect.

Interactions of the boson field with itself beyond the Gaussian approximation must also be taken into account, e.g. our model needs to be enhanced by a ϕ^4 interaction to describe the Ising-nematic critical point [105].

The interesting question will be which non-Fermi liquid features are retained and which change. The dynamical critical exponent z_f below the Landau damping scale is likely different from 1. Also, the splitting of the Fermi surface seems to be a subtle phenomenon, and whether it remains stable upon including fermionic loop corrections or going beyond the local patch approximation requires a careful investigation. On the other hand, the destruction of the quasi-particle poles and the fact that the spectrum is singular along the full dispersion curve is expected to be a robust effect that resembles that of a critical state. This is thought to be enhanced by the Landau damping.

2.A   Comparison with perturbation theory

We can expand (2.16) in the coupling constant. Although at first sight this expansion seems different from the usual perturbative expansion, we will show that in the case of zero fermi surface curvature they match at any order if we do not include fermion loops.

The λ^{2n} term in (2.16) is

$$
G_n(z) = \frac{G_0(z)}{2^n n!} \Big(\int dx' dx'' d\tau' d\tau'' \left[G_0\left(z - z'\right) + G_0\left(z'\right) \right] G_B\left(z' - z''\right)
$$
$$
\left[G_0\left(z - z''\right) + G_0\left(z''\right) \right] \Big)^n,
\tag{2.35}
$$

where $z = x + iv\tau$. The usual perturbative expansion result can be obtained by expanding

$$
\langle \psi(z)\psi(0)^\dagger \exp(\lambda\phi\psi^\dagger\psi)\rangle
\tag{2.36}
$$

and evaluating by Wick contraction

$$
G_n^{\text{pert}}(z) = \frac{(2n-1)!!}{(2n)!} \int dx_1...dx_{2n} d\tau_1...d\tau_{2n} I \cdot G_B(x_1 - x_2, \tau_1 - \tau_2)...\cdot
$$
$$
\cdot G_B(x_{2n-1} - x_{2n}, \tau_{2n-1} - \tau_{2n}),
\tag{2.37}
$$

$$I = \sum_{(i_1,..,i_{2n}) \in S_{2n}} G_0\left(z - z_{i_1}\right) G_0\left(z_{i_1} - z_{i_2}\right)...G_0\left(z_{i_{2n-1}} - z_{i_{2n}}\right) G_0\left(z_{i_{2n}}\right)$$

(2.38)

Here S_n is the set of permutations of the numbers 1 through n. The factor $1/(2n!)$ comes from the Taylor expansion of the exponential. By summing over the different assignments of internal points we are explicitly counting the different contractions of the fermion fields. There are however still $(2n-1)!!$ possibilities to pair the boson fields (each pairing gives rise to the same contribution after a change of variable in the integral). Since $(2n)!/(2n-1)!! = n! \cdot 2^n$ the identity which remains to be proved, once we have used our simple form of the free fermion Green's function, is

$$\sum_{(i_1,..,i_m) \in S_m} \frac{1}{z - z_{i_1}} \frac{1}{z_{i_1} - z_{i_2}} ... \frac{1}{z_{i_{m-1}} - z_{i_m}} \frac{1}{z_{i_m}} =$$

(2.39)

$$= \frac{z^{m-1}}{(z - z_1)(z - z_2)...(z - z_m) z_1...z_m}.$$

(2.40)

We need this for $m = 2n$, but the statement is true for odd m as well.

The identity can be proven by induction. The $m = 1$ case is easily checked and given that the equality holds for $m - 1$ we have

$$\sum_{(i_1,..,i_m) \in S_m} \frac{1}{z - z_{i_1}} \frac{1}{z_{i_1} - z_{i_2}} ... \frac{1}{z_{i_{m-1}} - z_{i_m}} \frac{1}{z_{i_m}} =$$

(2.41)

$$= \frac{1}{z_1...z_m} \sum_{k=1}^{m} \frac{1}{z - z_k} \frac{z_k^{m-1}}{(z_k - z_1)(z_k - z_2)...(z_k - z_m)}.$$

where the product in the last denominator excludes $(z_k - z_k)$. The right hand side of (2.40) and (2.41) are the same since they are both meromorphic functions of z with the same pole locations and residues and they both approach 0 at ∞.

2.B Calculating the real-space fermion Green's function

To find the real-space Euclidean fermionic Green's function we have to evaluate the integral (2.23). In order to do that, it is convenient to firstly

make a coordinate transformation of the following form

$$\omega = \frac{xk_1 + \tau k_2}{\sqrt{x^2 + \tau^2}},$$
$$k_x = \frac{xk_1 - \tau k_2}{\sqrt{x^2 + \tau^2}}.$$

(2.42)

The integral in k_2 can be then explicitly evaluated, giving

$$\int \mathrm{d}k_1 \mathrm{d}k_y \frac{\lambda^2 \left(\tau^2 + x^2\right) \left(\cos\left(k_1\sqrt{\tau^2 + x^2}\right) - 1\right)}{8\pi^2 \sqrt{k_1^2 + k_y^2} \left(x\left(\sqrt{k_1^2 + k_y^2} + |k_1|v\right) - i\tau\left(v\sqrt{k_1^2 + k_y^2} + |k_1|\right)\right)^2}.$$

(2.43)

Now switching to polar coordinates, $k_1 = k\cos\theta$, $k_y = k\sin\theta$, and performing the radial integral in k we obtain

$$I = \int_0^{2\pi} \mathrm{d}\theta \frac{\lambda^2 |\sin(\theta)| \left(\tau^2 + x^2\right)^{3/2}}{16\pi(\tau v + ix + |\sin(\theta)|(ivx + \tau))^2}.$$

(2.44)

Finally, integrating over θ for $v^2 \neq 1$ we derive

$$I = \frac{\lambda^2}{8\pi(1-v^2)} \left(\frac{(\tau + ivx)}{\sqrt{1-v^2}} \log\left(\frac{\tau + ivx + \sqrt{(1-v^2)(\tau^2 + x^2)}}{\tau + ivx - \sqrt{(1-v^2)(\tau^2 + x^2)}}\right) - 2\sqrt{\tau^2 + x^2}\right). \quad (2.45)$$

For the specific case $v^2 = 1$ the integration should be done independently and gives a simpler result

$$I = \lambda^2 \frac{(\tau - i\,\mathrm{sgn}(v)x)^2}{12\pi\sqrt{\tau^2 + x^2}}.$$

(2.46)

To Fourier transform the corresponding Green's function to momentum space, we will need an analytical continuation. For $0 < v < 1$, (2.16) with exponent (2.45) can be analytically continued in τ to the complex plane with two branch-cuts along parts of the imaginary axis

$$G_E(x,\tau) = -\frac{i}{2\pi} \frac{\mathrm{sgn}(v)}{x + iv\tau}.$$

$$\cdot e^{\frac{\lambda^2}{8\pi(1-v^2)} \left(\frac{(\tau+ivx)}{\sqrt{1-v^2}} \left(i\pi\mathrm{sgn}(x) + 2\tanh^{-1}\left(\frac{\tau+ivx}{\sqrt{(1-v^2)(\tau^2+x^2)}}\right)\right) - 2\sqrt{\tau^2+x^2}\right)}$$

(2.47)

2.C Fourier transforming the fermion Green's function

The next step is to calculate the retarded fermionic Green's function in momentum space. We know that the time-ordered momentum space Green's function of the Lorentzian signature theory, $G_T(\omega)$, is related to the Green's function of the Euclidean theory, $G_E(\omega)$, by analytical continuation

$$G_T(\omega, k_x) = G_E(\omega(-i + \epsilon), k_x). \tag{2.48}$$

$G_T(\omega, k_x)$ is analytic below the real line in the left half plane and above the real line in the right half plane. $G_E(\omega, k_x)$ is the Fourier transform in a generalized sense of (2.47). The (rather severe) divergence at infinity has to be regularized. Since the expression we found in Appendix 2.B permitted an analytic continuation to all of the first and third quadrants, we can continuously rotate the integration contour in the Fourier transform, $\tau = t(i + \delta)$, if additionally there is a regulator analytic in the first and third quadrant. We thus have

$$G_T(\omega, k_x) = \int dt(i + \delta)dx e^{i(\omega(-i+\epsilon)(i+\delta)t - k_x x)} G_E(t(i + \delta), x). \tag{2.49}$$

From this we see that the real-space time-ordered Green's function is given by analytically continuing the real-space Green's function of the Euclidean theory

$$G_T(t, x) = iG_E(t(i + \delta), x). \tag{2.50}$$

This slightly heuristic argument of analytical continuation in real space has been verified to give the correct Green's function up to one loop perturbation theory. The retarded Green's function is given by

$$G_R(\omega, k_x) = \int dt dx e^{i(\omega t - k_x x)} \theta(t)(G_T(t, x) + G_T^*(-t, -x)). \tag{2.51}$$

$G_T(t, x)$ is of the form $t^{-1} f_1(x/t) \exp(\lambda^2 t f_2(x/t))$. By performing a change of variable from x to $u = x/t$ we can perform the t integral. For this we need a regulator $\exp(-\epsilon t)$. The integrand of the remaining u integral has compact support, $u \in [-1, 1]$. We can perform a further change of variables

$$\sigma = \tanh^{-1}\left(\frac{\sqrt{(1 - v^2)(1 - u^2)}}{1 - uv}\right). \tag{2.52}$$

This function maps $[-1, v) \to \mathbb{R}^+$ and $(v, 1] \to \mathbb{R}^+$, both bijectively. The inverse thus has two branches that we need to integrate over, one for $u < v$ and one for $u > v$, and both integrals will be over $\mathbb{R}^+$. This change of variable is consistent with the principal value integral required for the singularity at $u = v$ if the $\sigma \to \infty$ limits are performed at the same time. The integrand obtained with this change of variable can be written as a sum of four pieces

$$G_R(\omega, k_x) = \int_0^\infty d\sigma \left[F(\sigma) + F(-\sigma) - F(\sigma + i\pi) - F(-\sigma + i\pi) \right], \quad (2.53)$$

where $F(\sigma)$ is defined as

$$F(\sigma) = \frac{i}{2\pi} \frac{\sinh(\sigma)}{\frac{\lambda^2 (\sinh(\sigma) - \sigma \cosh(\sigma))}{4\pi \sqrt{1-v^2}} + v\omega - k_x - \cosh(\sigma)(\omega - k_x v + i\epsilon)}. \quad (2.54)$$

Since $F(\sigma)$ is a meromorphic function and it approaches 0 as $\mathrm{Re}(\sigma) \to \pm\infty$, we can close the contour at $\pm\infty$ and obtain the integral as the residue of $F(\sigma)$'s single pole in the strip $0 < \mathrm{Im}(\sigma) < i\pi$,

$$G_R(\omega, k_x) = \frac{1}{\omega - k_x v + \frac{\lambda^2}{4\pi\sqrt{1-v^2}} \sigma(\omega, k_x)} \quad (2.55)$$

where $\sigma(\omega, k_x)$ is the solution, within $0 < \mathrm{Im}(\sigma) < i\pi$, of the equation

$$0 = \frac{\lambda^2}{4\pi\sqrt{1-v^2}} (\sinh(\sigma) - \sigma \cosh(\sigma)) + v\omega - k_x - \cosh(\sigma)(\omega - v k_x + i\epsilon). \quad (2.56)$$

The dispersion, $\omega(k_x)$, given by the location of the singularity of $G(\omega, k_x)$ is no longer monotonic as in the free case. The singularity occurs when the roots of (2.56) leave the real line. The dispersion can not be found analytically in general but for the two points where $d\omega/dk_x = 0$ we have,

$$\omega = \pm \lambda^2 \frac{\sqrt{1-v^2} - \cosh^{-1}\left(v^{-1}\right)}{4\pi (1-v^2)^{3/2}},$$

$$k_x = \pm \lambda^2 \frac{\sqrt{1-v^2} - v^2 \cosh^{-1}\left(v^{-1}\right)}{4\pi v (1-v^2)^{3/2}}. \quad (2.57)$$
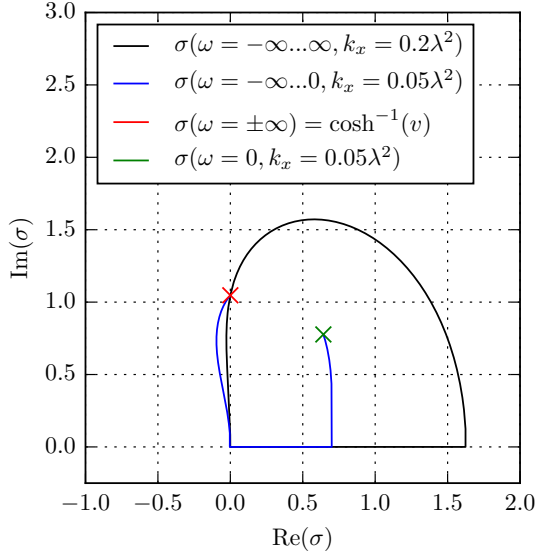
Figure 2.10. This figure shows a closed contour of integration for the sum rule and an open contour for calculating the occupation number integral. $v = .5$.

2.D   Integrals of the spectral function

Several important observables like the density of states or the occupation number are defined by momentum space integrals of the spectral function $A(\omega, k) = -2 \operatorname{Im} G_R(\omega, k)$. Despite the fact that we have only an implicit expression for the Green's function (2.55), these integrals can be relatively easily evaluated by bringing the imaginary axis projection outside the integral and then changing integration variable to σ. We then do not have a closed form expression for the (now complex) contour of integration but the integrand is greatly simplified.

For a fixed k_x we have ω as a closed form function of σ. Making this change of variable in integrals over ω gives the integrand

$$\int_C \mathrm{d}\omega\, A(\omega, k_x) = -2 \operatorname{Im} \left(\int_{\sigma(C)} \mathrm{d}\sigma \frac{\sinh(\sigma)}{v - \cosh(\sigma)} \right). \qquad (2.58)$$

The curve of integration, $\sigma(C)$, is now defined through the implicit expression for σ in (2.56).

First of all we check that the sum rule $\int d\omega A(\omega, k_x) = 2\pi$ is satisfied. Taking the $\omega \to \pm\infty$ limits in (2.56) we see that σ approaches $\cosh^{-1}(v)$ in both limits and the curve is thus closed. See Fig. 2.10. To solve the integral we thus just have to figure out what poles are within the contour. It turns out that the single pole is the one at $\sigma = \cosh^{-1}(v)$, which is on the contour. This gives divergences but since the residue is real they are in the real part and do not matter for the spectral density. The contribution to the imaginary part is just $2\pi i$ times half the residue since the contour is smooth at the pole. The result of the integral is then 2π as expected, for all values of k_x/λ^2 and v.

The occupation number at zero temperature is given by

$$n_{k_x} = \int_{-\infty}^{0} \frac{d\omega}{2\pi} A(\omega, k_x). \tag{2.59}$$

Since this contour is not closed we find a primitive function defined along the whole contour. The contribution from the point $\omega = 0$ depends on $\sigma(\omega = 0, k_x, v)$ so we can not get a closed form expression in this case. The contribution from $\omega \to -\infty$ now depends on the direction of the limit in the complex σ-plane since the point is only approached from one side. Summing the contributions from the two endpoints of the integral gives

$$n_{k_x} = \frac{1}{\pi} \arg \left[\frac{\cosh(\sigma(\omega = 0, k_x/\lambda^2, v)) - v}{v \cosh^{-1}(v) - \sqrt{1 - v^2}(i - 4\pi(1 - v^2)k_x/\lambda^2)} \right]. \tag{2.60}$$

From this we see that in the region where σ is real we actually have a closed form expression for the occupation number.

The density of states, $N(\omega) = \int dk_x A(\omega, k_x)$ is similarly calculated by changing variables to σ. For any ω there is a K_x such that $\sigma(k_x)$ is real for all $|k_x| > K_x$. The limits $k_x \to \pm\infty$ give $\sigma \to \pm\cosh^{-1}(1/v)$ and these are thus approached along the real line. Once again the integrand has poles (residue $1/v$) at these points and since we are only interested in the imaginary part of the integral of the retarded Green's function we will only need to know the direction we approach these poles from. Finding a primitive function is again trivial and in the end the result only depends on the direction the poles are approached from. Since σ is real in the limits, each pole is approached from either the left or the right. There are three different cases, for

$$\omega < -\lambda^2 \frac{\cosh^{-1}(v^{-1}) - \sqrt{1 - v^2}}{4\pi(1 - v^2)^{3/2}} \tag{2.61}$$
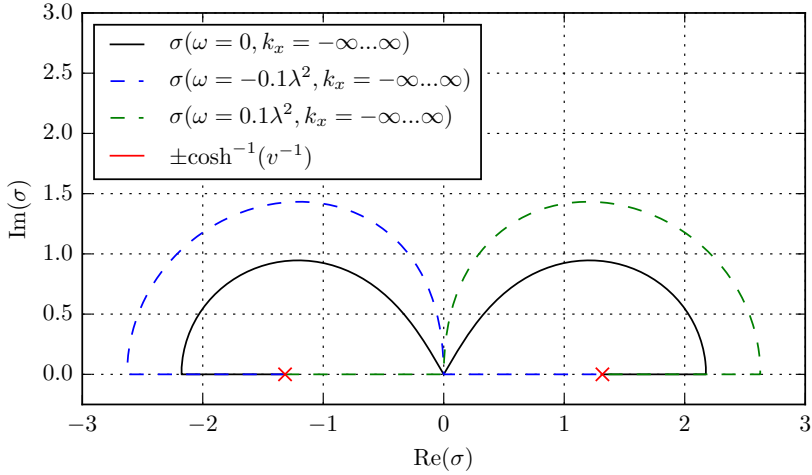
Figure 2.11. Integration contours for calculating density of states. The integrand and locations of the endpoints are independent of ω but since the integrand has poles at the endpoints the direction of approach matters. The poles are always approached along the real axis and this figure shows the three possible configurations. $v = .5$.

both poles are approached from the left. For

$$\omega > \lambda^2 \frac{\cosh^{-1}\left(v^{-1}\right) - \sqrt{1-v^2}}{4\pi(1-v^2)^{3/2}} \qquad (2.62)$$

both poles are approached from the right and for ω between these two values the left pole is approached from the left and the right pole from the right. See Fig. 2.11. Taking these different limits of the primitive function gives

$$N(\omega) = \frac{1}{v}\left[1 + \theta(\lambda^2 \frac{\cosh^{-1}\left(v^{-1}\right) - \sqrt{1-v^2}}{4\pi(1-v^2)^{3/2}} - |\omega|)\right]. \qquad (2.63)$$

The density of state takes two different values and we see that the ω where it changes are exactly the points where there are two instead of one solution in k_x to the equation $G^{-1}(\omega, k_x) = 0$.

Chapter 3

The two-point function of a $d = 2$ quantum critical metal in the limit $k_F \to \infty$, $N_f \to 0$ with $N_f k_F$ fixed

3.1 Introduction

The robustness of Landau's Fermi liquid theory relies on the protected gapless nature of quasiparticle excitations around the Fermi surface. Wilsonian effective field theory then guarantees that these protected excitations determine the macroscopic features of the theory in generic circumstances [107, 108]. Aside from ordering instabilities, there is a poignant exception to this general rule. These are special situations where the quasiparticle excitations interact with other gapless states. This is notably so near a symmetry breaking quantum critical point. The associated massless modes should also contribute to the macroscopic physics. In $d \geq 3$ dimensions this interaction between Fermi surface excitations and gapless bosons is marginal/irrelevant and these so-called quantum critical metals can be addressed in perturbation theory as first discussed by Hertz and Millis [109–112]. In 2+1 dimensions, however, the interaction is relevant and the theory is presumed to flow to a new interacting fixed point [112–115]. This unknown fixed point has been offered as a putative explanation of exotic physics in layered electronic materials near a quantum critical point

such as the Ising-nematic transition. As a consequence, the deciphering of this fixed point theory is one of the major open problems in theoretical condensed matter physics. There have been numerous earlier studies of Fermi surfaces coupled to gapless bosons but to be able to capture their physics one has almost always been required to study certain simplifying limits [116–126].

In this article we show that the fermionic and bosonic spectrum of the most elementary $d = 2$ quantum critical metal can be computed non-perturbatively in the double limit where the Fermi-momentum k_F is taken large, $k_F \to \infty$, while the number of fermion species N_f is taken to vanish, $N_f \to 0$, with the combination $N_f k_F$ held constant. This is an extension of previous work [127] where we studied the purely quenched limit $N_f \to 0$ *followed* by the limit $k_F \to \infty$. In this pure quenched $N_f \to 0$ limit the boson two-point function does not receive any corrections and the fermion two point function can be found exactly. However, it is well known that for finite N_f and k_F the boson receives so-called Landau damping contributions that dominate the IR of the theory. These Landau damping corrections are always proportional to N_f, and a subset of these are also proportional to k_F. These terms in particular influence the IR as the large scale, low energy behavior should emerge when k_F is large. Studying the double scaling limit where the combination $N_f k_F$ is held fixed gives a more complete understanding of the small N_f and/or large k_F limit and their interplay. In particular, this new double scaling limit makes precise previous results in the literature on the RPA approximation together with the $N_f \to 0$ limit and the strong forward scattering approximation [128–131]. Importantly, we shall show that the RPA results qualitatively capture the low energy at fixed momentum regime, but not the full IR of the theory in the double scaling limit. The idea of this limit is similar to the limit taken in [132] where they study a similar model, but in a matrix large N limit. In this limit they keep the quantity k_F^{d-1}/N fixed while taking both N and k_F large.

All the results here refer to the most elementary quantum critical metal. This is a set of N_f free spinless fermions at finite density interacting with a free massless scalar through a simple Yukawa coupling. Its action

88

reads (in Euclidean time)

$$S = \int \mathrm{d}x\mathrm{d}y\mathrm{d}\tau \left[\psi_j^\dagger \left(-\partial_\tau + \frac{\nabla^2}{2m} + \mu \right) \psi^j + \frac{1}{2} \left(\partial_\tau \phi \right)^2 + \frac{1}{2} \left(\nabla\phi \right)^2 + \lambda\phi\psi_j^\dagger\psi^j \right],$$

(3.1)

where $j = 1 \ldots N_f$ sums over the N_f flavors of fermions and $\mu = \frac{k_F^2}{2m}$. We will assume a spherical Fermi surface, meaning k_F both sets the size of the Fermi surface, $2\pi k_F$, and the Fermi surface curvature, $1/k_F$. We will study the fermion and boson two-point functions of this theory in the double scaling limit $N_f \to 0$, $k_F \to \infty$. By this we mean that we take $k_F \to \infty$ while keeping the external momenta (measured from Fermi surface), energies, the coupling scale λ^2 and the Fermi velocity $v = k_F/m$ fixed. We shall not encounter any UV-divergences, but to address any ambiguities that may arise the usual assumption is made that the above theory is an effective theory below an energy and momentum scale Λ_0, Λ_k, each of which is already much smaller than k_F ($\Lambda_0, \Lambda_k \ll k_F$). We do not address fermion pairing instabilities in this work. They have been studied and found for similar models in other limits, outside of the particular double scaling limit studied here [132–136].

3.2 Review of the quenched approximation ($N_f \to 0\, first, k_F \to \infty$ subsequently)

Let us briefly review the earlier results of [127] as they are a direct inspiration for the double scaling limit.

Consider the fermion two-point function for the action above, Eq. (3.1). Coupling the fermions to external sources and integrating them out, and taking two derivatives w.r.t. the source, the formal expression for this two point function is

$$G_{\mathrm{full}}(\omega, k) = \langle \psi^\dagger(-\omega, -k)\psi(\omega, k) \rangle =$$
$$= \int \mathcal{D}\phi \, \det{}^{N_f}(G^{-1}[\phi])G(\omega, k)[\phi]e^{-\int \frac{1}{2}(\partial_\tau\phi)^2 + \frac{1}{2}(\nabla\phi)^2}$$

(3.2)

where $G(\omega, k)[\phi]$ is the fermion two-point function in the presence of a

background field ϕ, defined by

$$\left(-\partial_\tau + \frac{\nabla^2}{2m} + \mu + \lambda\phi\right) G(t,x)[\phi] = \delta(t-t')\delta^2(x-x') \qquad (3.3)$$

In the limit $k_F \to \infty$, for external momentum k close to the Fermi surface, we may approximate the derivative part with $-\partial_\tau + iv\partial_x$. The defining equation for the Green's function can then be solved in terms of a free fermion Green's function dressed with the exponential of a linear functional of ϕ. In the quenched $N_f \to 0$ limit this single exponentially dressed Green's function can be averaged over the background scalar with the Gaussian kinetic term. The result in real space is again an exponentially dressed free Green's function

$$G_{R,N_f \to 0}(r,t) = G_{R,\text{free}}(r,t)e^{I(t,r)} \qquad (3.4)$$

with the exponent $I(r,t)$ given by

$$I(\tau,r) = \lambda^2 \int \frac{\mathrm{d}\omega \mathrm{d}k_x \mathrm{d}k_y}{(2\pi)^3} \frac{\cos(\tau\omega - rk_x) - 1}{(i\omega - k_x v)^2} G_B(\omega,k) , \qquad (3.5)$$

and r conjugate to momentum measured from the Fermi surface (k_x), not the origin. Here $G_B(\omega,k)$ is the free boson Green's function determined by the explicit form of the boson kinetic term in the action Eq. (3.1). This is of course a known function and due to this simple dressed expression the retarded Green's function and therefore the fermionic spectrum of this model can be determined exactly in the limit $N_f \to 0$. The retarded Green's function in momentum space reads [127] (here ω is Lorentzian)

$$G_{R,N_f \to 0}(\omega,k_x) = \frac{1}{\omega - k_x v + \frac{\lambda^2}{4\pi\sqrt{1-v^2}}\sigma(\omega,k_x)}, \qquad (3.6)$$

where σ is the solution of the equation

$$\frac{\lambda^2}{4\pi\sqrt{1-v^2}}(\sinh(\sigma) - \sigma\cosh(\sigma)) + v\omega - k_x - \cosh(\sigma)(\omega - k_x v + i\epsilon) = 0, \qquad (3.7)$$

with k_x the distance from the Fermi surface, $v = k_F/m$ is the Fermi velocity, and $\epsilon \to 0^+$ is an $i\epsilon$ prescription that selects the correct root.

This non-perturbative result already describes interesting singular fixed point behavior: the spectrum exhibits non-Fermi liquid scaling behavior

with multiple Fermi surfaces [127]. Nevertheless, it misses the true IR of the theory as the quenched limit inherently misses the physics of Landau damping. This arises from fermion loop corrections to the boson propagator that are absent for $N_f \to 0$. Below the Landau damping scale $\omega < \sqrt{\lambda^2 N_f k_F}$ the physics is expected to differ from the quenched approximation.

3.3 Loop-cancellations and boson two-point function

It is clear from the review of the quenched derivation that finite N_f, i.e. fermion loop corrections, that only change the boson two-point function, can readily be corrected for by replacing the free boson two-point function $G_B(\omega, k)$ by the (fermion-loop) corrected boson two-point function in Eq. (3.5) (valid at large k_F). This is the essence of many RPA-like approximations previously studied. A weakness is that finite N_f corrections will also generate higher-order boson interactions and these can invalidate the simple dressed expression obtained here.

At the same time, it has been known for some time that finite density fermion-boson models with simple Yukawa scalar-fermion-density interactions as in Eq. (3.1) have considerable cancellations in fermion loop diagrams for low energies and momenta after symmetrization [130, 137, 138]. These cancellations make loops with more than three interaction vertices $V \geq 3$ finite as the external momenta and energies are scaled uniformly to zero. We will now argue that this result also means that in the $N_f \to 0$, $k_F \to \infty$ limit with $N_f k_F$ fixed, these $V \geq 3$ loops vanish. In this limit *only* the boson two-point function is therefore corrected and only at one loop and we can directly deduce that in this double limit the exact fermion correlation function is given by the analogue of the dressed Green's function in Eq. (3.4). We comment on the limitations of considering this limit for subdiagrams in perturbation theory later in this section.

Consider the quantum critical metal before any approximations; i.e. we have a fully rotationally invariant Fermi surface with a finite k_F. The Yukawa coupling shows that the boson couples to the density operator $\psi^\dagger(x)\psi(x)$. All corrections to the boson therefore come from fermionic loops with fermion density vertices. These loops always show up symmetrized in the density vertices. Consider a fermion loop with a fixed

number V of such density vertices, dropping the overall coupling constant dependence, and arbitrary incoming energies and momenta. Such a loop (ignoring the overall momentum conserving δ-function) has energy dimension $3-V$. These fermionic loops are all UV finite so they are independent of the scale of the UV cut-offs. There are only two important scales, the external bosonic energies and momenta ω_i, k_i, the fermi momentum k_F. A symmetrized V-point loop can by dimensional analysis be written as
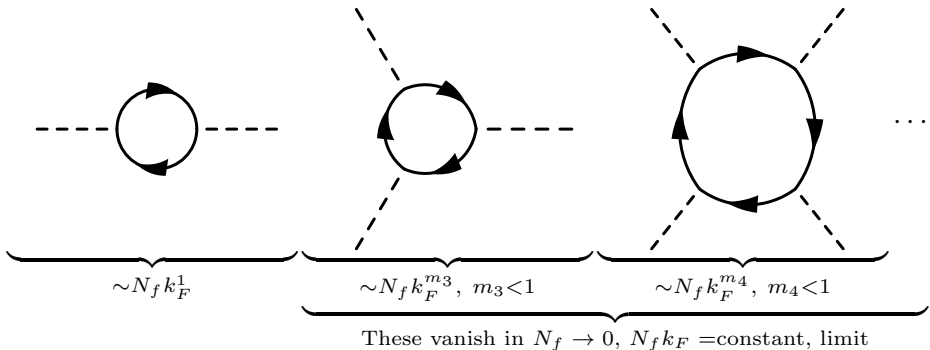
$$I(\{\omega_i\}, \{k_i\}) = k_F^{3-V} f(\{\omega_i/k_F\}, \{k_i/k_F\}) \tag{3.8}$$

Since fermion loops of our theory with $V \geq 3$ vertices have been shown to be finite as external energies and momenta are uniformly scaled to 0 [137], we thus have that f is finite as k_F is taken to infinity. This in turn means that $I(\{\omega_i\}, \{k_i\})$ scales as k_F^n with $n \leq 0$ for large k_F when $V \geq 3$. [1] Note that the use of the small external energies and momenta limit from [137] was merely a way of deducing the large k_F limit. We do not rely on the physical IR scaling to be the same as in [137], indeed we will find it not to be the same. All single fermionic loops additionally contain a sum over fermionic flavors so are therefore proportional to N_f. Combining this we see that a fermionic loop with $V \geq 3$ density vertices comes with a factor of $N_f k_F^{m_V}$ where $m_V \leq 0$ after symmetrizing the vertices. By now considering the combined limit of $N_f \to 0$ and $k_F \to \infty$ with $N_f k_F$ constant we see that these $V \geq 3$ loops all vanish. See Figure 3.1.

We have now concluded that for a fixed set of external momenta, all symmetrized fermion loops vanish in our combined limit, except the $V = 2$ loop. There is still a possibility that diagrams containing $V > 2$ loops are important when taking the combined limit *after* performing all bosonic momentum integrals and summing up the infinite series of diagrams. In essence, the bosonic integrals and the infinite sum of perturbation theory need not commute with the combined $N_f \to 0$, $k_F \to \infty$ limit. What the IR of the full theory (finite N_f) looks like is not known so taking the $N_f \to 0$ limit last is currently out of reach. In [139] the authors show that divergence of fermionic loops does not cancel under a non-uniform low-energy scaling of energies and momenta where the momenta are additionally taken to be increasingly collinear. The scaling they use is

---

[1] Naively corrections to the boson would be expected to scale as k_F since it receives corrections from a Fermi surface of size $2\pi k_F$. However k_F also sets the curvature of the Fermi surface and for a large k_F we approach a flat Fermi surface for which $V \geq 3$-loops completely cancel. This is shown in more detail in Appendix 3.A.

Here we show the dominant scaling of fermion loops with different
numbers of vertices in the limit of $N_f \to 0$ with $N_f k_F$ constant. This is the
scaling after symmetrizing the external momenta. The two-vertex loop on the
left does not get symmetrized and is the only loop that does not vanish in this
limit.

Figure 3.1. Here we show the dominant scaling of fermion loops with different
numbers of vertices in the limit of $N_f \to 0$ with $N_f k_F$ constant. This is the
scaling after symmetrizing the external momenta. The two-vertex loop on the
left does not get symmetrized and is the only loop that does not vanish in this
limit.

motivated by the perturbative treatment in [116] and if this is the true IR
scaling and it persists at small N_f, then there will be effects unaccounted
for in the above.

Regardless of the above mentioned caveat, in keeping the $V = 2$
fermion loops we take the combined limit *after* performing the fermionic
loop integrals and thus move closer than in our previous work [127] to the
goal of understanding the IR of quantum critical metals. To summarize:
the ordered limit we consider is

1. We first perform rotationally invariant finite k_F fermionic loop inte-
   grals.

2. Then we take the limit $N_f \to 0$, $k_F \to \infty$ with $N_f k_F$ fixed; this only
   keeps $V = 2$ loops.

3. Next we perform bosonic loop integrals.

4. Finally we sum all contributions at all orders of the coupling con-
   stant.

The result above means the fully quantum corrected boson remains Gaus-
sian in this ordered limit and only receives corrections from the $V = 2$
loops.

3.3.1 Boson two-point function

We now compute the one-loop correction to the boson two-point function; in our ordered double scaling limit this is all we need. We then substitute the Dyson summed one-loop corrected boson two-point function into the dressed fermion Green's function to obtain the exact fermionic spectrum.

The one-loop correction—the boson polarization—in the double scaling limit is given by the large k_F limit of the two-vertex fermion loop. This can be calculated using a linearized fermion dispersion:

$$\Pi_1\left(Q\right) = \lambda^2 N_f k_F \int \frac{\mathrm{d}k_0 \mathrm{d}k d\theta}{(2\pi)^3} \frac{1}{(ik_0 - vk)\left(i\left(k_0 + q_0\right) - v\left(k + |\vec{q}|\cos\theta\right)\right)}.$$
(3.9)

Note from the $\cos\theta$ dependence in the numerator that we are not making a "patch" approximation. In the low energy limit this angular dependence is the important contribution of the rotationally invariant fermi-surface, whereas the subleading terms of the dispersion can be safely ignored. As stated earlier, the result of these integrals is finite. However, it does depend on the order of integration. The difference is a constant C

$$\Pi_1\left(Q\right) = \frac{\lambda^2 N_f k_F}{2\pi v}\left(\frac{|q_0|}{\sqrt{q_0^2 + v^2 \vec{q}^2}} + C\right)$$

$$\equiv M_D^2\left(\frac{|q_0|}{\sqrt{q_0^2 + v^2 \vec{q}^2}} + C\right).$$
(3.10)

As pointed out in for instance [125, 126], the way to think about this ordering ambiguity is that one should strictly speaking first regularize the theory and introduce a one-loop counterterm. This counterterm has a finite ambiguity that needs to be fixed by a renormalization condition. Even though the loop momentum integral happens to be finite in this case, the finite counterterm ambiguity remains. The correct renormalization condition is the choice $C = 0$. This choice corresponds to the case when the boson is tuned to criticality since a non-zero C would mean the presence of an effective mass generated by quantum effects.

A more physical way to think of the ordering ambiguity is as the relation between the frequency (Λ_0) and momentum (Λ_k) cutoff. We will assume that $\Lambda_k \gg \Lambda_0$ — which means that we evaluate the k integral first and then the frequency k_0 integral. In this case $C = 0$ directly follows.

3.4 Fermion two-point function

With the single surviving one-loop correction to the boson two-point function in hand, we can immediately write down the expression for the full fermion two-point function. This is the same dressed expression Eq. (3.5) as in [127] but with a modified boson propagator $G_B = 1/(G_{B,0}^{-1} + \Pi)$, with Π the one-loop polarization of Eq. (3.10). Substituting this in we thus need to calculate the integral

$$I(\tau, r) = \lambda^2 \int \frac{\mathrm{d}\omega \mathrm{d}k_x \mathrm{d}k_y}{(2\pi)^3} \frac{\cos(\tau\omega - rk_x) - 1}{(i\omega - k_x v)^2 \left(\omega^2 + k_x^2 + k_y^2 + M_D^2 \frac{|\omega|}{\sqrt{v^2(k_x^2 + k_y^2) + \omega^2}}\right)}.$$
(3.11)

At this moment, we can explain clearly how our result connects to previous approaches. A similarly dressed propagator can be proposed based on extrapolation from 1d results [128, 130]. An often used approximation in the literature is to now study this below the scale M_D, see e.g [112, 129]. This is the physically most interesting limit since in the systems of interest N_f is order one and we are considering large k_F. In this limit the polarisation term will dominate over the kinetic terms, but since the rest of the integrand in (3.11) has no k_y dependence, it is necessary to keep the k_y term in the boson propagator. The ω and k_x momenta will suppress the integrand when they are of order λ^2 whereas the k_y term will do so once it is of order $\lambda^{2/3} M_D^{2/3}$. This means that for $M_D \gg \lambda^2$, the relevant k_y will be much larger than the relevant ω and k_x. This argues that we can truncate to the large M_D propagator

$$G_{B,M_D \to \infty}(\omega, k_x, k_y) = \frac{1}{k_y^2 + M_D^2 \frac{|\omega|}{v|k_y|}}.$$
(3.12)

This Landau-damped propagator has been used extensively, for instance [112, 129]. In [129] this propagator was used for the type of non-perturbative calculation we are proposing here. We discuss this here, as we will now show that using this simplified propagator has a problematic feature. This propagator only captures the leading large M_D contribution but the non-perturbative exponential form of the exact Green's function sums up powers of the propagator which then are subleading in M_D.

Using the large M_D truncated boson Green's function the integral

$I(\tau, r)$ to be evaluated simplifies to

$$I_{M_D \to \infty} = \lambda^2 \int \frac{\mathrm{d}\omega \mathrm{d}k_x \mathrm{d}k_y}{(2\pi)^3} \frac{\cos(\tau\omega - xk_x) - 1}{(i\omega - k_x v)^2 \left(k_y^2 + M_D^2 \frac{|\omega|}{v|k_y|}\right)}. \tag{3.13}$$

Writing the cosine in terms of exponentials we can perform the k_x integrals using residues by closing the contours in opposite half planes. Summing up the residues gives

$$I_{M_D \to \infty} = -\lambda^2 \int \mathrm{d}\omega \mathrm{d}k_y \frac{k_y^2 |r| e^{-|\omega|\left(\frac{|r|}{v} + i\,\mathrm{sgn}(r)\tau\right)}}{8\pi^2 M_D^2 \, |\omega k_y| + k_y^4 v}. \tag{3.14}$$

The k_y integral can be performed next to yield

$$I_{M_D \to \infty} = -\lambda^2 \int \mathrm{d}\omega \frac{|r| \, e^{-|\omega|\left(\frac{|r|}{v} + i\,\mathrm{sgn}(r)\tau\right)}}{12\sqrt{3}\pi(M_D^2 v^5 \, |\omega|)^{1/3}}. \tag{3.15}$$

The primitive function to this ω integral is the upper incomplete gamma function, with argument $2/3$. Evaluating this incomplete gamma function in the appropriate limits and substituting the final expression for $\underset{M_D \to \infty}{I}(\tau, r)$ into the expression for the fermion two-point function gives us:

$$\underset{M_D \to \infty}{G_f}(\tau, r) = \frac{1}{2\pi(ir - v\tau)} \exp\left(-\frac{|r|}{l_0^{1/3} \, (|r| + iv\,\mathrm{sgn}(r)\tau)^{2/3}}\right) \tag{3.16}$$

where the length scale l_0 is given by

$$l_0^{1/3} = \frac{6\sqrt{3}\pi v M_D^{2/3}}{\Gamma\left(\frac{2}{3}\right) \lambda^2}. \tag{3.17}$$

This result has been found earlier in [128] (see also [130]). However, this real space expression hides the inconsistency of the approach. This becomes apparent in its momentum space representation. The Fourier transform of the real space Green's function

$$\underset{M_D \to \infty}{G_f}(\omega, k) = \int \mathrm{d}\tau \mathrm{d}r \frac{e^{i(\omega\tau - kr)}}{2\pi(ir - v\tau)} \exp\left(-\frac{|r|}{l_0^{1/3} \, (|r| + iv\,\mathrm{sgn}(r)\tau)^{2/3}}\right) \tag{3.18}$$
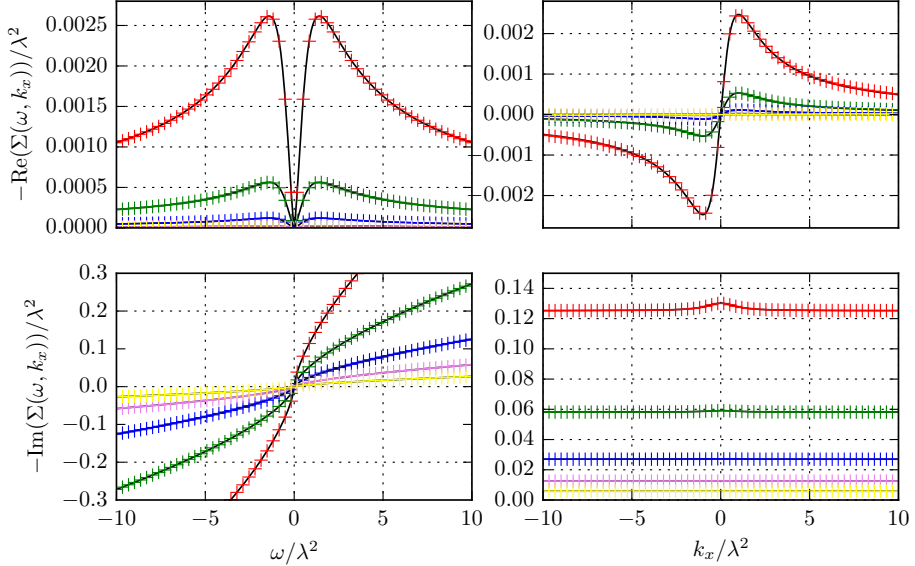
Figure 3.2. Real and imaginary parts of the self energy obtained using the large-k_F Landau-damped propagator. This plot shows the agreement between the numerics and the analytical solution, verifying that both solutions are correct. Notice the difference in magnitude between the real and imaginary part. The agreement of the real parts shows that the numerical procedure has a very small relative error. All plots are for the $k_x, \omega = \lambda^2$ slice with $v = 1$.

is tricky, but remarkably can be done exactly. We do so in appendix 3.B. The result is

$$
\begin{aligned}
\underset{M_D \to \infty}{G_f} (\omega, k_x) &= \frac{1}{i\omega - k_x v} \cos\left(\frac{\omega}{v l_0^{1/2}(\omega/v + ik_x)^{3/2}}\right) \\
&+ \frac{6\sqrt{3}i\Gamma\left(\frac{1}{3}\right)\omega^{2/3}}{8\pi l_0^{1/3} v^{5/3}(\omega/v + ik_x)^2} \, {}_1F_2\left(1; \frac{5}{6}, \frac{4}{3}; -\frac{\omega^2}{4 l_0 v^2(\omega/v + ik_x)^3}\right) + \\
&+ \frac{3\sqrt{3}i\Gamma\left(-\frac{1}{3}\right)\omega^{4/3}}{8\pi l_0^{2/3} v^{7/3}(\omega/v + ik_x)^3} \, {}_1F_2\left(1; \frac{7}{6}, \frac{5}{3}; -\frac{\omega^2}{4 l_0 v^2(\omega/v + ik_x)^3}\right).
\end{aligned}
\tag{3.19}
$$

This expression has been compared with numerics to verify its correctness; see Fig. 3.2.

97

We can now show the problematic feature. Recall that Eq. (3.19) is the Green's function in Euclidean signature. Continuing to the imaginary line, $\omega = -i\omega_R$, this becomes the proper retarded Greens function, $G_R(\omega_R, k_x)$, and from this we can obtain the spectral function

$$A(\omega_R, k_x) = -2 \operatorname{Im} \, G_R(\omega_R, k_x). \tag{3.20}$$

As it encodes the excitation spectrum, the spectral function ought to be a *positive* function that moreover equals 2π when integrated over all energies ω_R, for any momentum k. This large M_D spectral function contains an oscillating singularity at $\omega_R = vk_x$. We are free to move the contour into complex ω_R-plane by deforming $\omega_R \to \omega_R + i\Omega$ where Ω is positive but otherwise arbitrary. Upon doing this it is easy to numerically verify that indeed the integral over ω_R gives 2π. However, if we look at the behaviour close to the essential singularity, the function oscillates rapidly and does not stay positive as one approaches the singularity; see Fig. 3.3. This reflects that the large M_D approximation done in this way is not consistent. Even though the approximation for the exponent $I(\tau, r) \equiv \frac{\tilde{I}(\tau, r)}{(M_D)^{2/3}}$ is valid to leading order in $1/M_D$, this is not systematic after exponentiation to obtain the fermion two-point function

$$\underset{M_D \to \infty}{G_f}(\tau, r) = \frac{1}{2\pi(ir - v\tau)} \exp\left(\frac{\tilde{I}(\tau, r)}{M_D^{2/3}} + \mathcal{O}\left(\frac{1}{(M_D)^{4/3}} \right) \right). \tag{3.21}$$

Reexpanding the exponent one immediately sees that keeping only the leading term in $I(\tau, r)$ mixes at higher order with the subleading terms at lower order in $1/M_D$

$$\underset{M_D \to \infty}{G_f}(\tau, x) = \frac{1}{2\pi(ir - v\tau)} \left(1 + \frac{\tilde{I}(\tau, r)}{M_D^{2/3}} + \mathcal{O}(M_D^{-4/3}) + \right.$$
$$\left. + \frac{1}{2} \left(\frac{\tilde{I}(\tau, r)}{M_D^{2/3}} + \dots \right)^2 \right). \tag{3.22}$$

Despite this problematic feature, we will show from the exact result that in the IR $\underset{M_D \to \infty}{G_f}$ (with a small modification) does happen to capture the correct physics.
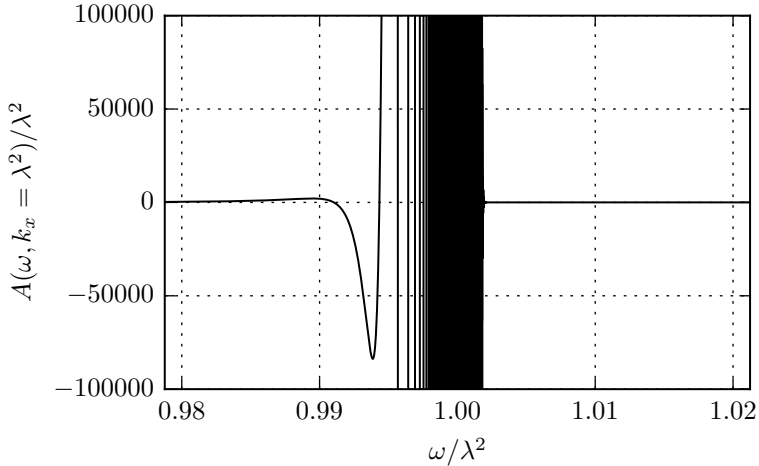
Figure 3.3. Exact fermion spectral function based on the large-M_D approximation for the exact boson propagator. Notice that the function is not positive everywhere. Here $k = \lambda^2$, $v = 1$ and $M_D = 2\pi\lambda^2$.

Exact fermion two-point function for large k_F with M_D fixed; $v = 1$

We therefore make no further assumption regarding the value of M_D and we return to the full integral Eq. (3.11) to determine the real space fermion two-point function. Solving this in general is difficult, and to simplify mildly we consider the special case $v = 1$. In our previous studies of the quenched $M_D = 0$ limit we saw that this choice for value of v is actually not very special, even though it appears that there is an enhanced symmetry. In fact, nothing abruptly happens as $v \to 1$, except that the quenched $M_D = 0$ solution can be written in closed form for this value of $v = 1$. Nor for the case of large M_D is the choice $v = 1$ in any way special. As can be seen above in Eq. (3.16) for large M_D all v are equivalent up to a rescaling of τ versus r and a rescaling of the single length scale l_0. We may therefore expect that for a finite M_D, the physics of $0 < v < 1$ is qualitatively the same as the (not-so-) special case $v = 1$.

After setting $v = 1$ and changing to spherical coordinates we have

$$I = \lambda^2 \int \mathrm{d}\tilde{r}\mathrm{d}\phi\mathrm{d}\theta\mathrm{e}^{2i\phi}\frac{\cos\left(\tilde{r}\sin(\theta)(\tau\sin(\phi) - r\cos(\phi))\right) - 1}{8\pi^3\sin(\theta)^2\left(M_D^2|\sin(\phi)| + \tilde{r}^2/\sin(\theta)\right)} . \qquad (3.23)$$

99

Performing the $\tilde{r}$ integral gives us

$$I = \pi^4 \lambda^2 \int \mathrm{d}\phi \mathrm{d}\theta e^{2i\phi} \frac{e^{-M_D|\tau \sin(\phi)-r\cos(\phi)|\sqrt{|\sin(\phi)|\sin(\theta)^3}} - 1}{16 M_D \sqrt{|\sin(\phi)|\sin(\theta)^3}} . \qquad (3.24)$$

Note that if the signs of both τ and r are flipped, then this is invariant. Changing the sign of only τ, and simultaneously making the change of variable $\phi \to -\phi$, then the (real) fraction is invariant but the exponent in the prefactor changes sign. Thus, I goes to I^* as the sign of either τ or r is changed. Without loss of generality, we can assume that both of them are positive from now on. We further see that the integrand is invariant under $\phi \to \phi + \pi$, so we may limit the range of ϕ to $(0, \pi)$ by doubling the value of integrand. Similarly we limit θ to $(0, \pi/2)$ and multiply by another factor of 2. We then make the changes of variables:

$$\begin{aligned} \phi &= \tan^{-1}(s) + \pi/2 \\ \theta &= \sin^{-1}(u^{2/3}) \end{aligned} \qquad (3.25)$$

with $s \in \mathbb{R}$ and u is integrated over the range $(0, 1)$. For convenience we introduce the function

$$z(s) = M_D |sr + \tau|(1 + s^2)^{-3/4}. \qquad (3.26)$$

Now the two remaining integrals can be written as

$$I = \frac{\lambda^2}{M_D} \int \mathrm{d}s \mathrm{d}u \frac{(e^{-uz(s)} - 1)(s - i)}{6\pi^2 (s+i)(1+s^2)^{3/4} u^{4/3}\sqrt{(1-u^{4/3})}}. \qquad (3.27)$$

After expanding the exponential we can perform the u integral term by term. We are left with

$$I = \frac{\lambda^2}{M_D} \int \mathrm{d}s \sum_{n=1}^{\infty} \frac{(1+s^2)^{1/4}(-z(s))^n}{8\pi^{3/2} n!(i+s)^2} \frac{\Gamma\left(\frac{3n-1}{4}\right)}{\Gamma\left(\frac{3n+1}{4}\right)}. \qquad (3.28)$$

This can be resummed into a sum of generalized hypergeometric functions, but this is not useful at this stage. Instead we once again integrate term by term. Collecting the prefactors and introducing the constant $a = \tau/r$, the n-th term can be written as

$$I = \sum_{n=1}^{\infty} c_n \int \mathrm{d}s \, (s - i)^2 |s + a|^n (1 + s^2)^{-(7+3n)/4}. \qquad (3.29)$$

This can be written as

$$I = \sum_{n=1}^{\infty} c_n \int \mathrm{d}s \mathrm{d}w \, (s-i)^2 |s+a|^n \frac{\mathrm{e}^{-w(s^2+1)} w^{3(1+n)/4}}{(3(1+n)/4)!}, \tag{3.30}$$

where w is integrated on $(0, \infty)$. After splitting the integral at $s = -a$ to get rid of the absolute value we can calculate the s integrals in terms of confluent hypergeometric functions $_1F_1(a, b; z)$. Adding the two halves $s < -a$ and $s > -a$ of the integral we have

$$I = \sum_{n=1}^{\infty} c_n \int \mathrm{d}w \frac{\Gamma\left(\frac{1+n}{2}\right) \mathrm{e}^{-(1+a^2)w}}{2(3(1+n)/4)!} \left(2w(i+a)^2 \, _1F_1\left(\frac{2+n}{2}, \frac{1}{2}; a^2 w\right) \right.$$

$$+ (2+n) \, _1F_1\left(\frac{4+n}{2}, \frac{1}{2}; a^2 w\right)$$

$$\left. - 4aw(2+n)(i+a) \, _1F_1\left(\frac{4+n}{2}, \frac{3}{2}; a^2 w\right). \right) \tag{3.31}$$

It may look like we have just exchanged the s-integral for the w-integral, but by writing the hypergeometric functions in series form,

$$I = \sum_{n=1}^{\infty} c_n \int \mathrm{d}w \sum_{m=0}^{\infty} \frac{2^{2m-1} a^{2m} \mathrm{e}^{-(1+a^2)w} w^{\frac{n-3}{4}+m} \Gamma\left(\frac{1+n}{2}+m\right)}{\Gamma\left(\frac{7+3n}{4}\right) \Gamma\left(2+2m\right)} \times$$

$$\times (n(1+2m-4a(i+a)w) + (1+2m)(1+2m-2(1+a^2)w)), \tag{3.32}$$

the w integral can now be performed. The result is

$$I = \sum_{n=1, m=0}^{\infty} c_n \frac{(a+i)4^{m-1} a^{2m} \left(a^2+1\right)^{-\frac{1}{4}(4m+n+5)}}{\Gamma(2m+2)\Gamma\left(\frac{7+3n}{4}\right)} \times$$

$$\times \Gamma\left(m + \frac{n+1}{4}\right) \Gamma\left(m + \frac{n+1}{2}\right) \times$$

$$\times \left(a\left(2m - 6mn - 2n^2 - n + 1\right) - i(2m+1)(n+1) \right). \tag{3.33}$$

101

The sum over m can be expressed in terms of the ordinary hypergeometric function, $_2F_1(a_1, a_2; b; z)$:

$$I = \sum_{n=1}^{\infty} c_n \frac{(n+1)\left(a^2 + 1\right)^{-\frac{n}{4}-\frac{1}{4}} \Gamma\left(\frac{n+1}{4}\right) \Gamma\left(\frac{n+1}{2}\right)}{24(a-i)^2(a+i)\Gamma\left(\frac{3n}{4}+\frac{7}{4}\right)} \times \tag{3.34}$$

$$\times \left(a^2(n+1)(-3an+a-i(n+1)) \, _2F_1\left(\frac{n+3}{2}, \frac{n+5}{4}; \frac{5}{2}; \frac{a^2}{a^2+1}\right) + \right. \tag{3.35}$$

$$\left. -6\left(a^2+1\right)(a(2n-1)+i) \, _2F_1\left(\frac{n+1}{4}, \frac{n+1}{2}; \frac{3}{2}; \frac{a^2}{a^2+1}\right)\right). \tag{3.36}$$

The space-time dependence in this expression is in $a = \tau/r$ and with additional r-dependence in the coefficients c_n The result above is the value for both τ and r positive. Using the known symmetries presented above, the solution can be extended to all values of τ and r by appropriate absolute value signs. Then changing variables to

$$\begin{aligned} \tau &= R\cos(\Phi) \\ r &= R\sin(\Phi) \end{aligned} \tag{3.37}$$

we have

$$I = \frac{\lambda^2 f\left(RM_D, \Phi\right)}{M_D} \tag{3.38}$$

with the function $f(\tilde{R}, \Phi)$ given by

$$f(\tilde{R}, \Phi) = \sum_{n=1}^{\infty} f_n \tilde{R}^n \tag{3.39}$$

$$f_n = \frac{e^{i\Phi} 2^{-1-n} (-1)^n \Gamma\left(\frac{n+1}{4}\right) |\sin(\Phi)|^{\frac{1+3n}{2}}}{9\pi(3n-1)\Gamma\left(\frac{n}{2}+1\right)\Gamma\left(\frac{1+3n}{4}\right)} \times \tag{3.40}$$

$$\times \left({}_2F_1\left(\frac{n+3}{2}, \frac{n+5}{4}; \frac{5}{2}; \cos^2(\Phi)\right)(n+1) \times \right. \tag{3.41}$$

$$\times \cos^2(\Phi)((1-3n)\cos(\Phi) - i(n+1)\sin(\Phi)) \tag{3.42}$$

$$+ {}_2F_1\left(\frac{n+1}{4}, \frac{n+1}{2}; \frac{3}{2}; \cos^2(\Phi)\right) \times$$

$$\left. \times 6((1-2n)\cos(\Phi) - i\sin(\Phi)) \right). \tag{3.43}$$

This exact infinite series expression for the exponent $I(\tilde{R}, \Phi)$ gives us the exact fermion two-point function in real (Euclidean) space (time). We have not been able to find a closed form expression for this final series. Note that $f_n \sim 1/n!$ for large n, and the series therefore converges rapidly. Moreover, numerically the hypergeometric functions are readily evaluated to arbitrary precision (e.g. with Mathematica), and therefore the value of $f(\tilde{R}, \Phi)$ can be robustly evaluated to any required precision.

As a check on this result, we can compare it to the exact result in the quenched $M_D = 0$ limit in [127], where the exact answer was found in a different way. In the limit where $M_D \to 0$ we see that only the first term of this series gives a contribution and the expression for the exponent collapses to

$$\lim_{M_D \to 0} I(R, \Phi) = \lambda^2 f_1 R = \lambda^2 \frac{e^{2i\Phi}}{12\pi} R. \tag{3.44}$$

In Cartesian coordinates this equals

$$\lim_{M_D \to 0} I(\tau, r) = \lambda^2 \frac{(\tau + ir)^2}{12\pi\sqrt{\tau^2 + r^2}}. \tag{3.45}$$

This is the exact same expression as found in [127] for $v = 1$.

There is one value of the argument for which $f(\tilde{R}, \Phi)$ drastically simplifies. For $r = 0$ ($\Phi = 0, \pi$) we have

$$f_n(\Phi = 0) = -\frac{(-1)^n}{6\pi\Gamma(n+2)} \qquad (3.46)$$

and thus

$$f(\tilde{R}, \Phi = 0) = \frac{1}{6\pi} + \frac{e^{-\tilde{R}} - 1}{6\pi\tilde{R}}. \qquad (3.47)$$

Further numerical analysis shows that the real part of $f(\tau, r)$ is maximal for $r = 0$.

The IR limit of the exact fermion two-point function compared to the large-M_D expansion

With this exact real space answer, we can now reconsider why the large M_D (large $N_f k_F$) limit fails and which expression does reliably capture the strongly coupled IR physics of interest. The expression obtained above, Eq. (3.43), is not very useful for extracting the IR Green's function or the Green's function at a large M_D as the expression is organized in an expansion around $RM_D = 0$. To study the limit where $RM_D \gg 1$ we can go back to Eq. (3.27). With this expression we see that the exponential in the integrand, $e^{-uz(s)}$ with $z \sim M_D|sr + \tau| \sim \tilde{r}$, is generically suppressed for large $\tilde{R} = RM_D$. The exceptions are when either $sr + \tau$ is small, s is large, or u is small. The first two cases are also unimportant in the $\tilde{R} \gg 1$ limit. In the first case we restrict the s integral to a small range of order $1/\tilde{R}$ around $-\tau/r$; this contribution therefore becomes more and more negligible in the limit $\tilde{R} \gg 1$. In the second case we will have a remaining large denominator in s outside the exponent that also suppresses the overall integral. Thus for large $\tilde{R}$, the only appreciable contribution of the exponential term to the integral in $I(\tau, r)$ arises when

u is small. To use this, we first write the integral as

$$I_{\text{IR}} = I_{\text{IR,exp}} + I_{\text{IR},-1}, \tag{3.48}$$

$$I_{\text{IR,exp}}(\tau, r) = \lambda^2 \int_{-\infty}^{\infty} ds \frac{s-i}{6\pi^2(s+i)(1+s^2)^{3/4}M_D} \times$$
$$\times \left(\int_0^1 du \frac{e^{-4uz(s)}-1}{u^{4/3}\sqrt{1-u^{4/3}}} - \int_1^{\infty} du \frac{1}{u^{4/3}} \right)$$
$$\simeq \lambda^2 \int_{-\infty}^{\infty} ds \frac{s-i}{6\pi^2(s+i)(1+s^2)^{3/4}M_D} \times$$
$$\times \left(\int_0^1 du \frac{e^{-4uz(s)}-1}{u^{4/3}} - \int_1^{\infty} du \frac{1}{u^{4/3}} \right),$$

$$I_{\text{IR},-1}(\tau, r) = \lambda^2 \int_{-\infty}^{\infty} ds \frac{s-i}{6\pi^2(s+i)(1+s^2)^{3/4}M_D} \times$$
$$\times \left(\int_1^{\infty} du \frac{1}{u^{4/3}} + \int_0^1 du \left(\frac{-u^{-4/3}}{\sqrt{1-u^{4/3}}} + u^{-4/3} \right) \right).$$

We have added and subtracted an extra term to each to ensure convergence of each of the separate terms. Since the important contribution to $I_{\text{IR,exp}}$ is from the small u region we can extend its range from $(0,1)$ to $(0,\infty)$. This way, the integrals can then be done

$$I_{\text{IR,exp}} = \int_{-\infty}^{\infty} ds \frac{-\lambda^2 |sr + \tau|^{1/3}}{3^{3/2}\pi M_D^{2/3}(s+i)^2 \Gamma\left(\frac{4}{3}\right)}$$
$$= -\frac{\Gamma\left(\frac{2}{3}\right)\lambda^2 |r|^{1/3}}{3^{3/2}\pi M_D^{2/3}\left(1+\frac{i\tau}{r}\right)^{2/3}}, \tag{3.49}$$

$$I_{\text{IR},-1} = \int_{-\infty}^{\infty} ds \frac{\lambda^2(s-i)}{6\pi^2(s+i)(1+s^2)^{3/4}M_D} \times$$
$$\times \left(\int_0^{\infty} du \Big(\frac{1}{u^{4/3}} - \frac{\theta(1-u)}{u^{4/3}\sqrt{1-u^{4/3}}} \Big) \right) = \frac{\lambda^2}{6\pi M_D}. \tag{3.50}$$

In total we have for large $\tilde{R}$:

$$I = -\frac{\Gamma\left(\frac{2}{3}\right)\lambda^2 |r|}{3^{3/2}\pi M_D^{2/3}\left(|r| + i\,\text{sgn}(r)\tau\right)^{2/3}} + \frac{\lambda^2}{6\pi M_D} + \mathcal{O}(\lambda^2 M_D^{-4/3}R^{-1/3}). \tag{3.51}$$

We see that the leading order term in R is the same as was obtained from the large M_D approximation of the exponent. The first subleading term is just a constant. This is good news because we already have the Fourier transform of this expression. This result is valid for length scales larger than $1/M_D$ with a bounded error of the order $R^{-1/3}$. Defining this approximation as G_{IR}, i.e.

$$G_{\mathrm{IR}} = G_0 \exp\left(-\frac{\Gamma\left(\frac{2}{3}\right)\lambda^2 |r|}{3^{3/2}\pi M_D^{2/3}(|r| + i\,\mathrm{sgn}(r)\tau)^{2/3}} + \frac{\lambda}{6\pi M_D}\right) \ , \qquad (3.52)$$

the error of this approximation follows from:

$$\Delta G_{\mathrm{IR}} = G - G_{\mathrm{IR}} = G_{\mathrm{IR}}\left(\exp\left(\mathcal{O}(\tilde{R}^{-1/3})\right) - 1\right). \qquad (3.53)$$

Since the exponential in G_{IR} is bounded we have that $\Delta G_{\mathrm{IR}} = \mathcal{O}(r^{-4/3})$. After Fourier transforming this translates to an error of order $\mathcal{O}(k^{-2/3})$.

3.4.1 The exact fermion two-point function in momentum space: Numerical method

Having understood the shortcomings of the naive large M_D answer, the way to derive the *exact* answer in real space, and the correct IR approximation, we can now analyze the behavior of the quantum critical metal at low energies. For this we need to transform to frequency-momentum space. As our exact answer is in the form of an infinite sum, this is not feasible analytically. We therefore resort to a straightforward numerical Fourier analysis.

To do so we first numerically determine the real space value of the exact Green's functions. To do so accurately, several observations are relevant

- The coefficients f_n in the infinite sum for $I(\tau, r)$ decay factorially in n so once n is of order $\tilde{R}$, convergence is very rapid.

- The hypergeometric functions for each n are costly to compute with high precision, but with the above choice of polar coordinates the arguments of the hypergeometric functions are independent of R and M_D. We therefore numerically evaluate the series over a grid in $\tilde{R}$ and Φ. We can then reuse the hypergeometric function evaluations many times and greatly decrease computing time.

- The real space polar grid will be limited to a finite size. The IR expansion from Eq. (3.52) can be used instead of the exact series for large enough $\tilde{R}$. To do so, we have to ensure an overlapping regime of validity. It turns out that a rather large value of $\tilde{R}$ is necessary to obtain numerical agreement between these two expansions, i.e. one needs to evaluate a comparably large number of terms in the expansion. For the results presented in this paper it has been necessary to compute coefficients up to order 16 000 in $\tilde{R}$, for many different angles Φ. The function is bounded for large τ and $\tilde{R}$ but each term grows quickly. This means that there are large cancellations between the terms that in the end give us a small value. We therefore need to calculate these coefficients to very high precision in evaluating the polynomial. For these high precision calculations, we have used the Gnu Multiprecision Library [140].

- On this polar grid we computed the exact answer for $\tilde{R} < \tilde{R}_0 \approx 1000$ and used cubic interpolation for intermediate values. For larger $\tilde{R}$ we use the asymptotic expansion in Eq. (3.52).

We then use a standard discrete numerical Fourier transform (DFT) to obtain the momentum space two-point function from this numeric prescription for $G(R, \Phi)$. Sampling $G(R, \Phi)$ at a finite number of discrete points, the size of the sampling grid will introduce an IR cut-off at the largest scales we sample and a UV-cut off set by the smallest spacing between points. These errors in the final result can be minimized by using the known asymptotic values analytically. Rather than Fourier transforming $G(\tau, r)$ as a whole, we Fourier transform $G_{\text{diff}}(\tau, r) = G(\tau, r) - G_{\text{IR}}(\tau, r)$ instead. Since both these functions approach the free propagator in the UV, the Fourier transform of its difference will decay faster for large ω and k. This greatly reduces the UV artefacts inherent in a discrete Fourier transform. These two functions *also* approach each other for large τ and x. In fact, with the numerical method we use to approximate $f(\tilde{R}, \Phi)$ described above, they will be identical for $\tilde{R}_0 < M_D \sqrt{\tau^2 + r^2}$. This means that we only need to sample the DFT within that area. With a DFT we will always get some of the UV tails of the function that gives rise to folding aliasing artefacts. Now our function decays rapidly so one could do a DFT to very high frequencies and discard the high frequency part. This unfortunately takes up a lot of memory so we have gone with a more CPU intensive but memory friendly approach. To address this we perform a convolution with a Gaussian kernel, perform the DFT, keep the lowest

1/3 of the frequencies and then divide by the Fourier transform of the kernel used. This gives us a good numeric value for $G_{\text{diff}}(\omega, k)$. To this we add our analytic expression for $G_{\text{IR}}(\omega, k)$.

## 3.5 The physics of 2+1 quantum critical metals in double scaling limit

With the exact real space expression and the numerical momentum space solution for the full non-perturbative fermion Green's function, we can now discuss the physics of the elementary quantum critical metal in the double scaling limit. Let us emphasize right away that all our results are in Euclidean space. Although a Euclidean momentum space Green's function can be used to find a good Lorentzian continuation with a well-defined and consistent spectral function, this function is not easily obtainable from our numerical Euclidean result. We leave this for future work. The Euclidean signature Green's function does not visually encode the spectrum directly, but for very low energies/frequencies the Euclidean and the Lorentzian expressions are nearly identical, and we can extract much of the IR physics already from the Euclidean correlation function.

In Fig. 3.4 we show density plots of the imaginary part of $G(\omega, k_x)$ for different values of M_D and in Fig. 3.5 we show cross-sections at fixed low ω. For the formal limit $M_D = 0$ we detect three singularities near $\omega = 0$ corresponding with the three Fermi surfaces found in Lorentzian signature in our earlier work [127]. However, for any appreciable value of the dimensionless ratio M_D/λ^2 one only sees a single singularity. As the plots for $G(\omega, k_x)$ at low frequency show, its shape approaches that of the strongly Landau-damped $M_D \to \infty$ result, Eq. (3.19), as one increases M_D/λ^2, though for low M_D it is still distinguishably different. Recall that our results are derived in the limit of large k_F and therefore a realistic ($N_f \sim 1$) value for M_D is $M_D \sim \lambda\sqrt{N_f k_F} \gg \lambda^2$.

This result is in contradistinction to what happens to the bosons. When the bosons are not affected in the IR, i.e. the quenched limit, the fermions are greatly affected by the boson: there is a topological Fermi surface transition and the low-energy spectrum behaves as critical excitations [127]. However, once we increase M_D to realistic values, the bosonic excitations are rapidly dominated in the IR by Landau damping but we now see that this *reduces* the corrections to the fermions. As M_D is increased for fixed ω, k_x, the deep IR fermion two-point function
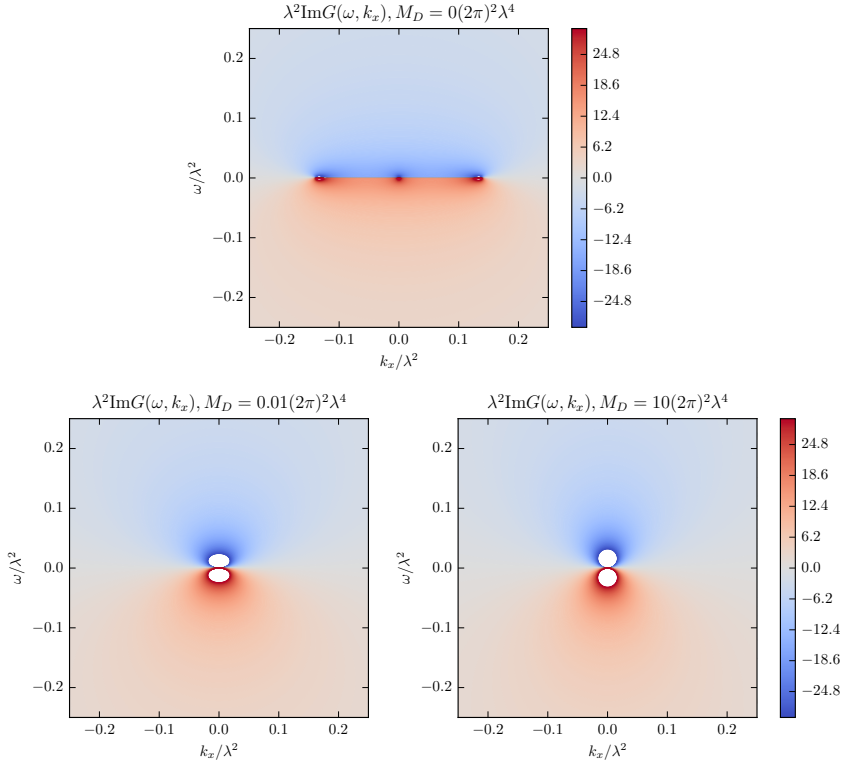
Figure 3.4. Density plots of the imaginary part of the exact (Euclidean) fermion Green's function $G(\omega, k_x)$ for three values of M_D. In the quenched limit $M_D = 0$ the three Fermi surface singularities are visible. For any appreciable finite M_D the Euclidean Green's function behaves as a single Fermi surface non-Fermi liquid.
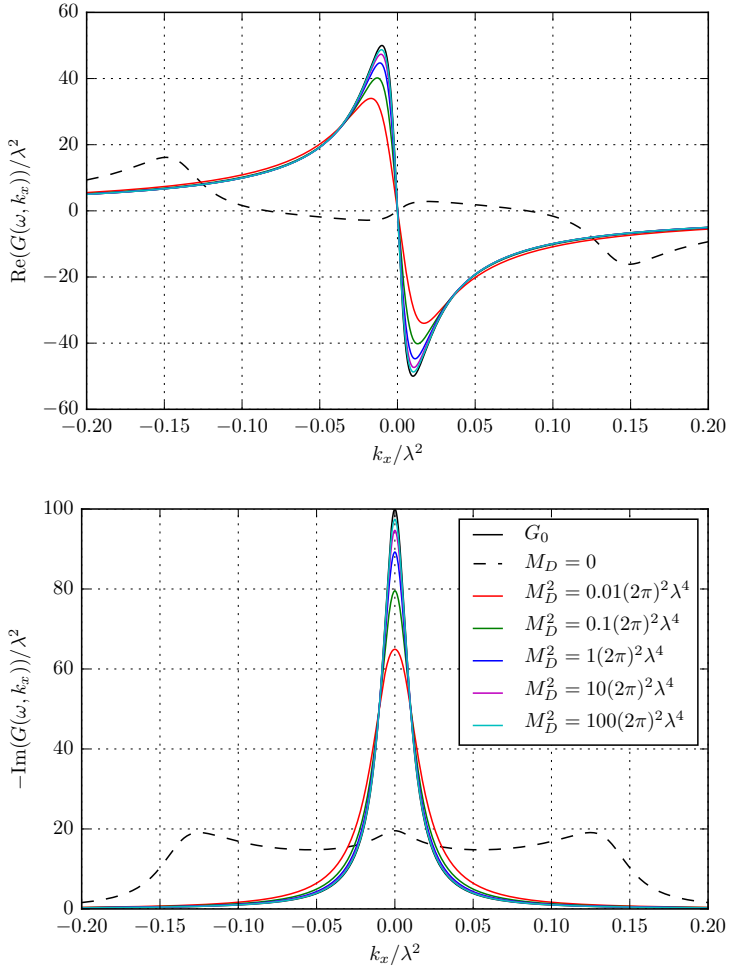
Figure 3.5. Real and imaginary parts of $G(\omega, k_x)$ for very small $\omega = 0.01\lambda^2$.

approaches more and more that of the simple RPA result with self-energy $\Sigma \sim i\omega^{2/3}$.

A more careful analysis of the IR reveals that there are several distinct $\omega \to 0$ limits of the two-point function:

$$\lim_{\substack{\omega \to 0, \\ k_x \text{ fixed}}} G_{\text{IR}}(\omega, k_x) \approx e^{\frac{\lambda^2}{6\pi M_D}} \frac{1}{i\omega - k_x - \Sigma_{\text{RPA}}}$$

$$\lim_{\substack{\omega \to 0, \\ k_x/\omega \text{ fixed}}} G_{\text{IR}}(\omega, k_x) \approx e^{\frac{\lambda^2}{6\pi M_D}} \frac{1}{i\omega - k_x - \frac{4\pi}{3\sqrt{3}}\Sigma_{\text{RPA}}}$$

However in the case of $\omega^2 \sim l_0 k_x^3$, the full expression for G_{IR} is necessary to describe the low energy limit,

$$\lim_{\substack{\omega \to 0, \\ l_0 k_x^3 \omega^{-2} \text{ fixed}}} G_{\text{IR}}(\omega, k_x) =$$

$$= e^{\frac{\lambda^2}{6\pi M_D}} \left[\frac{1}{i\omega - k_x} \cos\left(\frac{\omega}{l_0^{1/2}(\omega + ik_x)^{3/2}} \right) \right.$$

$$+ \frac{6\sqrt{3}i\Gamma\left(\frac{1}{3}\right)\omega^{2/3}}{8\pi l_0^{1/3}(\omega + ik_x)^2} \, {}_1F_2\left(1; \frac{5}{6}, \frac{4}{3}; -\frac{\omega^2}{4l_0(\omega + ik_x)^3} \right) +$$

$$\left. + \frac{3\sqrt{3}i\Gamma\left(-\frac{1}{3}\right)\omega^{4/3}}{8\pi l_0^{2/3}(\omega + ik_x)^3} \, {}_1F_2\left(1; \frac{7}{6}, \frac{5}{3}; -\frac{\omega^2}{4l_0(\omega + ik_x)^3} \right) \right],$$

This existence of multiple limits shows in fact that the RPA result is never a good low energy (less than M_D) approximation for any value of M_D/λ^2. We can illustrate this more clearly by studying the self-energy of the fermion $\Sigma(\omega, k_x) = G(\omega, k_x)^{-1} - G_0(\omega, k_x)^{-1}$. It is shown in Fig. 3.6 that the naive large M_D RPA result (dotted lines) does agree for large M_D at $\omega = 0, k_x = 0$ and the leading ω dependence of the imaginary part is captured. The leading k_x dependence is not captured by RPA. On the other hand, our improved approximation for the low energy regime G_{IR} (dashed lines) captures these higher order terms in the low energy expansion of $G(\omega, k_x)$ very well and also works for finite values of M_D/λ^2.

In all cases it is clear that the Fermion excitation, though qualitatively sharp, is not a Fermi liquid quasiparticle. We can calculate the occupation number and check whether it is consistent with the non-Fermi liquid nature of the Green's function. With a Fermi liquid by definition is meant a
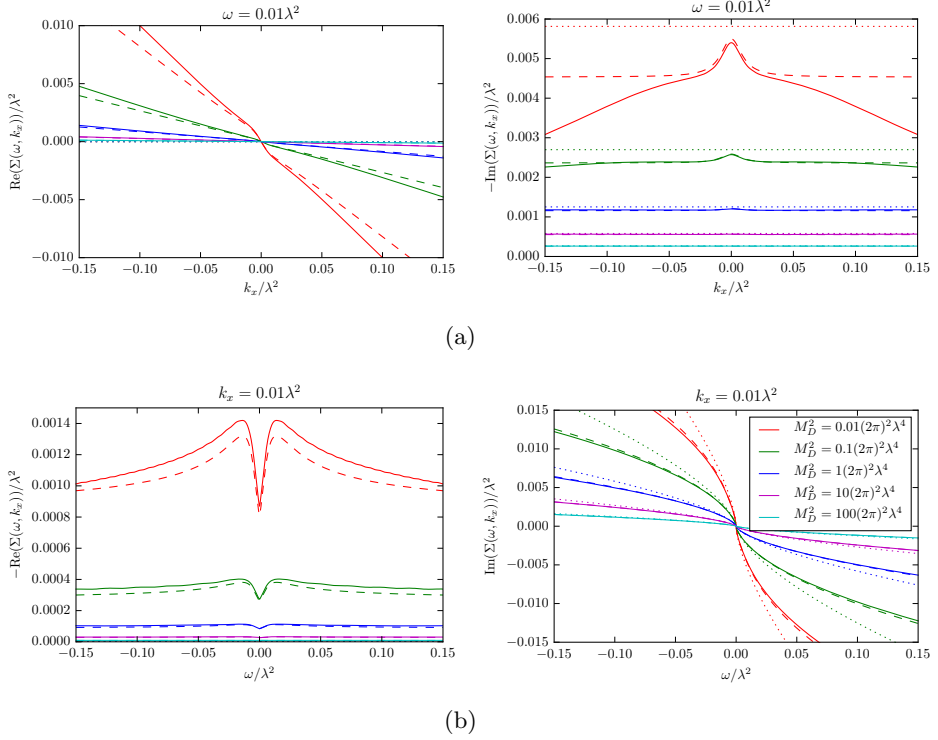
Figure 3.6. Real and imaginary parts of the fermion self-energy for (a) $\omega = 0.01\lambda^2$ and for (b) $k_x = 0.01\lambda^2$. Dashed lines show the G_{IR}-approximation; dotted lines show the RPA result.

spectrum with a discontinuity in the zero-temperature momentum distribution function $n_k = \int_{-\infty}^{0} d\omega_R A(\omega_R, k_x)/2\pi$ with $A(\omega_R, k_x)$ the spectral function. As the spectral function is the imaginary part of the retarded Green's functions and the latter is analytic in the upper half plane of ω_R we can move this contour to Euclidean ω and use the fact that $G(\omega, k_x)$ approaches $G_0(\omega, k_x)$ in the UV to calculate the momentum distribution function from our Euclidean results. In detail

$$
\begin{aligned}
n_{k_x} &= -\int_{-\infty}^{0} d\omega_R \operatorname{Im} \frac{G_R(\omega_R, k_x)}{\pi} \\
&= \operatorname{Im}\left[\int_{0}^{\Lambda} d\omega\, i \frac{G(\omega, k_x)}{\pi} + \int_{C} dz\, i \frac{G(z, k_x)}{\pi}\right] \; ;
\end{aligned}
\tag{3.54}
$$

the first integral can be done with the numerics developed in the preceding section. The contour C goes from Λ to $-\infty$ and for large enough Λ this is in the UV and can well be approximated by the free propagator. The resulting momentum distribution $n(k)$ is shown in Fig. 3.7. Within our numerical resolution, these curves are continuous as opposed to a Fermi liquid. This is of course expected; the continuity reflects the absence of a clear pole in the IR expansions in the preceding subsection. Note also that as M_D is lowered, the finite M_D curves approach the quenched result for $|k_x| > k_x^*$ where k_x^* is the point of the discontinuity of the derivative of the quenched occupation number. At k^* the (derivative) of the quenched momentum distribution number does have a discontinuity (reflecting the branch cut found in [127]).

3.6 Conclusion

We have presented a non-perturbative answer for the (Euclidean) fermion and boson two-point functions of the elementary quantum critical metal in the double limit of small N_f and large k_F with $N_f k_F$ fixed. This limit was taken order by order in perturbation theory and additionally before performing bosonic momentum integrals.

Our exact results clarify how approximations that have been made in the past hang together. The $N_f \to 0$, $k_F \to \infty$ theory is characterized by two energy scales λ^2 and M_D. For very large ω/λ^2 and ω/M_D^2 one can use perturbation theory in λ to understand the theory. This is the perturbation around the UV-fixed point of a free fermion plus a free boson.
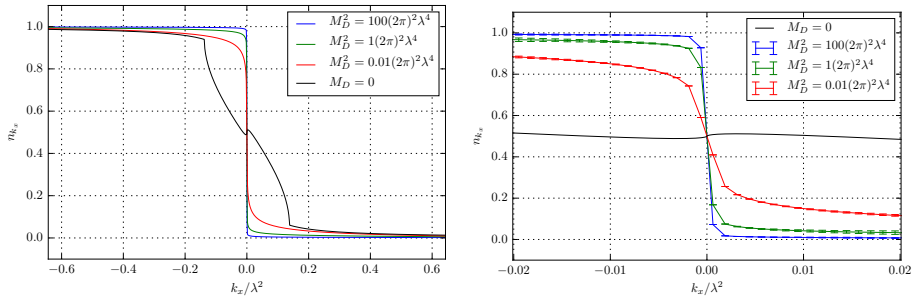
Figure 3.7. Momentum distribution function. The two plots show the same function for different ranges. The error bars of the lower figure show an estimate of the error due to using the free Green's function close to the UV. The error-bars are exaggerated by a factor 100.

In the deep IR region, $\omega \ll M_D^2$, we have an analytic expression for the two-point function, G_{IR}. This shows a $\omega^2 \sim l_0 k_x^3$ scaling.

In the intermediate regime, the full numerical results that we have presented are necessary.

The quenched result we obtained earlier [127] does not seem to have a useful regime of validity. As the momentum occupation number $n(k)$ indicates, its precise regime of applicability depends discontinuously on the momentum k/λ^2. The discontinuity is surprising, but it can be explained analytically as an order of limits ambiguity. Although it is hard to capture the deep IR region for very small N_f in the full numerics we find from G_{IR} that in the ω-k plane there is a region where the limit $N_f \to 0$ and $\omega, k_x \to 0$ do not commute. We show an indication of this in appendix 3.C. Thus for scales below λ^2, the quenched result is not useful. For scales above λ^2 with M_D small, we can use perturbation theory so also in this regime the quenched result is not useful. For small ω and k_x, below M_D, the IR approximation we presented above gives a good description of the physics. We have presented a pictorial overview of how the various approximations are related in Fig. 3.8.

As argued before the spectrum of the elementary quantum critical metal in the ordered double scaling limit obtained here is not the definitive one. Taking this limit after the bosonic integrals and the perturbative sum may give a different result. Another estimate for the true IR spectrum of the elementary quantum critical metal has been postulated before based on large N_f approximations [131, 141, 142], but our result
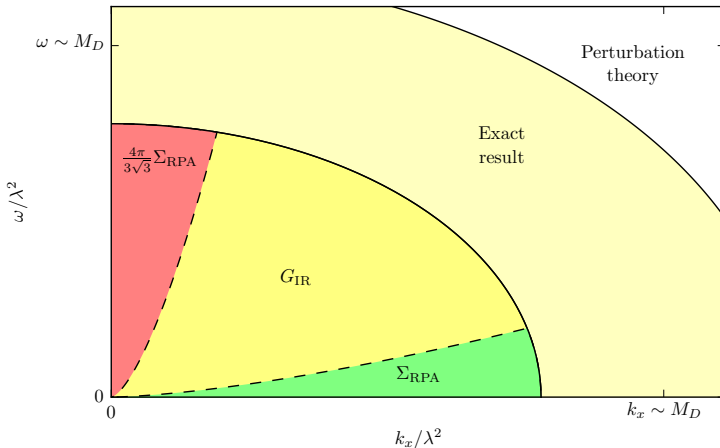
Figure 3.8. A sketch of the regimes of applicability of various approximations to the exact fermion Green's function of the elementary quantum critical metal in the double scaling limit. The G_{IR} approximation is applicable both in the deep yellow region and the red and green regions.

at small N_f gives a different IR. Our non-perturbative answer follows from the insight that in the limit of large k_F all fermion loops with more than two external boson legs have cancellations upon symmetrization such that their scaling in k_F is reduced. This higher loop cancellation has been previously put forward as a result of the strong forward scattering approximation. This approximation is engineered such that the Schwinger-Dyson equations combined with the fermion number Ward identity collapse to a closed set of equations. The solution to this closed set is the same dressed fermion correlator that we have presented. However the exact connection between the strong forward scattering approximation and the double scaling limit, is not clear. In the double scaling limit here, it is manifest that only the boson propagator is corrected and this in turn implies that the exact fermion Green's function in real space is an exponentially dressed version of the free Green's function.

At the physics level, an obvious next step is therefore to explore the spectrum of the elementary quantum critical metal including corrections in N_f that are not proportional to k_f. Since this necessarily involves higher-point boson correlations, the role of self-interactions of the boson needs to be considered. These are also relevant in the IR and may therefore give rise to qualitatively very different physics than found here. We leave this

for future work.

3.7 Acknowledgements

3.A Multiloop cancellation

The robustness of the one-loop result in case of linear fermionic dispersion was recognized before under the name of multiloop cancellation [130]. The technical result is that for a theory with a simple Yukawa coupling and linear dispersion around a Fermi surface, a symmetrized fermion loop with more than two fermion lines vanishes. In our context the linear dispersion is a consequence of the large k_F limit. In other words all higher loop contributions to the polarization Π should be subleading in $1/k_F$. This was explicitly demonstrated at two loops in [143].

We will give here a short derivation of this multiloop cancellation in the limit $k_F \to \infty$. We may assume in this limit that the momentum transfer at any fermion interaction is always much smaller than the size of the initial ($\vec{k}$) and final momenta ($\vec{k}'$) which are of the order of the Fermi momentum, i.e. $|\vec{k}' - \vec{k}| \ll k_F$ with $|\vec{k}|, |\vec{k}'| \sim k_F$. The free fermion Green's function then reflects a linear dispersion

$$G_0(\omega, k) = \frac{1}{i\omega - vk} \tag{3.55}$$

We now Fourier transform back to real space, as multiloop cancellation is most easily shown in this basis. The real space transform of the "linear" free fermion propagator above is

$$G_0(\tau, r) = -\frac{i}{2\pi} \frac{\text{sgn}(v)}{r + iv\tau}, \tag{3.56}$$

116

where as before r is the conjugate variable to $k = |\vec{k}| - k_F$. The essential step in the proof is that real space Green's function manifestly obeys the identity [127]

$$G_0\left(z_1\right)G_0\left(z_2\right) = G_0\left(z_1 + z_2\right)\left(G_0\left(z_1\right) + G_0\left(z_2\right)\right) \qquad (3.57)$$

with $z \equiv r + iv\tau$. Consider then (the subpart of any correlation function/Feynman diagram containing) a fermion loop with $n \geq 2$ vertices along the loop connected to indistinguishable scalars (i.e. no derivative interactions and all interactions are symmetrized). The corresponding algebraic expression in a real space basis will then contain the expression

$$F\left(z_1, ..., z_n\right) = \sum_{(i_1,..,i_n)\in S_n} G_0\left(z_{i_1} - z_{i_2}\right)G_0\left(z_{i_2} - z_{i_3}\right)...$$

$$...G_0\left(z_{i_{n-1}} - z_{i_n}\right)G_0\left(z_{i_n} - z_{i_1}\right), \qquad (3.58)$$

where S_n is the set of permutations of the numbers 1 through n. Using the "linear dispersion" identity Eq. (3.57) and the shorthand notation $G_0\left(z_{i_1} - z_{i_2}\right) = G_{12}$ we obtain

$$F\left(z_1, ..., z_n\right) = \sum_{(i_1,..,i_n)\in S_n} G_{12}G_{23}...G_{n-1,1}\left(G_{n-1,n} + G_{n,1}\right). \qquad (3.59)$$

Next we cyclically permute the indices from 1 to $n-1$: $1 \to 2, 2 \to 3, ...,$ $n-1 \to 1$ in the sum

$$\sum_{(i_1,..,i_n)\in S_n} G_{12}G_{23}...G_{n-1,1}G_{n-1,n} = \sum_{(i_1,..,i_n)\in S_n} G_{23}G_{34}...G_{12}G_{1,n}. \qquad (3.60)$$

This gives us

$$F\left(z_1, ..., z_n\right) = \sum_{(i_1,..,i_n)\in S_n} G_{12}G_{23}...G_{n-1,1}\left(G_{1,n} + G_{n,1}\right). \qquad (3.61)$$

Then since $G_{i,j}$ corresponds to a (spinless) fermionic Green's function, it is antisymmetric $G_{i,j} = -G_{j,i}$, and we can conclude that F vanishes for $n \geq 3$. For $n = 2$ it is not possible to use the identity Eq. (3.57) since we would need to evaluate $G(0)$ which is infinite.

3.B The Fourier transform of the fermion Green's function in the large M_D approximation

We will now show how to perform this Fourier transform. We need to calculate the following integral:

$$
\underset{M_D \to \infty}{G_f} (\omega, k) = \int \mathrm{d}\tau \mathrm{d}x \frac{e^{i(\omega\tau - kx)}}{2\pi(ix - v\tau)} \exp\left(-\frac{|x|}{l_0^{1/3} \left(|x| + iv\,\mathrm{sgn}(x)\tau\right)^{2/3}}\right)
$$

$$(3.62)$$

First we note that integrand is τ-analytic in the region $\{\tau \in \mathbb{C} : \min(0, vx) < \mathrm{Im}(\tau) < \max(0, vx)\}$. Since the integrand necessarily goes to 0 at ∞ we can thus shift the τ contour, $\tau \to \tau + ix/v$. We now have

$$
\underset{M_D \to \infty}{G_f} (\omega, k) = -\int \frac{\mathrm{d}\tau \mathrm{d}x}{2\pi v\tau} \exp\left(i\omega\tau + \right.
$$
$$
\left. - x\left(ik + \omega/v + \frac{\mathrm{sgn}(x)}{l_0^{1/3} \left(iv\,\mathrm{sgn}(x)\tau\right)^{2/3}}\right)\right) \quad (3.63)
$$

We have allowed ourselves to choose the order of integration, shift the contour, and then change the order. We see that the x integral now is trivial but only converges for

$$
-\frac{v^{1/3}}{2l_0^{1/3}|\tau|^{2/3}} < \mathrm{Re}(\omega) < \frac{v^{1/3}}{2l_0^{1/3}|\tau|^{2/3}} \quad (3.64)
$$

This is fine since we know that the final result is ω-analytic in both the right and left open half-planes. As long as we can obtain an answer valid within open subsets of both of these sets we can analytically continue the found solution to the whole half planes. We thus proceed assuming $\mathrm{Re}(\omega)$ is in this range. One can further use symmetries of our expression to relate the left and right ω-half-planes, so to simplify matters, from now on we additionally assume ω to be positive. Let us now consider a negative x, we then see that the τ integral can be closed in the upper half plane and since it is holomorphic there the result will be 0. We can thus limit the x

integrals to $\mathbb{R}^+$. We then have

$$\underset{'N_f k_F \to \infty}{G_f}(\omega, k) = \int d\tau \frac{e^{i\omega\tau}}{2\pi v\tau} \frac{-1}{a + \frac{1}{l_0^{1/3}(iv\tau)^{2/3}}} \tag{3.65}$$

where $a = ik + \omega/v$. The integrand has a pole at

$$(i\tau)^{2/3} = -1/(a l_0^{1/3} v^{2/3}). \tag{3.66}$$

Now break the integral in positive and negative τ and write it as

$$\underset{M_D \to \infty}{G_f}(\omega, k) = \frac{h((-i)^{2/3} u_0^*)^* - h((-i)^{2/3} u_0)}{2\pi v a} \tag{3.67}$$

where

$$h(u) = \int_0^\infty d\tau \frac{e^{i\tau}}{\tau + u\tau^{1/3}},$$
$$u_0 = \frac{\omega^{2/3}}{a l_0^{1/3} v^{2/3}}. \tag{3.68}$$

Usng Morera's theorem we can prove that h is holomorphic on $\mathbb{C}/\mathbb{R}^-$. Consider any closed curve C in $\mathbb{C}/\mathbb{R}^-$. We need to show that

$$\int_C du\, h(u) = 0 \tag{3.69}$$

We do this by rotating the contour slightly counter clockwise. For any curve C there is clearly a small $\epsilon > 0$ such that we will still not hit the pole $\tau + u\tau^{1/3} = 0$.

$$\int_C du \int_0^{(1+i\epsilon)\infty} d\tau \frac{e^{i\tau}}{\tau + u\tau^{1/3}}, \tag{3.70}$$

The piece at ∞ converges without the denominator and thus goes to 0. Since the integral now converges absolutely we can use Fubini's theorem to change the orders of integration

$$\int_0^{(1+i\epsilon)\infty} d\tau \int_C du \frac{e^{i\tau}}{\tau + u\tau^{1/3}} = 0 \tag{3.71}$$

119

$$h(u) \qquad\qquad G_{3,5}^{5,3}\left(\begin{matrix} 0, \frac{1}{3}, \frac{2}{3} \\ 0, 0, \frac{1}{3}, \frac{1}{2}, \frac{2}{3} \end{matrix} \ \middle| \ -\frac{u^3}{4} \right)$$
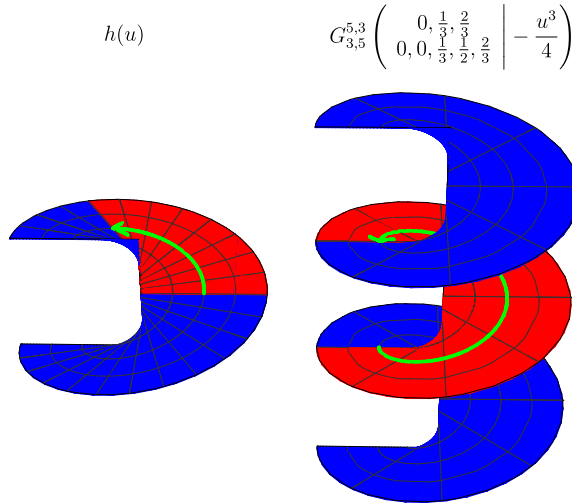
Figure 3.9. The left image shows part of the Riemann surface of the function h and the right image shows part of the Riemann surface of the G-function. The part in red of the left image can be expressed as the G-function evaluated on its first sheet, the red part of the right image. The green arrow shows how points are mapped from one Riemann surface to the other by the mapping $u \mapsto -u^3/4$

And since also the integrand is holomorphic on a connected open set containing C the proof is finished.

The function h can for $0 < \arg(u) < 2\pi/3$ be expressed as a Meijer G-function:

$$h(u) = \frac{3}{8\pi^{5/2}} G_{3,5}^{5,3}\left(\begin{matrix} 0, \frac{1}{3}, \frac{2}{3} \\ 0, 0, \frac{1}{3}, \frac{1}{2}, \frac{2}{3} \end{matrix} \ \middle| \ -\frac{u^3}{4} \right) \qquad (3.72)$$

The G-function has a branch cut at $\mathbb{R}^-$ and because of that we can not easily write $h(u)$ in terms of it since the argument u appears cubed in the argument of the G-function and we know that h is holomorphic on all of $\mathbb{C}/\mathbb{R}-$. We can however express h as an analytic continuation of the G-function past this branch cut, onto the further sheets of its Riemann surface. We will write the G-function as a function with two real arguments, first the absolute value and second the phase of its otherwise

complex argument. We will allow the phase to be any real number and when outside the range $[-\pi, \pi]$, we let the function be defined by its analytical continuation to the corresponding sheet. We hereafter omit the constant parameters of the G-function. We then have:

$$
\begin{aligned}
\underset{M_D \to \infty}{G_f}(\omega, k) &= 3 \frac{G_{3,5}^{5,3}\big(\frac{|u_0|^3}{4}, -2\pi - 3\arg(u_0)\big)^*}{16\pi^{7/2}va} + \\
&\quad - 3 \frac{G_{3,5}^{5,3}\big(\frac{|u_0|^3}{4}, -2\pi + 3\arg(u_0)\big)}{16\pi^{7/2}va} \\
&= 3 \frac{G_{3,5}^{5,3}\big(\frac{|u_0|^3}{4}, 3\arg(u_0) + 2\pi\big) - G_{3,5}^{5,3}\big(\frac{|u_0|^3}{4}, 3\arg(u_0) - 2\pi\big)}{16\pi^{7/2}va}
\end{aligned}
$$

In the last step we used the fact that the G-function commutes with complex conjugation. We see that the Green's function is given by a certain monodromy of the G-function. It is given by the difference in its value starting at a point $u_0^3/4$ on the sheet above the standard one and then analytically continuing clockwise around the origin twice to the sheet below the standard one and there return to $u_0^3/4$. Since we only need this difference, we might expect this to be a, in some sense, simpler function as would happen for e.g. monodromies of the logarithm. To see how to simplify this we look at the definition of the G-function. It is defined as an integral along L:

$$
\begin{aligned}
G_{p,q}^{m,n}\left(\begin{array}{c} a_1, \ldots, a_p \\ b_1, \ldots, b_q \end{array} \middle| z\right) &= \\
&= \frac{1}{2\pi i} \int_L \frac{\prod_{j=1}^m \Gamma(b_j - s) \prod_{j=1}^n \Gamma(1 - a_j + s)}{\prod_{j=m+1}^q \Gamma(1 - b_j + s) \prod_{j=n+1}^p \Gamma(a_j - s)} z^s \, ds, \quad (3.73)
\end{aligned}
$$

There are a few different options for L and which one to use depends on the arguments. In our case L starts and ends at $+\infty$ and circles all the poles of $\Gamma(b_i - s)$ in the negative direction. Using the residue theorem we can recast the integral to a series. We have double poles at all negative integers and some simple poles in between. The calculation to figure out the residues of all these single and double poles is a bit too technical to present here but in the end the series can be written as

$$
G_{3,5}^{5,3}(z) = \sum_{n=0}^{\infty} \left(a_n z^n + b_n z^n \log(z) + c_n z^{n+1/3} + d_n z^{n+1/2} + e_n z^{n+2/3} \right)
$$

$$(3.74)$$

Now we perform the monodromy term by term and a lot of these terms cancel out.

$$G_{3,5}^{5,3}(|z|, \arg(z) + 2\pi) - G_{3,5}^{5,3}(|z|, \arg(z) - 2\pi) =$$

$$\sum_{n=0}^{\infty} \left(4\pi i b_n z^n + i\sqrt{3} c_n z^{n+1/3} - i\sqrt{3} e_n z^{n+2/3} \right) \tag{3.75}$$

The coefficients a_i contain both the harmonic numbers and the polygamma function whereas the other coefficients are just simple products of gamma functions. This simplification now lets us sum this series to a couple of generalized hypergeometric functions. Inserting the expressions for a and u_0 we have

$$\begin{aligned}
\underset{M_D \to \infty}{G_f}(\omega, k) &= \frac{1}{i\omega - kv} \cos\left(\frac{\omega}{v l_0^{1/2}(\omega/v + ik)^{3/2}} \right) \\
&+ \frac{6\sqrt{3} i \Gamma\left(\frac{1}{3}\right) \omega^{2/3}}{8\pi l_0^{1/3} v^{5/3}(\omega/v + ik)^2} \, {}_1F_2\left(1; \frac{5}{6}, \frac{4}{3}; -\frac{\omega^2}{4 l_0 v^2(\omega/v + ik)^3} \right) \\
&+ \frac{3\sqrt{3} i \Gamma\left(-\frac{1}{3}\right) \omega^{4/3}}{8\pi l_0^{2/3} v^{7/3}(\omega/v + ik)^3} \, {}_1F_2\left(1; \frac{7}{6}, \frac{5}{3}; -\frac{\omega^2}{4 l_0 v^2(\omega/v + ik)^3} \right).
\end{aligned} \tag{3.76}$$

Note that this expression is ω-holomorphic for ω in the right half plane so our previous assumptions on ω can be relaxed as long as ω is in the right half plane. We note from expression (3.62) that if we change sign on both ω and k and do the changes of variables $\tau \to -\tau$ and $x \to -x$ we end up with the same integral up to an overall minus sign. We can thus get the left half plane result using the relation

$$\underset{M_D \to \infty}{G_f}(-\omega, k) = - \underset{M_D \to \infty}{G_f}(\omega, -k). \tag{3.77}$$

As mentioned in the main text, this expression has been compared with numerics to verify that we have not made any mistakes. See Fig. 3.2. We have also done the two integrals for the Fourier transform in the opposite order, first obtaining a different Meijer G-function then using the G-function convolution theorem to do the second integral. In the end one obtains the same monodromy of the G-function as above. This expression can also be found in Appendix A.2 of [131], however it was not entirely clear from the phrasing of the last paragraph that this function is actually the exact Fourier transform, Eq. (3.62).

3.C The discontinuous transition from the quenched to the Landau-damped regime

We show here why including Landau damping (finite M_D) physics starting from the quenched $N_f \to 0$ result, is discontinuous in the IR. To do so we calculate the Green's function by imposing the $N_f \to 0$ limit from the begining. We need to evaluate the Fourier transform integral:

$$G_L\left(\omega, k\right) = \int_{-\infty}^{\infty} dx \int_{-L}^{L} d\tau G_0 \exp\left(I_0 + i\omega \cdot \tau - ik \cdot x\right), \qquad (3.78)$$

where as before the free propagator is

$$G_0(\tau, x) = -\frac{i}{2\pi} \frac{1}{x + i \cdot \tau} \qquad (3.79)$$

and the $N_f \to 0$ limit of the exponent of the real space Green's function:

$$I_0 = \frac{(\tau + i \cdot x)^2}{12\pi\sqrt{\tau^2 + x^2}}. \qquad (3.80)$$

Note however that the τ integral is divergent in this limit. Therefore in (3.78) we have introduced a cutoff L in this direction. By looking at the full expansion of I we can see that the natural value of L is of the order $1/M_D$. For larger values of τ the asymptotic expansion describes I better. We expect that for large enough momenta and frequencies the asymptotic region does not contribute to the Fourier transform and therefore the cutoff can be removed. This naive epxectation however is only partly true. We will shortly see that the region in the $\omega - k$ plane where the cutoff can be removed is more complicated and asymmetric in terms of the momenta and frequency.

Let us turn now to the evaluation of (3.78). After making the coordinate change $\tau \to \tau$, $x \to u \cdot \tau$ one of the integrals (τ) can be evaluated analytically:

$$G_L\left(\omega, k\right) = \int_{-\infty}^{\infty} du \left(I_1(u) + I_2(u) + I_3(u)\right), \qquad (3.81)$$

where

$$I_1(u) = \frac{6\exp\left(ikLu\sqrt{u^2+1} - iL\omega\sqrt{u^2+1} - \frac{L(u-i)^2}{12\pi}\right)}{12\pi(u+i)(ku-\omega) + i\sqrt{u^2+1}u + \sqrt{u^2+1}}, \qquad (3.82)$$
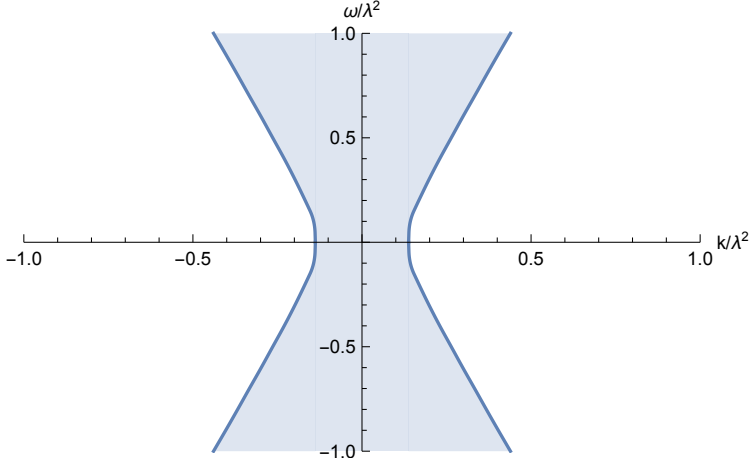
Figure 3.10. The region of convergence. In the shaded area the $L \to \infty$ ($N_f \to 0$) limit is not convergent while outside this area $\lim_{L \to \infty} G_L = G_{quenched}$.

$$I_2(u) = \frac{6i \exp\left(-ikLu\sqrt{u^2+1} + iL\omega\sqrt{u^2+1} - \frac{L(u-i)^2}{12\pi}\right)}{12i\pi k(u+i)u + \sqrt{u^2+1}u - i\sqrt{u^2+1} + 12\pi(1-iu)\omega}, \quad (3.83)$$

$$\begin{aligned} I_3(u)^{-1} = &-\frac{u\left(-3 + u\left(144\pi^2 k^2(u+i) + u - 3i\right)\right)}{144\pi(ku-\omega)} \\ &+ \frac{288\pi^2 ku(u+i)\omega - 144\pi^2(u+i)\omega^2 - i}{144\pi(ku-\omega)}. \end{aligned} \quad (3.84)$$

By numerically performing the single integral u we can obtain $G_{M_D \to 0}$. Since it is easier than evaluating the Fourier transform of the true real-space version of the Green's function it is worth understanding how the $L \to \infty$ (which is equivalent to $M_D \to 0$) works. The result is depicted on Fig. 3.10. In the shaded region (which corresponds to small k) the limit is not well defined while outside of this region the limit is equal to the quenched result. The numerics shows that for zero frequency, the edge of this region is at k^*, where the Green's function is singular.

We can qualitatively determine the line separating the convergent and divergent region. For this we assume that when L is large one can expand

the exponent in u

$$I_1(u) \sim \exp\left[u^2\left(-\frac{1}{12\pi} - \frac{1}{2}i\omega\right)L + \frac{iu(6\pi k + 1)}{6\pi}L - iL + \omega\right.$$
$$\left. + \frac{L}{12\pi} + \mathcal{O}\left(Lu^3\right)\right]. \qquad (3.85)$$

We see that because of the term $-L \cdot u^2/(12\pi)$, the integrand is non-zero only in a narrow region around $u = 0$. For the same reason we approximate the denominator of (3.82) by replace u by zero there. With these simplifications we arrive to a gaussian integral which can be evaluated analytically:

$$\int_{-\infty}^{\infty} I_1(u)du \approx \frac{12i\sqrt{3}\pi \exp\left(\frac{iL\left(6\pi k^2 + 2k + \omega(-12\pi\omega + i)\right)}{12\pi\omega - 2i}\right)}{(12\pi\omega + i)\sqrt{L(1 + 6i\pi\omega)}}. \qquad (3.86)$$

The real part of (3.86) is

$$L\frac{3\left(\omega^2 - k^2\right)\pi - k}{36\pi^2\omega^2 + 1}. \qquad (3.87)$$

It is clear that if this value is positive (i.e. $3\left(\omega^2 - k^2\right)\pi - k > 0$) than the $L \to \infty$ limit is divergent. Looking at the numerical result in Fig. 3.10 we indeed see that the boundary of the shaded region is indeed a hyperbola. Note, however, that the exact location of this hyperbola obtained from expanding the exponent is slightly off.

It is interesting to note that if we are in the divergent region G_L is not convergent for large L but for some intermediate values it can still get close to the quenched result $G_{quenched}$. To quantify this let us introduce a relative "error" function

$$\text{error}(L) = \left|\frac{G_L - G_{quenched}}{G_{quenched}}\right|. \qquad (3.88)$$

In Fig. 3.11 we show the behavior of this function for various points in the $\omega - k$ plane. For a point which is outside the shaded region the error approaches zero when L is large. For $\omega = 1$, $k = 0$ which is inside the divergent region the error is oscillating but there is an interval of L where the amplitude of this oscillation has a minimum. If the frequency is small ($\omega = 0.1$), the amplitude is larger.
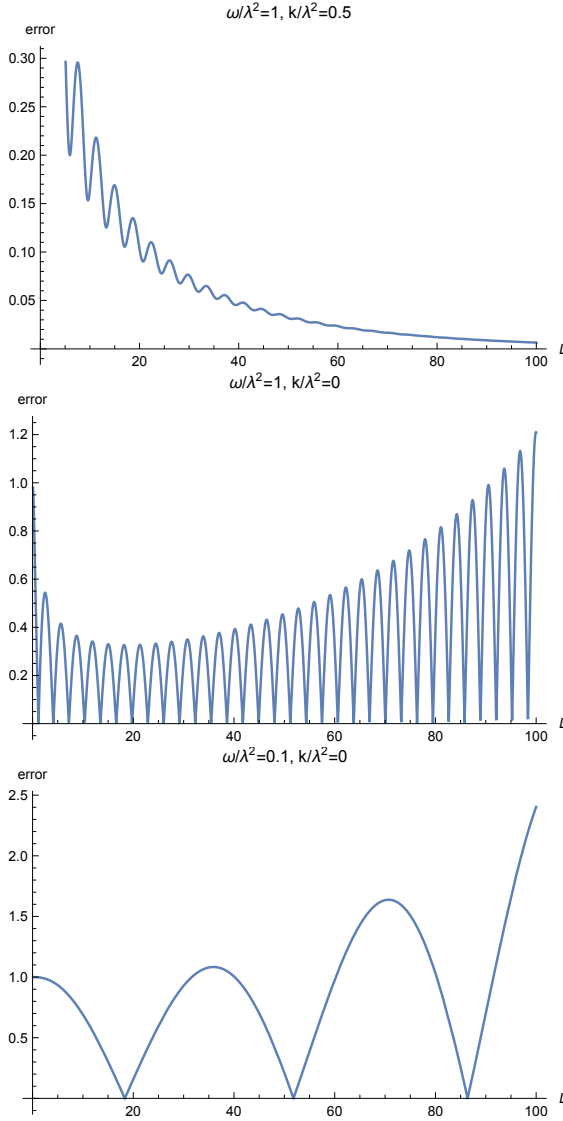
Figure 3.11. The relative difference between G_L and the quenched result as a function of L for different frequencies and momenta. Left: for a point in the (ω, k) plane which is outside of the shaded region of Fig. 3.10 the "error" goes to zero for large L. Middle: inside the shaded region the error is oscillating with diverging amplitude as L goes to larger values. However, for larger values of ω there is an intermediate range of L, where the relative error is smaller than 0.3. Therefore the quenched approximation is qualitatively correct. Right: for small ω the amplitude of the oscillation is large.

126

Chapter 4

A framework for studying quantum critical metals in the limit $N_f \to 0$

In Chapter 2 we studied a Fermi surface coupled to a quantum critical boson:

$$S = \int \mathrm{d}^3x \left[\psi_j^\dagger \left(\partial_\tau - \frac{\nabla^2}{2k_F} - \frac{k_F}{2} \right) \psi^j + \frac{1}{2} \left(\partial_\tau \phi \right)^2 + \frac{1}{2} \left(\nabla \phi \right)^2 - \lambda \phi \psi_j^\dagger \psi^j \right].$$

(4.1)

This theory has a strongly coupled IR which makes the use of conventional methods to study this intractable. We took the limit of vanishing fermion flavor number and showed that after taking this limit it is possible to calculate the all order in λ low-energy fermion two-point function of the above action. We obtained analytical results for the two-point function both in real and momentum space. The two-point function can be used to calculate the fermion spectral function which is an important observable. There are, however, further observables that characterize this theory, but that can not be obtained from the two-point function. In this chapter we expand upon the work of Chapter 2 by showing how to calculate general fermion n-point functions in the same limit. We present here a closed form expression that gives the low energy fermion n-point function in real space. The low-energy limit means that the insertion points of the various fields are well separated in both (Euclidean) time and space compared to

$1/k_F$. As in Chapter 2 it is important that the $N_f \to 0$ limit is taken before this low energy limit.

By having a closed form expression for the fermion n-point functions we have in essence solved this theory completely. Since we are in the $N_f \to 0$ limit also mixed fermion and boson n-point functions are readily obtained from this expression. With the general expression for n-point functions we explicitly calculate the $n = 2$-point function, verifying our previous result, and we calculate the fermion density-density correlator and study its properties. Further investigations of this solution involving more observables are left for future work. Of immediate interest is the current-current correlator from which the optical conductivity can be computed.

Apart from the satisfaction of having a full solution of this theory and being able to calculate observables at $N_f \to 0$, we can use the result obtained here to very efficiently calculate any diagrams of quantum critical metal perturbation theory that survive the $N_f \to 0$ limit. Several studies of high order perturbation theory have been performed in these theories. The large N_f limit was thought to be controlled [22] until S.S. Lee performed a 2-loop calculation of the vertex correction [60]. In that work, only considering one FS patch, it was however found that the large N_f limit classify diagrams in a genus expansion similar to the genus expansion of a matrix large N gauge theory. Later, M. Metlitski and S. Sachdev performed several 3-loop calculations and showed that the genus expansion breaks down when studying two opposite FS patches [24]. They note that their three loop result is consistent with a dynamical critical exponent $z = 3$. Most recently T. Holder and W. Metzner performed a four-loop calculation that showed that $z = 3$ scaling doesn't survive 4-loop corrections [144]. Qualitatively different physics has thus been found at each loop order up until 4 loops. We therefore think our result can be useful for further perturbative studies also away from $N_f = 0$ since there is overlap with the perturbative expansions with nonzero N_f.

In Chapter 2 we found that for the case of equal Fermi velocity v_F and boson velocity c (set to 1 in our above action) we get a considerably simpler result. The limit of $v_F \to c$ is found to be continuous and qualitatively similar to the case of $0 < v_F < c$ ($c < v_F$ has not been studied yet for $N_f \to 0$) for the two-point function. The cases of $v_F/c \to 0$ or ∞ are qualitatively different. However, we believe that $v_F/c = 1$ captures the physics of $v_F \sim c$ also for general n-point functions (See Chapter

128

3). We therefore exclusively consider this case since it makes analytical calculations much simpler. The reason that these simplifications occur is covered thoroughly in Chapter 5. The techniques that we present here for calculating expectation values in the $N_f \to 0$ limit do not crucially depend on these velocities being the same and much of the calculation can be done for a general $v_F \sim c$. It is only a final set of integrals that for the general case $v_F \sim c$ would likely only be numerically amenable whereas for $v_F = c$ we can find closed-form expressions.

In the next section we present a framework for calculating general n-point functions. We do this by writing down a background Green's function for the fermion in the presence of the background field ϕ. This is similar to the work of Chapter 2. However, now we can no longer assume that the fermion momentum is in a certain patch of the FS, but can be anywhere close to the FS. Finally we integrate out the field ϕ and obtain the fermion n-point function. This is only valid for long wavelengths and times. Nevertheless we show that this expression can still be used to calculate the leading small N_f contribution to density correlators where two fermions operators coincide in time and space. In Section 4.2 we apply this result to calculate the density-density correlator. We discuss the different processes that contribute to this result and compare to some earlier works on related models.

4.1 A framework for calculating fermion n-point functions in the $N_f \to 0$ limit

In this section we provide a framework for calculating fermion n-point functions in real space. We take $N_f \to 0$ right from the start and calculate n-point functions in real space for time and length scales larger than $1/k_F$.

We start by adding sources for the fermion to the action in (4.1), $\int \mathrm{d}^3z (J^i \psi_i^\dagger + J_i^\dagger \psi^i)$, and perform the fermionic path integral to get the generating functional:

$$Z[J^\dagger, J] =$$
$$= \int \mathcal{D}\phi \exp\left(-S_{\det}[\phi] - S_b[\phi] - \int \mathrm{d}^3z \mathrm{d}^3z' J_i^\dagger(z) G_j^i[\phi](z,z') J^j(z') \right)$$
$$\tag{4.2}$$

where

$$S_{\text{det}}[\phi] = -\operatorname{tr}\log G^i_j[\phi](z,z') = -N_f \operatorname{tr}\log G[\phi](z,z') \qquad (4.3)$$

and $G^i_j[\phi](z,z')$ is the fermion Green's function with a background field ϕ. We use a simple z to denote (τ, x, y). This determinant action vanishes for $N_f \to 0$. The determinant is responsible for all fermionic loops in a perturbative expansion of this theory. By differentiating with respect to the sources and setting them to vanish we find

$$\lim_{N_f \to 0} \langle \psi^\dagger_{i_1}(z_1)\psi^{j_1}(w_1)...\psi^\dagger_{i_n}(z_n)\psi^{j_n}(w_n) \rangle =$$

$$Z[0]^{-1}\int \mathcal{D}\phi \sum_{\sigma \in S_n} \prod_k \operatorname{sgn}(\sigma) G^{i_k}_{j_{\sigma_k}}[\phi](z_k, w_{\sigma_k}) \mathrm{e}^{-S_b}. \qquad (4.4)$$

Here the sum is over permutations of the integers $1, 2, ..., n$ and $\operatorname{sgn}(\sigma)$ is the parity of the permutation σ.

4.1.1 Background-field fermion two-point function

We will here calculate the background field fermion Greens function for a general background field ϕ. We do this while keeping in mind that we will later perform the above integral over ϕ and that we are only interested in energies small compared to k_F. The background field Greens function is defined through

$$\left(-\partial_{\tau_1} + \frac{\nabla^2_1}{2k_F} + \frac{k_F}{2} + \lambda\phi(z_1) \right) G^i_j[\phi](z_1, z_2) = \delta^3(z_1 - z_2)\delta_{ij} \qquad (4.5)$$

In momentum space $k = (\omega, k_x, k_y)$,

$$G(z_1, z_2) = \int \frac{\mathrm{d}^3 k_1 \mathrm{d}^3 k_2}{(2\pi)^6} \mathrm{e}^{i(-\omega_1\tau_1 + k_{x1}x + k_{y1}y_1) - i(-\omega_2\tau_2 + k_{x2}x_2 + k_{y2}y_2)} G(k_1, k_2),$$
$$(4.6)$$

we have

$$\left(i\omega_1 - \frac{k^2_1}{2k_F} + \frac{k_F}{2} \right) G[\phi](k_1, k_2) + \lambda \int \frac{\mathrm{d}^3 k'}{(2\pi)^3} \phi(k') G[\phi](k_1 - k', k_2) =$$
$$= (2\pi)^3 \delta(k_1 - k_2). \qquad (4.7)$$

130

For momenta k_2 in the vicinity of a point $\hat{n}k_F$ on the Fermi surface we can approximate this as

$$(i\omega_1 - \hat{n} \cdot k_1 + k_F)G_{\hat{n}}[\phi](k_1, k_2) + \lambda \int \frac{\mathrm{d}^3 k'}{(2\pi)^3} \phi(k')G_{\hat{n}}[\phi](k_1 - k', k_2) =$$
$$= (2\pi)^3 \delta^3(k_1 - k_2). \tag{4.8}$$

Fourier transforming back to real space this now reads

$$\left(-\partial_{\tau_1} + i\hat{n} \cdot \nabla_1 + k_F + \lambda\phi(z_1)\right) G_{\hat{n}}[\phi](z_1, z_2) = \delta^3(z_1 - z_2) \tag{4.9}$$

The solution to this first order PDE can be written

$$G_{\hat{n}}[\phi](z_1, z_2) = f_{\hat{n}}(z_1 - z_2) \times$$
$$\times \exp\left(ik_F\hat{n} \cdot (z_1 - z_2) + \lambda \int \mathrm{d}^3 z \phi(z)(f_{\hat{n}}(z - z_1) - f_{\hat{n}}(z - z_2))\right) \tag{4.10}$$

where $f_{\hat{n}}(z) = \delta(\hat{m} \cdot z)(2\pi)^{-1}/(i\hat{n} \cdot z - \tau)$. $\hat{m}$ is a spatial unit vector perpendicular to $\hat{n}$. This solution is now only valid for momenta close to $\hat{n}k_F$ but since it is written in real space this statement might seem confusing. $G[\phi]$ should be viewed as an operator on fields that obeys the operator equation (4.5). $G_{\hat{n}}[\phi]$ is an approximation to this operator that is valid when acting on fields with momentum components close to $k_F\hat{n}$. The operator $G_{\hat{n}}[\phi]$ can be represented in either real or momentum space.

So far this calculation has paralleled that of Chapter 2 albeit in the true real space coordinates instead of the coordinates conjugate to patch momentum coordinates used there. $G_{\hat{n}}[\phi]$ is all we need to calculate the fermion two-point function. However, to calculate general n-point functions we cannot restrict ourselves to having all fermion momenta in a single patch of the FS, i.e. in the vicinity of a single point. For low energies and long wavelengths we can still restrict ourselves to momenta close to the FS, but we must include all directions.

We now construct an operator $G_{\mathrm{IR}}[\phi]$ that approximates $G[\phi]$ well everywhere close to the FS. See Fig. 4.1 for a comparison between the approximations $G_{\hat{n}}[\phi]$ and $G_{\mathrm{IR}}[\phi]$. We do this by projecting out momentum components in different directions and applying the corresponding $G_{\hat{n}}[\phi]$.

We use the resolution of identity,

$$
\begin{aligned}
\delta^3(z, z') =& \delta(\tau, \tau') \int \frac{\mathrm{d}^2 k}{(2\pi)^2} \mathrm{e}^{i(k_x(x-x')+k_y(y-y'))} \\
=& \delta(\tau, \tau') \int \frac{\mathrm{d}k k \mathrm{d}\theta}{(2\pi)^2} \mathrm{e}^{ik\hat{n}(\theta)\cdot(z-z')}.
\end{aligned} \tag{4.11}
$$

Operating with $G_{\mathrm{IR}}[\phi]$ on identity we have

$$
\begin{aligned}
G_{\mathrm{IR}}[\phi](z_1, z_2) =& \int \mathrm{d}^3 z' \int \frac{\mathrm{d}k k \mathrm{d}\theta}{(2\pi)^2} G_{\mathrm{IR}}(z_1, z')[\phi]\delta(\tau', \tau_2)\mathrm{e}^{ik\hat{n}(\theta)\cdot(z'-z_2)} \\
=& \int \mathrm{d}^3 z' \int \frac{\mathrm{d}k k \mathrm{d}\theta}{(2\pi)^2} G_{\hat{n}(\theta)}[\phi](z_1, z')\delta(\tau', \tau_2)\mathrm{e}^{ik\hat{n}(\theta)\cdot(z'-z_2)} \\
=& \int \mathrm{d}^3 z' \int \frac{\mathrm{d}k k \mathrm{d}\theta}{(2\pi)^2} f_{\hat{n}(\theta)}(z_1 - z')\delta(\tau', \tau_2)\times \\
& \times \mathrm{e}^{i\hat{n}(\theta)\cdot(k_F(z_1-z')+k(z'-z_2))}\mathrm{e}^{\lambda I_{\hat{n}(\theta)}[\phi](z_1,z')}
\end{aligned} \tag{4.12}
$$

where we have used that the action of $G_{\mathrm{IR}}[\phi]$ and $G_{\hat{n}}[\phi]$ are the same when acting on a momentum mode close to $k_F \hat{n}$. Here we have defined

$$
I_{\hat{n}(\theta)}[\phi](z_1, z_2) = \int \mathrm{d}^3 z \phi(z)(f_{\hat{n}}(z - z_1) - f_{\hat{n}}(z - z_2)). \tag{4.13}
$$

In the large k_F limit we can perform these integrals using a saddle point approximation. Here we make use of the fact that ϕ will not contain frequencies of order k_F for configurations relevant in the large k_F limit. In principle we could first integrate out ϕ and then perform the saddle point approximation. However, the result turns out to be the same and the calculation is more instructive done in the other order. We make the change of variable $z' = z_1 + (\eta\hat{n}(\theta) + \nu\hat{m}(\theta), \sigma)$

$$
\begin{aligned}
G_{\mathrm{IR}}[\phi](z_1, z_2) =& \int \mathrm{d}\eta \mathrm{d}\nu \int \frac{\mathrm{d}k k \mathrm{d}\theta}{(2\pi)^3} \frac{\delta(\nu)}{-i\eta + \tau_2 - \tau_1} \mathrm{e}^{i((k-k_F)\eta + k\hat{n}(\theta)\cdot(z_1-z_2))}\times \\
& \times \mathrm{e}^{\lambda I_{\hat{n}(\theta)}[\phi](\tau_1, z_1; \tau_2, z_1 + \eta\hat{n}(\theta))}
\end{aligned} \tag{4.14}
$$

The exponential oscillates faster in η than any other factor of the integrand unless $k \approx k_F$. The dominant contribution to the integral will therefore be from $k \approx k_F$. In this k-region, the exponential oscillates faster in θ than any other part of the integrand (since $k_F|z_2 - z_1| \gg 1$), except for the two points where $\hat{n}(\theta)$ is parallel or anti-parallel to $z_{12} = z_2 - z_1$. We

(a) $G_{\hat{n}}$ region of validity   (b) G_{IR} region of validity
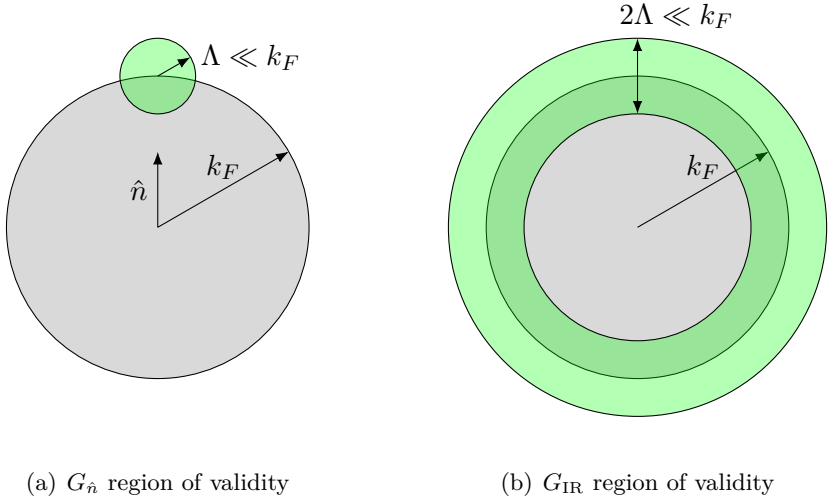
Figure 4.1. The green areas indicate the regions in momentum space where the approximate background-field Green's functions $G_{\hat{n}}[\phi]$ (a) and $G_{\mathrm{IR}}[\phi]$ (b) are accurate. The boundary of the gray area is the FS.

therefore perform saddle-point expansions around these two points and perform the θ integral to obtain

$$G_{\mathrm{IR}}[\phi](z_1, z_2) = \int \mathrm{d}\eta \int \frac{\mathrm{d}k}{(2\pi)^{5/2}} \frac{1}{-i\eta + \tau_2 - \tau_1} \mathrm{e}^{i(k-k_F)\eta} \sqrt{k/|z_{12}|} \times$$
$$\times \left(\mathrm{e}^{-ik|z_{12}|+i\pi/4+\lambda I_{\hat{z}_{12}}[\phi](\tau_1, z_1; \tau_2, z_1+\eta\hat{z}_{12})} + \right.$$
$$\left. + \mathrm{e}^{ik|z_{12}|-i\pi/4+\lambda I_{-\hat{z}_{12}}[\phi](\tau_1, z_1; \tau_2, z_1-\eta\hat{z}_{12})} \right). \tag{4.15}$$

Next we proceed with the k integral. It is of the form $\int_0^\infty \mathrm{d}k \mathrm{e}^{ikz}\sqrt{k}$ and diverges. In principle these integrals should be performed last for convergence but we can introduce a small imaginary component to η so that the Fourier transform integral is regularized. In the end the result is independent of the imaginary part so we can remove it. This amounts to using the result

$$\int_0^\infty \mathrm{d}k \mathrm{e}^{ikz}\sqrt{k} \to \frac{\sqrt{\pi}}{2(-iz)^{3/2}} \tag{4.16}$$

133

for these integrals. We then have

$$G_{\mathrm{IR}}[\phi](z_1, z_2) = \int \frac{\mathrm{d}\eta}{(2\pi)^{5/2}} \frac{1}{-i\eta + \tau_2 - \tau_1} e^{-ik_F\eta} \frac{\sqrt{\pi}}{2\sqrt{|z_{12}|}} \times$$

$$\times \Big(\frac{e^{i\pi/4 + \lambda I_{\hat{z}_{12}}[\phi](\tau_1, z_1; \tau_2, z_1 + \eta \hat{z}_{12})}}{(-i(\eta - |z_{12}|))^{3/2}} +$$

$$+ \frac{e^{-i\pi/4 + \lambda I_{-\hat{z}_{12}}[\phi](\tau_1, z_1; \tau_2, z_1 - \eta \hat{z}_{12})}}{(-i(\eta + |z_{12}|))^{3/2}} \Big). \qquad (4.17)$$

Next we integrate η and take the large k_F limit. We see that this is the high frequency limit of the Fourier transform in η. For $|\tau_2 - \tau_1| \gg 1/k_F$, the high frequency part of this function is dominated by the singularities at $\eta = \pm|z_{12}|$. We can expand around them to get the leading large k_F limit.

$$G_{\mathrm{IR}}[\phi](z_1, z_2) = \frac{\sqrt{k_F}}{(2\pi)^{3/2}\sqrt{|z_{12}|}} \times$$

$$\times \Big(\frac{e^{-ik_F|z_{12}| + i\pi/4 + \lambda I_{\hat{z}_{12}}[\phi](\tau_1, z_1; \tau_2, z_2)}}{-i|z_{12}| + \tau_2 - \tau_1} +$$

$$+ \frac{e^{ik_F|z_{12}| - i\pi/4 + \lambda I_{-\hat{z}_{12}}[\phi](\tau_1, z_1; \tau_2, z_2)}}{i|z_{12}| + \tau_2 - \tau_1} \Big)$$

$$= \frac{2\sqrt{k_F}}{(2\pi)^{3/2}\sqrt{|z_{12}|}} \operatorname{Re} \left(\frac{e^{-ik_F|z_{12}| + i\pi/4 + \lambda I_{\hat{z}_{12}}[\phi](\tau_1, z_1; \tau_2, z_2)}}{-i|z_{12}| + \tau_2 - \tau_1} \right)$$

$$(4.18)$$

These two terms can be understood as momentum modes of momenta parallel and anti-parallel to $z_2 - z_1$ giving the dominant contributions to $G_{\mathrm{IR}}[\phi](z_1, z_2)$. These two contributions couple in different ways to the background field ϕ.

4.1.2 Integrating over $\phi(z)$

We now have an expression for the background field fermion two-point function that we can substitute into Eq. (4.4). The next step is to integrate over the field ϕ. Eq. (4.4) gives a product of $G_{\mathrm{IR}}[\phi]$ so in performing the ϕ integral we will need to evaluate expressions like

$$H_\lambda(\{\hat{n}_i\}, \{z_i\}, \{w_i\}) = Z[0]^{-1} \int \mathcal{D}\phi \exp \left(\lambda \sum_i I_{\hat{n}_i}[\phi](z_i, w_i) - S_B[\phi] \right)$$

$$(4.19)$$

where $\hat{n}_i$ is either parallel or antiparallel to the spatial part of $w_i - z_i$. The result of this Gaussian path-integral is

$$
H_\lambda = \exp\left(\frac{\lambda^2}{2}\int \mathrm{d}^3Z\mathrm{d}^3W\left(\sum_i f_{\hat{n}_i}(z_i - Z) - f_{\hat{n}_i}(w_i - Z)\right)\times\right.
$$

$$
\left.\times\left(\sum_j f_{\hat{n}_j}(z_j - W) - f_{\hat{n}_j}(w_j - W)\right)G_B(Z - W)\right)
$$

$$
= \exp\left(\lambda^2\sum_{i<j}\left(h_{\hat{n}_i,\hat{n}_j}(z_j - z_i) - h_{\hat{n}_i,\hat{n}_j}(z_j - w_i)+\right.\right.
$$

$$
\left.- h_{\hat{n}_i,\hat{n}_j}(w_j - z_i) + h_{\hat{n}_i,\hat{n}_j}(w_j - w_i)\right)+
$$

$$
\left.- \lambda^2\sum_i h_{\hat{n}_i,\hat{n}_i}(z_i - w_i)\right) \tag{4.20}
$$

where h is defined as

$$
h_{\hat{n}_1,\hat{n}_2}(z) = \int \mathrm{d}^3z'\mathrm{d}^3z'' f_{\hat{n}_1}(z')\left(f_{\hat{n}_2}(z'' - z) - f_{\hat{n}_2}(z'')\right)G_B(z' - z''). \tag{4.21}
$$

Transforming to momentum space and using that $G_B(k)$ is even, we have

$$
h_{\hat{n}_1,\hat{n}_2}(z) = \int \frac{\mathrm{d}^3k}{(2\pi)^3}\left(\cos(\omega\tau - k_x x - k_y y) - 1\right)f_{\hat{n}_1}(k)f_{\hat{n}_2}(-k)G_B(k) \tag{4.22}
$$

where $f_{\hat{n}}(k)$ is given by

$$
f_{\hat{n}}(k) = \int \mathrm{d}^3z\, e^{i(\omega\tau - k_x x - k_y y)}f_{\hat{n}}(z) = \frac{1}{i\omega - \hat{n}\cdot k}. \tag{4.23}
$$

The function $h_{\hat{n}_1,\hat{n}_2}(z)$ can be obtained in closed form for the boson kinetic term of our action. The result is presented in Appendix 4.A. We now have

a closed form expression for all fermion n-point functions of our theory:

$$\lim_{N_f \to 0} \langle \psi_{i_1}^\dagger(z_1)\psi^{j_1}(w_1)...\psi_{i_n}^\dagger(z_n)\psi^{j_n}(w_n) \rangle = \frac{k_F^{n/2}}{(2\pi)^{3n/2}} \times$$

$$\times \sum_{\substack{\sigma \in S_n \\ s_1 = \pm 1 \\ ... \\ s_n = \pm 1}} \left[\prod_{l=1}^{n} \delta_{i_l}^{j_\sigma(l)} \frac{\mathrm{e}^{-ik_F s_l |z_{l,\sigma(l)}| + i s_l \pi/4}}{\sqrt{|z_{l,\sigma l}|}(-i s_l |z_{l,\sigma(l)}| + \tau_{\sigma(l)} - \tau_l)} \right] \times$$

$$\times H_\lambda(\{s_i \hat{z}_{i,\sigma(i)}\}, \{z_i\}, \{w_{\sigma(i)}\}) + o(k_F^{n/2}) \tag{4.24}$$

where $z_{ij} = w_j - z_i$. Here $o(k_F^{n/2})$ (little-o notation) signify terms subleading to $k_F^{n/2}$ when k_F is large compared to the scale set be the z_{ij}. We will use the notation $\langle O \rangle_{k_F^{n/2}}$ to signify expectation values calculated to leading order using this expression.

4.1.3   Density n-point functions

The fermion density of species i is given by $\rho_i(z) = \psi_i^\dagger(z)\psi_i(z)$. To use the framework of the previous section to calculate correlation functions of this composite operator it will be necessary to contract $\psi_i^\dagger(z)$ and $\psi_i(z)$ at the same point using the the background field Green's function. We only have the approximate function G_{IR}, which is not valid for length scales of order $1/k_F$ or shorter so it cannot be used for this. We will instead only study correlations of the total fermion density operator that is invariant under the global $U(N_f)$:

$$\rho(z) = \sum_i \psi_i^\dagger(z)\psi_i(z). \tag{4.25}$$

In calculating a correlation function $\langle \rho(z_1)\rho(z_2)... \rangle$ using Eq. (4.4) we sum over the different permutations of the contractions of $\psi_i^\dagger$ and ψ_i, and over the flavor indices i. The background field Green's function is diagonal in indices so each contraction constrains the sums over flavor indices. One sum over a flavor index will remain for each cycle of the permutation so each permutation σ will come with a factor $N_f^{\mathrm{cycles}(\sigma)}$ where cycles(σ) is the number of cycles in permutation σ. In the small N_f limit that we consider we have only kept the leading contribution and we should thus only sum over the permutations with a single cycle since all other permutations are

(a) Small N_f leading part   (b) Small N_f subleading part
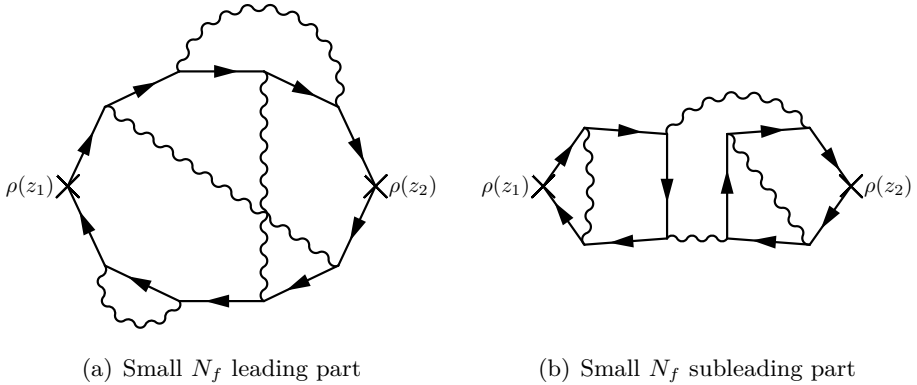
Figure 4.2. Once the fermionic fields have been integrated out and the resulting determinant set to 1 (by the small N_f limit) there are two classes of diagrams contributing to the fermion density-density correlator. (a) Shows one of the diagrams in the first class that contributes at order N_f (b) Shows a diagram in the second class that contributes at order N_f^2.

subleading in small N_f. For density n-point functions with $n > 1$ we will then never contract $\psi_i^\dagger(z)$ and $\psi_i(z)$ at the same point (since that would contribute an extra cycle) unless two of the z_i are equal. The G_{IR} of the previous section is thus sufficient for calculating correlation functions of $\rho(z)$ to leading order in small N_f. See Fig. 4.2 for an example of this in the case of the density-density correlator. For a fermion density n-point function we have:

$$
\begin{aligned}
\langle \rho(z_1)...\rho(z_n) \rangle_{k_F^{n/2}} = & N_f \frac{k_F^{n/2}}{(2\pi)^{3n/2}} \times \\
& \times \sum_{\substack{\sigma \in S_n^{\text{cyclic}} \\ s_1 = \pm 1 \\ \cdots \\ s_n = \pm 1}} \left[\prod_{i=1}^{n} \frac{\mathrm{e}^{-ik_F s_i |z_{i,\sigma i}| + is_i \pi/4}}{\sqrt{|z_{i,\sigma i}|}(-is_i |z_{i,\sigma i}| + \tau_{\sigma i} - \tau_i)} \right] \times \\
& \times H(\{s_i \hat{z}_{i,\sigma i}\}, \{z_i\}, \{z_{\sigma(i)}\}) + \mathcal{O}(N_f^2) \qquad (4.26)
\end{aligned}
$$

137

4.2 Results

In this section we apply the framework developed in the preceding section to explicitly calculate some observables in the $N_f \to 0$ limit. As a consistency check we expand these results in the coupling constant and compare with perturbation theory in Appendix 4.B.

4.2.1 Fermion two-point function

Since we have rotational symmetry we need only consider a positive separation r. We find the real-space fermion two point function:

$$\langle \psi^\dagger(0)\psi(\tau,r) \rangle_{k_F^{1/2}} = -\sqrt{\frac{k_F}{r}} \frac{e^{\frac{\lambda^2\left(\tau^2-r^2\right)}{12\pi\sqrt{\tau^2+r^2}}}}{2\pi^{3/2}\left(\tau^2+r^2\right)} \times$$

$$\times \left[(\tau-r)\sin\left(k_F r + \frac{\lambda^2 \tau r}{6\pi\sqrt{\tau^2+r^2}} \right) + \right.$$

$$\left. + (\tau+r)\cos\left(k_F r + \frac{\lambda^2 \tau r}{6\pi\sqrt{\tau^2+r^2}} \right) \right] \qquad (4.27)$$

This is equivalent to what is found in [65] and we refer to that work for an in-depth analysis of this fermion two-point function.
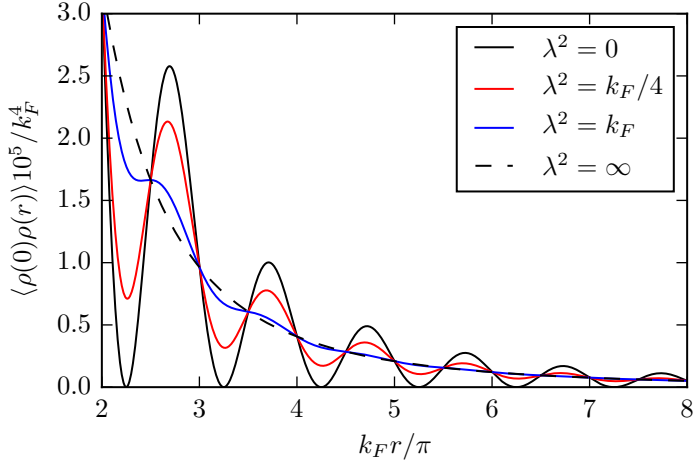
4.2.2 Density-density correlator

We note the property of the function I

$$I_{\hat{n}}(z_1, z_2) + I_{\hat{n}}(z_2, z_3) = I_{\hat{n}}(z_1, z_3) \qquad (4.28)$$

This, together with the fact that $I_{\hat{n}}(z,z) = 0$ means that there are considerable cancellations in the sum of Eq. 4.19 for density correlators where some $z_i - z_j$ are parallel to each other for different i, j. This is true for the density 2-point function and therefore it is given by the rather simple expression:

$$\langle \rho(0)\rho(\tau,r) \rangle_{k_F^1} = N_f k_F \frac{\tau^2 - r^2 + \left(\tau^2+r^2\right)\sin(2k_F r)e^{-\frac{\lambda^2\left(\tau^2+2r^2\right)}{3\pi\sqrt{\tau^2+r^2}}}}{4\pi^3 r \left(\tau^2+r^2\right)^2}.$$

$$(4.29)$$

Figure 4.3. Equal time density-density correlator. Note that for any finite λ the correlator exponentially approaches the $\lambda = \infty$ case for large separations r.

The equal time correlator is given by $|\tau| \ll r$. We can not set $\tau = 0$ directly since this expression is only valid for $\tau \gg k_F^{-1}$, though we see that the limit $|\tau| \ll r$ has the same effect.

$$\langle \rho(0)\rho(r)\rangle_{k_F^1} = N_f k_F \frac{\sin(2k_F r)e^{-\frac{2\lambda^2 r}{3\pi}} - 1}{4\pi^3 r^3}. \tag{4.30}$$
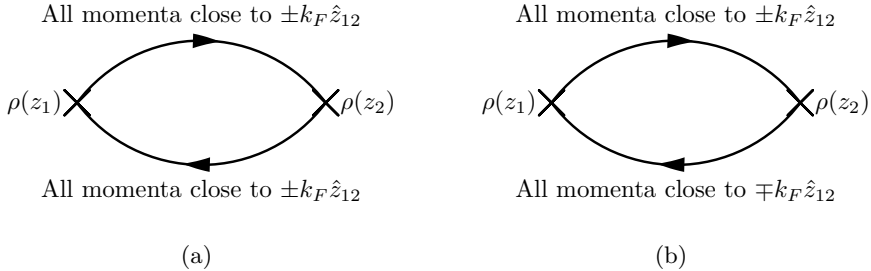
For $\lambda = 0$ we see the familiar Friedel oscillations with wave-vector $2k_F$ and a power-law decay. For a finite coupling λ the oscillations decay exponentially in the separation r with decay length set by $1/\lambda^2$. See Fig. 4.3. For separations longer than $1/\lambda^2$ we have

$$\langle \rho(0)\rho(\tau, r)\rangle_{k_F^1} \approx \langle \rho(0)\rho(\tau, r)\rangle_{\mathrm{IR}} \equiv N_f k_F \frac{\tau^2 - r^2}{4\pi^3 r \left(\tau^2 + r^2\right)^2}. \tag{4.31}$$

In momentum space this is

$$\langle \rho(-\omega, -k)\rho(\omega, k)\rangle_{\mathrm{IR}} = N_f k_F \frac{|\omega|}{2\pi\sqrt{\omega^2 + k^2}}. \tag{4.32}$$

In this limit the scale λ^2 drops out and the IR behavior of the density-density correlator is independent of λ^2. The value of λ^2 only sets the scale of a crossover to this IR behavior.

139

All momenta close to $\pm k_F \hat{z}_{12}$

All momenta close to $\pm k_F \hat{z}_{12}$

$\rho(z_1)$ $\rho(z_2)$

$\rho(z_1)$ $\rho(z_2)$

All momenta close to $\pm k_F \hat{z}_{12}$

All momenta close to $\mp k_F \hat{z}_{12}$

(a)

(b)

Figure 4.4. These two diagrams correspond to the two dominant classes of momentum configurations for large separations $z_2 - z_1$. Here we imagine an infinite series of boson exchanges attached in all possible combinations on the upper and lower lines. Since the boson carries momentum much smaller than k_F, this will still keep the fermion momenta in the same patch along the upper and lower lines. The two lines however need not belong to the same patch. Since only two opposite patches dominate in the large separation limit the upper and lower lines are either in the same (a) or opposite patches (b). In the former case the dominant external momentum is small compared to k_F, in the latter case the dominant external momentum is close to $\pm 2 k_F \hat{z}_{12}$.

The result in (4.29) can be understood by considering the infinite sum of diagrams contributing to it. Each diagram will have two fermion lines, one going from the insertion of $\rho(0)$ to $\rho(\tau, r)$ and one in the opposite direction. A general diagram will have many boson exchanges along these lines. Each fermion propagator will have its momentum close to the Fermi surface for low energy processes. The boson will carry a momentum much smaller than k_F for the dominant processes. Therefore each of these two fermions lines will have their momenta confined to one patch each of the Fermi surface. We know from section 4.1.1 that the two dominating patches are in the directions parallel to $z_{12} = z_2 - z_1$. There are thus four dominant regions of the multidimensional momentum space associated to each diagram. All momenta on the line from $\rho(z_1)$ to $\rho(z_2)$ can be either in the patch close to $-k_F \hat{z}_{12}$ or $k_F \hat{z}_{12}$, and similarly for the momenta on the line from $\rho(z_2)$ to $\rho(z_1)$. See Fig. 4.4. We separate the contributions from processes where the two patches are the same, $G_{\rho\rho}^+$, and where they are opposite, $G_{\rho\rho}^-$:

$$\langle \rho(0)\rho(\tau, r) \rangle_{k_F^1} = G_{\rho\rho, k_F^1}^+(\tau, r) + G_{\rho\rho, k_F^1}^-(\tau, r) \qquad (4.33)$$

Processes with opposite patches have external momenta $k \approx \pm 2 k_F \hat{z}_{12}$

and are thus the oscillating part of Eq. (4.29) while processes where the patches are the same have external momenta $k \ll k_F$:

$$G^+_{\rho\rho,k_F^1}(\tau,r) = N_f k_F \frac{\tau^2 - r^2}{4\pi^3 r \left(\tau^2 + r^2\right)^2} \tag{4.34}$$

$$G^-_{\rho\rho,k_F^1}(\tau,r) = N_f k_F \sin(2k_F r) \frac{e^{-\frac{\lambda^2\left(\tau^2+2r^2\right)}{3\pi\sqrt{\tau^2+r^2}}}}{4\pi^3 r \left(\tau^2 + r^2\right)} \tag{4.35}$$

The non-oscillating part, $G^+_{\rho\rho,k_F^1}(\tau,r)$, receives no corrections from interactions at all. This is expected since the diagrams contributing to this are completely symmetrized fermionic loops. It was shown by Feldman et. al that the leading contribution to this, as $\omega_i, k_i \ll k_F$, cancels out completely in the symmetrized sum (this point of their calculation was specifically pointed out in [145]). Only the non-interacting diagram is not a symmetrized fermionic loop and it survives the cancellation.

The oscillating part, $G^-_{\rho\rho,k_F^1}(\tau,r)$, does not have this cancellation since now two of the vertices in the fermionic loop has momenta of order k_F. Here however it turns out that the sum of all these diagrams exponentiates and for large separations they completely cancel. The density-density large separation result above is therefore exactly what is obtained by a simple one loop calculation, only taking into account the process where both fermions are on the same patch. The fact that all processes with opposite patches cancel out is, however, non-trivial and requires the above non-perturbative calculation to be seen. The exponentiation and subsequent cancellation for large separations is the main new result obtained from applying the framework of the previous section to the density-density correlator.

4.3 Conclusion

The limit of low energies compared to the Fermi energy constrains fermions to live very close to the Fermi surface and only scatter in the forward direction. This makes the fermions almost one-dimensional. This "hidden" one-dimensionality and its consequences has been noted before, see [146] for an overview. We write *almost* one-dimensional because for some processes the fermions still see the curvature of the Fermi surface. There are, however, sectors where the curvature is not seen and the fermions

can be exactly described as one-dimensional albeit coupled to a two-dimensional boson. The $N_f \to 0$ limit singles out this sector precisely. Only the fermionic loops see the curvature. Studying the effectively one-dimensional fermions in the $N_f \to 0$ limit in this work allowed us to calculate all fermion n-point function of a quantum critical metal. In Section 4.1.2 we presented a closed form expression for the fermion-fermion n-point function. In Section 4.2.2 we used this expression to calculate the fermion density two-point function. As a next step we would like to also use this expression to calculate the current-current correlator to obtain the optical conductivity.

The physics of the $N_f \to 0$ limit quantum critical metal is not expected to be similar to the, currently intractable, finite N_f case. We can however use it to gain some insights into how the different diagrams of the full perturbation theory behave as we saw for the density-density correlator. It provides an alternative to the studies of the opposite limit of large N_f [24, 60, 144, 147].

Another extension of this theory is the matrix large N limit. This has been studied in the context of quantum critical metals both directly in field theory [42, 148] and in many works through the use of the AdS/CFT correspondence [149]. All fermionic loops are gone in this limit as well, so we believe it can be solved similarly to how the $N_f \to 0$ case was. The matrix large N case is more limiting since additionally only planar diagrams are kept so we have chosen not to study it here. In [150] the authors study a Reissner-Nordström black hole in AdS$_4$. This is dual to a CFT in 2+1 dimensions at a finite temperature with a global $U(1)$ symmetry with the corresponding chemical potential turned on. The CFT contains fermions charged under the $U(1)$ so one might expect a FS to form. They calculate the charge density two-point function numerically and indeed see oscillations, below a critical temperature. Similarly to what we found, and in contrast to Friedel oscillations, the authors of [150] find that the density-density oscillations decay exponentially even at $T = 0$. Whether this $T = 0$ exponential decay is a general feature of strongly interacting fermions at finite density or a consequence of the boson dominated limits $N_f \to 0$ or matrix large N is too early to tell.

Acknowledgements

4.A   Calculating $h_{\hat{n}_1,\hat{n}_2}(z)$

In this section we calculate the function $h_{\hat{n}_1,\hat{n}_2}(z)$ as defined in Eq. 4.22. Up till now we have not had to consider the form of the boson propagator. To continue we need to use the specific form of the free boson propagator of our theory:

$$G_B(k) = \frac{1}{\omega^2 + k_x^2 + k_y^2}. \tag{4.36}$$

We need to perform three integrals to find h. First we make the change of variables $k = r\hat{n}_1 \times \hat{n}_2 + rs_2 z \times \hat{n}_1 + rs_3 z \times \hat{n}_2$. After integrating r over all of $\mathbb{R}$ we have

$$
\begin{aligned}
h_{\hat{n}_1,\hat{n}_2}(z) = - \int \frac{\mathrm{d}s_2 \mathrm{d}s_3}{(2\pi)^3} & \frac{\pi |\tau \hat{n}_1 \times \hat{n}_2 \cdot z|^3}{(n_s \times z - \hat{n}_1 \times \hat{n}_2)^2} \times \\
& \frac{1}{((1 + is_2\tau)\hat{n}_1 \times \hat{n}_2 + \tau n_s \times \hat{\tau}) \cdot z} \times \\
& \frac{1}{((1 - is_3\tau)\hat{n}_1 \times \hat{n}_2 + \tau n_s \times \hat{\tau}) \cdot z}
\end{aligned}
\tag{4.37}
$$

where $n_s = s_2 \hat{n}_1 + s_3 \hat{n}_2$ and $\hat{\tau} = (1,0,0)$. We can now do the s_2 integral using the residue theorem. The denominator is a fourth order polynomial in s_2. Two roots are polynomials in s_3 whereas the the remaining second order polynomial in s_2 has roots in terms of radicals of s_3. The contribution from the first two poles can thus easily be integrated once again, now over s_3, since it is a rational function. The range is no longer $\mathbb{R}$ since the

pole in s_2 will leave the upper half plane where we close the s_2-contour for certain values of s_3. The contribution from the last two poles is more involved because of the radicals. One of these poles is always in the UHP and the other in the LHP so we only need to account for one of them. By making the change of variables

$$s_3 \mapsto \frac{\sqrt{\tau^2 + y^2}\sinh(w) - x}{\tau^2 + x^2 + y^2},$$
(4.38)

we get rid of the radicals and can carry out the w integral. In the end the total result can be written as

$$
\begin{aligned}
h_{\hat{n}_1,\hat{n}_2}(z) =& \frac{1}{4\pi(1 - \hat{n}_1 \cdot \hat{n}_2)} \Bigg[|\hat{n}_1 \diamond z| + |\hat{n}_2 \diamond z| - 2r+ \\
& - 2\frac{\tau\hat{n}_1 \cdot \hat{n}_2 - i(\hat{n}_1 \cdot z + \hat{n}_2 \cdot z + i\tau)}{|\hat{n}_1 \diamond \hat{n}_2|} \times \\
& \times \Big(\pi\theta(-\tau) + i\,\mathrm{sgn}(\hat{n}_l \diamond z)\log(A) + \\
& \quad + i\big[\theta(-\hat{n}_1 \diamond z) - \theta(\hat{n}_2 \diamond z)\big] \times \\
& \qquad \times \log\Big[\frac{i\tau\hat{n}_1 \diamond \hat{n}_2 + \hat{n}_1 \diamond z - \hat{n}_2 \diamond z}{\hat{n}_1 \diamond \hat{n}_2(\hat{n}_k \cdot z + i\tau)}\Big] \Big) \Bigg],
\end{aligned}
$$
(4.39)

where

$$z = (\tau, x, y) \tag{4.40}$$
$$n_i = (x_i, y_i) \tag{4.41}$$
$$\tilde{r} = \mathrm{sgn}(\hat{n}_l \diamond z)\sqrt{\tau^2 + x^2 + y^2} \tag{4.42}$$
$$\hat{n}_1 \cdot \hat{n}_2 = x_1 x_2 + y_1 y_2 \tag{4.43}$$
$$\hat{n}_1 \diamond \hat{n}_2 = x_1 y_2 - y_1 x_2 \tag{4.44}$$
$$\hat{n}_1 \diamond z = x_1 y - y_1 x \tag{4.45}$$
$$k = \begin{cases} 1, & \text{for} \quad \hat{n}_1 \diamond \hat{n}_2 < 0 \\ 2, & \text{for} \quad 0 < \hat{n}_1 \diamond \hat{n}_2 \end{cases} \tag{4.46}$$
$$l = 3 - k \tag{4.47}$$

and

$$A = \frac{(\hat{n}_1 \cdot \hat{n}_2 - 1)(\tau(1 + \hat{n}_1 \cdot \hat{n}_2) - i(\hat{n}_1 + \hat{n}_2) \cdot z)}{(\hat{n}_1 \diamond \hat{n}_2)^2(i\tau + \hat{n}_1 \cdot z)(i\tau + \hat{n}_2 \cdot z)} \times$$

$$\times \left(i\tilde{r}\tau |\hat{n}_1 \diamond \hat{n}_2| + (\hat{n}_l \diamond z - \tilde{r})(\hat{n}_k \diamond z + \tilde{r}) + \right.$$

$$\left. + \tau^2 \hat{n}_1 \cdot \hat{n}_2 - i\tau(\hat{n}_1 \cdot z + \hat{n}_2 \cdot z) + \tau^2 \right)^{1/2}. \tag{4.48}$$

We see that the prefactor of this expression diverges for $\hat{n}_1 = \hat{n}_2$ and this case has to be treated separately. The function is continuous at this point however, and we can simply take the limit $\hat{n}_1 = \hat{n}_2$ to obtain

$$h_{\hat{n},\hat{n}}(z) = \frac{r^3 - |\hat{n} \diamond z| \left(3(\hat{n} \cdot z)^2 + 3i\tau\hat{n} \cdot z + (\hat{m} \cdot z)^2 \right)}{12\pi(\hat{n} \cdot z + i\tau)^2}. \tag{4.49}$$

This can be compared to the calculation for the two-point function. There we have $\hat{n} \diamond z = 0$, and using this we get

$$h_{\hat{n},\hat{n}}(z) = \frac{r^3}{12\pi(\hat{n} \cdot z + i\tau)^2} = \frac{(\hat{n} \cdot z - i\tau)^2}{12\pi\sqrt{(\hat{n} \cdot z)^2 + \tau^2}}. \tag{4.50}$$

This agrees with the previous result of [65]. For the density-density correlator we additionally need h for $\hat{n}_1 = -\hat{n}_2$ and $n_1 \diamond z = 0$. Taking the limits simultaneously we find

$$h_{\hat{n},-\hat{n}}(z) = -\frac{\sqrt{\tau^2 + (\hat{n} \cdot z)^2}}{4\pi}. \tag{4.51}$$

We note that A diverges as $\sim 1/\hat{n}_1 \diamond \hat{n}_2$ for $\hat{n}_1 = -\hat{n}_2$. The prefactor of the logarithm is proportional to $\hat{n}_1 \diamond z$.

$$h_{\hat{n}_1,\hat{n}_2}(z) = \frac{|\hat{n}_1 \diamond z| \log(|\hat{n}_1 \diamond \hat{n}_2|)}{4\pi} + \text{finite}. \tag{4.52}$$

We have an additional constraint in Eq. (4.20) however, the n_i are parallel or anti-parallel to $w_i - z_i$. Using this one can show that this divergence in h as $\hat{n}_1$ and $\hat{n}_2$ become anti-parallel cancels out in the sum of Eq. (4.20) and is not seen in observables.

4.B Perturbative verification

To verify our non-perturbative results we can expand in the coupling constant λ and compare with perturbation theory. We do so here for both the fermion two-point function and the density-density correlator, both up to order λ^2. Since our non-perturbative results are only valid at long wavelengths and low energies, we will expand around singularities in momentum space and verify that the leading singularities agree with perturbation theory. We start off by verifying the two-point function (4.27) at tree level:

$$\langle \psi^\dagger(0)\psi(\tau,r) \rangle_{k_F^{1/2},\lambda^0} = -\frac{\sqrt{\frac{k_F}{r}}\left((\tau-r)\sin(k_F r) + (\tau+r)\cos(k_F r)\right)}{2\pi^{3/2}\left(\tau^2 + r^2\right)}. \tag{4.53}$$

In momentum space this is

$$\langle \psi^\dagger(0)\psi(\omega,k) \rangle_{k_F^{1/2},\lambda^0} = -\sqrt{\pi k_F}(1 + i\,\mathrm{sgn}(\omega)) \times$$
$$\times \int_0^\infty \mathrm{d}r\sqrt{r}J_0(kr)e^{-r|\omega|+ik_F r\,\mathrm{sgn}(\omega)} \tag{4.54}$$

where J_0 is the zeroth Bessel function of the first kind. We look for singularities and therefore want the integral to diverge. The only possibility for this is when $\omega = 0$, so there is no exponential decay, and when $k = k_F$, so the oscillations of the Bessel function cancels those of the exponential. To expand around this point we can approximate the Bessel function with its asymptotic oscillatory behaviour. In doing so we only modify the finite part of the integral. We find

$$\langle \psi^\dagger(0)\psi(\omega,k_F + k_x) \rangle_{k_F^{1/2},\lambda^0} = \left(1 - \frac{i\omega}{2k_F}\right)\frac{1}{i\omega - k_x} +$$
$$+ \frac{1}{8k_F}\log\left(\frac{k_F}{i\omega - k_x}\right) + \text{finite}. \tag{4.55}$$

The full fermion two-point function of our toy model at tree level is given by

$$\langle \psi^\dagger(0)\psi(\omega,k) \rangle_{\lambda^0} = \frac{1}{i\omega - k^2/(2k_F) + k_F/2}$$
$$\approx \frac{1}{i\omega - (k - k_F)} \equiv G_0^{\text{patch}}(\omega, k - k_F) \tag{4.56}$$
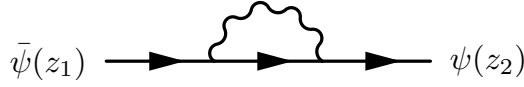
Figure 4.5. The single diagrams that contributes at order λ^2 to the fermion two-point function.

(a)   (b)   (c)
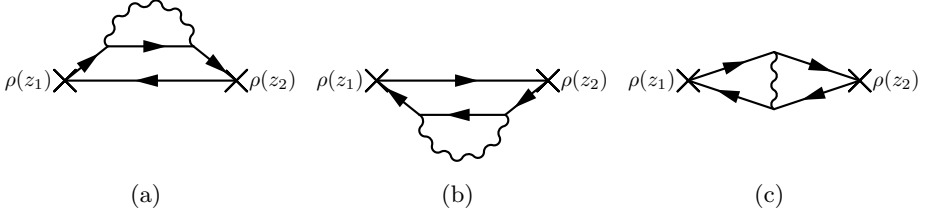
Figure 4.6. The three diagrams that contribute at order λ^2 to the density-density correlation function.

We see that the results agree to leading order for $\omega \ll k_F$ and k close to k_F. This same technique is used below to find the leading divergences of the higher point correlators and also of the higher order in λ contributions to the correlators. The two-point function, Eq. (4.27), expanded to second order in λ is found to be

$$\langle \psi^\dagger(0)\psi(\omega, k_F + k_x)\rangle_{k_F^{1/2},\lambda^2} = -\lambda^2 \frac{\sqrt{k_x^2 + \omega^2}}{4\pi(k_x - i\omega)^3} + \text{subleading.} \quad (4.57)$$

This is to be compared to the diagram in Fig. 4.5. Evaluating this diagram with all fermion propagators linearized at the patch of the Fermi surface at $k = (k_F + k_x)\hat{x}$ gives

$$\begin{aligned}
D_{4.5} &= \lambda^2 G_0^{\hat{x}}(\omega, k_x)^2 \int \frac{\mathrm{d}\omega_1 \mathrm{d}q_x \mathrm{d}q_y}{(2\pi)^3} G_0^{\hat{x}}(\omega + \omega_1, k_x + q_x) G_B(\omega_1, q) \\
&= \lambda^2 \frac{\sqrt{k_x^2 + \omega^2}}{4\pi(i\omega - k_x)^3}
\end{aligned} \quad (4.58)$$

where $G_0^{\hat{x}}$ is defined in Eq. 4.56. The density-density correlator (4.29) at order λ^0 is easily verified in real space using (4.27) at the same order. To verify the density-density correlator at order λ^2 we need to calculate the three diagrams in Fig. 4.6. Diagram 4.6ab can similarly be obtained by

147

combining the fermion two-point function at order λ^0 and λ^2 in real space:

$$D_{4.6\text{a}}(\tau, r) = -N_f G_{\lambda^0}(\tau, r) G_{\lambda^2}(-\tau, r) \tag{4.59}$$

$$D_{4.6\text{b}}(\tau, r) = -N_f G_{\lambda^2}(\tau, r) G_{\lambda^0}(-\tau, r) \tag{4.60}$$

Subtracting these two diagrams in real space from Eq. (4.29) and Fourier transforming we find for small ω and $k \approx 2k_F$:

$$\langle \rho(-\omega, -k) \rho(\omega, k) \rangle_{k_F, \lambda^2, N_f^1} - D_{4.6\text{ab}}(\omega, k) =$$

$$= -\frac{N_f \lambda^2 \sqrt{k_F}}{4\pi^3 \sqrt{|\omega|}} \operatorname{Re}\left[(1+i) K \left(\frac{i(|k| - 2k_F) + |\omega|}{2|\omega|} \right) \right] +$$

$$+ \text{ subleading.} \tag{4.61}$$

where K is the complete Elliptic integral of the first kind. Calculating Diagram 4.6c requires a more involved calculation. Since we are interested in the external momentum $k = (2k_F + k_x)\hat{x}$, $|k_x| \ll k_F$, we can expand the fermion propagators in momenta in the patches at $\pm k_F \hat{x}$. After this we can perform all the momentum integrals to obtain:

$$D_{4.6\text{c}} = -N_f \lambda^2 \int \frac{\mathrm{d}^3 k_1}{(2\pi)^3} \frac{\mathrm{d}^3 q}{(2\pi)^3} G_0^{\hat{x}}((2k_F + k_x)\hat{x} + k_1) \times$$

$$\times G_0^{\hat{x}}((2k_F + k_x)\hat{x} + k_1 + q) G_0^{-\hat{x}}(k_1 + q) G_0^{-\hat{x}}(k_1) G_B(q)$$

$$= N_f \lambda^2 \sqrt{k_F} \int \frac{\mathrm{d}\omega_B \mathrm{d}^2 q}{(2\pi)^3} \frac{\sqrt{k_x + i\omega} - \sqrt{k_x + q_x - i(\omega_B - \omega)}}{\pi \left(q_x^2 + \omega_B^2 \right)} G_B(\omega_B, q)$$

$$+ \text{ subleading}$$

$$= -\frac{N_f \lambda^2 \sqrt{k_F}}{4\pi^3 \sqrt{|\omega|}} \operatorname{Re}\left[(1+i) K \left(\frac{ik_x + |\omega|}{2|\omega|} \right) \right] + \text{ subleading.} \tag{4.62}$$

We have thus verified the density-density correlator at order λ^2.

Chapter 5

Boson-dominated quantum critical metals at Lorentz symmetric point

5.1   Introduction

In Sec. 1.4 we studied several, rather exotic, limits of a quantum critical metal in which fermion loops are suppressed. This results in a theory where fermions get non-perturbative corrections from the bosons but the boson does not receive any corrections from the fermion.

In this chapter we consider a general extension of the theory of the quantum critical metal such that all diagrams contributing to the fermion self-energy may differ in their numerical weight but they retain their dependence on the external parameters. The only constraint is that all diagrams containing fermionic loops are suppressed. We thus study a more general class of theories within which the matrix large N or small N_f limits are included. This class of theories contains more than these two extreme limits. One example is a theory with a global $SU(N)$ symmetry such as the matrix large N, fermions in the fundamental and boson in the adjoint and additionally a global $U(N_f)$ under which only the fermions transform, in the fundamental. Taking $N_f \to 0$ suppresses all fermion loops, but each value of N gives a different theory. We refer to these theories, with suppressed fermionic loops, as *boson-dominated* theories.

Only fermion momenta close to the Fermi surface are important when

Figure 5.1. One-loop correction to fermion two-point function.

considering low energies. When calculating the fermion two-point function without corrections from fermionic loops we only need to consider a single patch of the Fermi surface. Let us consider a patch centered at $\mathbf{k} = k_F\hat{\mathbf{x}}$ and introduce patch coordinates $\mathbf{k} = (k_F + k_x)\hat{\mathbf{x}} + k_y\hat{\mathbf{y}}$. We can then approximate the free fermion two-point function by

$$G_0(k) = \frac{1}{i\omega - vk_x - k_y^2/2m} \tag{5.1}$$

The term quadratic in k_y is important for convergence of the boson momentum integrals, but after performing them we can take $m \to \infty$ to find the low energy behavior. This amounts to taking $m \to \infty$ from the start, but keeping in mind that we should take the $k_y \to \pm\infty$ limits at the same time, a type of principal value integral with the divergence at ∞.

The one-loop correction to the fermion two-point function is given by the diagram in Fig. 5.1. The integral corresponding to this diagram is

$$\Sigma_{\lambda^2}(\omega, k_x) \sim \lambda^2 \int \frac{\mathrm{d}^3 p}{(2\pi)^3} \lim_{m\to\infty} G_0(k+p)D_0(p), \tag{5.2}$$

possibly with some prefactor coming from the specific theory one is interested in. Calculating this we find

$$\Sigma_{\lambda^2}(\omega, k_x) = \lambda^2 \frac{\log\left(\frac{iv\omega - k_x + \sqrt{(1-v^2)(k_x^2 + \omega^2)}}{iv\omega - k_x - \sqrt{(1-v^2)(k_x^2 + \omega^2)}}\right)}{8\pi\sqrt{1-v^2}} \tag{5.3}$$

This expression is valid for $0 < v < 1$ and $1 < v$. The square roots are defined by analytical continuation in the upper half plane for negative arguments. For $v = 1$ we have

$$\Sigma_{\lambda^2, v=1}(\omega, k_x) = \lambda^2 \frac{\sqrt{\omega^2 + k_x^2}}{4\pi(i\omega - k_x)}. \tag{5.4}$$

We see that the point $v = 1$ gives a considerably simpler result. Recall that we set the boson velocity to $c = 1$ in Sec. 1.2.2 by a choice of coordinates.

This means that for $v = 1$ the UV Fermi velocity and UV boson velocity are equal. The extreme limits of $v \to 0, \infty$ represents different physics but the point $v = 1$ is not considerably less interesting than the case of a general v of order one. With this motivation we will study this special case.

5.2 Consequences of $v = 1$ for a boson dominated quantum critical metal

We will now study the extra symmetry gained at the point $v = 1$ and what it entails for a general boson dominated theory as discussed in the previous section.

   As we saw in the calculation of the fermion self-energy, we do not need to keep the curvature term in the free fermion two point function when considering the low energy limit. This is true for higher loop diagrams as well, as long as they do not contain any fermionic loops. For our purposes the relevant propagators are then

$$G_0(\omega, k_x) = \frac{1}{i\omega - k_x} \tag{5.5}$$

$$D(\omega, k_x, k_y) = \frac{1}{\omega^2 + k_x^2 + k_y^2} \tag{5.6}$$

were we now implicitly consider the patch used earlier for the fermion momenta. Writing $w = i\omega + k_x$, we see that the boson propagator is invariant under a rotation $w \mapsto e^{i\theta} w$, $\theta \in \mathbb{R}$, whereas the fermion propagator receives a phase $e^{i\theta}$ under the same rotation. The measure in momentum integrals is invariant under this rotation so any diagram containing only these propagators will only receive a rotation by a phase $e^{in\theta}$ upon rotating all external energies and momenta by an angle θ. Since we are in Euclidean space this rotation corresponds to a Lorentz transformation, where the speed of light is equal to unity, $c = 1$. The integer n is given by the number of fermion propagators which equals to the number of vertices plus one. On dimensional grounds one can then conclude that the fermion two-point function is given by

$$G(\omega, k_x) = \sum_{n=0}^{\infty} \frac{f_n \lambda^{2n}(\omega^2 + k_x^2)^{n/2}}{(i\omega - k_x)^{2n+1}} \equiv f\left(\lambda^2 \frac{\sqrt{\omega^2 + k_x^2}}{(i\omega - k_x)^2}\right) \frac{1}{i\omega - k_x} \tag{5.7}$$

where $f(z)$ is independent of $\bar{z}$. The two-point function is thus greatly constrained, a general two-point function would be described by a general function of two real variables. In our case the two-point function is described by a general function of a complex variable, but since it is holomorphic this is morally a function of a single real variable. We call $f(z)$ the characteristic function of a boson dominated $v = 1$ theory. The single scale set by the coupling constant is redundant and we set to $\lambda^2 = 1$ from now on. We introduce the map z from Euclidean energy-momentum space to $\mathbb{C}$:

$$z : (\omega, k_x) \mapsto \frac{\sqrt{\omega^2 + k_x^2}}{(i\omega - k_x)^2} \tag{5.8}$$

and we can then write $G(\omega, k_x) = f(z(\omega, k_x))/(i\omega - k_x)$. This is the main result of this chapter. We will now proceed by studying properties of the characteristic function.

5.2.1 Properties of the characteristic function

From the self-energy calculation we see that the 1-loop fermion Green's function is of the anticipated form and we have $f_0 = 1, f_1 = n_1/4\pi$ where n_1 is the multiplicity of the diagram in Fig. 5.1 in our particular boson-dominated scheme. We see that negating the external frequency, $\omega \to -\omega$, and making the change of variable for all integrated frequencies $\omega_i \to -\omega_i$, we obtain the complex conjugate of the integrand. Assuming the multiplicities of all diagrams are real, this means that all $f_n \in \mathbb{R}$ and thus $f(\bar{z}) = \overline{f(z)}$. To calculate further coefficients we need to calculate higher diagrams, but since they all come with different multiplicities that depend on the particular scheme used to remove fermion loops we will refrain from that and instead study general properties of the function f.

From causality we have that $G(\omega, k_x)$ is ω-analytic when continued to the open right half plane (RHP) (ω is Euclidean) for all values of k_x. We analytically continue the mapping z in ω and consider the image of the ω-RHP. We find that for $0 < k_x$, z is onto $\mathbb{C}$ with the fourth quadrant and the line $0 < -iz < 3^{-3/2}k_x$ cut out. See Fig. 5.2. Similarly for $k_x < 0$, z is onto $\mathbb{C}$ with the first quadrant and the line $3^{-3/2}k_x < -iz < 0$ cut out. Since the analyticity requirement is true for all k_x we thus see that f has to be analytic everywhere except the positive real axis.

Now we consider unitarity. The spectral function $A(\omega_R, k_x)$ can be obtained from the retarded two-point function. This is obtained by eval-
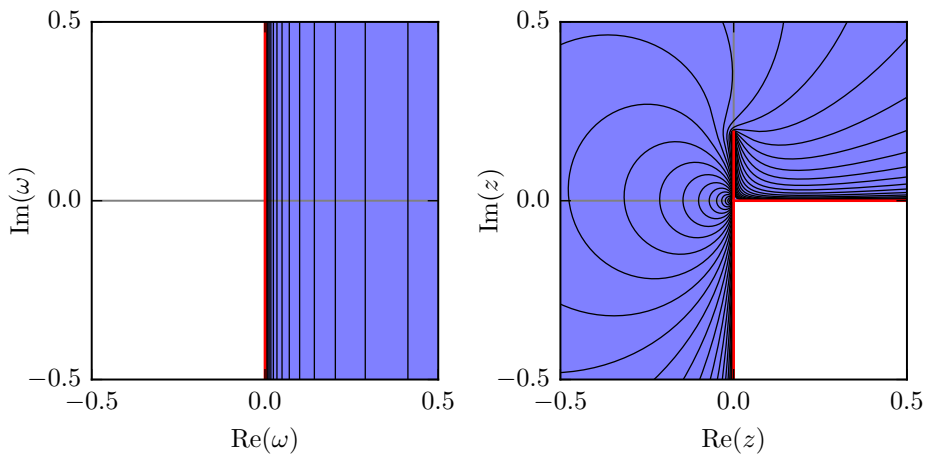
Figure 5.2. These figures show how the ω-region where G is analytic (left) is mapped by z onto a subset of $\mathbb{C}$ (right). Here $k = 1$ but a different k would just rescale the image, and flip it upside down for a negative k. We thus see that for every point $z_0 \in \mathbb{C}/\mathbb{R}^+$, there is a k such that a neighbourhood of z_0 is contained in the image of the ω-RHP under the mapping z. The red line shows the real frequency contour.

uating the Euclidean two-point function on a contour slightly right of the imaginary axis, we indicate this with a +0 below

$$A(\omega_R, k_x) = -2\operatorname{Im}(G(-i\omega_R + 0, k_x)). \tag{5.9}$$

The spectral density obeys the sum rule

$$\int \frac{\mathrm{d}\omega_R}{2\pi} A(\omega_R, k_x) = 1 \tag{5.10}$$

This relation depends on A at all scales but we only have an expression for A in terms of f at scales below the Fermi energy. We push the Fermi energy to infinity and so all spectral weight is contained below this scale and the above sum rule should then be obeyed by our low-energy spectral functions. Since $G(\omega, k_x)$ is ω-analytic in the RHP we can shift the contour to infinity and we have

$$-2 \lim_{r\to\infty} \operatorname{Im} \int_{-\pi/2}^{\pi/2} \frac{-i\mathrm{d}\theta i r e^{i\theta}}{2\pi} \frac{f\left(\frac{\sqrt{re^{i\theta}+k_x^2}}{(ire^{i\theta}-k_x)^2}\right)}{ire^{i\theta}-k_x} = 1 \tag{5.11}$$

Taking the limit we find

$$\lim_{r\to\infty} \operatorname{Re} \int_{-\pi/2}^{\pi/2} \frac{\mathrm{d}\theta}{\pi} f\left(-(re^{i\theta})^{-3/2}\right) = 1 \tag{5.12}$$

For f regular at 0 this simply means $f(0) = 1$.

Unless the dispersion of the interacting theory is identical to that of the free theory, we have that $G(-i\omega, \omega)$ is finite. If we make this slightly stronger by assuming the two-point function is ω-analytic here we have that

$$\lim_{i\omega \to k_x} \frac{f(z(\omega, k_x))}{i\omega - k_x} = C. \tag{5.13}$$

Here C is a constant independent of the direction the limit is taken. Now consider taking this limit in a general direction with $i\omega$ in the UHP. Writing $i\omega = k_x + ire^{i\theta}$, $\theta \in [-\pi/2, \pi/2]$ we have that

$$\lim_{r\to 0^+} \frac{f\left(-r^{-3/2}\sqrt{2|k_x|}e^{i\left(-\frac{3\theta}{2}-\frac{1}{4}\pi\operatorname{sgn}(k)\right)}\right)}{re^{i\theta}} = C \tag{5.14}$$

154

We thus have

$$f(z) = \frac{C}{(-z)^{2/3}} + \text{subleading}. \tag{5.15}$$

For a non-zero C, f will necessarily have a branch-cut going to infinity which from our previous considerations has to be along $\mathbb{R}^+$. By the reality condition we have $C \in \mathbb{R}$. If the two-point function is not analytic at $i\omega = k_x$ and some remnant of the free theory dispersion remains in the interacting case, then f can have different asymptotics. For a simple discontinuity at this point f still has this asymptotic form in the directions $1+0, 1-0, i, -i$ though the constants C are different in these directions.

5.2.2   Implications for the retarded two-point function

The retarded two-point function is given by analytically continuing the Euclidean two-point function in the RHP.

$$G_R(\omega_R, k_x) = G(-i\omega_R + 0, k_x) \tag{5.16}$$

When analytically continuing z we need to separate two cases, in analogy with relativistic theories we call these time-like and space-like:

$$z(-i\omega_R + 0, k_x) = \begin{cases} \frac{\sqrt{k_x^2 - \omega_R^2}}{(\omega_R - k_x)^2} + 0\,\text{sgn}(k_x) & \omega_R^2 < k_x^2, \text{ timelike} \\ -i\,\text{sgn}(\omega_R)\frac{\sqrt{\omega_R^2 - k_x^2}}{(\omega_R - k_x)^2} & \omega_R^2 > k_x^2, \text{ spacelike} \end{cases} \tag{5.17}$$

This mapping is shown in Fig. 5.3. It is useful to go to light-cone coordinates, $\alpha = \omega_R - k_x$ and $\beta = \omega_R + k_x$, $\tilde{G}_R(\alpha, \beta) = G_R(\omega_R, k_x)$. We then have

$$\tilde{z}(\alpha, \beta) = \begin{cases} \frac{\sqrt{-\alpha\beta}}{\alpha^2} + 0\,\text{sgn}(\beta - \alpha) & \alpha\beta < 0, \text{ timelike} \\ -i\,\text{sgn}(\alpha + \beta)\frac{\sqrt{\alpha\beta}}{\alpha^2} & 0 < \alpha\beta, \text{ spacelike} \end{cases} \tag{5.18}$$

We see that z is invariant under the "boost" $\alpha, \beta \to s\alpha, s^3\beta$. This is not an actual Lorentz boost under which we would instead have $\alpha, \beta \to s\alpha, s^{-1}\beta$. This invariance means that

$$\tilde{G}_R(\alpha, \beta) = s\tilde{G}_R(s\alpha, s^3\beta) \tag{5.19}$$

for any $s \in \mathbb{R}$. Fourier transforming to real space we similarly have

$$\mathcal{F}\tilde{G}_R(x^+, x^-) = s^{-1}\mathcal{F}\tilde{G}_R(sx^+, s^3x^-) \tag{5.20}$$
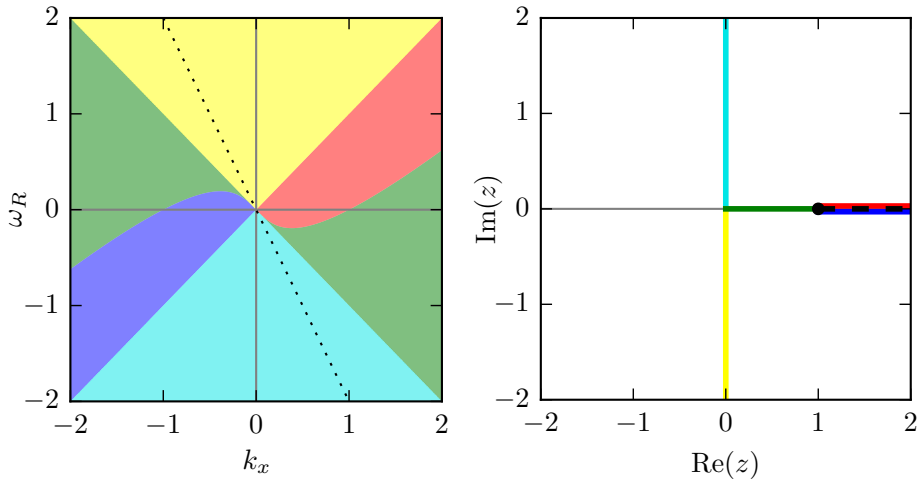
Figure 5.3. These figures show how different regions of (ω_R, k_x) space (left) are mapped onto the complex z plane (right). Considering a function f with branch cut from $z = 1$ to $z = +\infty$ (indicated with dashed line), it is important what side of the branch-cut z is for $1 < z$. The ϵ-prescription has been indicated by separating the red and blue lines slightly. f is real for $0 < z < 1$ and therefore the spectral function is identically 0 in the green regions. The cyan and yellow regions map to the imaginary axis where f is analytic and therefore the two-point function is analytic in these regions. The dotted line indicates a turning point where $\mathrm{d}z/\mathrm{d}\omega_R = 0$.

where

$$\mathcal{F}\tilde{G}_R(x^+, x^-) = \int \frac{\mathrm{d}\alpha \mathrm{d}\beta}{(2\pi)^2} e^{-i(x^+\alpha + x^-\beta)/2} \tag{5.21}$$

and thus $x^+ = x + t$ and $x^- = t - x$. Analogously with Lorentz-boosts, these "boosts" do not take time-like separations to space-like separations and vice versa. For spacelike arguments $\omega_R^2 < k_x^2$, z is always on the imaginary axis. Since f is guaranteed to be analytic there, so is G_R and there are no excitations with velocity larger than 1. For timelike arguments, z is on the positive real line. We have noted that f could have singularities and branch cuts on $\mathbb{R}^+$. Let us denote the singular point closest to 0 by r_0. This is also the radius of convergence of the series defining f in Eq. (5.7). For now this could be 0, ∞ or a finite value. In the next section we will see that in the $N_f \to 0$ limit we have a finite r_0 and this is what we will focus on. Before doing so let us see what the other cases entail:

- **$r_0 = 0$** : In this case the series in (5.7) is asymptotic and needs to be regularized somehow to give a meaningful answer. This is more rule than exception in quantum field theories, however—in addition to the $N_f \to 0$ limit—this is not the case for a class of two-dimensional Fermi liquids [151]. From Eq. (5.17) we see that an f that is not analytic at 0 means that G is not ω analytic at $\omega_R = -k_x$, all the way into the UV.

- **$r_0 = \infty$** : If f were an entire function, G is non-analytic in ω at the dispersion of the free theory. To show this assume the opposite for contradiction. We then have that f is bounded by the above argument and since it is entire it is necessarily constant and by unitarity $f = 1$ and thus we have a contradiction.

- **$r_0 = $ finite** : This is the case we study in detail now.

We now assume a finite r_0. f is necessarily not analytic at $z = r_0$. The preimage of this point is the curve $\beta = -\alpha^3 r_0$. This is shown for $r_0 = 1$ as the interface between the green and the blue or red areas of Fig. 5.3. A singularity in f at r_0 corresponds to an excitation in the spectral function. The dispersion, $\omega_R(k_x)$, of this is then not monotonic. It generally crosses $\omega_R = 0$ for three momenta: $k_x = 0, \pm 1/\sqrt{r_0}$. For small k_x the dispersion is $\omega_R = -k_x + \mathcal{O}(k_x^2)$, for large $|k_x|$ the dispersion is $\omega_R = k_x + $ subleading.

Since all $a_n \in \mathbb{R}$ we have that $f(z < r_0) \in \mathbb{R}$. The spectral function is thus identically zero in the timelike regions above $(k_x < 0)$ and below $(0 < k_x)$ the dispersion. f may have a branch cut for $r_0 < z$ and complex values on either side of it. The reality condition still gives us that $f(z + 0i) = \bar{f}(z - 0i)$. In this case the spectral function would have a continuum in the timelike regions below $(k_x < 0)$ and above $(0 < k_x)$ the dispersion. f could also have additional singularities for $r_0 < z$.

Finally we explore the "null" arguments $\omega_R = \pm k_x$. If G_R is analytic at $\omega_R = k_x$ then from (5.15) we have that

$$G_R(k_x, k_x) = \text{sgn}(k_x)\frac{C}{(-2|k_x|)^{1/3}} \qquad (5.22)$$

By demanding that G_R is analytic at $\omega_R = -k_x$ we find that all $f_n = 0$ for n odd. This means that under quite general assumptions G_R is not analytic at $\omega_R = -k_x$. For $0 < r_0$ we have that $f(0) = 1$ and thus

$$G_R(-k_x, k_x) = \frac{1}{2k_x} \qquad (5.23)$$

A finite r_0 means that perturbation theory converges inside a disc of radius r_0 in complex z-plane, and diverges outside it. The region this corresponds to in energy-momentum space is shown in Fig. 5.4. The properties derived in this section are summarized in Table 5.1.

5.3 $N_f \to 0$ limit

In [65] the authors find that the fermion two-point function for $0 < v < 1$ is given by

$$G_R(\omega_R, k_x) = \frac{1}{\omega_R - k_x v + \frac{\lambda^2}{4\pi\sqrt{1-v^2}}\sigma(\omega_R, k_x)}, \qquad (5.24)$$

where $\sigma(\omega_R, k_x)$ is the root, within $0 < \text{Im}(\sigma) < i\pi$, of the equation

$$\frac{\lambda^2}{4\pi\sqrt{1-v^2}}(\sinh(\sigma) - \sigma\cosh(\sigma)) + v\omega_R - k_x +$$
$$- \cosh(\sigma)(\omega_R - k_x v + 0i) = 0 \qquad (5.25)$$

Taking the $v \to 1$ limit of this we find that the characteristic function obeys the equation

$$3f^3 z^2 - 16\pi^2 (f+2)(f-1)^2 = 0. \qquad (5.26)$$

Assumption	$\implies$ Property of G_R
none	- $\tilde{G}_R(\alpha, \beta) = s\tilde{G}_R(s\alpha, s^3\beta)$ - analytic for $\omega_R^2 > k_x^2$
$r_0 = 0$	not analytic at $\omega_R = -k_x$
r_0 finite	- not analytic at $\omega_R + k_x = r_0(k_x - \omega_R)^3$ - $A(\omega_R, k_x) = 0$ for $r_0\|\alpha\|^3 < \|\beta\|$ - perturbation theory converges for $\|k_x^2 - \omega^2\| < r_0^2(\omega_R - k_x)^4$
$r_0 = \infty$	- not analytic at $\omega_R = k_x$ - $A(\omega_R, k_x) = 0$ for $\omega_R^2 < k_x^2$
$r_0 > 0$	$G_R(-k_x, k_x) = (2k_x)^{-1}$
G_R analytic at $\omega_R = -k_x$	- $r_0 > 0$ - all $f_n = 0$ for n odd
G_R analytic at $\omega_R = k_x$	- $r_0 \neq \infty$ - $G_R(k_x, k_x) = \text{sgn}(k_x)C(-2\|k_x\|)^{-1/3}$

Table 5.1. Summary of properties of the retarded Green's function given different assumptions.
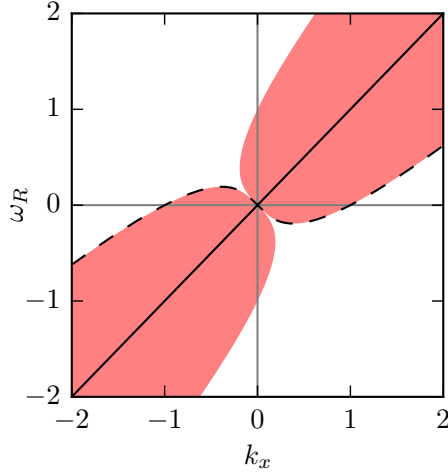
Figure 5.4. The red area indicates where perturbation theory diverges for $r_0 = 1$. Perturbation theory converges outside of this area. The dashed line indicates where the singularity at $z = r_0$ shows up in ω_R, k_x-space, the solid line indicates $\omega_R = k_x$.

This third order polynomial in f generally has three solutions and $f(z)$ has a triply sheated Riemann surface. From (5.26) we see that the equation is first order in f at the points $z^2 = 16\pi^2/3$. Two solutions necessarily go to ∞ and only one sheet remains finite at these points. f is required to be analytic on the negative real axis so the relevant sheet is the one where f is finite at $z = -4\pi/\sqrt{3}$. Analytically continuing from this point and directing the branch cut starting at $z = 4\pi/\sqrt{3}$ towards $+\infty$ we find

$$f(z) = 2\pi^{2/3} \frac{\sqrt[3]{-2}\left(1 - \frac{3iz}{\sqrt{48\pi^2 - 9z^2}}\right)^{2/3} - \frac{2(-2\pi)^{2/3}}{\sqrt[3]{16\pi^2 - 3z^2}}}{\sqrt[3]{16\pi^2 - z\left(3z + i\sqrt{48\pi^2 - 9z^2}\right)}}, \tag{5.27}$$

where the branch-cuts of all fractional powers are taken to be along the negative real axis. We have thus found the unique characteristic function f that both obeys Eq. 5.26 and has the correct analytic structure. The radius of convergence is given by $r_0 = 4\pi/\sqrt{3}$ and there are no further singularities along $\mathbb{R}^+$. Directly from (5.26) we find the asymptotic

160

behavior

$$f(z) = \left(\frac{32\pi^2}{3}\right)^{1/3} \frac{1}{(-z)^{2/3}} + \text{subleading}. \qquad (5.28)$$

with the branch-cut towards $+\infty$.

5.4   Matrix large N limit

We believe the matrix large N limit can be found with a similar method as the $N_f \to 0$ limit. The determinant of the fermion background field two-point function is a constant also in this case. Another approach would be to apply the gap equation (see the introduction to this thesis, Eq. (1.67)), to G expressed in terms of the coefficients $\{f_n\}$. Performing the integral results in a recurrence relation for the coefficients $\{f_n\}$. Although relatively straightforward, we will not perform this analysis in this thesis.

We will, however, mention some expectations of the result. As noted in the introduction to this thesis, the authors of [62] study the RG flow of a matrix large N theory similar to ours in $3 - \epsilon$ dimensions and find that the Fermi velocity flows to 0 in the IR. Based on this they make an ansatz for the fixed-point fermion two-point function and find a solution to the gap equation

$$G(\omega, \mathbf{k}) = A\omega^{2\gamma-1} \qquad (5.29)$$

where A is a constant and the anomalous dimension $\gamma = \epsilon/4$. Their calculation is based on a general UV Fermi velocity but their solution does not obey the symmetry found here. Understanding this discrepancy between our results would be interesting. The fixed point found in [62] is found for a small ϵ so one explanation could simply be that it does not survive to $\epsilon = 1$.

5.5   Conclusions

We have studied a spherical Fermi surface coupled to massless bosons in 2+1 dimensions in a general limit where fermion loops are suppressed. At the point where the UV Fermi velocity and boson velocities are the same we found a symmetry for energies far below the Fermi energy that greatly constrains the fermion two-point function. The constraints were found by considering perturbation theory but since they hold to all orders the

constraint on the two-point function holds into the IR. This allowed us to find the dispersion relation. For interacting theories with perturbative series converging in the UV we found a continuous excitation spectrum with dispersion that is universally non-monotonic and thus showing a splitting of the FS. The exact behavior of the two-point function is parametrized with a single holomorphic function $f(z)$ that needs to be determined using other methods. We showed what this function is for the $N_f \to 0$ case.

In [65] the authors calculated the fermion two-point function in the $N_f \to 0$ limit of a quantum critical metal for $0 < v < 1$. The expression they find is consistent with most predictions we make in this paper for a $v = 1$ quantum critical metal without fermion loops. We therefore believe that our results are rather robust and gives a good intuition about strongly coupled boson dominated quantum critical metals despite that we have assumed $v = 1$ to obtain these predictions.

Within the theories we studied here we could extend the analysis to higher point functions and compare with the results found in [67]. One can also perform two immediate extensions beyond the theories we have studied that still retain the employed symmetry. Going to higher or lower dimension by adding more dimensions transverse to the FS will still keep the ω, k_x rotational symmetry. Changing the boson dynamical critical exponent so we have a low energy boson two-point function

$$D(k) = \frac{1}{k^{2(1-\gamma_\phi)}} \tag{5.30}$$

will not ruin the symmetry, however it will change the mapping z:

$$z : (\omega, k_x) \mapsto \frac{\left(\omega^2 + k_x^2\right)^{1/2+\gamma_\phi}}{(i\omega - k_x)^2} \tag{5.31}$$

One could for example consider $g\phi^4$ interacting bosons. If the interaction scale g is larger than λ^2, then for energies of order λ the boson is described by the Wilson-Fisher fixed point with $\gamma_\phi \neq 0$ [63], since we are in a limit where the boson does not receive fermion corrections.

Acknowledgements

this manuscript. This work was supported in part by a VICI (Koenraad Schalm) award of the Netherlands Organization for Scientific Research (NWO), by the Netherlands Organization for Scientific Research/Ministry of Science and Education (NWO/OCW), and by the Foundation for Research into Fundamental Matter (FOM).

Samenvatting

In het algemeen worden de interacties tussen fermionen bij een eindige dichtheid beschreven door de Fermi vloeistof theorie, waarbij men storingsrekening kan gebruiken om de interacties tussen de fermionen in beschouwing te nemen. Wanneer deze fermionen ook reageren met massaloze bosonen, resulteert dit in een niet-Fermi vloeistof, dit systeem kan niet langer op de conventionele manier bestudeerd worden door terug te vallen op storingsrekening. Deze theorieën zijn belangrijk wanneer men kwantum kritische metalen wil beschrijven; metaalachtige systemen in de nabijheid van een kwantum kritisch punt (KKP). Het is bekend dat zulke kwantum kritische punten voorkomen in fermionische systemen, er is daardoor een algemene behoefte zulke systemen te begrijpen. Het bestaan van zulke kwantum kritische punten wordt daarnaast gezien als een mogelijk mechanisme waarmee zogenaamde "vreemde metalen" en hoge-temperatuur supergeleiders begrepen zouden kunnen worden.

In dit proefschrift bestuderen we een twee dimensionaal sferisch Fermi oppervlak, gekoppeld aan massaloze bosonen, overeenkomend met een KKP orde parameter bij nul momentum. We breiden deze theorie uit naar een theorie waarin de fermionen N_f smaken hebben en een globale $U(N_f)$ smaak symmetrie groep. De essentie van deze scriptie is dat in de $N_f \to 0$ limiet met daaropvolgend een lage energie limiet we de twee-punt correlatie functie van de fermionen en de dichtheid-dichtheid correlatie functie kunnen berekenen zonder terug te hoeven vallen op de eerder genoemde storingsrekening technieken.

Beide functies vertonen inderdaad gedrag dat typerend is voor een niet-Fermi vloeistof. De pool in de twee-punt correlatiefunctie verbreedt zich als $(\omega - ..)^{-1/2}$, met een vertakkingslijn die resulteert in een continuüm in de dispersierelatie. Hierdoor verdwijnt de discontinuïteit in de momentum verdeling die normaal typerend is voor een Fermi vloeistof. De dispersiere-

latie wordt hierdoor een niet-monotone functie, waarbij het singuliere punt van de twee-punt correlatie functie $\omega = 0$ snijdt bij drie verschillende momenta. Dit resulteert in drie verschillende lage energie excitaties en een splitsing van het Fermi oppervlak. Het centrale Fermi oppervlak heeft een negatieve Fermi snelheid gelijk aan minus de ongerenormaliseerde boson snelheid, onafhankelijk van de Fermi snelheid in het UV (bij korte lengteschalen).

De dichtheid-dichtheid correlatiefunctie laat oscillaties zien met een momentum $2k_F$ en neemt exponentieel af als functie van de afstand, in tegenstelling tot de correlatiefunctie van een Fermi vloeistof die normaal afneemt met een machtsfunctie.

Een nadeel van de $N_f \to 0$ limiet is dat we belangrijke effecten in het infrarood (op lange lengteschalen) hier niet kunnen bestuderen. We kijken daarom ook naar de dubbele limiet waarin we ook $N_F \to 0$ nemen en we $N_f k_F$ constant houden. De fermion lus diagrammen die overblijven in deze limiet kunnen behandeld worden met niet-perturbatieve technieken. De niet-monotoniciteit van de twee-punt correlatie functies verdwijnt en het infrarood wordt gekarakteriseerd door een $\omega^2 \sim k_x^3$ schaling, de twee-punt correlatie functie verschilt echter van de RPA vorm. Hoewel dit resultaat hetzelfde is voor eindige N_f, laat het zien dat de resultaten die we vinden in de limiet waar we eerst $N_f \to 0$ nemen specifiek zijn voor deze limiet.

Een interessante vondst is dat de storingsrekening expansie van de $N_f = 0$ fermion n-punt correlatie functies een eindige convergentiestraal heeft. Hoewel dit niet gebruikelijk is voor quantum velden theorieën komt dit in ons geval niet geheel onverwacht, gezien hetzelfde zich ook voordoet in tweedimensionale Fermi vloeistoffen [3]. De straal wordt hier in principe bepaald door de energieschaal waardoor storingsrekening niet langer gebruikt kan worden om het infrarood te bereiken. Het is onbekend of dit convergente gedrag specifiek is voor $N_f = 0$ of dat het ook blijft bestaan bij een eindige N_f. We presenteren een heuristisch argument in sectie 1.4.6 waarin we beargumenteren dat de convergentiestraal voor N_F niet groter zal zijn dan 1.

Tenslotte nemen we een stap terug en beschouwen we de theorie waarin een Fermi oppervlak reageert met een massaloos boson in een meer algemene benadering dan de $N_f \to 0$ limiet, maar nog steeds op zo'n manier dat het boson geen correcties van het fermion ondervindt. Naast de $N_f \to 0$ limiet bevat dit andere theorieën in de (matrix) grote N limiet en generalisaties van deze theorieën. We bestuderen de symmetrie eigen-

schappen van deze klasse van theorieën wanneer de UV Fermi snelheid gelijk is aan de ongerenormaliserde boson snelheid. We vinden dat het non-Fermi vloeistof gedrag, dat we eerder vonden in de limiet waar we eerst $N_F \to 0$ nemen, algemeen is voor deze klasse van theorieën en we bewijzen dat dit in het algemeen het geval is wanneer storingsrekening in de koppelingsconstante een eindige convergentiestraal heeft.

Summary

Generic interacting fermions at finite density in two dimensions are described by Fermi liquid theory (FLT) and can be studied using perturbation theory in the interaction strengths. Coupling such a theory to a massless boson however results in a non-Fermi liquid that can not be studied using conventional methods. These theories show up in particular when studying quantum critical metals, metallic systems in the vicinity to a quantum critical point (QCP). Quantum critical points are known to exist in fermionic systems so there is general need for understanding of such systems. Most interestingly—though not conclusively—existence of a QCP has been suggested as a mechanisms for strange-metallicity and high-T_c superconductivity.

In this thesis we study a two-dimensional spherical Fermi surface (FS) coupled to a massless boson corresponding to a QCP order parameter at zero momentum. We extend the theory to have N_f flavors of fermions and a global $U(N_f)$ flavor symmetry group. The core of this thesis is that in the $N_f \to 0$ limit followed by a low-energy limit we need not rely on perturbation theory, but can non-perturbatively calculate the zero temperature fermion two-point function and the fermion density-density correlation function.

Both quantities indeed show non-Fermi liquid behavior. The pole in the two-point function gets broadened into a fractional power, $(\omega - ..)^{-1/2}$, with a branch cut resulting in a continuum in the spectral function. This completely removes the discontinuity of the momentum distribution function that is found in Fermi liquids. The dispersion becomes non-monotonic, with the singular point of the two-point function crossing $\omega = 0$ at three momenta. This results in three species of low-energy excitations and a splitting of the FS. The central FS has a negative Fermi velocity equal to minus the unrenormalized boson velocity, independent

of the UV Fermi velocity.

The density-density correlator shows oscillations at momentum $2k_F$, however they die off exponentially in the separation as opposed to the power-law decay of a Fermi liquid.

A drawback of performing the $N_f \to 0$ limit first is that we are still unable to study important effects in the IR. We therefore also study the double limit $N_f \to 0$ with $N_f k_F$ constant. Some of the fermion loop diagrams survive this limit but are still amenable to a non-perturbative treatment. The non-monotonicity of the two-point function disappears and the IR is characterized by a $\omega^2 \sim k_x^3$ scaling, however, the two-point function is distinct from the RPA form. While this result is not necessarily similar to the finite N_f case, it shows that the results obtained in the $N_f \to 0$-first case are specific to that limit.

An interesting finding is that the perturbative expansions of $N_f = 0$ fermion n-point functions have finite radii of convergence. This is not common for quantum field theories. However, it is not completely unexpected in our case since the same thing has been found for two-dimensional Fermi-liquids [3]. The radius is set by the energy scale so perturbation theory can nevertheless not be used to access the IR directly. We do not know whether this convergence is specific to $N_f = 0$ or if it survives to finite N_f. We do present a heuristic argument in Section 1.4.6 why the radius of convergence in N_f is not larger than 1.

Lastly we take a step back and consider the theory of a FS interacting with a massless boson, in a more arbitrary approximation than the $N_f \to 0$ limit, but such that the boson still receives no corrections from the fermion. In addition to the $N_f \to 0$ limit this contains theories in the matrix large N limit and generalizations of these theories. The symmetry properties of this class of theories is studied at the point where the UV Fermi velocity and the unrenormalized boson velocities are equal. It is found that the non-Fermi liquid behavior found in the $N_f \to 0$-first limit is rather general in such theories and is proven to exist whenever perturbation theory in the coupling constant has a finite radius of convergence.

List of Publications

The thesis is based on the following publications:

[65]   Balazs Meszena et al. "Nonperturbative emergence of non-Fermi-liquid behavior in $d = 2$ quantum critical metals". In: *Phys. Rev. B* 94 (11 Sept. 2016), p. 115134. URL: `http://link.aps.org/doi/10.1103/PhysRevB.94.115134`.

[66]   Petter Säterskog, Balazs Meszena, and Koenraad Schalm. "Two-point function of a $d = 2$ quantum critical metal in the limit $k_F \to \infty$, $N_f \to 0$ with $N_f k_F$ fixed". In: *Phys. Rev. B* 96 (15 Oct. 2017), p. 155125. URL: `https://link.aps.org/doi/10.1103/PhysRevB.96.155125`.

[67]   Petter Säterskog. "A Framework for Studying a Quantum Critical Metal in the Limit $N_f \to 0$". In: *To be submitted* (2017).

[68]   Petter Säterskog. "Boson-Dominated Quantum Critical Metals at Lorentz Symmetry Point". In: *To be submitted* (2017).

Other publications by the author:

[152]   Irina Arefeva et al. "Holographic dual of a time machine". In: *Phys. Rev. D* 94 (4 Aug. 2016), p. 044059. URL: `https://link.aps.org/doi/10.1103/PhysRevD.94.044059`.

Curriculum Vitæ

I was born the 8th of February 1989 in Gothenburg, Sweden.

In 2008 I started my studies at the bachelor's program "Physics Engineering" at Chalmers University in Gothenburg. I obtained my degree in 2011 and was admitted to the master's program "Physics and Astronomy" at the same university. The first year of this program was done as an exchange student at Hong Kong University of Science and Technology and the second year back in Gothenburg. I obtained my master's degree in 2013.

I was the same year hired as a Ph.D. student in the group of Koenraad Schalm at the Lorentz Institute at Leiden University in the Netherlands to conduct research on strongly coupled condensed matter systems using methods from high-energy physics. My work there resulted in this thesis.

During the fall of 2016 I presented my work at the "Applications of Gauge/Gravity Duality 2016" workshop at Chalmers University, at the Perimeter Institute, Harvard University, Stanford University and UC Berkeley.

From October 2017 I will be working as a postdoctoral researcher at the "Nordic Institute for Theoretical Physics" in Stockholm.

Acknowledgments

Foremost, I would like to express my sincere gratitude to my advisor Koenraad Schalm for the continuous support of my Ph.D. study and research, for his patience, enthusiasm and the freedom he allowed me in choosing research directions during my final year.

I am grateful to my collaborators Andrey Bagrov and Balazs Meszena whom it was a pleasure to work with.

I would especially like to thank Vadim Cheianov and Jan Zaanen for useful discussions and for providing a critical view on my work. Though not directly involved in my work I would like to thank many other members of the Lorentz Institute for providing interesting discussions and a nice atmosphere. In particular I would like to thank Aurelio, Bartosz, Jaakko, Ke, Nick, Nikos, Miguel, Philippe, Richard, Robert-Jan, Sasha, Sašo, Steffen, Vincenzo and Yujie.

Outside of the Lorenz Institute I express my gratitude to Ulf Gran at Chalmers University who was the advisor of my master's project. I thoroughly enjoyed the research we did together and this motivated me to pursue a Ph.D. in theoretical physics.

Lastly I would like to thank my family and friends outside the Lorentz Institute. While not directly contributing to this work they kept me sane and happy and were thus integral for the completion of this thesis.

Bibliography

[1] K. Marx et al. *Capital, Volume I: A Critique of Political Economy.* Dover Publications, 2011.

[2] LD Landau. "The theory of a Fermi liquid". In: *Soviet Physics Jetp-Ussr* 3.6 (1957), pp. 920–925.

[3] Joel Feldman, Horst Knörrer, and Eugene Trubowitz. "A Two Dimensional Fermi Liquid. Part 1: Overview". In: *Communications in Mathematical Physics* 247.1 (May 2004), pp. 1–47. URL: http://dx.doi.org/10.1007/s00220-003-0996-0.

[4] J. Bardeen, L. N. Cooper, and J. R. Schrieffer. "Microscopic Theory of Superconductivity". In: *Phys. Rev.* 106 (1 Apr. 1957), pp. 162–164. URL: https://link.aps.org/doi/10.1103/PhysRev.106.162.

[5] Adam Mann. "High-temperature superconductivity at 25: Still in suspense". In: *Nature* 475.7356 (July 2011), pp. 280–282. URL: https://doi.org/10.1038/475280a.

[6] Matthias Troyer and Uwe-Jens Wiese. "Computational Complexity and Fundamental Limitations to Fermionic Quantum Monte Carlo Simulations". In: *Phys. Rev. Lett.* 94 (17 May 2005), p. 170201. URL: https://link.aps.org/doi/10.1103/PhysRevLett.94.170201.

[7] P. Coleman. *Introduction to Many-Body Physics.* Cambridge University Press, 2015. URL: https://books.google.nl/books?id=PDg1HQAACAAJ.

[8]   J. M. Luttinger. "Fermi Surface and Some Simple Equilibrium Properties of a System of Interacting Fermions". In: *Phys. Rev.* 119 (4 Aug. 1960), pp. 1153–1163. URL: https://link.aps.org/doi/10.1103/PhysRev.119.1153.

[9]   I Ja Pomeranchuk et al. "On the stability of a Fermi liquid". In: *Sov. Phys. JETP* 8 (1958), p. 361.

[10]   Joel Feldman et al. "An intrinsic 1/N expansion for many-fermion systems". In: *EPL (Europhysics Letters)* 24.6 (1993), p. 437.

[11]   Joseph Polchinski. "Effective field theory and the Fermi surface". In: *Theoretical Advanced Study Institute (TASI 92): From Black Holes and Strings to Particles Boulder, Colorado, June 3-28, 1992.* 1992, pp. 0235–276. arXiv: hep-th/9210046 [hep-th].

[12]   R. Shankar. "Renormalization-group approach to interacting fermions". In: *Rev. Mod. Phys.* 66 (1 Jan. 1994), pp. 129–192. URL: https://link.aps.org/doi/10.1103/RevModPhys.66.129.

[13]   J. Feldman et al. "An Intrinsic 1/ N Expansion for Many-Fermion Systems". In: *EPL (Europhysics Letters)* 24.6 (1993), p. 437. URL: http://stacks.iop.org/0295-5075/24/i=6/a=002.

[14]   Joel Feldman et al. "Superconductivity in a repulsive model". In: *Helvetica Physica Acta* 70.1-2 (1997), pp. 154–191.

[15]   W. Kohn and J. M. Luttinger. "New Mechanism for Superconductivity". In: *Phys. Rev. Lett.* 15 (12 Sept. 1965), pp. 524–526. URL: https://link.aps.org/doi/10.1103/PhysRevLett.15.524.

[16]   Andrey V. Chubukov. "Kohn-Luttinger effect and the instability of a two-dimensional repulsive Fermi liquid at T=0". In: *Phys. Rev. B* 48 (2 July 1993), pp. 1097–1104. URL: https://link.aps.org/doi/10.1103/PhysRevB.48.1097.

[17]   A. Altland and B.D. Simons. *Condensed Matter Field Theory.* Cambridge books online. Cambridge University Press, 2010. URL: https://books.google.nl/books?id=GpF0Pgo8CqAC.

[18]   J. G. Bednorz and K. A. Müller. "Possible highTc superconductivity in the Ba-La-Cu-O system". In: *Zeitschrift für Physik B Condensed Matter* 64.2 (1986), pp. 189–193. URL: http://dx.doi.org/10.1007/BF01303701.

[19] J. A. N. Bruin et al. "Similarity of Scattering Rates in Metals Showing T-Linear Resistivity". In: *Science* 339.6121 (2013), pp. 804–807. eprint: `http://science.sciencemag.org/content/339/6121/804.full.pdf`. URL: `http://science.sciencemag.org/content/339/6121/804`.

[20] C.M. Varma, Z. Nussinov, and Wim van Saarloos. "Singular or non-Fermi liquids". In: *Physics Reports* 361.5 (2002), pp. 267–417. URL: `http://www.sciencedirect.com/science/article/pii/S0370157301000606`.

[21] L. B. Ioffe and A. I. Larkin. "Gapless fermions and gauge fields in dielectrics". In: *Phys. Rev. B* 39 (13 May 1989), pp. 8988–8999. URL: `https://link.aps.org/doi/10.1103/PhysRevB.39.8988`.

[22] Joseph Polchinski. "Low-energy dynamics of the spinon-gauge system". In: *Nuclear Physics B* 422.3 (1994), pp. 617–633. URL: `http://www.sciencedirect.com/science/article/pii/0550321394904499`.

[23] B. I. Halperin, Patrick A. Lee, and Nicholas Read. "Theory of the half-filled Landau level". In: *Phys. Rev. B* 47 (12 Mar. 1993), pp. 7312–7343. URL: `https://link.aps.org/doi/10.1103/PhysRevB.47.7312`.

[24] Max A. Metlitski and Subir Sachdev. "Quantum phase transitions of metals in two spatial dimensions. I. Ising-nematic order". In: *Phys. Rev. B* 82 (7 Aug. 2010), p. 075127. URL: `https://link.aps.org/doi/10.1103/PhysRevB.82.075127`.

[25] Matthias Vojta. "Quantum phase transitions". In: *Reports on Progress in Physics* 66.12 (2003), p. 2069. URL: `http://stacks.iop.org/0034-4885/66/i=12/a=R01`.

[26] Matthias Eschrig. "The effect of collective spin-1 excitations on electronic spectra in high- Tc superconductors". In: *Advances in Physics* 55.1-2 (2006), pp. 47–183. eprint: `http://dx.doi.org/10.1080/00018730600645636`. URL: `http://dx.doi.org/10.1080/00018730600645636`.

[27] D. N. Basov and Andrey V. Chubukov. "Manifesto for a higher Tc". In: *Nat Phys* 7.4 (Apr. 2011), pp. 272–276. URL: `http://dx.doi.org/10.1038/nphys1975`.

[28]   G. Ghiringhelli et al. "Long-Range Incommensurate Charge Fluctuations in (Y,Nd)Ba2Cu3O6+x". In: *Science* 337.6096 (2012), pp. 821–825. eprint: `http://science.sciencemag.org/content/337/6096/821.full.pdf`. URL: `http://science.sciencemag.org/content/337/6096/821`.

[29]   M. Brando et al. "Metallic quantum ferromagnets". In: *Rev. Mod. Phys.* 88 (2 May 2016), p. 025006. URL: `https://link.aps.org/doi/10.1103/RevModPhys.88.025006`.

[30]   Ke Liu et al. "Classification of nematic order in $2 + 1$ dimensions: Dislocation melting and $O(2)/Z_N$ lattice gauge theory". In: *Phys. Rev. B* 91 (7 Feb. 2015), p. 075103. URL: `https://link.aps.org/doi/10.1103/PhysRevB.91.075103`.

[31]   P. Jakubczyk, W. Metzner, and H. Yamase. "Turning a First Order Quantum Phase Transition Continuous by Fluctuations: General Flow Equations and Application to d-Wave Pomeranchuk Instability". In: *Phys. Rev. Lett.* 103 (22 Nov. 2009), p. 220602. URL: `https://link.aps.org/doi/10.1103/PhysRevLett.103.220602`.

[32]   M. P. Lilly et al. "Evidence for an Anisotropic State of Two-Dimensional Electrons in High Landau Levels". In: *Phys. Rev. Lett.* 82 (2 Jan. 1999), pp. 394–397. URL: `https://link.aps.org/doi/10.1103/PhysRevLett.82.394`.

[33]   Eduardo Fradkin et al. "Nematic Fermi Fluids in Condensed Matter Physics". In: *Annual Review of Condensed Matter Physics* 1.1 (2010), pp. 153–178. eprint: `https://doi.org/10.1146/annurev-conmatphys-070909-103925`. URL: `https://doi.org/10.1146/annurev-conmatphys-070909-103925`.

[34]   C. M. Varma. "Pseudogap Phase and the Quantum-Critical Point in Copper-Oxide Metals". In: *Phys. Rev. Lett.* 83 (17 Oct. 1999), pp. 3538–3541. URL: `https://link.aps.org/doi/10.1103/PhysRevLett.83.3538`.

[35]   Y. Li et al. "Unusual magnetic order in the pseudogap region of the superconductor HgBa2CuO4+[dgr]". In: *Nature* 455.7211 (Sept. 2008), pp. 372–375. URL: `http://dx.doi.org/10.1038/nature07251`.

[36] Yuan Li et al. "Hidden magnetic excitation in the pseudogap phase of a high-Tc superconductor". In: *Nature* 468.7321 (Nov. 2010), pp. 283–285. URL: http://dx.doi.org/10.1038/nature09477.

[37] Chandra Varma. "High-temperature superconductivity: Mind the pseudogap". In: *Nature* 468.7321 (2010), pp. 184–185.

[38] H. A. Mook et al. "Observation of magnetic order in a superconducting YBa$_2$Cu$_3$O$_{6.6}$ single crystal using polarized neutron scattering". In: *Phys. Rev. B* 78 (2 July 2008), p. 020506. URL: https://link.aps.org/doi/10.1103/PhysRevB.78.020506.

[39] B. Keimer et al. "From quantum matter to high-temperature superconductivity in copper oxides". In: *Nature* 518.7538 (Feb. 2015). Review, pp. 179–186. URL: http://dx.doi.org/10.1038/nature14165.

[40] Sudip Chakravarty, Richard E. Norton, and Olav F. Syljuåsen. "Transverse Gauge Interactions and the Vanquished Fermi Liquid". In: *Phys. Rev. Lett.* 74 (8 Feb. 1995), pp. 1423–1426. URL: https://link.aps.org/doi/10.1103/PhysRevLett.74.1423.

[41] A. Liam Fitzpatrick et al. "Non-Fermi-liquid fixed point in a Wilsonian theory of quantum critical metals". In: *Phys. Rev. B* 88 (12 Sept. 2013), p. 125116. URL: https://link.aps.org/doi/10.1103/PhysRevB.88.125116.

[42] A. Liam Fitzpatrick et al. "Non-Fermi-liquid behavior of large-N_B quantum critical metals". In: *Phys. Rev. B* 89 (16 Apr. 2014), p. 165114. URL: https://link.aps.org/doi/10.1103/PhysRevB.89.165114.

[43] Gonzalo Torroba and Huajia Wang. "Quantum critical metals in $4 - \epsilon$ dimensions". In: *Phys. Rev. B* 90 (16 Oct. 2014), p. 165144. URL: https://link.aps.org/doi/10.1103/PhysRevB.90.165144.

[44] A. Liam Fitzpatrick, Gonzalo Torroba, and Huajia Wang. "Aspects of renormalization in finite-density field theory". In: *Phys. Rev. B* 91 (19 May 2015), p. 195135. URL: https://link.aps.org/doi/10.1103/PhysRevB.91.195135.

[45]   Joel Feldman et al. "Evaluation of Fermion Loops by Iterated Residues". In: *Singularities: The Brieskorn Anniversary Volume*. Ed. by V. I. Arnold, G.-M. Greuel, and J. H. M. Steenbrink. Basel: Birkhäuser Basel, 1998, pp. 361–398. URL: http://dx.doi.org/10.1007/978-3-0348-8770-0_18.

[46]   Gonzalo Torroba and Huajia Wang. "Quantum critical metals in $4 - \epsilon$ dimensions". In: *Phys. Rev. B* 90 (16 Oct. 2014), p. 165144. URL: https://link.aps.org/doi/10.1103/PhysRevB.90.165144.

[47]   John A. Hertz. "Quantum critical phenomena". In: *Phys. Rev. B* 14 (3 Aug. 1976), pp. 1165–1184. URL: https://link.aps.org/doi/10.1103/PhysRevB.14.1165.

[48]   AJ Millis. "Effect of a nonzero temperature on quantum critical points in itinerant fermion systems". In: *Physical Review B* 48.10 (1993), p. 7183.

[49]   Subir Sachdev. *Quantum phase transitions*. Wiley Online Library, 2007.

[50]   Kenneth G. Wilson and Michael E. Fisher. "Critical Exponents in 3.99 Dimensions". In: *Phys. Rev. Lett.* 28 (4 Jan. 1972), pp. 240–243. URL: https://link.aps.org/doi/10.1103/PhysRevLett.28.240.

[51]   L. N. Lipatov. "Divergence of the Perturbation Theory Series and the Quasiclassical Theory". In: *Sov. Phys. JETP* 45 (1977). [Zh. Eksp. Teor. Fiz.72,411(1977)], pp. 216–223.

[52]   Daniele Dorigoni. "An Introduction to Resurgence, Trans-Series and Alien Calculus". In: (2014). arXiv: 1411.3585 [hep-th].

[53]   John A. Hertz. "Quantum critical phenomena". In: *Phys. Rev. B* 14 (3 Aug. 1976), pp. 1165–1184. URL: https://link.aps.org/doi/10.1103/PhysRevB.14.1165.

[54]   Kenneth A. Intriligator and N. Seiberg. "Mirror symmetry in three-dimensional gauge theories". In: *Phys. Lett.* B387 (1996), pp. 513–519. arXiv: hep-th/9607207 [hep-th].

[55]   Andrea Allais and Subir Sachdev. "Spectral function of a localized fermion coupled to the Wilson-Fisher conformal field theory". In: *Phys. Rev. B* 90 (3 July 2014), p. 035131. URL: https://link.aps.org/doi/10.1103/PhysRevB.90.035131.

[56] AB Migdal. "Interaction between electrons and lattice vibrations in a normal metal". In: *Sov. Phys. JETP* 7.6 (1958), pp. 996–1001.

[57] Ipsita Mandal and Sung-Sik Lee. "Ultraviolet/infrared mixing in non-Fermi liquids". In: *Phys. Rev. B* 92 (3 July 2015), p. 035141. URL: https://link.aps.org/doi/10.1103/PhysRevB.92.035141.

[58] Olexei I. Motrunich and Matthew P. A. Fisher. "*d*". In: *Phys. Rev. B* 75 (23 June 2007), p. 235116. URL: https://link.aps.org/doi/10.1103/PhysRevB.75.235116.

[59] B. L. Altshuler, L. B. Ioffe, and A. J. Millis. "Low-energy properties of fermions with singular interactions". In: *Phys. Rev. B* 50 (19 Nov. 1994), pp. 14048–14064. URL: https://link.aps.org/doi/10.1103/PhysRevB.50.14048.

[60] Sung-Sik Lee. "Low-energy effective theory of Fermi surface coupled with U(1) gauge field in $2 + 1$ dimensions". In: *Phys. Rev. B* 80 (16 Oct. 2009), p. 165102. URL: https://link.aps.org/doi/10.1103/PhysRevB.80.165102.

[61] David F. Mross et al. "Controlled expansion for certain non-Fermi-liquid metals". In: *Phys. Rev. B* 82 (4 July 2010), p. 045121. URL: https://link.aps.org/doi/10.1103/PhysRevB.82.045121.

[62] A. Liam Fitzpatrick et al. "Non-Fermi-liquid behavior of large-N_B quantum critical metals". In: *Phys. Rev. B* 89 (16 Apr. 2014), p. 165114. URL: https://link.aps.org/doi/10.1103/PhysRevB.89.165114.

[63] Kenneth G. Wilson and Michael E. Fisher. "Critical Exponents in 3.99 Dimensions". In: *Phys. Rev. Lett.* 28 (4 Jan. 1972), pp. 240–243. URL: https://link.aps.org/doi/10.1103/PhysRevLett.28.240.

[64] F. J. Dyson. "Divergence of Perturbation Theory in Quantum Electrodynamics". In: *Phys. Rev.* 85 (4 Feb. 1952), pp. 631–632. URL: https://link.aps.org/doi/10.1103/PhysRev.85.631.

[65] Balazs Meszena et al. "Nonperturbative emergence of non-Fermi-liquid behavior in $d = 2$ quantum critical metals". In: *Phys. Rev. B* 94 (11 Sept. 2016), p. 115134. URL: http://link.aps.org/doi/10.1103/PhysRevB.94.115134.

[66] Petter Säterskog, Balazs Meszena, and Koenraad Schalm. "Two-point function of a $d = 2$ quantum critical metal in the limit $k_F \to \infty$, $N_f \to 0$ with $N_f k_F$ fixed". In: *Phys. Rev. B* 96 (15 Oct. 2017), p. 155125. URL: https://link.aps.org/doi/10.1103/PhysRevB.96.155125.

[67] Petter Säterskog. "A Framework for Studying a Quantum Critical Metal in the Limit $N_f \to 0$". In: *To be submitted* (2017).

[68] Petter Säterskog. "Boson-Dominated Quantum Critical Metals at Lorentz Symmetry Point". In: *To be submitted* (2017).

[69] LD Landau. "The theory of a Fermi liquid". In: *Soviet Physics Jetp-Ussr* 3.6 (1957), pp. 920–925.

[70] C. M. Varma et al. "Phenomenology of the normal state of Cu-O high-temperature superconductors". In: *Phys. Rev. Lett.* 63 (18 Oct. 1989), pp. 1996–1999. URL: https://link.aps.org/doi/10.1103/PhysRevLett.63.1996.

[71] Yafis Barlas and Kun Yang. "Non-Fermi Liquid behavior in Neutral Bilayer Graphene". In: (2009). arXiv: 0908.1238.

[72] F. Guinea and M. I. Katsnelson. "Many body renormalization of the minimal conductivity in graphene". In: (2013). arXiv: 1307.6221.

[73] D. van der Marel et al. "Powerlaw optical conductivity with a constant phase angle in high Tc superconductors". In: (2003). arXiv: cond-mat/0309172.

[74] Philipp Gegenwart, Qimiao Si, and Frank Steglich. "Quantum Criticality in Heavy Fermion Metals". In: (2007). arXiv: 0712.2045.

[75] T. Senthil. "Theory of a continuous Mott transition in two dimensions". In: (2008). arXiv: 0804.1555.

[76] Takahiro Misawa and Masatoshi Imada. "Quantum criticality around metal-insulator transitions of strongly correlated electrons". In: (2006). arXiv: cond-mat/0612632.

[77] John A. Hertz. "Quantum critical phenomena". In: *Phys. Rev. B* 14 (3 Aug. 1976), pp. 1165–1184. URL: https://link.aps.org/doi/10.1103/PhysRevB.14.1165.

[78] A. J. Millis. "Effect of a nonzero temperature on quantum critical points in itinerant fermion systems". In: *Physical Review B* 48.10 (Sept. 1993), pp. 7183–7196. URL: https://doi.org/10.1103%2Fphysrevb.48.7183.

[79] S. Sachdev. *Quantum Phase Transitions*. Cambridge University Press, 2001. URL: https://books.google.nl/books?id=Ih%5C_E05N5TZQC.

[80] J. Rech, C. Pepin, and A. V. Chubukov. "Quantum critical behavior in itinerant electron systems – Eliashberg theory and instability of a ferromagnetic quantum-critical point". In: (2006). arXiv: cond-mat/0605306.

[81] Sudip Chakravarty, Bertrand I. Halperin, and David R. Nelson. "Two-dimensional quantum Heisenberg antiferromagnet at low temperatures". In: *Physical Review B* 39.4 (Feb. 1989), pp. 2344–2371. URL: https://doi.org/10.1103%2Fphysrevb.39.2344.

[82] Qimiao SI, J. Lleweilun Smith, and Kevin Ingersent. "Quantum Critical Behaviour in Kondo Systems". In: *International Journal of Modern Physics B* 13.18 (July 1999), pp. 2331–2342. URL: https://doi.org/10.1142%2Fs0217979299002435.

[83] Hilbert v. Löhneysen et al. "Fermi-liquid instabilities at magnetic quantum phase transitions". In: *Rev. Mod. Phys.* 79 (3 Aug. 2007), pp. 1015–1075. URL: https://link.aps.org/doi/10.1103/RevModPhys.79.1015.

[84] Max A. Metlitski and Subir Sachdev. "Quantum phase transitions of metals in two spatial dimensions. I. Ising-nematic order". In: *Physical Review B* 82.7 (Aug. 2010). URL: https://doi.org/10.1103%2Fphysrevb.82.075127.

[85] Sung-Sik Lee. "Low-energy effective theory of Fermi surface coupled with U(1) gauge field in $2+1$ dimensions". In: *Phys. Rev. B* 80 (16 Oct. 2009), p. 165102. URL: https://link.aps.org/doi/10.1103/PhysRevB.80.165102.

[86] Max A. Metlitski and Subir Sachdev. "Quantum phase transitions of metals in two spatial dimensions. II. Spin density wave order". In: *Physical Review B* 82.7 (Aug. 2010). URL: https://doi.org/10.1103%2Fphysrevb.82.075128.

[87] Tobias Holder and Walter Metzner. "Anomalous dynamical scaling from nematic and U(1) gauge field fluctuations in two-dimensional metals". In: *Phys. Rev. B* 92 (4 July 2015), p. 041112. URL: https://link.aps.org/doi/10.1103/PhysRevB.92.041112.

[88] Tobias Holder and Walter Metzner. "Fermion loops and improved power-counting in two-dimensional critical metals with singular forward scattering". In: *Phys. Rev. B* 92 (24 Dec. 2015), p. 245128. URL: https://link.aps.org/doi/10.1103/PhysRevB.92.245128.

[89] David F. Mross et al. "Controlled expansion for certain non-Fermi-liquid metals". In: *Phys. Rev. B* 82 (4 July 2010), p. 045121. URL: https://link.aps.org/doi/10.1103/PhysRevB.82.045121.

[90] A. Liam Fitzpatrick et al. "Non-Fermi-liquid fixed point in a Wilsonian theory of quantum critical metals". In: *Phys. Rev. B* 88 (12 Sept. 2013), p. 125116. URL: https://link.aps.org/doi/10.1103/PhysRevB.88.125116.

[91] A. Liam Fitzpatrick et al. "Non-Fermi-liquid behavior of large-N_B quantum critical metals". In: *Phys. Rev. B* 89 (16 Apr. 2014), p. 165114. URL: https://link.aps.org/doi/10.1103/PhysRevB.89.165114.

[92] R. Mahajan et al. "Quantum critical metals in $d = 3 + 1$ dimensions". In: *Phys. Rev. B* 88 (11 Sept. 2013), p. 115116. URL: https://link.aps.org/doi/10.1103/PhysRevB.88.115116.

[93] Gonzalo Torroba and Huajia Wang. "Quantum critical metals in $4 - \epsilon$ dimensions". In: *Phys. Rev. B* 90 (16 Oct. 2014), p. 165144. URL: https://link.aps.org/doi/10.1103/PhysRevB.90.165144.

[94] Jean-Paul Blaizot and Edmond Iancu. "Bloch-Nordsieck propagator at finite temperature". In: *Phys. Rev. D* 56 (12 Dec. 1997), pp. 7877–7892. URL: https://link.aps.org/doi/10.1103/PhysRevD.56.7877.

[95] Maarten F. L. Golterman. "Chiral perturbation theory and the quenched approximation of QCD". In: *Acta Phys. Polon.* B25 (1994), pp. 1731–1756. arXiv: hep-lat/9411005 [hep-lat].

[96]   A. Jakovác and P. Mati. "Resummations in the Bloch-Nordsieck model". In: *Phys. Rev. D* 85 (8 Apr. 2012), p. 085006. URL: `https://link.aps.org/doi/10.1103/PhysRevD.85.085006`.

[97]   Andrea Kernemann and N. G. Stefanis. "Exact solutions for fermionic Green's functions in the Bloch-Nordsieck approximation of QED". In: *Phys. Rev. D* 40 (6 Sept. 1989), pp. 2103–2111. URL: `https://link.aps.org/doi/10.1103/PhysRevD.40.2103`.

[98]   A. Jakovác and P. Mati. "Spectral function of the Bloch-Nordsieck model at finite temperature". In: *Phys. Rev. D* 87 (12 June 2013), p. 125007. URL: `https://link.aps.org/doi/10.1103/PhysRevD.87.125007`.

[99]   A. Jakovác and P. Mati. "Validating the 2PI resummation: The Bloch-Nordsieck example". In: *Phys. Rev. D* 90 (4 Aug. 2014), p. 045038. URL: `https://link.aps.org/doi/10.1103/PhysRevD.90.045038`.

[100]   A.I. Karanikas, C.N. Ktorides, and N.G. Stefanis. "On the infrared structure of the one-fermion Green function in QED". In: *Physics Letters B* 289.1 (1992), pp. 176–183. URL: `http://www.sciencedirect.com/science/article/pii/037026939291381I`.

[101]   D. V. Khveshchenko and P. C. E. Stamp. "Low-energy properties of two-dimensional fermions with long-range current-current interactions". In: *Phys. Rev. Lett.* 71 (13 Sept. 1993), pp. 2118–2121. URL: `https://link.aps.org/doi/10.1103/PhysRevLett.71.2118`.

[102]   L. B. Ioffe, D. Lidsky, and B. L. Altshuler. "Effective lowering of dimensionality in the strongly correlated two dimensional electron gas". In: *Phys. Rev. Lett.* 73 (3 July 1994), pp. 472–475. URL: `https://link.aps.org/doi/10.1103/PhysRevLett.73.472`.

[103]   B. L. Altshuler, L. B. Ioffe, and A. J. Millis. "Low-energy properties of fermions with singular interactions". In: *Phys. Rev. B* 50 (19 Nov. 1994), pp. 14048–14064. URL: `https://link.aps.org/doi/10.1103/PhysRevB.50.14048`.

[104]   Arne Neumayr and Walter Metzner. "Fermion loops, loop cancellation, and density correlations in two-dimensional Fermi systems". In: *Phys. Rev. B* 58 (23 Dec. 1998), pp. 15449–15459. URL: `https://link.aps.org/doi/10.1103/PhysRevB.58.15449`.

[105] Andrea Allais and Subir Sachdev. "Spectral function of a localized fermion coupled to the Wilson-Fisher conformal field theory". In: *Phys. Rev. B* 90 (3 July 2014), p. 035131. URL: https://link.aps.org/doi/10.1103/PhysRevB.90.035131.

[106] J. Quintanilla and A. J. Schofield. "Pomeranchuk and topological Fermi surface instabilities from central interactions". In: *Phys. Rev. B* 74 (11 Sept. 2006), p. 115126. URL: https://link.aps.org/doi/10.1103/PhysRevB.74.115126.

[107] Joseph Polchinski. "Effective field theory and the Fermi surface". In: *Theoretical Advanced Study Institute (TASI 92): From Black Holes and Strings to Particles Boulder, Colorado, June 3-28, 1992*. 1992, pp. 0235–276. arXiv: hep-th/9210046 [hep-th].

[108] R. Shankar. "Renormalization-group approach to interacting fermions". In: *Rev. Mod. Phys.* 66 (1 Jan. 1994), pp. 129–192. URL: https://link.aps.org/doi/10.1103/RevModPhys.66.129.

[109] John A. Hertz. "Quantum critical phenomena". In: *Phys. Rev. B* 14 (3 Aug. 1976), pp. 1165–1184. URL: https://link.aps.org/doi/10.1103/PhysRevB.14.1165.

[110] A. J. Millis. "Effect of a nonzero temperature on quantum critical points in itinerant fermion systems". In: *Physical Review B* 48.10 (Sept. 1993), pp. 7183–7196. URL: https://doi.org/10.1103%2Fphysrevb.48.7183.

[111] Hilbert v. Löhneysen et al. "Fermi-liquid instabilities at magnetic quantum phase transitions". In: *Rev. Mod. Phys.* 79 (3 Aug. 2007), pp. 1015–1075. URL: https://link.aps.org/doi/10.1103/RevModPhys.79.1015.

[112] S. Sachdev. *Quantum Phase Transitions*. Cambridge University Press, 2001. URL: https://books.google.nl/books?id=Ih%5C_E05N5TZQC.

[113] Patrick A. Lee. "Gauge field, Aharonov-Bohm flux, and high-T_c superconductivity". In: *Phys. Rev. Lett.* 63 (6 Aug. 1989), pp. 680–683. URL: https://link.aps.org/doi/10.1103/PhysRevLett.63.680.

[114] Vadim Oganesyan, Steven A. Kivelson, and Eduardo Fradkin. "Quantum theory of a nematic Fermi fluid". In: *Phys. Rev. B* 64 (19 Oct. 2001), p. 195109. URL: https://link.aps.org/doi/10.1103/PhysRevB.64.195109.

[115] W. Metzner, D. Rohe, and S. Andergassen. "Soft Fermi Surfaces and Breakdown of Fermi-Liquid Behavior". In: *Phys. Rev. Lett.* 91 (6 Aug. 2003), p. 066402. URL: https://link.aps.org/doi/10.1103/PhysRevLett.91.066402.

[116] Max A. Metlitski and Subir Sachdev. "Quantum phase transitions of metals in two spatial dimensions. I. Ising-nematic order". In: *Phys. Rev. B* 82 (7 Aug. 2010), p. 075127. URL: https://link.aps.org/doi/10.1103/PhysRevB.82.075127.

[117] Max A. Metlitski and Subir Sachdev. "Quantum phase transitions of metals in two spatial dimensions. II. Spin density wave order". In: *Phys. Rev. B* 82 (7 Aug. 2010), p. 075128. URL: https://link.aps.org/doi/10.1103/PhysRevB.82.075128.

[118] D. V. Khveshchenko and P. C. E. Stamp. "Low-energy properties of two-dimensional fermions with long-range current-current interactions". In: *Phys. Rev. Lett.* 71 (13 Sept. 1993), pp. 2118–2121. URL: https://link.aps.org/doi/10.1103/PhysRevLett.71.2118.

[119] A. Liam Fitzpatrick et al. "Non-Fermi-liquid fixed point in a Wilsonian theory of quantum critical metals". In: *Phys. Rev. B* 88 (12 Sept. 2013), p. 125116. URL: https://link.aps.org/doi/10.1103/PhysRevB.88.125116.

[120] A. Liam Fitzpatrick et al. "Non-Fermi-liquid behavior of large-N_B quantum critical metals". In: *Phys. Rev. B* 89 (16 Apr. 2014), p. 165114. URL: https://link.aps.org/doi/10.1103/PhysRevB.89.165114.

[121] Andrea Allais and Subir Sachdev. "Spectral function of a localized fermion coupled to the Wilson-Fisher conformal field theory". In: *Phys. Rev. B* 90 (3 July 2014), p. 035131. URL: https://link.aps.org/doi/10.1103/PhysRevB.90.035131.

[122] Tobias Holder and Walter Metzner. "Fermion loops and improved power-counting in two-dimensional critical metals with singular forward scattering". In: *Phys. Rev. B* 92 (24 Dec. 2015), p. 245128.

URL: https://link.aps.org/doi/10.1103/PhysRevB.92.245128.

[123] R. Mahajan et al. "Quantum critical metals in $d = 3 + 1$ dimensions". In: *Phys. Rev. B* 88 (11 Sept. 2013), p. 115116. URL: https://link.aps.org/doi/10.1103/PhysRevB.88.115116.

[124] Jérôme Rech, Catherine Pépin, and Andrey V. Chubukov. "Quantum critical behavior in itinerant electron systems: Eliashberg theory and instability of a ferromagnetic quantum critical point". In: *Phys. Rev. B* 74 (19 Nov. 2006), p. 195126. URL: https://link.aps.org/doi/10.1103/PhysRevB.74.195126.

[125] A. Liam Fitzpatrick, Gonzalo Torroba, and Huajia Wang. "Aspects of renormalization in finite-density field theory". In: *Phys. Rev. B* 91 (19 May 2015), p. 195135. URL: https://link.aps.org/doi/10.1103/PhysRevB.91.195135.

[126] Gonzalo Torroba and Huajia Wang. "Quantum critical metals in $4 - \epsilon$ dimensions". In: *Phys. Rev. B* 90 (16 Oct. 2014), p. 165144. URL: https://link.aps.org/doi/10.1103/PhysRevB.90.165144.

[127] Balazs Meszena et al. "Nonperturbative emergence of non-Fermi-liquid behavior in $d = 2$ quantum critical metals". In: *Phys. Rev. B* 94 (11 Sept. 2016), p. 115134. URL: https://link.aps.org/doi/10.1103/PhysRevB.94.115134.

[128] L. B. Ioffe, D. Lidsky, and B. L. Altshuler. "Effective lowering of dimensionality in the strongly correlated two dimensional electron gas". In: *Phys. Rev. Lett.* 73 (3 July 1994), pp. 472–475. URL: https://link.aps.org/doi/10.1103/PhysRevLett.73.472.

[129] B. L. Altshuler, L. B. Ioffe, and A. J. Millis. "Low-energy properties of fermions with singular interactions". In: *Phys. Rev. B* 50 (19 Nov. 1994), pp. 14048–14064. URL: https://link.aps.org/doi/10.1103/PhysRevB.50.14048.

[130] Walter Metzner, Claudio Castellani, and Carlo Di Castro. "Fermi systems with strong forward scattering". In: *Advances in Physics* 47.3 (1998), pp. 317–445. eprint: http://dx.doi.org/10.1080/000187398243528. URL: http://dx.doi.org/10.1080/000187398243528.

[131] Tigran A. Sedrakyan and Andrey V. Chubukov. "Fermionic propagators for two-dimensional systems with singular interactions". In: *Phys. Rev. B* 79 (11 Mar. 2009), p. 115129. URL: https://link.aps.org/doi/10.1103/PhysRevB.79.115129.

[132] S. Raghu, Gonzalo Torroba, and Huajia Wang. "Metallic quantum critical points with finite BCS couplings". In: *Phys. Rev. B* 92 (20 Nov. 2015), p. 205104. URL: https://link.aps.org/doi/10.1103/PhysRevB.92.205104.

[133] Philipp Gegenwart, Qimiao Si, and Frank Steglich. "Quantum criticality in heavy-fermion metals". In: *Nat Phys* 4.3 (Mar. 2008), pp. 186–197. URL: http://dx.doi.org/10.1038/nphys892.

[134] Max A. Metlitski et al. "Cooper pairing in non-Fermi liquids". In: *Phys. Rev. B* 91 (11 Mar. 2015), p. 115111. URL: https://link.aps.org/doi/10.1103/PhysRevB.91.115111.

[135] A. Liam Fitzpatrick et al. "Enhanced pairing of quantum critical metals near $d = 3+1$". In: *Phys. Rev. B* 92 (4 July 2015), p. 045118. URL: https://link.aps.org/doi/10.1103/PhysRevB.92.045118.

[136] Huajia Wang, Srinivas Raghu, and Gonzalo Torroba. "Non-Fermi-liquid superconductivity: Eliashberg approach versus the renormalization group". In: *Phys. Rev. B* 95 (16 Apr. 2017), p. 165137. URL: https://link.aps.org/doi/10.1103/PhysRevB.95.165137.

[137] Arne Neumayr and Walter Metzner. "Fermion loops, loop cancellation, and density correlations in two-dimensional Fermi systems". In: *Phys. Rev. B* 58 (23 Dec. 1998), pp. 15449–15459. URL: https://link.aps.org/doi/10.1103/PhysRevB.58.15449.

[138] Peter Kopietz, Joachim Hermisson, and Kurt Schönhammer. "Bosonization of interacting fermions in arbitrary dimension beyond the Gaussian approximation". In: *Phys. Rev. B* 52 (15 Oct. 1995), pp. 10877–10896. URL: https://link.aps.org/doi/10.1103/PhysRevB.52.10877.

[139] Stephan C. Thier and Walter Metzner. "Singular order parameter interaction at the nematic quantum critical point in two-dimensional electron systems". In: *Phys. Rev. B* 84 (15 Oct. 2011), p. 155133. URL: https://link.aps.org/doi/10.1103/PhysRevB.84.155133.

[140] Torbjörn Granlund et al. "GNU Multiple Precision Arithmetic Library". In: (Dec. 2002). `https://gmplib.org/`.

[141] Sung-Sik Lee. "Low-energy effective theory of Fermi surface coupled with U(1) gauge field in $2+1$ dimensions". In: *Phys. Rev. B* 80 (16 Oct. 2009), p. 165102. URL: `https://link.aps.org/doi/10.1103/PhysRevB.80.165102`.

[142] David F. Mross et al. "Controlled expansion for certain non-Fermi-liquid metals". In: *Phys. Rev. B* 82 (4 July 2010), p. 045121. URL: `https://link.aps.org/doi/10.1103/PhysRevB.82.045121`.

[143] Yong Baek Kim et al. "Gauge-invariant response functions of fermions coupled to a gauge field". In: *Phys. Rev. B* 50 (24 Dec. 1994), pp. 17917–17932. URL: `https://link.aps.org/doi/10.1103/PhysRevB.50.17917`.

[144] Tobias Holder and Walter Metzner. "Anomalous dynamical scaling from nematic and U(1) gauge field fluctuations in two-dimensional metals". In: *Phys. Rev. B* 92 (4 July 2015), p. 041112. URL: `https://link.aps.org/doi/10.1103/PhysRevB.92.041112`.

[145] Arne Neumayr and Walter Metzner. "Fermion loops, loop cancellation, and density correlations in two-dimensional Fermi systems". In: *Phys. Rev. B* 58 (23 Dec. 1998), pp. 15449–15459. URL: `https://link.aps.org/doi/10.1103/PhysRevB.58.15449`.

[146] Andrey Chubukov. "Hidden one-dimensional physics in 2D critical metals". In: *Physics* 3 (Aug. 2010). URL: `https://doi.org/10.1103/physics.3.70`.

[147] Max A. Metlitski and Subir Sachdev. "Quantum phase transitions of metals in two spatial dimensions. II. Spin density wave order". In: *Phys. Rev. B* 82 (7 Aug. 2010), p. 075128. URL: `https://link.aps.org/doi/10.1103/PhysRevB.82.075128`.

[148] A. Liam Fitzpatrick et al. "Enhanced pairing of quantum critical metals near $d = 3+1$". In: *Phys. Rev. B* 92 (4 July 2015), p. 045118. URL: `https://link.aps.org/doi/10.1103/PhysRevB.92.045118`.

[149] J. Zaanen et al. *Holographic Duality in Condensed Matter Physics.* Cambridge University Press, 2015. URL: `https://books.google.nl/books?id=2Gw7rgEACAAJ`.

[150]   Mike Blake, Aristomenis Donos, and David Tong. "Holographic charge oscillations". In: *Journal of High Energy Physics* 2015.4 (2015), p. 19. URL: `http://dx.doi.org/10.1007/JHEP04(2015)019`.

[151]   Joel Feldman, Horst Knörrer, and Eugene Trubowitz. "Convergence of Perturbation Expansions in Fermionic Models. Part 1: Nonperturbative Bounds". In: *Communications in Mathematical Physics* 247.1 (May 2004), pp. 195–242. URL: `http://dx.doi.org/10.1007/s00220-004-1039-1`.

[152]   Irina Arefeva et al. "Holographic dual of a time machine". In: *Phys. Rev. D* 94 (4 Aug. 2016), p. 044059. URL: `https://link.aps.org/doi/10.1103/PhysRevD.94.044059`.